NATIONAL COOPERATIVE HIGHWAY RESEARCH PROGRAM REPORT

DONE

304

DETERMINING DETERIORATED AREAS IN PORTLAND CEMENT CONCRETE PAVEMENTS USING RADAR AND VIDEO IMAGING

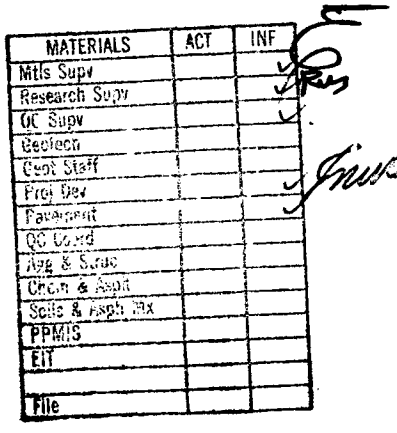

TRANSPORTATION RESEARCH BOARD
NATIONAL RESEARCH COUNCIL

NATIONAL COOPERATIVE HIGHWAY RESEARCH PROGRAM
REPORT 304

DETERMINING DETERIORATED AREAS IN PORTLAND CEMENT CONCRETE PAVEMENTS USING RADAR AND VIDEO IMAGING

L. C. BOMAR, W. F. HORNE, D. R. BROWN
and
J. L. SMART
Gulf Applied Research
Marietta, Georgia

RESEARCH SPONSORED BY THE AMERICAN ASSOCIATION OF STATE HIGHWAY AND TRANSPORTATION OFFICIALS IN COOPERATION WITH THE FEDERAL HIGHWAY ADMINISTRATION

AREAS OF INTEREST:

Pavement Design and Performance
Cement and Concrete
General Materials
Maintenance
(Highway Transportation, Air Transportation)

TRANSPORTATION RESEARCH BOARD
NATIONAL RESEARCH COUNCIL
WASHINGTON, D.C.

DECEMBER 1988

NATIONAL COOPERATIVE HIGHWAY RESEARCH PROGRAM

Systematic, well-designed research provides the most effective approach to the solution of many problems facing highway administrators and engineers. Often, highway problems are of local interest and can best be studied by highway departments individually or in cooperation with their state universities and others. However, the accelerating growth of highway transportation develops increasingly complex problems of wide interest to highway authorities. These problems are best studied through a coordinated program of cooperative research.

In recognition of these needs, the highway administrators of the American Association of State Highway and Transportation Officials initiated in 1962 an objective national highway research program employing modern scientific techniques. This program is supported on a continuing basis by funds from participating member states of the Association and it receives the full cooperation and support of the Federal Highway Administration, United States Department of Transportation.

The Transportation Research Board of the National Research Council was requested by the Association to administer the research program because of the Board's recognized objectivity and understanding of modern research practices. The Board is uniquely suited for this purpose as: it maintains an extensive committee structure from which authorities on any highway transportation subject may be drawn; it possesses avenues of communications and cooperation with federal, state, and local governmental agencies, universities, and industry; its relationship to the National Research Council is an insurance of objectivity; it maintains a full-time research correlation staff of specialists in highway transportation matters to bring the findings of research directly to those who are in a position to use them.

The program is developed on the basis of research needs identified by chief administrators of the highway and transportation departments and by committees of AASHTO. Each year, specific areas of research needs to be included in the program are proposed to the National Research Council and the Board by the American Association of State Highway and Transportation Officials. Research projects to fulfill these needs are defined by the Board, and qualified research agencies are selected from those that have submitted proposals. Administration and surveillance of research contracts are the responsibilities of the National Research Council and the Transportation Research Board.

The needs for highway research are many, and the National Cooperative Highway Research Program can make significant contributions to the solution of highway transportation problems of mutual concern to many responsible groups. The program, however, is intended to complement rather than to substitute for or duplicate other highway research programs.

NCHRP REPORT 304

Project 10-28 FY '85

ISSN 0077-5614

ISBN 0-309-04601-7

L. C. Catalog Card No. 88-51064

Price $14.00

NOTICE

The project that is the subject of this report was a part of the National Cooperative Highway Research Program conducted by the Transportation Research Board with the approval of the Governing Board of the National Research Council. Such approval reflects the Governing Board's judgment that the program concerned is of national importance and appropriate with respect to both the purposes and resources of the National Research Council.

The members of the technical committee selected to monitor this project and to review this report were chosen for recognized scholarly competence and with due consideration for the balance of disciplines appropriate to the project. The opinions and conclusions expressed or implied are those of the research agency that performed the research, and, while they have been accepted as appropriate by the technical committee, they are not necessarily those of the Transportation Research Board, the National Research Council, the American Association of State Highway and Transportation officials, or the Federal Highway Administration, U.S. Department of Transportation.

Each report is reviewed and accepted for publication by the technical committee according to procedures established and monitored by the Transportation Research Board Executive Committee and the Governing Board of the National Research Council.

Special Notice

The Transportation Research Board, the National Research Council, the Federal Highway Administration, the American Association of State Highway and Transportation Officials, and the individual states participating in the National Cooperative Highway Research Program do not endorse products or manufacturers. Trade or manufacturers' names appear herein solely because they are considered essential to the object of this report.

Published reports of the

NATIONAL COOPERATIVE HIGHWAY RESEARCH PROGRAM

are available from:

Transportation Research Board
National Research Council
2101 Constitution Avenue, N.W.
Washington, D.C. 20418

Printed in the United States of America

FOREWORD

By Staff
Transportation
Research Board

Improvements to the application of ground penetrating radar and high resolution video to detect deteriorated areas of portland cement concrete pavements were researched. Developments in radar technology and the interpretation of radar signals were studied as a means for detecting subsurface deterioration, while studies on video imaging were intended to provide a method for recording and cataloging surface deterioration or distress. Advances in both technologies have made it possible to apply them as practical tools for sampling purposes. The research also provides a basis for further study to enhance the capabilities of both technologies and make them more suitable for project level decisions. Engineers and scientists interested in the two technologies and their applications for assessing the condition of concrete pavements will benefit from the research documented in this report.

The need for maintenance and repair of portland cement concrete pavements has increased over the years as these facilities have deteriorated from the effects of age and accumulated traffic loads. This has produced a need for a method to accurately and rapidly determine the location and extent of deteriorated concrete.

An accurate method would enhance the preparation of project plans for needed repairs by permitting more precise calculations of quantities and boundary conditions. And, a rapid method would be desirable for surveying long lengths of pavements, minimizing the interference with traffic on heavily traveled roads. To further increase its utility, the method should be suitable for reinforced and nonreinforced concrete pavements with and without overlays.

Various technologies, such as radar, sonics, infrared, and others, have demonstrated to some degree the feasibility of rapid and accurate detection of deteriorated areas; but, data reduction and interpretation are slow and require expertise not generally available in most state highway agencies. Furthermore, the data may not always be sufficient for determining quantities and exact locations and boundaries of the needed repairs at the project level.

Recognizing that existing technologies showed promise, the NCHRP solicited research proposals to improve accuracy and speed of operation in one or more technologies of the proposer's choosing and to produce results more simply displayed and understandable. Gulf Applied Research, Marietta, Georgia, was selected to study the benefits of ground-penetrating, short-pulsed radar, and high-resolution video imaging.

The researchers performed all the tasks that they proposed, and, as noted in the report, research was successful to varying degrees; however, improvements to both technologies were accomplished. Practical applications are possible for sampling concrete pavement deterioration to make overall assessments of highway segments or networks. Both technologies have also demonstrated enough potential to warrant continued support for which this report provides an excellent foundation and resource for any future endeavors.

CONTENTS

1 SUMMARY

PART I

2 CHAPTER ONE Introduction and Research Approach
Introduction, 2
Research Approach, 2

3 CHAPTER TWO Findings and Interpretation
Subsurface Data Acquisition Subsystem Design, 3
Void-Sizing Algorithm, 6
Video Data Acquisition Subsystem Design, 9
Real Time, Surface Video Analysis System Design, 12
Surface Video Analysis Software Development, 12
Laboratory Testing, 14
Field Testing, 14

16 CHAPTER THREE Conclusions and Suggested Research
Radar as a Survey Tool, 16
Multichannel Radar System Development, 16
Radar Laboratory Tests, 16
Void-Sizing Algorithm, 17
Video Recording Subsystem, 17
Video Data Analysis System Software Development, 17
Real Time, Video Data Analysis System Design, 17

18 REFERENCES

PART II

18 APPENDIX A Technology Background

22 APPENDIX B Enhanced Radar System Design

30 APPENDIX C Void Sizing Algorithm Test Data

40 APPENDIX D Development of the Surface Anomaly Detection Algorithm

52 APPENDIX E Video Analysis Subsystem Design

56 APPENDIX F Laboratory Testing

72 APPENDIX G Field Testing Program

85 APPENDIX H Development of Void Radar Return Equation

88 APPENDIX I SIGMOD Source Listing

94 APPENDIX J CRAKFIND Source Listing

ACKNOWLEDGMENTS

The research reported herein was performed under NCHRP Project 10-28 by Gulf Applied Research, Incorporated. Lucien C. Bomar, President, Walter F. Horne, Danny R. Brown and Jeff L. Smart were principal investigators. Other contributors include William J. Steinway former President, Charles N. Neil Jr., Engineer, and James Thomas, Engineer. A special thanks goes to Dr. Michael Darter of ERES Inc. and Bill Yrjanson of the ACPA and personnel of the Georgia, Florida, North Carolina, Mississippi, Texas, and Illinois Departments of Transportation for their contributions.

DETERMINING DETERIORATED AREAS IN PORTLAND CEMENT CONCRETE PAVEMENTS USING RADAR AND VIDEO IMAGING

SUMMARY

The ability to determine the existence, extent, and rate of progression of deterioration in portland cement concrete (PCC) pavements has been a concern of highway engineers for many years. A method to detect deteriorated areas of PCC pavements rapidly and accurately would be of significant value to the industry and was the subject of this research. The goal of this research was the design of a system which identifies and assesses both surface and subsurface deterioration in PCC pavements. To achieve this goal two existing technologies were chosen for integration into the proposed system. Ground-penetrating short-pulse radar was chosen for subsurface measurements and high-resolution video was selected for pavement surface evaluation. Algorithms for both technologies were developed to allow the detection of several types of surface and subsurface deterioration. Hardware was obtained or designed and built to implement the radar and video technologies for actual laboratory and field testing. Software was written to allow for the automatic detection, recognition, and measurement of various pavement surface defects by the video system. A special algorithm was developed and evaluated for the determination of the volume of subsurface voids. Laboratory testing involved the use of concrete slabs to model subsurface distresses in reinforced and nonreinforced pavements.

Field testing was performed on various roadways to evaluate both the video and radar system capabilities. The radar system was capable of detecting several different types of subsurface distresses after some field sampling for verification. The video system was capable of automatically detecting and measuring very small ($\frac{1}{16}$-in. void cracks) surface targets during the field tests. The radar system was operated at a speed as high as 40 mph, but because of the constant pulse rate of the system, some accuracy in the measurements was lost. For the purpose of this project most data were collected at 10 to 20 mph.

Two different video system designs were developed for future implementation. One design involves the use of off-the-shelf components to collect pavement surface video data for off-line processing. This design can be implemented at a reasonable cost, but will require maximum survey speeds of 10 to 20 mph and data processing at a central location. The second video system design will be capable of data collection at highway speeds and real-time processing of the data. This system will be much more expensive to implement.

Future suggested research includes additional development and testing of a void volume measurement algorithm. Additional field measurements to study in-depth the radar return signals associated with the various types of subsurface distresses will also be of considerable value.

CHAPTER ONE

INTRODUCTION AND RESEARCH APPROACH

INTRODUCTION

Several thousand miles of portland cement concrete (PCC) pavements are in service in the United States. Large portions of these pavements were built prior to 1975 and have reached their design life. A design life of PCC pavement is usually 20 years and is based on a predicted traffic loading. Many PCC pavements received the traffic loading predicted for the 20-year design life in significantly less than 20 years. When a PCC pavement reaches its design life, it usually has begun to exhibit deterioration. This deterioration manifests itself in various types of distress, both surface and subsurface. Once these distresses occur, they steadily increase in severity, reducing the serviceability of the pavement. Extensive study has been dedicated to the causes of the various types of PCC distresses and to the relationship between traffic loading and rate of deterioration.

Type and severity of each pavement distress and the rate of deterioration are vital information required to make the most cost-effective decisions for the type, extent, and scheduling of rehabilitation work on PCC pavements. PCC distresses that are visible on the pavement surface have been defined for standardization and have been classified based on severity in *NCHRP Report 277*. That NCHRP-sponsored project studied concrete pavement distresses nationwide and developed a visual inspection method that defines the most critical distresses, defines severity levels for these distresses, and develops a method to combine these visual distress data into a rating system.

Although *NCHRP Report 277* effectively addresses the definition of visual distresses in PCC pavements, the in-depth visual inspection of these pavements is a relatively slow process requiring trained technicians. A sampling method can be used to speed up the visual inspection process, but a method to "rapidly" collect 100 percent of the distress information, periodically, would be of extreme value in determining deterioration rates and in estimating certain quantities for rehabilitation efforts.

Another major area of concern in PCC pavements is subsurface distresses. Wet base materials, voids, D-cracking, delaminations, saturated subgrade materials, are all subsurface distresses that are difficult to detect in their early stages. When subsurface distresses become severe enough to be evidenced as surface distresses, the PCC pavement is usually in very poor condition. A method to determine the existence and severity of subsurface distresses prior to any major deterioration would be very useful in preventive maintenance and could be employed to prolong the "life" of PCC pavements.

Various deflection methods and sonic methods have been used in an attempt to determine the subsurface condition of PCC pavements. Although some of these methods have met with some success, the techniques are limited because many factors affect the deflection (or sonic) response of a PCC pavement—such as, environmental conditions, slab curl, voids, condition of subsurface layers, and pavement thickness. Deflection methods can determine a "loss of support" condition, but have difficulty determining the cause and extent of this condition and these type tests are slow. A method to assess subsurface conditions accurately, rapidly, and nondestructively is needed.

Current ground-penetrating radar technology has shown great promise in the nondestructive assessment of PCC pavement subsurface conditions. Voids under PCC pavements have been successfully located using ground-penetrating radar (*1*), and delaminations have been located in bridge decks via the same technology (*2,3*). Certain surface distresses in asphaltic concrete pavements have been successfully quantified using a video analysis process in Arizona (*4*). Another private company has a surface video system that is capable of surface distress recognition at highway speeds (*5*). Nevertheless, additional efforts are required in order to refine existing technologies, automate data acquisition and analysis, and integrate these technologies into a mobile unit. This research project, NCHRP Project 10-28, has as its goal the definition and demonstration of a PCC pavement survey system capable of locating, assessing, and defining the extent of surface and subsurface deterioration. The system should be nondestructive, fast, accurate, easy to operate and report survey results in a format easily understood by those charged with pavement maintenance.

RESEARCH APPROACH

The approach taken to fulfill the goals previously mentioned was through the accomplishment of the following six major tasks:

1. Assess and refine existing technologies.
2. Develop algorithms that allow for the location and assessment of distresses.
3. Design a system that implements the algorithms in a fast, accurate, easy-to-operate and useful manner.
4. Implement a sufficient portion of each technology to demonstrate the usefulness and feasibility of the proposed system.
5. Verify the usefulness and feasibility of the proposed system through both field and laboratory tests.
6. Assess the system design to determine limitations and recommend future improvements.

It was the intent of this project to integrate proven technologies rather than to discover new technologies. In order to fully address the two types of distresses (surface and subsurface), two technologies were selected for integration into the final system: high-resolution video and ground-penetrating radar.

Ground-Penetrating Radar

The Gulf Applied Research RODAR™ system was used for

the ground penetrating radar portion of the system. This system normally has a dual-channel, short-pulse, non-ground-contact radar unit for the detection and assessment of subsurface distresses, as well as a video camera and recording unit for the manual assessment of surface distresses for correlation with the subsurface radar data. The RODAR™ offered the state-of-the-art ground-penetrating radar capability. It had been in use commercially as a pavement assessment tool for 2 years prior to this project, and it had been used extensively for non-destructive pavement thickness measurements, void detection, subsurface distress assessment, and bridge deck delamination detection. However, several needs existed that were addressed in this research project, the most important of which were: (1) increased automation of the data analysis process; and (2) improved techniques for, and experience in, the detection and assessment of subsurface distresses other than voids.

To this end, an algorithm based on ground-penetrating radar capabilities was developed to allow for the location, assessment, and sizing of voids beneath PCC pavement. This algorithm has application to certain other subsurface distresses. The algorithm involves a multiple channel radar system that simultaneously surveys closely spaced parallel "paths" across the roadway as the system is moved longitudinally along the roadway. As the target (void or other distress) appears in one or more radar "paths", the existence and length of the target is noted. The result is an approximation of the two-dimensional shape of the target. In the case of voids, previous research conducted under NCHRP Project 10-14 developed a relationship between target signal return amplitude and vertical dimension of the void. This relationship is used in the ground-penetrating radar-based algorithm to determine the vertical dimension of the void.

To implement the ground-penetrating radar-based algorithm, a system was designed, incorporating both hardware and software components. The hardware portion of the system design involved the modification of the existing RODAR™ technology into a five-channel system. This design directed attention to both the electronic problems of a multiple antenna system and the physical problems of producing a road-worthy system. The software portion of the system design uses digitized radar return data to detect the existence of a target, determines the amplitude of a target signal return, and recognizes the length (longitudinally) of the target (based on fifth wheel distance data). The signal processing software designed for this project can be effective in detecting and sizing a void.

To implement a portion of the system design, a five-channel radar system was built, which consisted of five independent radar units combined into a multichannel system. Both laboratory and field tests were undertaken to determine the usefulness of the system design. Laboratory tests were conducted using cast concrete blocks and a large substantial number of variables for experimentation. Field tests were conducted on PCC pavements in several states to test a variety of pavement types and subsurface distresses.

High-Resolution Video

High-resolution video was chosen as the surface distress detection technology. Since considerable work had been done in the video imaging processing area, in general, existing camera systems, video recorders, and video image processing development software were assessed. A camera system and an image processing software development package were acquired for use with this research project.

Algorithms were also developed for the location, identification, and assessment of PCC pavement surface distresses. The PCC pavement distress definitions developed for *NCHRP Report 277* were identified as the distresses to be used for the algorithm development. Certain of the distresses defined in *NCHRP Report 277,* however, could not be identified by video image processing. Those distresses that could be identified by image processing were studied. A system was defined to implement the video processing algorithms using the equipment and software, on hand, in the laboratory. To implement the video processing algorithms in a very high-resolution, real-time format based on existing technology, a second system was designed giving special attention to resolution, background intensity, and system calibration.

A video recording system was implemented in the RODAR™ vehicle for the collection of actual surface distress data. A special camera mounting system was built to allow significant flexibility in the height, angle, and number of cameras to be used in the tests. Special attention was paid to the recording of fifth wheel-generated location information and its optimum use. The field data collected with this system were used to assess the system performance.

CHAPTER TWO

FINDINGS AND INTERPRETATION

SUBSURFACE DATA ACQUISITION SUBSYSTEM DESIGN

The existing radar-based pavement survey system chosen for this project normally operates with two antennas. With this dual antenna system, a subsurface anomaly can be detected in two 12-in. to 18-in. wide paths along a roadway. This makes a crude estimate of horizontal anomaly dimensions possible. Additional transverse data density is required to more accurately determine the horizontal dimensions of the anomaly. The most straightforward method for achieving the requisite information is the use of an antenna array with sufficient coverage to provide the

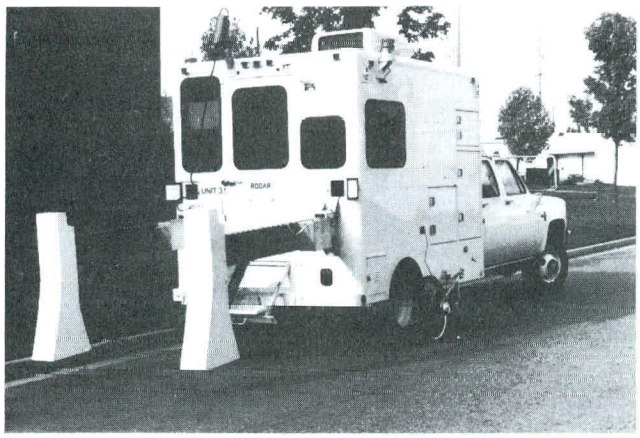

Figure 1. Conventional RODAR™ vehicle.

desired resolution. There are two difficulties with such an approach, however. First, as more antenna/transducer units are added to the array and the spacing between adjacent units is decreased, the mitigation of intrasystem interference becomes increasingly more important if valid data are to be obtained. Second, the magnitude of the data acquisition and analysis task increases in proportion to the number of antennas in the array because the return signal from each antenna must be processed to retrieve the desired information. These two problems were addressed and solved during this project.

The approach chosen to accomplish the determination of subsurface anomaly dimensions is a multichannel, short-pulse radar system. The multichannel system was designed (overcoming the many inherent technical problems), tested, and used in the field to collect actual survey data. Appendix B describes the design modifications made to produce a working, multichannel, short-pulse radar-based, PCC pavement survey system.

In order to demonstrate the validity of the radar subsystem design discussed in Appendix B, a RODAR™ vehicle was dedicated for the integration of the enhanced radar subsystem prototype components. A conventional RODAR™ vehicle can be seen in Figure 1. This type vehicle utilizes a two-antenna system. The antennas are attached to the ends of 5-ft long fiberglass booms to eliminate reflections from the metal body of the vehicle. Enclosures attached to the booms contain the transducer hardware. A fifth wheel, for location information, is a part of the system. The remainder of the system electronics is contained in racks inside the vehicle. The modifications made to the conventional RODAR™ system for the integration of the enhanced radar subsystem are discussed in the following paragraphs.

A smaller flared version of the RODAR™ operating antenna (Figure 2) was used for this project. This type antenna allows for a significant reduction in system size and weight with only moderate reductions in system performance. Mounting the transmitter hardware inside the antenna enclosure also contributes to size reduction and has signal performance gains. Accordingly, special antenna enclosures and new smaller antennas were designed and fabricated. Transducer hardware was moved from the conventional enclosures and mounted, along with the new antennas, in the new antenna enclosures. In total, six new

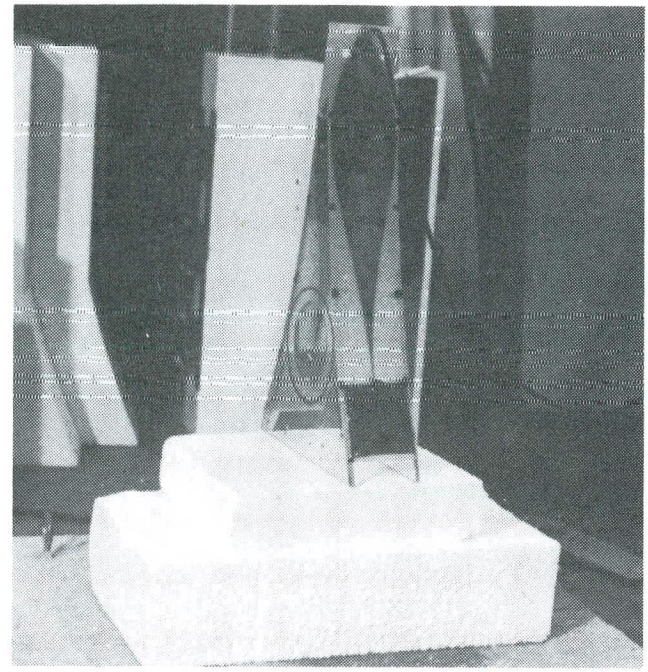

Figure 2. Short flare antenna.

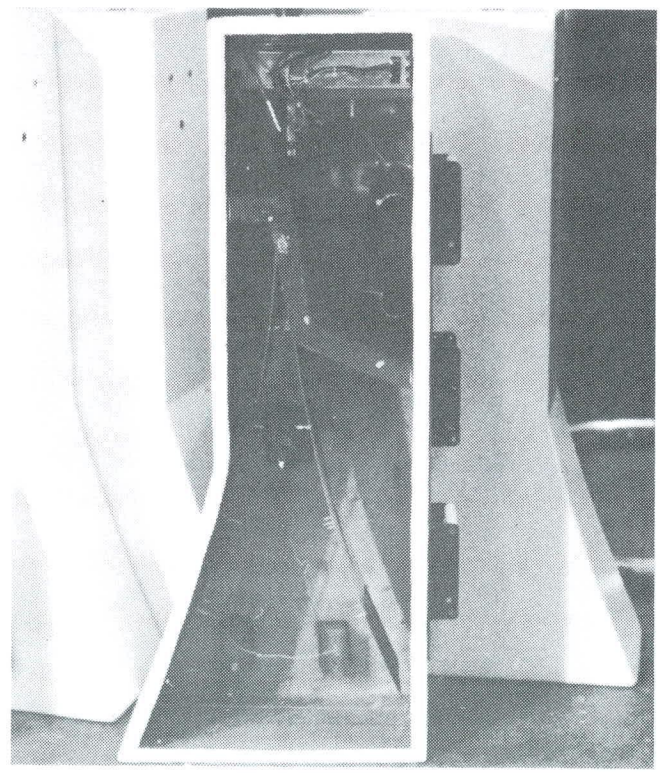

Figure 3. Short flare antenna/transducer unit.

antenna/transducer units were constructed. Figure 3 shows one of these units.

In order to suspend five of the aforementioned antenna/transducer units across the roadway in a manner acceptable for

field operations, a mounting system was devised. To make the mounting system as simple as possible, the two existing fiberglass booms on the RODAR™ vehicle were used. These two booms offered sufficient structural capacity for the proposed multiple radar system antenna units and the required mounting system. A transverse boom was designed and constructed using the same structural fiberglass material as in the two existing booms. The transverse boom was designed so that it could be quickly broken into two pieces for transportability. Additional structure necessary to support the five antenna units in a field operation was designed and fabricated also using the same structural fiberglass components. Figure 4 illustrates the modified boom arrangement used in this project.

The modifications to the conventional RODAR™ system electronic components required considerable design and fabrication effort and resulted in new assemblies, panels, and units. Figure 5 shows an overall view of these modified systems in the vehicle.

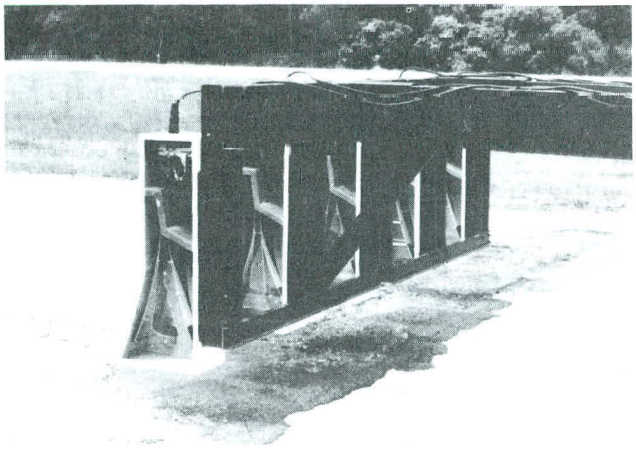

Figure 4. Modified antenna boom.

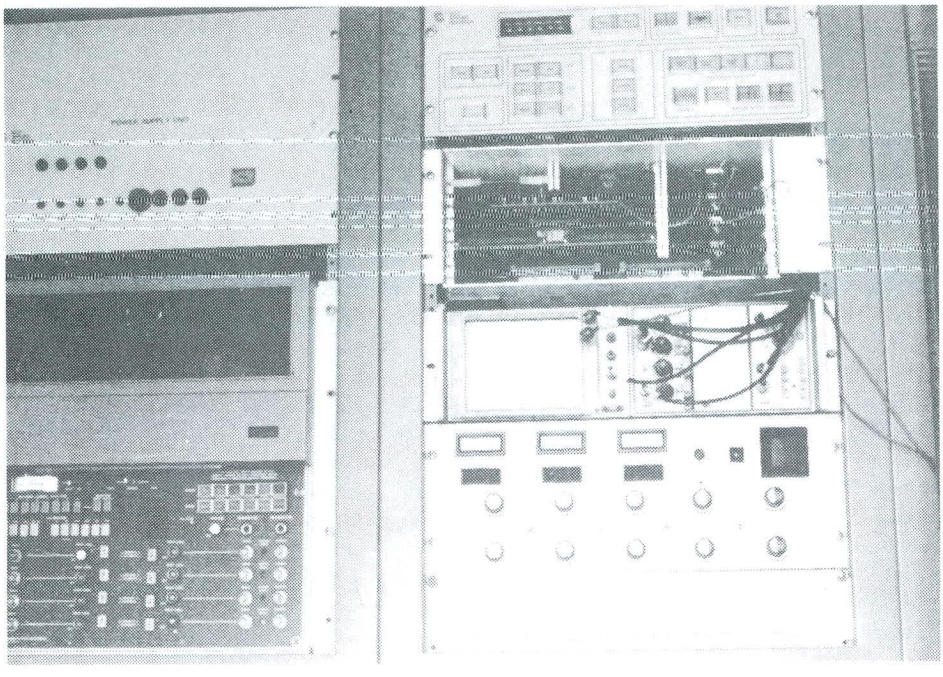

Figure 5. Overall view of enhanced radar subsystem hardware integrated in vehicle.

Thus, the enhanced radar subsystem integration effort led to a properly functioning multiantenna system that was compact, road-worthy, easily assembled and disassembled, capable of real-time processing and display of subsurface anomaly data, capable of recording all data, and capable of playing back the data through the system for later analysis.

The highly modified radar system—designed, fabricated, and integrated for this project—was tested under several different conditions. First, the antenna/transducer units were tested to determine if there was any interference between units caused by the transverse spacing of the antenna array. The short-flared antennas used in this subsystem were also tested for transmitted power and penetration capability, and the results were compared to those of the standard RODAR™ antennas. Second, the entire subsystem was operated in the field, on a number of occasions, to test the entire system function, including the recording of the multiplexed data. Third, after the field data collection, the system was further tested by playing the recorded data back through the system to demultiplex the data and allow for further experimentation with the data processing capability of the system.

Horn-type antennas, such as those used in the RODAR™ vehicle, are very effective at directing the radar pulse, but a small portion of the energy is emitted to the sides of the antenna forming a "field." Objects that come inside this "field" affect the received pulse by contributing clutter. Because of this phenomenon, the antenna/transducer units have to be separated

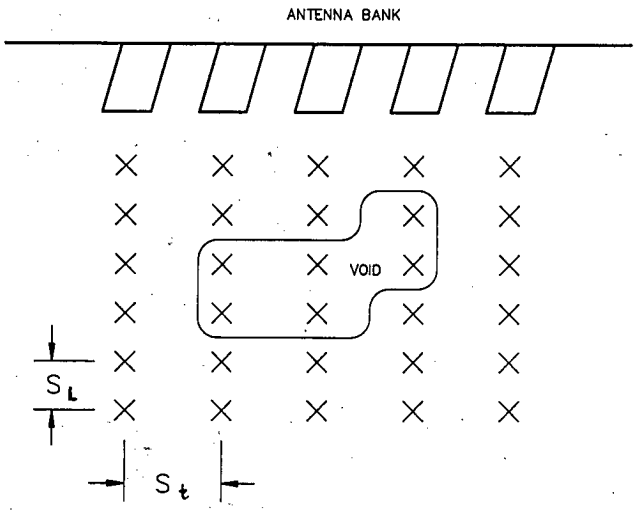

Figure 6. Void measurement sample points.

by a certain minimum distance. The alternate radar pulse firing scheme used in this system reduced the minimum spacing between antennas significantly, but it was still necessary to determine if the spacing of the antennas used for this project was sufficient to avoid this source of clutter. The test to determine the minimum antenna spacing involved varying the spacing between the actual antenna units and evaluating the effects on the signal returns. The results obtained indicated that the spacing between the antenna/transducer units (28 in.) in this subsystem was adequate.

The capability of the short-flare antennas used in this system was evaluated. The short-flare antennas performed in an acceptable manner, were compact and helped prove the feasibility of mounting the transducer hardware inside the antenna enclosure. The transmitted power and depth of penetration were tested and compared to the standard RODAR™ antenna. This testing was carried out as part of the laboratory testing phase of this project and is covered in Appendix F. The results of these tests indicated that the short-flare antennas had somewhat less transmitted power and correspondingly less penetration than the longer standard RODAR™ antennas. It would appear that the use of the standard RODAR™ antenna would enhance the system's capabilities. The implementation of the standard antennas into the system would be a relatively simple process involving only the physical substitution of antennas.

The dedicated RODAR™ vehicle, with the enhanced radar subsystem, was taken to several field sites for testing. The system was assembled, was placed on the roadway, and data were recorded. While on the roadway, experiments were performed to establish the radar data "windows" and "threshold", described in Appendix B, that make up the automatic data processing features of this system. The adjustments to establish the time "window" around the target proved to be relatively quick, simple, and accurate. The adjustments to vary voltage thresholds for target amplitude detection were also simple and relatively quick, but the positioning of the thresholds to measure the vertical dimension of very thin voids proved to be more difficult. This difficulty was not associated with the enhanced radar subsystem equipment, but was related to the effects on target amplitudes of moisture variations in the pavement materials. These relationships are discussed in more depth in Appendix C.

Because the signal return amplitudes from a similar target (subsurface distress) can vary from one roadway project to another, a method to "field" calibrate the enhanced radar subsystem's threshold position for automatic detection was required. A method was developed to establish the appropriate voltage threshold for amplitude-based void detection. To perform this calibration, because the target signal return amplitudes were dependent on material and moisture variables, some physical evidence at each job site was necessary. A few slabs, where void signatures were in evidence, were chosen and the horizontal extent of the void was determined using the water infiltration test (described later in this chapter.) The information from these few slabs could be used for calibration to set the voltage thresholds for the remainder of the test. However, this process would be relatively time consuming for a field operation because each of the five radar units had to have the thresholds set based on these calibration slabs. Since the enhanced radar subsystem is capable of recording the raw radar data for each channel and playing the data back through the data processing hardware (where the window and threshold are applied), the time required to set windows and thresholds could be employed in the office and not while on the roadway, for safety considerations.

Thus, although the feasibility of making the necessary adjustments in the data processing hardware for real-time detection of voids (or certain other subsurface distresses) on the job site was proven, most of the field data were recorded and evaluated back in the office. The enhanced radar subsystem data, the physical evidence from the calibration slabs, and the data from a standard RODAR™ vehicle were used for calibration and verification in the office.

VOID-SIZING ALGORITHM

As part of this project, an algorithm was developed to allow for the automated detection of a void and a computation of the volume of the void. In order to compute the volume of a void, a measure of the extent of the void must be made in three dimensions. The transverse and longitudinal extent of the void under the road surface as well as the thickness of the void must be measured and entered into the algorithm for computation of the volume of the void. Therefore, the basic approach of the void-sizing algorithm is to measure the parameters at regular points on the road surface as shown in Figure 6. The equation governing the size of the void is given as follows:

$$\text{Void Volume} = \sum_j \sum_i \left[t_{i,j} * S_T * S_L \right] = S_T * S_L * \left[\sum_j \sum_i t_{i,j} \right]$$

where S_T = spacing of samples in transverse direction; S_L = spacing of samples in longitudinal direction; and $t_{i,j}$ = void thickness at any point i,j.

The accuracy of the technique improves as S_T and S_L get smaller, and as $t_{i,j}$ is more precisely known. The sample spacing in the transverse direction, S_T, is determined by the number of antenna paths covering the width of the roadway. The sample spacing in the longitudinal direction, S_L, is determined by the speed of the vehicle and the firing rate of the radar. The algorithm for determining the thickness of the void is described in this section.

The void thickness measurement technique used and evaluated during this research project was based on work performed by Steinway, Echard, and Luke for NCHRP Project 10-14. According to the results published in that project's final report, *NCHRP Report 237,* an algorithm to accurately measure void thickness had been identified from time domain analysis of the radar return waveform. The approach adopted in that project for analyzing the radar void signature was to write a computer program which modeled the return signal. The researchers then analyzed the output from the computer and sought to identify characteristic features of the time domain waveform which reliably correlated with the thickness of the void being illuminated by the radar. The approach used during the current program was to expand the analysis presented in *NCHRP Report 237* in order to provide the measurement of void thickness at the sample points of the roadway. This expansion of the original work includes the addition of more terms in the equation for the radar return waveform simulated on the computer, thus resulting in a more complex model for the received signal. A derivation of the equation for the radar return waveform from a void is included in Appendix H of this report.

However, the major difference between the current research project and the one conducted in Project 10-14 is the choice of the form of the transmitted waveform ($X_{(t)}$). In that project the researchers used the monocycle waveform shown in Figure 7. Although this is the waveform that is generated in the transducer of the radar, it is not the form of the wave transmitted from the radar antenna. This is because of the antenna frequency characteristics which modulate the transducer-generated waveform during transmission. The antenna possesses the frequency response of a high-pass filter which serves to differentiate the transducer signal, thus producing the transmitted wave shape shown in Figure 8. Therefore, to provide a more accurate model of the radar received signal, the transmitted waveform shown in Figure 8 was used during this project. The template waveform was obtained directly from the radar system used during the laboratory tests by capturing the return from a metal plate. The digitized pulse was upsampled from 32 samples to 256 samples, resulting in a real-time separation between samples in the template of 3.906 picoseconds. This sample rate produces a minimum detectable void size of 0.023 in. The DC offset of the template waveform was removed, and the signal was inverted to compensate for the inversion of the received signal from the metal plate.

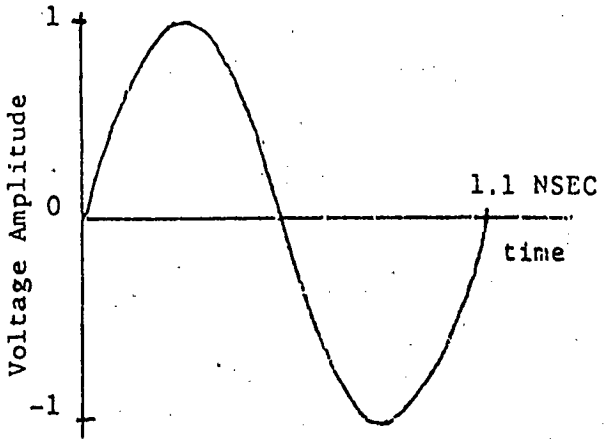

Figure 7. NCHRP Project 10-14 transmitted waveform template.

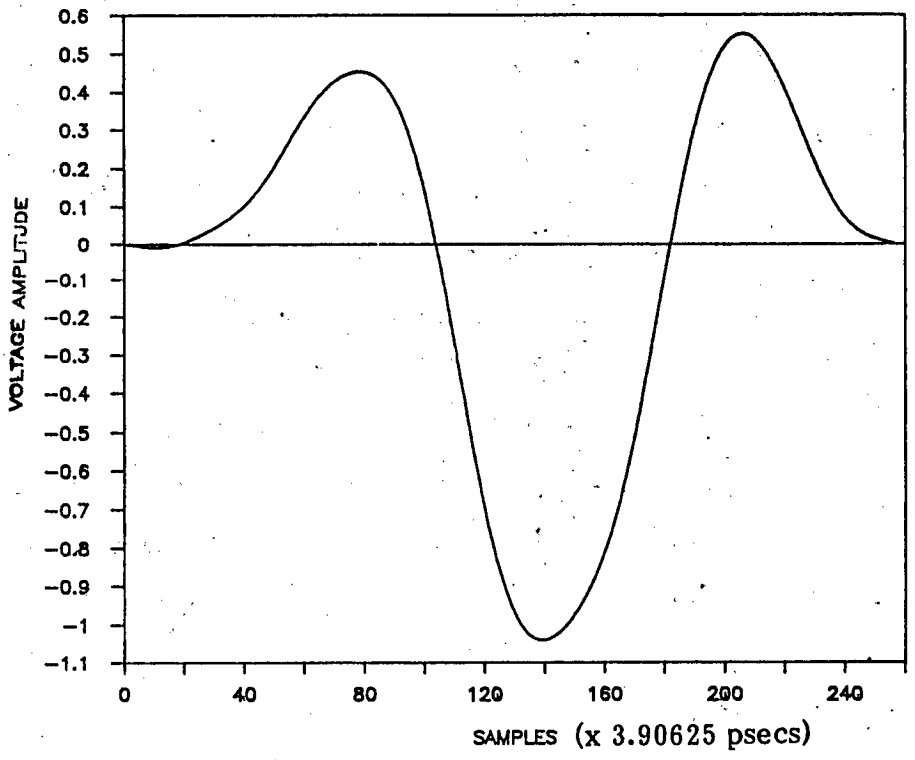

Figure 8. Current project's transmitted waveform.

The return signal modeling program, SIGMOD (refer to Appendix I for program listing) was provided input parameters that corresponded to the conditions of the laboratory and the Florida test slab used as part of the field testing phase. The program then produced a series of waveforms simulating a series of voids in the test pavement. If the void is assumed to contain air, the return from the top of the void corresponds to reflection from a higher dielectric to lower dielectric discontinuity. Therefore, the reflected waveform has the same polarity as the incident waveform. The return from the bottom of the void corresponds to a reflection from a lower dielectric to higher dielectric discontinuity which produces a 180-deg phase shift from the transmitted waveform. If the simulated void was smaller than a range bin of the transmitted pulse, the two returns from the top and bottom overlapped and could not be resolved independently. The research work performed in Project 10-14 proposed that a measure of void size for small voids could be obtained by measuring the magnitude of the return which corresponded to the interference between the returns from the top and bottom of the void. Specifically, the magnitude of the negative peak corresponding to the contribution from the return at the top of the void and the magnitude of the positive peak corresponding to the contribution from the return at the bottom of the void could be directly related to void size. Once the void size was large enough to separate the two reflections into two independently resolvable returns, then the measurement of the time between the negative peak of the first return and the positive peak of the second return could be directly related to the size of the void.

A range of void sizes was entered into the signal modeling program allowing a set of curves relating the magnitude of the peaks and the separation between the peaks versus void size to be created for the laboratory and test lane environments. The amplitude versus void size curves exhibited the same shape as that presented in the Project 10-14 *NCHRP Report 237*. The magnitudes of the negative and positive peaks begin to increase with void size because of constructive interference between the two returns until a critical void size is reached where the magnitudes begin to decrease as the two returns begin to separate. A least squares polynomial curve fit was used to calculate the coefficients of a cubic function which best fits the peak amplitude versus void size curves. The void-sizing algorithm will be required to choose a void size given the magnitude of the peak amplitude in the radar return. Therefore, only that portion of the curve where the amplitude is monotonically increasing with void size can be used because it produces a unique void depth for each given amplitude. A least squares polynomial curve fit was used to calculate the slope and offset of a line of best fit for the linear portion of the separation between peaks versus void size curves. In this region of the curve, the two returns have separated and become two independent returns.

Thus, one task in the research effort was to examine the effectiveness of these curves in predicting void sizes less than ½ in. The peak amplitude versus void size curves are used for small voids until a "switch point" void size is reached, at which point the separation between the peaks can be used as the void size determinant. A graphical representation of the algorithm is shown in Figure 9. This measurement of void thickness provides the value of $t_{i,j}$ for the proposed method of calculating void volume.

In order to test the algorithm, the void modeling program was used to construct peak amplitude versus void size and time separation peaks versus void size curves for the Florida test lane and several different laboratory configurations. The laboratory configurations simulated voids of various sizes in a wet silty clay base and a sand base. The accuracy of the curves produced by the computer model was tested by comparison against actual radar measurements of the test configurations. The results of the test configurations are covered in Appendix C of this report.

A substantial discrepancy was found between the actual radar return data and the peak amplitude values predicted by the theoretical signal modeling program. These prediction errors were much greater than those reported in Project 10-14. During the analysis of the laboratory configuration with the wet silty clay base material, errors as high as 112 percent were found to exist between the predicted values from the theoretical curves and the actual radar return data. There exist several factors that could cause these measured discrepancies.

One possible cause is clutter and noise contaminants that enter the radar return waveform. The effects of system noise and clutter on the radar return waveform are relatively minor. However, because the amplitudes associated with a void must be accurately measured for accurate void sizing, even the small effects from system noise and clutter can have an effect on these amplitudes. Therefore, to implement an algorithm that uses the amplitude of the return to accurately measure void size, the system noise and clutter must be reduced to a negligible level in comparison to the magnitude of the return from the void. During the laboratory testing phase of this project an antenna configuration was tested that reduced the system clutter significantly.

Another possible cause for the measurement error is the amount of pulse stretching which occurs in the pavement. The phase velocity of the radar wave through the pavement is a function of the conductivity of the concrete and the frequency of the transmitted wave. The transmitted pulse is composed of a band of frequencies that peak at approximately 800 MHz. Therefore, because the phase velocity is different for the different frequencies in the spectrum of the transmitted pulse, the pulse spreads or disperses as it travels through the pavement. This dispersion causes the pulse to distort, which changes the magnitudes of the peaks of the waveform.

These discrepancies, which were not included in the model, could contribute to the measurement errors. The signal modeling program produced the simulated return waveform by simply scaling and time-shifting the original transmitted wave shape. These factors, however, could have served to produce a return waveform whose shape was different from that of the transmitted waveform. Therefore, it is believed that a more complex model is needed to simulate the frequency dependent factors that serve to distort the waveform as it travels through the pavement. Initially, it was believed that a more complex model was not necessary because acceptable results had been documented in Project 10-14. However, those results could not be duplicated by the research staff of this project.

There are additional problems involved with implementing an algorithm, which uses peak amplitudes, into an operational highway system for void measurement. The primary problem is the dependence of the peak amplitude on the dielectric properties of the material into which the radar signal is propagating. For example, Figure 10 shows the dependence of the positive peak amplitude versus void size curves on the dielectric of the base material. The plots in the figure are curves generated from the signal modeling program produced by changing only the

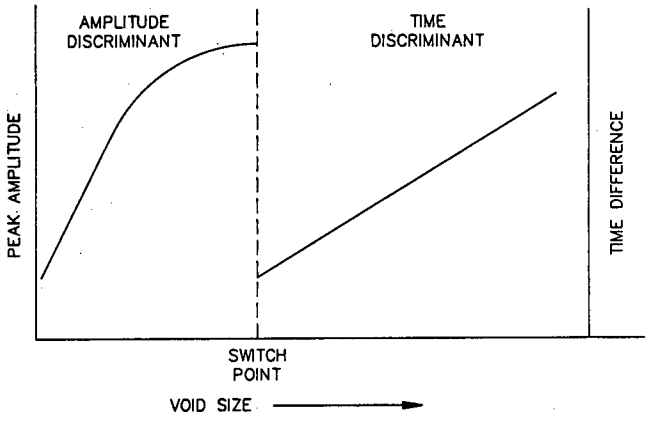

Figure 9. Void sizing algorithm.

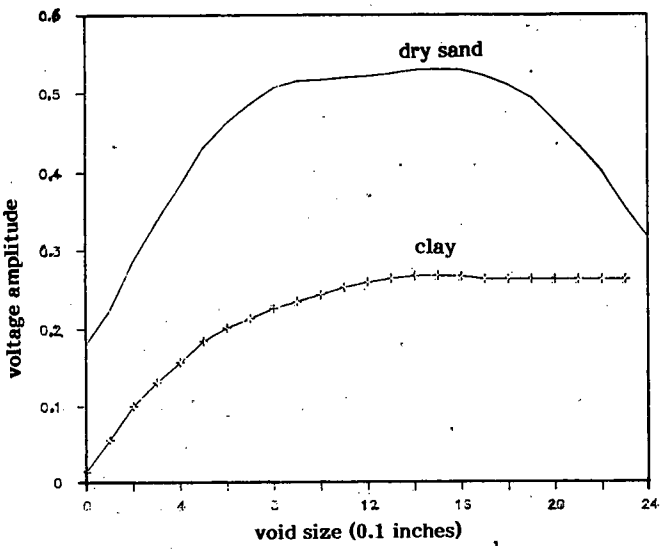

Figure 10. Positive peak versus void size for wet silty clay and dry sand base materials.

dielectric constant of the base from wet silty clay ($\epsilon_r = 37$) to dry sand ($\epsilon_r = 4$). Therefore, given the amplitude of a peak return from the radar signal, the algorithm must know which curve is applicable to determine the size of the void. In Project 10-14 it was suggested that a calibration procedure could be performed before a void-sizing run, which could determine the proper amplitude curve. However, the base material may not be homogeneous over the extent of the run, therefore, the amplitude curve that was valid at the point where the calibration was taken may no longer be correct at a point some distance down the road. This is particularly relevant because most voids tend to form around the joints in the pavement where water has infiltrated. This moisture, which collects near the joints, is not necessarily present under the middle of the slabs; therefore, the dielectric constant of the base material at the joints can be much higher than in the middle of the slab, making calibration difficult. Although this variation in moisture content would result in inaccuracies in determining the vertical dimension of the void, the horizontal extent of the void could still be determined with reasonable accuracy.

VIDEO DATA ACQUISITION SUBSYSTEM DESIGN

The video recording subsystem designs were based on several goals:

1. The system should accommodate the entire width of a roadway lane and the entire length of the required survey area.
2. The system should have the capability of resolving very small targets (i.e. $\frac{1}{16}$-in. cracks) if required.
3. Footage information should accompany the video data for the accurate location of targets.
4. The system should be flexible so that the system can be changed to meet specific survey requirements (i.e., survey speed, resolution, continuous survey vs. sample scheme).
5. The analysis software portion of the system should be capable of enhancing the video image for maximum resolution and be capable of "recognizing" surface defects and assessing them.
6. The data analysis should be done automatically, after the initial setup.
7. The system should utilize existing technology wherever possible to enhance reliability and reduce costs.

To achieve these goals, it was necessary to consider some basic video concepts and how these concepts apply to detecting pavement surface defects. The concepts include video resolution, video contrast, and data location referencing. On the basis of these considerations and the previously mentioned goals, it was decided that two separate designs would be generated: one design that would record the surface video data for off-line analysis and could be implemented with off-the-shelf components at a reasonable cost; and a second design that would involve real-time processing of the surface video data and would be considerably more expensive.

The off-line video analysis design was implemented by obtaining components and integrating them into a RODAR™ vehicle. This implementation of the off-line video analysis design was necessary to test the design concept and to collect data for the development of the surface video analysis algorithms and software. The following sections discuss some basic video considerations, the integration of video recording components into a vehicle, and the designs for an off-line and a real-time surface video analysis system.

Basic Considerations—Resolution

A video camera produces an image by varying the intensity of light and color at each point (pixel) of a matrix. The number of pixels in this matrix determines the resolution of the image. Commercial-quality, high-resolution video cameras vary in the density of the matrix from 380 by 380 pixels to 2048 by 2048 pixels or higher. A standard format is usually 512 by 512 pixels or 1024 by 1024 pixels.

Although the resolution of the video camera is a very important performance criterion, the ability to resolve a small target on the pavement surface is a complex function of camera

resolution, amount of pavement surface in the image matrix, and the contrast between the surface targets and the surface background intensity.

The effect of camera resolution (number of pixels in the image matrix) on the ability to resolve small pavement surface targets can easily be illustrated with an example. Assume a camera with a 512 by 512 pixel matrix is used to record the image of the entire width of a 12-ft wide lane. Then, each pixel would represent 12 ft/512 pixels = 0.28 in. of surface.

On the basis of this example, a crack ¼-in. wide would represent about one pixel width. To be able to resolve very small targets, several possibilities exist: use a higher resolution camera, use several cameras in parallel so that less pavement surface is covered by each camera, or use video data enhancement techniques to detect targets less than one pixel wide. Figure 11 exhibits some of the relationships between width of camera coverage, pixel width, and video enhancement effects for crack detection in a 512 by 512 pixel image format.

The two surface video analysis system designs developed for this project (a low-cost, off-line system and a real-time system) call for multiple cameras and the use of video data enhancement techniques. Multiple cameras are a good choice because extremely high resolution cameras are very expensive and usually not suitable for field use. The disadvantages of using multiple cameras are that each camera requires a separate recorder, and the analysis software is slightly more complicated because the data from the parallel operation of each of the cameras must be correlated.

Video cameras generally operate at a rate of 30 "frames" per second. With a video camera used for pavement surface imaging at highway speeds, simple mathematics indicates that considerable movement can occur during each frame. This movement results in the smearing of the data and a substantial loss of resolution. Because the detection of targets as small as 1/16 in. is a goal, a very small loss of resolution by data smearing can result in the inability to detect the desired targets. A number of cameras exist that have a shuttering system. These cameras use a standard video format but employ a very fast shutter to "stop" the action. This type of camera has been used for several years in applications with data rate requirements similar to those of pavement surface distress imaging at highway speeds.

To record the video data for off-line analysis, a video cassette recorder (VCR) is considered the best choice because of its ease of operation, ruggedness, cost, and data storage capacity. The only drawback to the VCR method of data storage is resolution. VCR systems have 500 lines of resolution or less, as compared to available video cameras which have 1000 to 2000 lines of resolution.

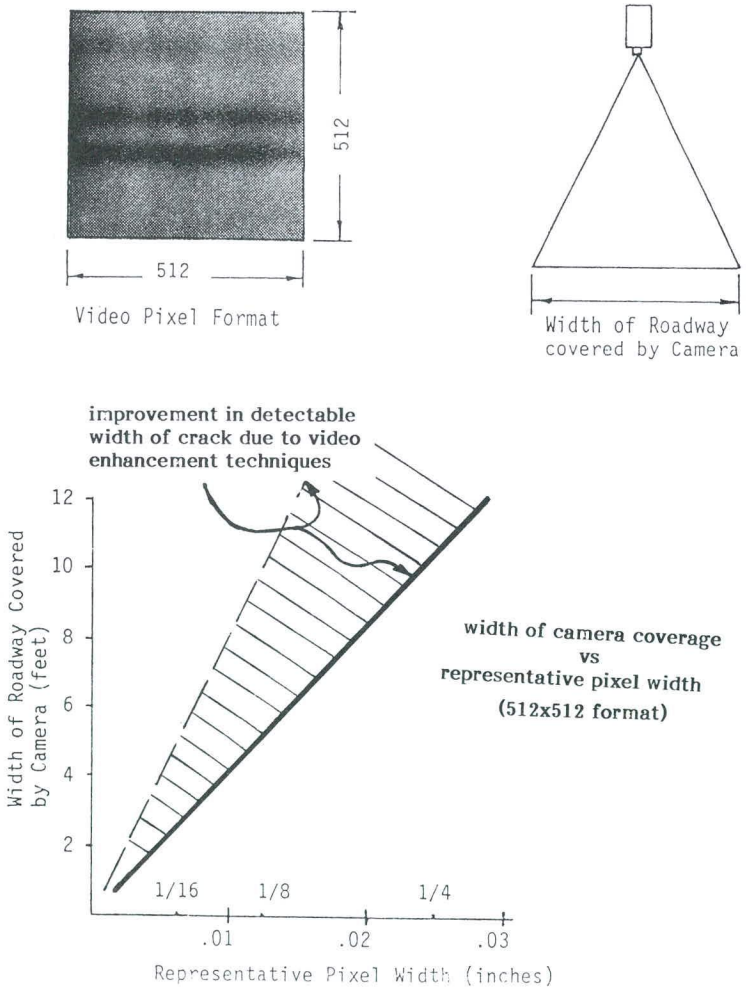

Figure 11. Effects of video image format, roadway width coverage, and computerized video enhancement on target resolution.

The best VCR system available for this application is a broadcast quality unit, with a ½-in. format. These systems can have 450 lines (pixels) of resolution and a signal-to-noise ratio of 48 dB. The systems are rugged enough for field use and capable of reasonably high resolution data storage.

Because of the unavailability of a very high resolution VCR, the video image recording system is the deciding factor in the choice of other off-line system components, such as the camera and image analysis software. It does no good to have a camera capable of reproducing a 1024 by 1024 pixel matrix, or image analysis software designed to handle such a matrix, when the video recording system is only capable of reproducing a 450 by 450 pixel matrix.

Another factor that affects video resolution is camera vibration during data collection. If the camera is mounted rigidly to a support system, the camera will experience some vibration during a video data collection survey. During the field testing phase of this project, acceptable video data were taken at 5 to 8 mph using a mounting system rigidly attached to the vehicle. It is feasible that somewhat higher speeds than this may be possible with a rigid mounting system, but with higher survey speeds (25+ mph) and roads of "average" roughness, good camera stability is a must. A commercially available camera stabilizing system should be included in this video recording subsystem.

Surface Video Contrast Considerations

Contrast is the difference between the color and the intensity of the target image as compared to the color and intensity of the background. Video image contrast, as it pertains to this subsystem, is a function of the camera, recorder, lighting, and the actual difference in color between the target and the background. The contrast capabilities of any video hardware component are generally well known and the information is readily available before acquisition of the part. The contrast capabilities of the video hardware are usually expressed in terms of a signal-to-noise ratio. A signal-to-noise ratio of 45 dB or greater is highly desirable.

The actual contrast in color, between background and target, can pose a severe problem to any surface video analysis system. Some aggregates and cement materials are dark in color and produce a surface that is relatively dark. Also, the area of the road surface between the wheelpaths is usually dark because of oil stain. These factors, which serve to darken the surface, make the resolution of small targets (distressed areas) difficult. A procedure was developed, and is discussed in Appendix D, to determine what size targets are resolvable under existing contrast conditions. Also discussed in Appendix D are efforts that were undertaken to enhance the contrast between the target and background of recorded surface video data using computer processing methods.

The use of lighting to increase video contrasts can be a useful approach. Properly placed and directed lighting can brighten the pavement surface and create shadows and darken certain targets, thus increasing contrast. Lighting can be of value during daytime operation to reduce the effects of shadows on the roadway from overhanging objects or from clouds. Lighting used for surface video enhancement should offer a level of illumination appoximating the sun for a particular target area. Less than this level of illumination offers little improvement during daylight operations and offers a less than optimum video contrast during nighttime operations. To generate this level of continuous lighting, a considerable power generation capability must be available. If a shuttered camera is used in the system, a strobe lighting system can be employed requiring much less power. A strobe lighting system must be triggered by the shuttered camera to avoid timing problems.

Location Considerations

The ability to accurately determine the location of all detected pavement distresses is vital to the usefulness of the video image analysis subsystem. The location of distresses is valuable for correlation of data with other sensors and also in recognition of certain types of features.

The location information for the video system implemented for this project was provided by a fifth wheel with an optical encoder. The RODAR™ system hardware counts the number of passes from the encoder and calculates footage and speed based on this pulse count. These pulses can be recorded on the audio channel of the system VCR and used to determine the relative location of each video frame during off-line processing.

At highway speeds the pulses from the fifth wheel enter the recorder at a frequency that can result in recording problems due to bandwidth limitations of the audio channel (Appendix E). To solve this problem an intermediate step is required. This intermediate step is a counter that receives the high rate of pulses from the fifth wheel and generates its own pulses at predetermined distance increments. The audio channel is able to handle the reduced data rate from the counter output, because pulses are generated by the counter much less frequently than by the fifth wheel.

The fifth wheel generates pulses at a rate of 25 per foot. The RODAR™ system "paint mark controller" circuit counts these pulses and generates its own pulse at an interval fully controlled by the operator. This pulse currently controls the application of a reference mark on the pavement surface by the paint system, but recording this pulse on the audio channel of the video recording system VCR for location reference is a simple matter.

There are several advantages to placing a single pulse on the video subsystem VCR tape for reference. Because this pulse can be set at any distance, it can be used to inform the analysis software where a surface video frame begins and ends. The frequency of pulses recorded on the VCR audio channel is greatly reduced, solving bandwidth-related recording problems. Thus, the video image analysis software has significantly fewer incoming pulses with which to contend, thereby reducing the work load on the system.

Surface Video Analysis System Implementation

A RODAR™ vehicle was modified to implement a surface video recording system. This system was used to demonstrate the design concept and to gather surface video data to aid in the design and development of the computer-based data analysis algorithms and software. It was also used for experimentation in the areas of video contrast, lighting, camera angle, and surface defect resolution. The video recording subsystem integrated into the RODAR™ vehicle consisted of: video camera, camera mounting framework, video recorder, fifth wheel, and wheel pulse counting system for generation of distance reference pulse to be recorded on the VCR audio channel.

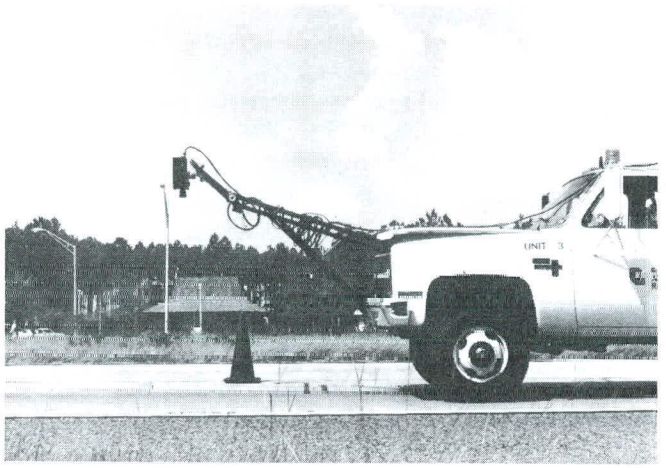

Figure 12. Camera mounting framework, camera at 6-ft height.

Two types of cameras were used for video data collection: a shuttered, high resolution (512 by 512 pixel matrix) unit and a more conventional video camera (380 by 380 pixels) with higher video contrast capability (signal-to-noise ratio). The cameras were mounted on a specially designed framework, without antivibration mounting systems.

The camera mounting framework was attached to the front of the RODAR™ vehicle (Figure 12). The framework was designed so that multiple cameras could be mounted or a single camera could be mounted at any transverse position. The camera mounting framework was also capable of simple camera height adjustment. The relatively simple framework allowed a greater degree of flexibility and ease in camera mounting both transversely and vertically. This flexibility allows for accurate camera placement to obtain the required surface coverage and required resolution.

A commercial-quality video cassette recorder capable of recording and accurately reproducing a 380 by 380 pixel matrix was used in the subsystem. A high-resolution video monitor was also employed for the operator's use in camera placement, aiming, focus, and f-stop adjustment. For location reference, the standard fifth wheel from the RODAR™ system was used. An optical encoder on the fifth wheel generates 25 pulses per foot of movement and these pulses are counted and computed into footage and speed data. These data are displayed on a monitor in the vehicle for reference via a title generator. The data are also recorded directly onto the video tape.

Off-Line Surface Video Analysis System Components

On the basis of the experience gained from the field operation of the video recording system and from the implementation of the laboratory video data analysis system, it is recommended that the video recording system include a camera with the following features: 450 by 450 pixel matrix resolution (minimum), shuttered, 45-dB signal-to-noise ratio (minimum). The number of cameras are dependent on the resolution required. The cameras should be mounted on the front of the vehicle with a vertical orientation, and the camera mounting system should be antivibration in nature.

Natural sunlight can be used for lighting, but the orientation of the sun and survey direction must be considered to avoid vehicle shadows in the camera field of view. Artificial lighting, if required for night operations or heavily shaded areas, should be mounted on the front of the survey vehicle. For improved contrast, the lights should be directed at an angle toward the field of view to create shadows internal to the surface features of interest. To compensate for shadows on the roadway or for night operations, lighting should be sufficient to illuminate the camera field of view to produce approximately the intensity of sunlight. A strobe lighting system, triggered by the shuttered camera, would require much less power than continuous lighting, and is thus preferable.

The video image recorders should be capable of a minimum of 450 lines of resolution with a signal-to-noise ratio of 45 dB (minimum). A video monitor with resolution comparable to other system components is required to aid the operator in field operations.

A fifth wheel optical encoder is included for location measurements. An intermediate circuit is included to count the fifth wheel optical encoder pulses and replace them with a single pulse at a predetermined distance interval equal to the required video frame size. The location pulses are recorded on the audio channel of the video tape recorder.

A further discussion of the design of the off-line surface video analysis system is contained in Appendix E.

REAL TIME, SURFACE VIDEO ANALYSIS SYSTEM DESIGN

A real time, surface video analysis system that will analyze surface video data at highway speeds requires much more sophisticated hardware and streamlined software than the previously discussed off-line system. This system will require a faster video sensor and an on-board computer system with high speed, dedicated processors to handle the high data rates. A discussion of this type of system is included in Appendix E.

SURFACE VIDEO ANALYSIS SOFTWARE DEVELOPMENT

The primary software components of the automated pavement surface distress analysis system can be divided into two main bodies of code: the Main Administrative Program and the Video Frame Analyzer.

The task of the administrative program is to control the hardware functions necessary to capture a video image, execute the video frame analyzer subroutine, and record a running, cumulative count of the surface distress identified by the frame analyzer during the pavement analysis. The Video Frame Analyzer is required to examine the video image made available to it by the main program for the surface distresses of interest and report the number found in the frame to the Main Administrative Program for storage.

Certainly, the Video Frame Analyzer, which forms the heart of the automated system, poses the more difficult programming problem. Therefore, the main emphasis of the software portion of this research effort was to develop a working prototype video frame analyzer and identify the problems associated with enhancing and extracting surface distress features from the video data.

To conduct this portion of the research effort, a board-level video digitizer and display module that is "plug-compatible" with the IBM Personal Computer was purchased by Gulf Applied Research. This hardware card captures a standard RS-170 or RS-330 video signal at a rate of 30 frames per second, stores the image in an on-board 512 by 512 by 4 or 8 bit frame memory, and simultaneously displays the stored image on an external monitor. In addition, an advanced, menu-driven software package containing a variety of image acquisition and processing functions developed for use on an IBM PC was acquired for this project. The software menu was necessary to provide some of the common image processing functions used to enhance the raw video data. Extensive experimentation with individual and combinations of these image processing functions led to the development of a very effective feature enhancement method to help detect pavement surface defects. The results of this experimentation are covered in detail in Appendix D.

The video analysis software developed for this project consists of two major components: a feature enhancement process and a feature extractor. The feature enhancement process serves to increase the contrast between the desired features and the surrounding background. Therefore, this process increases the computer's ability to detect small, faint features in the video frame. In addition, it makes it easier for the feature extractor to determine which pixels belong to the feature and which belong to the background.

The feature extractor must be capable of taking the enhanced video data and locating and cataloging the surface distresses of interest. The extractor begins by reducing the video data to a binary image containing only feature pixels and background pixels. Once the silhouette of the feature has been created in the video image, the extractor must be able to identify and catalog the feature shape.

Several feature enhancement schemes were implemented and tested for improving the contrast in the raw video data. A detailed description of the enhancement schemes and the results of this application on three sample test images are provided in Appendix D of this report. A block diagram of the most successful image enhancement configuration is shown in Figure 13. This configuration consists of a Sobel Operator, Look-Up Table Inverter, Median Filter, and Low-Pass Filter. These special-purpose image processing functions were provided by the purchased image processing software menu.

The Sobel Operator, SOBELOP, is an image filter which enhances fine, continuous edges in the video data. An edge enhancement filter is an obvious choice for enhancing the raw image, since cracks in the pavement appear as edges in the video data. The Sobel Operator Subroutine assigns high pixel intensities (white) to the edges in the image. However, the feature extractor was designed to search for dark features on a white background; therefore, it was necessary to invert the intensities of the pixels in the image with a Look-Up Table Inverter, INVERT LUT.

An undesirable side effect of the Sobel Operator is the creation of a large amount of "speckle" noise in the image. This type of noise is characterized by isolated areas of dark pixels that form on the image. Generally, these patches are caused by discolorations due to variations in lighting of the raw image, which are enhanced by the edge enhancer. The most effective means of reducing the "speckle" noise is by smoothing the image with median and Gaussian low-pass filters. In addition to reducing the "speckle" noise in the background of the image, the smoothing filters serve to make the enhanced edges more continuous, which aids the feature extractor in following the outline of the feature's silhouette.

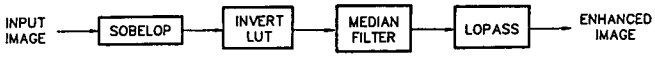

Figure 13. Image enhancement process block diagram.

Once the image has been enhanced to improve the contrast between the desired features and the image background, the video data are passed to the feature extractor for identification of the surface distresses. The feature extraction algorithm, CRAKFIND, which was developed during this research project, is described in detail in Appendix D of this report. The CRAKFIND algorithm was implemented in the Microsoft FORTRAN programming language and a listing of the source code can be found in Appendix J. This feature extraction algorithm was designed to locate, identify, and quantify cracks as well as popouts and spalls in the concrete pavement.

The program begins by separating the cracks from the pavement background by reducing the video data to a binary (black/white) image consisting of black cracks and white background. This is accomplished by determining an intensity threshold which lies between the dark surface features and the lighter pavement background. The value of the intensity threshold is adaptive in order to allow for variations in the lighting of different images. Once the feature pixels of the image have been identified, the algorithm must be able to recognize and classify the silhouette of the surface distress.

Classification of surface distresses is accomplished by providing the feature extractor with a set of "frame analysis parameters" that describe the shape of the desired features. For example, the frame analysis parameters define a "typical longitudinal crack as a long slender silhouette which has a predominant vertical orientation in the frame. Similarly, a long slender silhouette running horizontally in the frame is considered to be a transverse crack. The parameters define a spall as a wide section of a silhouette which otherwise appears to be a crack. A popout is defined as a relatively large clustering of black pixels in the frame whose dimensions are greater than the width of a crack. By programming the computer with this set of rules that describe the geometries of common surface distresses, the algorithm is capable of discerning the features from the "speckle" noise in the background of the enhanced image.

The ability of the algorithm to detect and classify a crack was found to be largely dependent on actual contrast conditions and resolution of the video acquisition system. However, the frame analyzer was able to identify cracks as small as $\frac{1}{16}$ in. in 4 ft by 4 ft video data frames taken on a continuously reinforced pavement (I-95 near Brunswick, Georgia). The surface of this roadway was dark in color and had very thin cracks ($\frac{1}{32}$–$\frac{3}{16}$ in.). This combination offered a good example of poor natural contrast between targets and background and served as excellent data to determine the limits of the system capabilities. (Refer to Appendixes D and G for more detail.)

A valuable feature of the surface video analysis algorithms and software is the ability to use the system with any type sensor that results in a digital format output. This software can be used with other pavement surface sensor systems, such as lasers and charged couple devices. The surface video analysis algorithm

development resulted in a system that can detect cracking, crack width, crack length, crack location, crack orientation, spalling, spalled area, spalling associated with cracks and joints, localized distress (popouts), asphalt patches, and asphalt patch area.

These detectable items were verified with actual field data, and were also compared with the distress identification definitions found in *NCHRP Report 277.* The results of these comparisons are given in Tables 1, 2, and 3.

Some of the distresses in *NCHRP Report 277* are associated with pavement deformations (blow-ups, depressions, faulting), which may have few surface manifestations for a video system to detect. Also, some of these distresses are not directly on the pavement surface (pumping, shoulder joint separation). The tables point out that a significant number of the major structural distresses of concrete pavements can be detected by the surface video analysis system.

LABORATORY TESTING

For the laboratory investigation of detection of small voids, concrete slabs 4 ft by 4 ft were constructed to simulate PCC pavement. These 4 ft by 4 ft pavement models were constructed in various thicknesses, with and without reinforcing steel, and with the ability to simulate delaminations at the steel interface. Figures 14, 15, and 16 are drawings of the three typical types of test slabs used in this experiment. Concrete slabs 4 ft by 4 ft were satisfactory in this case, because the measurements were performed near the centers of these slabs. Since the 3-dB beamwidth of the RODAR™ antenna encompasses an area approximately 12 in. in diameter, edge effects could be neglected, as could possible interference from any eye bolts embedded in the corners of the concrete for hoisting purposes. In brief, the RODAR™ system surveys such a small area at any one time, that whether this area is part of a 4 ft by 4 ft slab or part of an entire pavement system, the measurement results will remain valid.

Voids were modeled between pairs of test slabs, and different types of base materials were used to determine the effects on void return. The effects of water-filled voids and delaminations were investigated during this phase. Some tests with different radar antenna configurations were performed for comparison purposes. Also, the effect on the radar return antenna orientations relative to the reinforcing steel orientation was studied.

A special laboratory test was designed to model the PCC test slab at the Materials Laboratory of the Florida Department of Transportation. This test slab is a full scale roadway with known voids formed at the time of construction. Data were taken on the Florida DOT test slab as part of the field testing phase. A laboratory model of the "known" field data was constructed to more accurately assess the system. Certain surface defects were also modeled in the laboratory to aid in the development of the video system. A more detailed discussion of the laboratory testing phase of this project is given in Appendix F.

FIELD TESTING

Several sites (refer to Appendix G) were chosen to conduct field tests of the radar and video systems. The five-antenna, modified RODAR system was used on most test sites to verify operational performance. A standard RODAR™ vehicle was used on each test site for comparison with the five-channel system and in the determination of the limits of ground-penetrating radar in determining various subsurface distresses. The surface video system was also employed on several of these test

Table 1. Pavement distress detection capabilities of computer-based surface video analysis system—jointed plain concrete pavements.

Distress (NCHRP Report 277)	Detection	Determine Severity Levels	Measurement
Blow-up	no	-	-
Corner Break	yes	yes	yes
Cracking from Improper Jt. Construction	(1)	yes	yes
Depression	no	-	-
"D"- Cracking	(2)	-	-
Faulting, Transverse	no	-	-
Joint Seal Damage	no	-	-
Shoulder Joint Separation	no	-	-
Longitudinal Cracks	yes	yes	yes
Faulting, Longitudinal	no	-	-
Patch Deterioration	(3)	yes	yes
Pumping	no	-	-
Reactive Aggregate Distress	(2)	-	-
Scaling, Map Cracking	no	-	-
Spalling	yes	yes	yes
Studded Tire Damage	no	-	-
Swell	no	-	-
Transverse and Diagonal Cracking	yes	yes	yes

(1) Distress can be detected but distinction as to cause is difficult.

(2) Distress can be detected in higher severity levels only and as evidenced by spalling, wider cracking patterns or asphalt patches.

(3) The deterioration of the patch can be detected, severity determined and measurements made, but some difficulty exists in discriminating between large slab replacements and original slabs.

Table 2. Pavement distress detection capabilities of computer-based surface video analysis system—jointed reinforced concrete pavements.

Distress (NCHRP Report 277)	Detection	Determine Severity Level	Measurement
Blow-up	no	-	-
Corner Break	yes	yes	yes
Cracking from Improper Jt. Construction	(1)	yes	yes
Depression	no	-	-
"D"- Cracking	(2)	-	-
Faulting, Transverse	no	-	-
Joint Seal Damage	no	-	-
Shoulder Joint Separation	no	-	-
Longitudinal Cracks	yes	yes	yes
Faulting, Longitudinal	no	-	-
Patch Deterioration	(3)	yes	yes
Patch Adjacent Slab Deterioration	(3)	yes	yes
Pumping	no	-	-
Reactive Aggregate Distress	(2)	-	-
Scaling, Map Cracking	no	-	-
Spalling	yes	yes	yes
Studded Tire Damage	no	-	-
Swell	no	-	-
Transverse and Diagonal Cracking	yes	yes	yes

(1) Distress can be detected but distinction as to cause is difficult.

(2) Distress can be detected in higher severity levels only and as evidenced by spalling, wider cracking patterns or asphalt patches.

(3) The deterioration of the patch can be detected, severity determined and measurements made, but some difficulty exists in discriminating between large slab replacements and original slabs.

Table 3. Pavement distress detection capabilities of computer-based surface video analysis system—continuously reinforced concrete pavements.

Distress (NCHRP Report 277)	Detection	Determine Severity Level	Measurement
Blow-up	no	-	-
Construction Joint Deterioration	(1)	yes	yes
Depression	no	-	-
"D"- Cracking	(2)	-	-
Edge Punchout	yes	yes	yes
Shoulder Joint Separation	no	-	-
Localized Distress	(1)	yes	yes
Longitudinal Cracks	yes	yes	yes
Faulting, Longitudinal	no	-	-
Patch Deterioration	(3)	yes	yes
Patch Adjacent Slab Deterioration	(1)	yes	yes
Pumping	no	-	-
Reactive Aggregate Distress	(2)	-	-
Scaling, Map Cracking	no	-	-
Spalling	yes	yes	yes
Studded Tire Damage	no	-	-
Swell	no	-	-
Transverse and Diagonal Cracking	yes	yes	yes

(1) Distress can be detected but distinction as to cause is difficult.

(2) Distress can be detected in higher severity levels only as evidenced by spalling, wider cracking patterns or asphalt patches.

(3) The deterioration of the patch can be detected, severity determined and measurements made, but some difficulty exists in discriminating between large slab replacements and original slabs.

sites. Verification of the subsurface distresses was carried out with a variety of methods: deflection tests (Falling Weight Deflectometer, Dynaflect, Benklemen Beam), grouting, slab removal, and a special "water infiltration" test. The water infiltration test was widely used during the field testing program.

The water-infiltration test involves the drilling of a series of 1-in. diameter holes at 12-in. to 18-in. intervals longitudinally along the roadway, where a void or other anomaly has been indicated by the radar. These holes are placed in a manner that will determine the actual length of the anomaly (longitudinal) for comparison with the anomaly length indicated by radar. The holes are drilled with a carbide tipped rotary hammer and no water is used during drilling. The drill bit is fluted to remove dislodged material. These flutes also serve to "bring up" some of the base material after the concrete has been penetrated. Because water is used in the drilling operation, this small "sample" of the base material can give an indication of the existence of excess moisture and the general condition of the base material at the concrete-base interface. The sample can also give general information such as washing out of fines by pumping, excess moisture, leaching of stabilization materials, and so forth. After the holes have been drilled and the base "samples" inspected, the holes themselves are inspected to determine if free water is present at the bottom of the slab. After these functions have been carried out, water is poured into each hole and the general rate of water descent (infiltration) down the hole is noted. Obviously, this infiltration test is not precise, but the following general observations can be made: (1) a sound pavement/base interface will result in no short-term infiltration of water (within

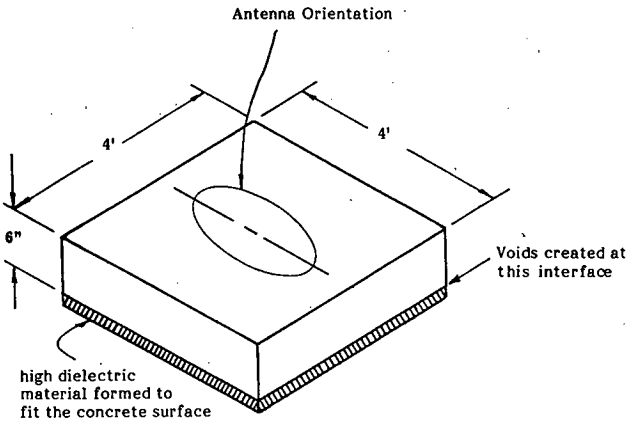

Figure 14. Typical test slab, nonreinforced.

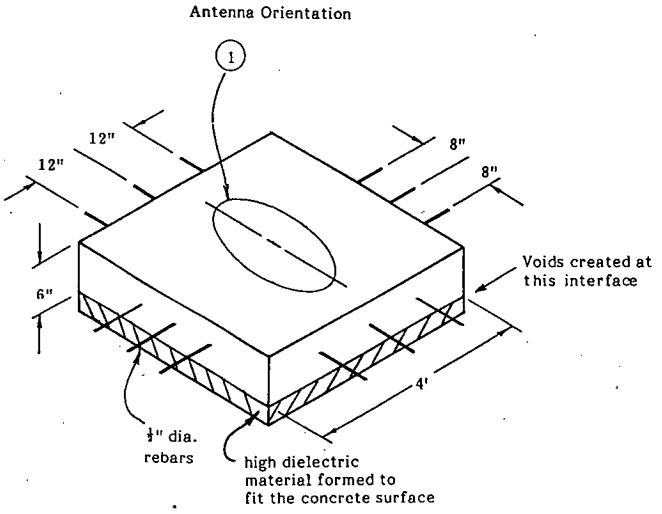

Figure 15. Typical test slab, reinforced.

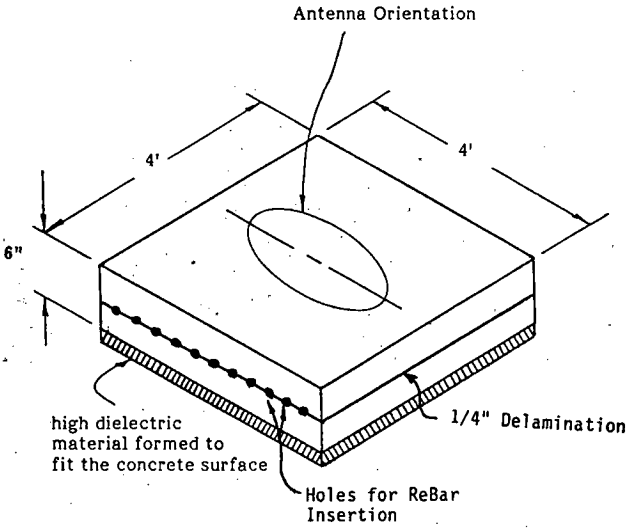

Figure 16. Typical test slab, delaminations.

30 sec or so), (2) a loose deteriorated base material or very small voids will result in a slow-to-moderate infiltration rate, and (3) an air void beneath the drilled hole will make filling the hole with water difficult because water runs down the hole into the void very rapidly. Even a void filled with water will usually exhibit a very rapid infiltration rate. Used prudently, in conjunction with ground-penetrating radar, this water infiltration test has proven to be very useful in verifying the existence and horizontal extent of voids and also in determining the existence of moisture in base materials. The advantage of this type of test over conventional core drilling is that the holes are smaller, drilling is quicker, and water is not introduced into the pavement system during drilling.

During the field testing phase several subsurface anomalies were detected: voids, free water under slabs, wet base materials, wet subgrade materials, and subsurface effects of D-cracking. A more detailed discussion of each field test is given in Appendix G.

CHAPTER THREE

CONCLUSIONS AND SUGGESTED RESEARCH

RADAR AS A SURVEY TOOL

Short-pulse ground-penetrating radar proved to be capable of detecting a number of different types of subsurface defects (anomalies) on different types of portland cement concrete pavements. Radar can collect data at 10 to 20 mph and detect the existence (and equally important the nonexistence), location, lateral extent, and, to some degree, the severity of subsurface anomalies. Survey speeds higher than 20 mph result in horizontal resolution reduction caused by a fixed pulse rate. Several types of subsurface anomalies were detected during the field test portion of this project including those within the concrete pavement, at the pavement/base interface, and at the base/subgrade interface. During the field testing portion of this project, a number of subsurface anomalies were detected by the radar system: air-filled voids, water-filled voids, deteriorated base material, base material contaminated with subgrade material, wet base material, wet subgrade material, and subsurface effects of "D" cracking. Additional field testing to quantify these various types of subsurface distresses and develop algorithms to detect them are suggested as additional research. The exact nature of some of these subsurface anomalies could not always be determined based on the radar signal return waveforms alone. Other inputs (cores or some knowledge of pavements) are usually necessary to determine the exact nature of the anomalies and to verify the existence and severity of the anomaly. A few physical tests to verify the relationship between radar signal return and distress type prior to the survey allowed for the rapid survey of the entire project to determine location, lateral extent, and severity of these distresses, because it can be generally assumed that the type of subsurface distress is constant within the limits of an original, uniform construction project.

MULTICHANNEL RADAR SYSTEM DEVELOPMENT

The multichannel radar system hardware was successfully designed, fabricated, tested, and implemented. A five-antenna radar array was mounted on a vehicle. As this vehicle moved along the roadway, each of the five antennas, equally spaced across the lane, collected data in a path oriented longitudinally down the roadway. Hardware was implemented in this system, which permitted near real-time processing and display of the horizontal extent and severity of subsurface anomalies. Adjustments were possible to detect anomalies at preselected depths in the pavement system and to display anomalies only above a selected severity level. This equipment was taken into the field for testing, where it functioned in an acceptable manner and recorded all of the data for later analysis. During the field tests, coring was used to verify the existence, type, extent, and severity of anomalies at a few locations to allow for the calibration of the automated radar system. This effort proved the feasibility of operating a multichannel radar survey system in the field with the capability of detecting and displaying the horizontal extent of certain subsurface anomalies in near real-time or recording the data for later analysis.

RADAR LABORATORY TESTS

During the laboratory testing phase of this project several different radar antenna configurations were tested to evaluate performance as related to PCC pavement assessment. It was determined that antennas used in the bistatic mode were superior to ones operated in a monostatic configuration. The orientation of the radar antennas in relation to the orientation of reinforcing steel in pavements was investigated. It was demonstrated that if reinforcing steel is oriented predominantly in one direction (as in CRC pavements), the proper orientation of the radar antenna results in greatly improved penetration of the pavement structure. If the electric field of the antenna is perpendicular to the predominant orientation of the reinforcing steel, the reinforcing steel becomes nearly "invisible" to the radar.

VOID-SIZING ALGORITHM

The development of the void-sizing algorithm involved the estimation of three void dimensions. The longitudinal extent of the void can be accurately measured based on the output of the fifth-wheel unit included with the modified RODAR™ vehicle. The multichannel approach to determining the horizontal extent of a void also produced satisfactory results and can be used for estimating the surface extent of other pavement anomalies, provided appropriate detection criteria are available. Estimation of void thickness or depth proved more problematic, however.

The time domain approach to void, vertical dimension measurement proposed during NCHRP Project 10-14 and examined during this project possesses several inherent problems which make it difficult to use as an accurate technique for an operational, automatic system. The primary problem is the dependence of the void return peak amplitudes on the dielectric properties of the concrete and base materials. The dependence of these amplitudes on the type of base material was demonstrated theoretically and confirmed by data taken during this project. This dependence requires the use of a different amplitude versus void size relationship for different pavements and base materials. *NCHRP Report 237* proposed that a calibration routine could be devised which would determine the proper amplitude curve for a given roadway. However, the pavement base material usually will not contain homogenous dielectric properties over the extent of a subsurface survey because of water infiltration through joints and cracks. This is true even if the type of base material does not change over the survey run, because the dielectric properties of the base are also dependent on the water content of the material. Therefore, the algorithm for void vertical dimension detection would be unable to determine if an increase in the peak amplitude was due to a void or an increase in the water content of the base material near a joint or crack. This problem is particularly troublesome because most voids form in the wet base material near joints, rather than in the dryer material below the center of the slab. The problem was addressed to some extent during the field testing phase by assuming that all voids occur in wet base materials and by calibrating, based on coring, at a few locations prior to a survey.

An alternative approach, therefore, must be found which is less affected by the constantly varying dielectric properties of the pavement and base materials. One approach, which might prove successful, involves the analysis of the void return in the frequency domain. It is believed from a theoretical standpoint that the round-trip transit time through a void can be measured directly from the phase of the complex Fourier transform of the void return. This measurement will require a high degree of accuracy because the round-trip transit time through a ⅛-in. air void is only 21 picoseconds. Also, the frequency domain approach would be affected by the spectral spreading of the radar signal caused by attenuation in the pavement. Therefore, additional research must be done to characterize the effects of pavement attenuation on the spectrum of the radar transmitted pulse. Also, the frequency domain approach to measurement of void size does not depend on the dielectric properties of the base material; therefore, additional research should be conducted to explore the use of frequency domain analysis on the measurement of void thickness.

VIDEO RECORDING SUBSYSTEM

A relatively simple and inexpensive video recording system was designed and implemented for assessment of PCC pavement surface defects. This system can record surface video data of reasonably high resolution, along with location data. The recording can be taken to a central location and an automated analysis system can be employed to assess the video data, enhancing and extracting surface defect information. With a small amount of operator interface prior to the video survey to establish optimum camera settings, lighting, and so on, the video data can be recorded continuously. Likewise, a small amount of operator interface will be necessary to establish certain constants in the automated video data analysis system for optimum data enhancement and extraction, but the system can then run unaided until the data analysis is complete.

VIDEO DATA ANALYSIS SYSTEM SOFTWARE DEVELOPMENT

The video data analysis software developed for this project proved to be very effective. A considerable amount of pavement surface video data with very thin cracks and/or dark backgrounds was analyzed. After a considerable amount of effort, data enhancement methods were developed that were capable of enhancing poor contrast targets and recognizing cracks thinner than one-half video pixel. After enhancement, the software detected cracks, joints, spalling, and certain other distresses; determined widths, lengths, locations, and orientations for classification and cataloging. Also developed during this project was a method to determine the effects of lighting, equipment adjustments, surface color, enhancement techniques, and feature intensity threshold selection on the detectability of surface features. This method was implemented in the software and is valuable for the field calibration of the video equipment.

REAL TIME, VIDEO DATA ANALYSIS SYSTEM DESIGN

This design effort proposes a system capable of obtaining high-resolution video data, enhancing the data, extracting distress features, and classifying the features as the survey vehicle operates at highway speeds. This system would be composed of existing technology, with most components available off-the-shelf, for reliability and cost consideration as well as for ease of implementation. This design can well serve as the starting point for development of an operational prototype video data analysis system. Such a prototype unit can then be laboratory and field tested to assess and quantitize system performance capabilities.

REFERENCES

1. STEINWAY, W. J., ECHARD, J. D., and LUKE, C. M., "Locating Voids Beneath Pavement Using Pulsed Electromagnetic Waves." *NCHRP Report 237* (Nov. 1981) 40 pp.
2. MANNING, D. G., and HOLT, F. B., "Detecting Deterioration in Asphalt-Covered Bridge Decks." *Transportation Research Record 899* (1983) pp. 10–20.
3. CANTOR, T. R., and KNEETER, C. P., "Radar as Applied To Evaluation of Bridge Decks." *Transportation Research Record 853* (1982) pp. 37–42.
4. MACKENZIE, J. S., "Pavement Cracking Inventory Study." Arizona Department of Transportation, *FHWA/AZ DOT Report No. 82/181.*
5. COX, G., CURPHEY, D., FRONEK, D., and WILSON, J., "Remote Video Sensing of Highway Pavements at Road Speeds: Using the Motorola 68020 Microprocessor." *Microcomputers in Civil Engineering,* Vol. 1, No. 1 (July 1986).

APPENDIX A

TECHNOLOGY BACKGROUND

Because the ultimate goal of this project was to develop a system which identifies and assesses both surface and subsurface deterioration in concrete pavements, two existing nondestructive technologies were selected for integration into the proposed system. The first, short-pulse ground-penetrating radar, provides detection and location of voids and other subsurface distresses in concrete pavement systems. The second, high-resolution video imaging, permits identification and assessment of surface distresses such as cracking, breakoffs, and spalling. The following outlines the capabilities of each of these technologies as tools for determining deteriorated areas in portland cement concrete pavement.

GROUND-PENETRATING RADAR

Theoretical Background

The ability of short-pulse radar to detect, locate, and characterize surface and airborne targets is well established and well documented. The use of short-pulse radar as a tool for subsurface exploration is a more recent application but has received considerable attention, especially over the last 15 years. In fact, an operational short-pulse radar system designed specifically for continuous profiling of subsurface conditions has been available since 1970. Short-pulse radar has been used in a multitude of subsurface assessment applications, including finding buried cables and sewer lines; measurement of ice thickness; assessment of glaciers and snowpacks; profiling the bottoms of lakes and rivers; and even examining the subsurface of the moon. Over the last few years, a great deal of interest has been generated in using short-pulse radar to perform pavement assessment, with void-detecting being of particular interest.

The following paragraphs give a more in-depth description of short-pulse radar technology and discuss its usefulness as a subsurface anomaly detection tool. The major components and the functional operation of a short-pulse radar will also be discussed. A brief outline of the theoretical background of short-pulse radar is presented here. Some practical applications of radar theory to pavement condition assessment are also noted.

Consider Figure A-1, which is a simplified model of the interaction of impinging electromagnetic waves with a dielectric discontinuity. As shown in this figure, a portion of the incident electromagnetic wave is reflected by this discontinuity and a portion continues to propagate down into the second medium. The proportion of the incident wave that is reflected at the interface is determined by the reflection coefficient, ρ, associated with the boundary. This reflection coefficient is given by:

$$\rho = (n_2 - n_1)/(n_2 + n_1) \qquad \text{(A-1)}$$

where n_1 and n_2 are the wave impedances of medium 1 and medium 2, respectively. In general, the wave impedance is a complex number, but simplification is possible for certain groups of materials. For example, the wave impedance for a highly conductive material, such as silver or copper, is essentially zero, whereas that for a nonferrous, nonconducting material, such as dry concrete or soil, is given by:

$$n = \left[\frac{\mu_o}{\epsilon_o \epsilon_r}\right]^{1/2} \qquad \text{(A-2)}$$

where μ_o is the permeability of free space (a constant), ϵ_o is

the permittivity of free space (a constant), and ϵ_r is the relative dielectric constant of the material in question. Since ϵ_r is the only variable in the wave impedance expression in Eq. A-2, the reflection coefficient expression shown in Eq. A-1 can be reduced as follows for interfaces between nonferrous, nonconducting materials:

$$\rho = \frac{\sqrt{\epsilon_{r1}} - \sqrt{\epsilon_{r2}}}{\sqrt{\epsilon_{r1}} + \sqrt{\epsilon_{r2}}} \qquad \text{(A-3)}$$

where ϵ_{r1} and ϵ_{r2} are the relative dielectric constants for medium 1 and medium 2, respectively.

Note from Eq. A-3 that if medium 1 has a smaller relative dielectric constant than medium 2, ρ is negative; and if medium 1 has a larger relative dielectric constant than medium 2, ρ is positive. Furthermore, the magnitude of ρ is proportional to the difference between ${\epsilon_{r1}}^{1/2}$ and ${\epsilon_{r2}}^{1/2}$. Thus, at an interface between materials with similar dielectric properties, most of the impinging wave energy passes through the interface and little is reflected back toward the transmitting source. On the other hand, a large reflection and a correspondingly small transmission occur at an interface between two materials with greatly different relative dielectric constants. This reflection phenomenon is the theoretical basis for the production of specific signatures by various subsurface objects and features.

As a practical application, consider the case of an individual portland cement concrete slab. If no void is present, there are only two discontinuities or boundaries from which reflections of the incident radar waves will occur: the air-concrete interface at the top of the concrete slab and the concrete-base interface at the bottom of the slab. In contrast, if a void is present between the concrete slab and the underlying base material, there are three boundaries that produce reflections: the air-concrete interface at the top of the concrete slab, the concrete-air interface at the bottom of the slab, and the air-base interface at the bottom of the void. One should note from Eq. A-1 that the reflection coefficient, ρ, produced by a transition from air to concrete has the opposite sign from that produced by a transition from concrete to air. Thus, two factors which affect the radar return distinguish the case in which a void is present. The first is the number of reflections, because three such reflections characterize a void, whereas two are produced when no void exists. The second is the amplitude and sign of the reflections, which is determined by the respective reflection coefficients. In both cases (no void and void present), an identical reflection occurs at the air-concrete interface at the top of the slab. However, the second reflection when no void is present is produced by the concrete-base interface at the bottom of the slab, which differs significantly from that produced by either the concrete-air or the air-base interfaces which result from the presence of a void.

SHORT-PULSE RADAR SYSTEM COMPONENTS

Short-pulse radar systems were developed for ground-penetrating applications more than a decade ago. Only in the last few years have they been used as a highway survey tool. The existing radar system that is most applicable, in a rapid PCC pavement survey mode, is a system using the air-coupled "horn" antenna. A schematic of the functional components of this existing radar system is shown in Figure A-2.

Six essential components are identified in this figure: a transmitter, an isolator, an antenna, a receiver, a signal processor, and a display.

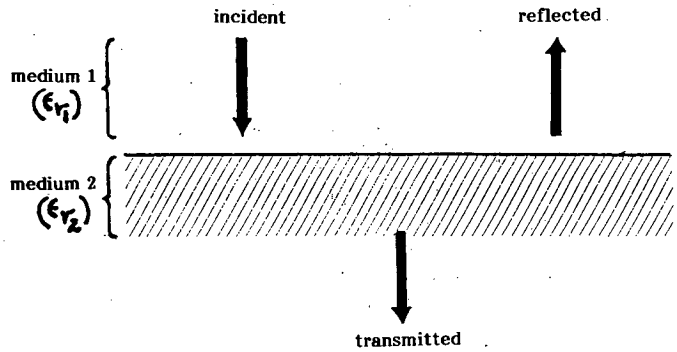

Figure A-1. Simplified model of interaction of electromagnetic waves impinging upon a dielectric discontinuity.

Each of these will be discussed, in turn, in the paragraphs that follow.

The function of the transmitter is to generate a known waveform that is used to probe the environment for targets. The name "short-pulse radar" is derived from the fact that the transmitted waveform of such a system is actually a very narrow pulse, which typically might last on the order of one-billionth of a second (1 nanosecond). Such a short pulse is necessary to achieve adequate depth resolution in the ground. In other words, the use of a narrower pulse improves the ability of the radar to distinguish smaller objects and features under the ground. Thus, the task of the transmitter of a short-pulse radar (SPR) system is to produce a suitable narrow pulse for transmission.

During the transmit cycle, the isolator shown in Figure A-2 provides a direct path from the transmitter to the antenna. The narrow pulse formed in the transmitter is thus routed to the antenna for radiation into the environment. The antenna actually serves two functions. First, it provides a smooth electromagnetic transition from the transmitter to the environment. Without such a smooth transition, the efficiency with which the narrow pulse is radiated into the environment is greatly reduced. A detrimental side effect of such a reduction in efficiency is that undesirable internal system reflections (called "ringing") are often created which can partially or completely mask actual target reflection or can be falsely classified as target reflections themselves.

The second function of the antenna for this application is to direct the radiated electromagnetic energy into the ground in a desirable pattern. In general, the antenna has a three-dimensional radiation pattern and, thus, will direct energy in all directions. The antenna is designed so that the majority of the radiated energy is directed into the ground and very little is radiated in other directions. The shape of the beam directed into the ground is also of interest because the antenna essentially integrates the return received over this characteristic beam shape. If the antenna beam shape is poor, each beam covers a relatively large area (called a "footprint") on the ground. The advantage of employing such a large footprint is that fewer antennas can cover a given linear swath. The disadvantage is that each antenna integrates over a larger area because of the broader beam and, thus, a high-intensity target return is effectively diluted by the lower intensity return of the surrounding

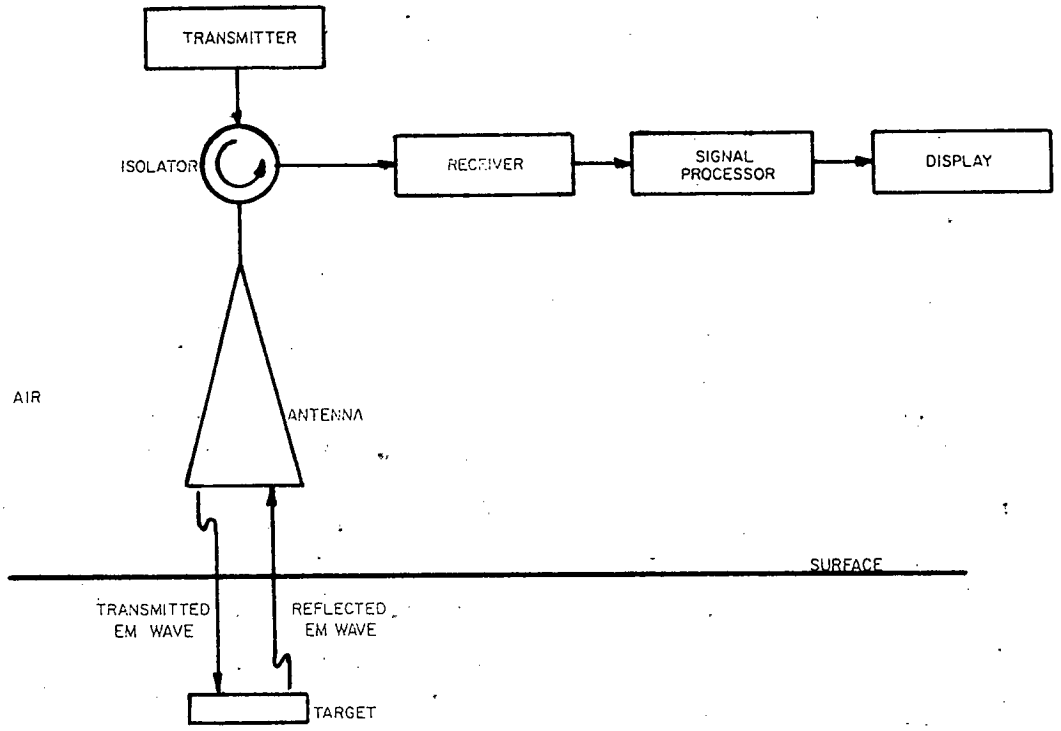

Figure A-2. Basic functional components of short pulse radar system for highway.

media. Thus, the probability of overlooking the return from a small object is increased.

On the other hand, use of an antenna with a narrower beam offers the opposite tradeoff. More antennas are needed to completely cover a given swath, but detection performance is improved because integration is performed over a smaller area surrounding and including the object, thus reducing the dilution effect. A technical problem is involved in this approach because antennas with very narrow beams are typically more difficult and expensive to construct than those with broader beams. Often, the reduction of the antenna main beam width results in some undesirable side effects, such as increasing the energy radiated in directions away from the ground.

The electromagnetic wave launched by the antenna travels in the radiated direction until it strikes a discontinuity in the electromagnetic properties of the media. A portion of the wave passes through the discontinuity, and a portion is scattered or reflected in other directions away from the discontinuity. Such a discontinuity is almost always associated with a material change in the media.

The first such discontinuity encountered by the wave in Figure A-2 is associated with the air-pavement interface. At this interface, a portion of the incident wave is scattered back away from the earth and a portion propagates into the earth. Next, the wave traveling within the pavement strikes a discontinuity such as a pavement layer interface. Again, a portion of the incident energy is reflected away from the target, with the remainder continuing along the downward path. The portion of the wave reflected by the target forms the basis for target detection and assessment.

As described previously, the isolator connects the transmitter to the antenna input port during pulse transmission. Shortly after this transmission, the isolator connects the radar receiver to this same antenna port for signal reception (assuming the system is operating in a monostatic mode). This isolation function protects the radar receiver components from overload and possible damage. However, once transmission is complete, the isolator must connect the receiver to the antenna so that any returning reflections from targets can be detected. In this receiving mode, the antenna collects the electromagnetic energy of the return reflection or echo and delivers it to the receiver. By the reciprocity theorem, the receiving characteristics of the antenna are equivalent to its transmitting characteristics, so that the performance parameters described in the previous antenna discussion are valid for the receiving case as well.

The task of the receiver is to capture weak target signals and amplify them for subsequent processing. The receiver typically gates, filters, mixes, and samples the incoming signal to shift the incoming waveform to a desired frequency band and to reduce the signal contamination produced by electrical noise and reflections (called "clutter") from objects that are not of interest to the radar operator. Of the two primary signal contaminants, noise and clutter, clutter is the more severe in typical ground-penetration applications and is the principal limitation of the radar system's ability to detect faint target echoes.

Following reception, the output of the receiver is then passed to the signal processor which extracts the desired information from the received signal. The specific signal processing techniques used for a particular radar system depend on the primary "targets" that the system is designed to detect or assess. Signal processing can be performed either off-line or in real-time. In an off-line processing mode, data are acquired by the radar system and stored in some fashion for subsequent processing, often at a central data reduction and analysis facility. A real-

time processing approach requires that data be processed as they are received. Thus, one waveform from the receiver must be processed before the next one is available. The advantage is that anomalies can be detected virtually as soon as they pass into the field of view of the radar. The disadvantage is that only a limited amount of time is available for processing, typically given in milliseconds. Thus, time is available to perform processing algorithms of only limited sophistication, and expensive high-speed processing hardware must often be used even to perform such limited algorithms.

The final radar system component depicted in Figure A-2 is the display, the purpose of which is to present the information contained in the radar return signal in an appropriate format for interpretation by the operator. This display unit is often a two-dimensional screen; and because the data to be displayed are typically four-dimensional (three spatial dimensions as well as intensity) or even more complex (should phase, frequency, or polarization descriptors be of interest), a variety of display formats have been used. Typically, the radar data must be correlated with or "mapped into" a specific spatial reference system. In this case, additional information, omitted from Figure A-2 for the sake of simplicity, must be provided to the display to properly locate the received data with respect to the chosen frame of reference. An example of such additional positional information is the output of a fifth wheel or that of a shaft encoder connected to the wheel of the vehicle on which the radar is mounted, which gives the relative position of the radar sensor along the path of travel of the vehicle.

The particular radar system chosen for this research project has the following advantages: (1) is based on short-pulse technology, (2) uses air-coupled antenna (non-ground contact), (3) uses narrow beam width, (4) offers high resolution, (5) is based on a complete field proven system, (6) has been used extensively in actual pavement surveys, and (7) has associated with it an existing advanced data enhancement, display and analysis system.

VIDEO TECHNOLOGY

The current state of the art in video/image processing encompasses a broad range of disciplines ranging from optics and photography to pattern recognition and multidimensional digital signal processing. The three basic tasks of any image analysis system can be generally described as follows: (1) image acquisition, (2) image/feature enhancement, and (3) feature recognition and extraction.

First, the image to be processed by the system is acquired from some optical source. One technique for acquiring the image is to use the output of a high-resolution color or black and white TV camera which produces a standard RS-170 analog video signal. Also, shuttered cameras and line scan cameras are commercially available for taking high-speed images of an object in motion. The shuttered camera is basically a standard video camera which contains a disc, with a small slit in it, spinning at a very high rate of speed in front of the lens of the camera. This spinning disc has a stroboscopic effect on the image that is shown to the camera. The line scan camera uses a CCD (charge coupled device) linear sensor to scan only one horizontal line of the image at a time. The CCD linear image sensors contained in these cameras are monolithic components which contain a single row of image sensing elements called photosites or pixels. The output of the sensor is a series of pulses whose magnitudes are related to the amount of light encountered by the photosites. Generally, the output of the line scan camera is the photosite pulse train in either binary or analog format.

If the video signal is to be computer-enhanced, it must be read into the computer to form a two-dimensional array of pixel values that make up the image. If the input video from the camera is an analog signal, RS-170 standard for example, the signal must be digitized with an analog-to-digital (A/D) converter. The digital signal is then quantized into gray levels which represent different levels of light for the pixels in the image array. The image processing hardware purchased by Gulf is capable of digitizing an RS-170 video signal into a 512 by 512 array of pixels that are quantized at 256 gray levels. The 0 gray level corresponds to black (no light) and the 255 gray level is white (maximum light). The quantized pixel array can then be written into the memory of the computer for enhancement and automated feature extraction.

Computer enhancement of the image is accomplished with software algorithms which manipulate the values of the image pixels stored in the memory of the computer. Generally, these algorithms involve convolving the raw, input image with a mask that is meant to achieve some desired change in the appearance of the image. The most effective of these programs takes advantage of the geometry of the feature in order to enhance it. For example, a program that enhances edges in the image is an effective technique for enhancing cracks in images of the road surface. The process of two-dimensional convolution is a well-documented technique in the field of multidimensional digital signal processing, and a brief description is provided here. The equation which governs a two-dimensional convolution is given as follows:

$$Y(i,j) = \sum_m \sum_n X(m,n)\, H(i - m, j - n) \qquad \text{(A-4)}$$

where $X(m,n)$ = input two-dimensional image pixel array; $H(i-m, j-n)$ = inverted, space shifted enhancement filter mask or kernel; and $Y(i,j)$ = output processed two-dimensional image pixel array.

The convolution begins by determining the coefficients in a mask, or kernel, $H(m,n)$ which will be used to compute the values of the new pixels in the processed image $Y(i,j)$. One example of a convolution mask is the 3 by 3 Laplacian mask shown in Figure A-3, which is used to enhance edges by selectively passing only high spatial frequency image components. The pixel intensities of the processed image are computed by sliding the mask over the input image while multiplying the input image pixels which fall inside the mask by the coefficients of the mask.

Once the contrast between the desired features and the rest of the image has been enhanced, then the features are more easily recognized by a human operator or the computer. Typically, it is the unique geometry of the desired feature that distinguishes it from the background of the image. Therefore, to accomplish feature extraction, the computer must somehow be taught what the desired feature "looks like". This is done by providing the computer with a set of rules that describe the typical geometry of the feature. For example, the EarthTech research team chose to calculate a "shape factor" which they defined as the length-to-width ratio of an object in the image (see Ref. 5). If the value of this shape factor was within an

−1	−1	−1
−1	8	−1
−1	−1	−1

Figure A-3. 3 × 3 Laplacian convolution kernel.

acceptable range of values for typical road surface cracks, the object was labeled a crack.

However, the pattern recognition algorithm, which identifies the features, must be fairly sophisticated if it is to be reasonably reliable. First, the designer must define the "typical" geometry of the desired feature. This problem is a function of the amount of physical area included in the image as well as the type and amount of enhancement that the image undergoes. In many cases the enhancement algorithms will distort the original image, making a feature slightly larger or smaller than that of the original image. Ideally, the program should also be able to identify all of the pixels that belong to a feature. For example, a physically large feature, which has been separated into pieces in the image because of lack of system resolution due to degradations during the feature enhancement process, should be identified as one feature. An effective feature extractor must be able to recognize and group together pieces of the same feature rather than to identify the pieces themselves as separate features. Also, the feature extractor must be able to identify two features that overlap in the image. This simple occurrence requires a great deal of flexibility in the algorithm because two features overlapping in the frame can produce a contiguous object in the image which does not satisfy the rules governing recognition of either of the individual features.

These technically sophisticated tasks of acquiring, processing, and analyzing the video data are further complicated when the job is required to operate in real time. Obviously, a real-time system must contain software that is very efficient with respect to execution. Also, the hardware must be able to handle data rates that for video imaging are very high—for example, CCD line scan cameras are commercially available with output data rates up to 20×10^6 pixels per second.

APPENDIX B

ENHANCED RADAR SYSTEM DESIGN

The enhanced radar system is composed of nine subsystems. A schematic of the enhanced radar system is shown in Figure B-1. The designations and brief descriptions of the components are as follows:

UNIT	DESCRIPTION
A	Antenna/Transducer Assembly
B	Radar Control Unit
C	Master Control Panel
D	Auxiliary Control Panel
E	Odometer/Speedometer
F	5th Wheel Assembly
G	FM Tape Recorder
H	Line Scan Recorder

The following paragraphs describe each of these components.

A—ANTENNA/TRANSDUCER ASSEMBLY

The transducer contains the short-pulse transmitter power supply, receiver sampler, sweep circuitry, and transmitter delay line, and is housed within the antenna case mounted on the boom. Along with the antenna, this enclosure comprises the microwave portion of the system. The antenna designed for this project was a smaller flared version of the RODAR™ operating antenna. This smaller antenna allowed for a much smaller system size and weight without excessive deterioration in the performance of the system. This project was the first to incorporate the transducer subassembly into the enclosure of the RODAR antenna. Mounting the transducer subassembly inside the antenna enclosure, instead of placing it at the end of a long cable, significantly reduces the losses in the received signal associated with this longer cable. The transducer receives DC power from the power supply unit, and receives a 5-MHz reference signal, sweep delay, and range control voltage from the Master Control Unit. A block diagram of the transducer is shown in Figure B-2. All five of the antenna/transducer assemblies are identical.

B—RADAR CONTROL UNIT

The Radar Control Unit (RCU) contains all the timing, control, signal conditioning, and tracking circuitry for the system.

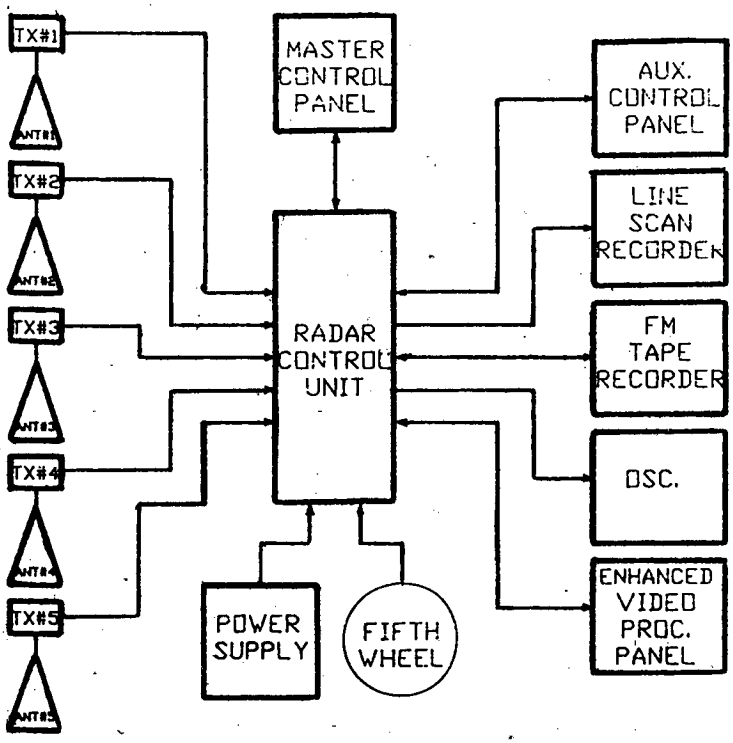

Figure B-1. Radar subsystem component schematic.

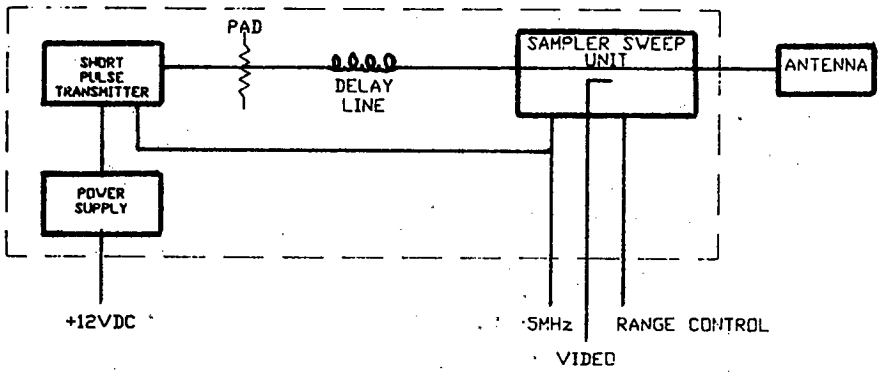

Figure B-2. Radar transducer block diagram.

The RCU contains 10 circuit boards that are designated: Timing and Control Board, Position Reference Boards, Surface Tracker No. 1 through No. 5, Video Buffer Board, Video Processing Board, and Enhanced Video Processor Board.

Figure B-3 is a block diagram of the Radar Control Unit. The RCU interfaces to all other functional units. The RCU synchronizes all recording and data gathering, conditions signals, and encodes distance references. The following paragraphs describe the characteristics of each board in the Radar Control Unit.

Timing And Control Board

The timing and control board generates the 5-MHz reference clock, the scan ramp, the early gate, and the late gate. Because this system has five channels, two additional clock phases are needed in addition to those already provided in the standard RODAR™ system. To prevent interference between the different radar channels, a multiphase reference clock is needed. The timing board takes a 15-MHz clock and divides it into three phases, each being 120-deg apart and each being at a frequency of 5 MHz. This 120 deg of phase shift allows each channel to operate with no interference from other channels. Channels 1, 2, and 3 are operated from phases zero, 1, and 2, respectively. Channel 4 is operated from phase zero, while channel 5 is operated from phase one. The difference in phase between channels is sufficient to minimize interference between any two channels. The board block diagram is shown in Figure B-4.

Position Reference Board

The position reference board (PRU) functions as the master control for all operator interface. The operator selects a given parameter (positive video, record, playback, start, stop, etc.), and the board generates the correct logic which performs that function. These logic levels are passed between the different

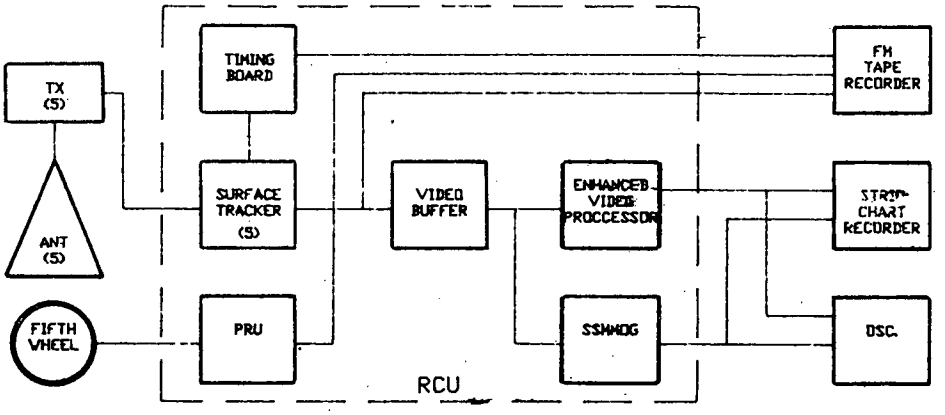

Figure B-3. Radar control unit block diagram.

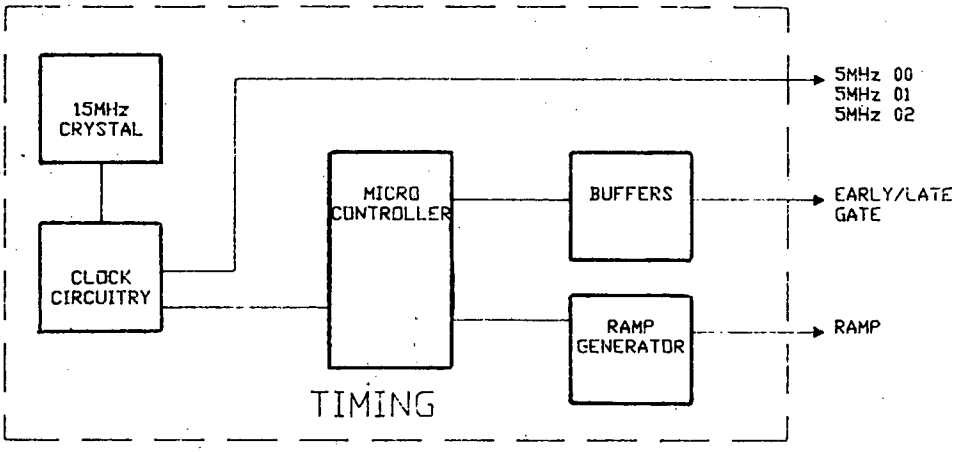

Figure B-4. Timing and control board block diagram.

boards so that a particular function can be carried out. This board is microprocessor-controlled and has a default state that is used on all power-up conditions. The board block diagram is shown in Figure B-5.

Surface Tracker Boards

The surface tracker boards have two functions. They must maintain the surface return signal at a fixed, predetermined location, and buffer and amplify the signals from the receiver sampler. This surface lock eliminates any system drift and any signal variations caused by the antenna vertical movement. The tracker circuit uses the early and late gates and a portion of the video in a comparator circuit that locks the surface in a fixed position. This circuit also can be used out of lock so that the video can be displayed and investigated anywhere in the range.

The surface tracker board also is used to buffer and amplify the video from the receiver sampler. To ensure proper operation of the tracker circuit, the video from the receiver sampler must be amplified by a gain of 10. This stage of amplification also acts as a buffer stage between the tracker and receiver sampler. The configuration of the board is shown in Figure B-6.

Video Buffer Board

The video buffer board has several data collection functions. Figure B-7 shows an overall block diagram of this board. The

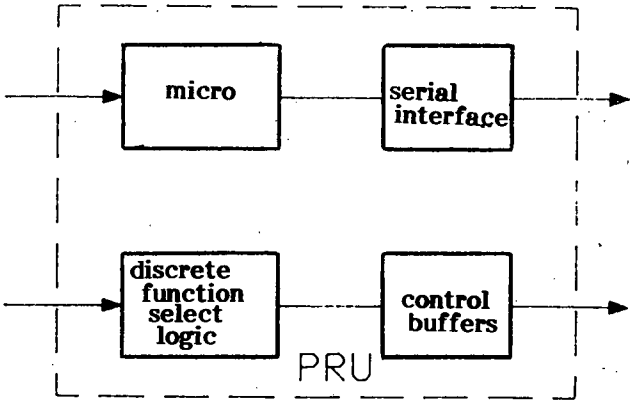

Figure B-5. Position reference unit block diagram.

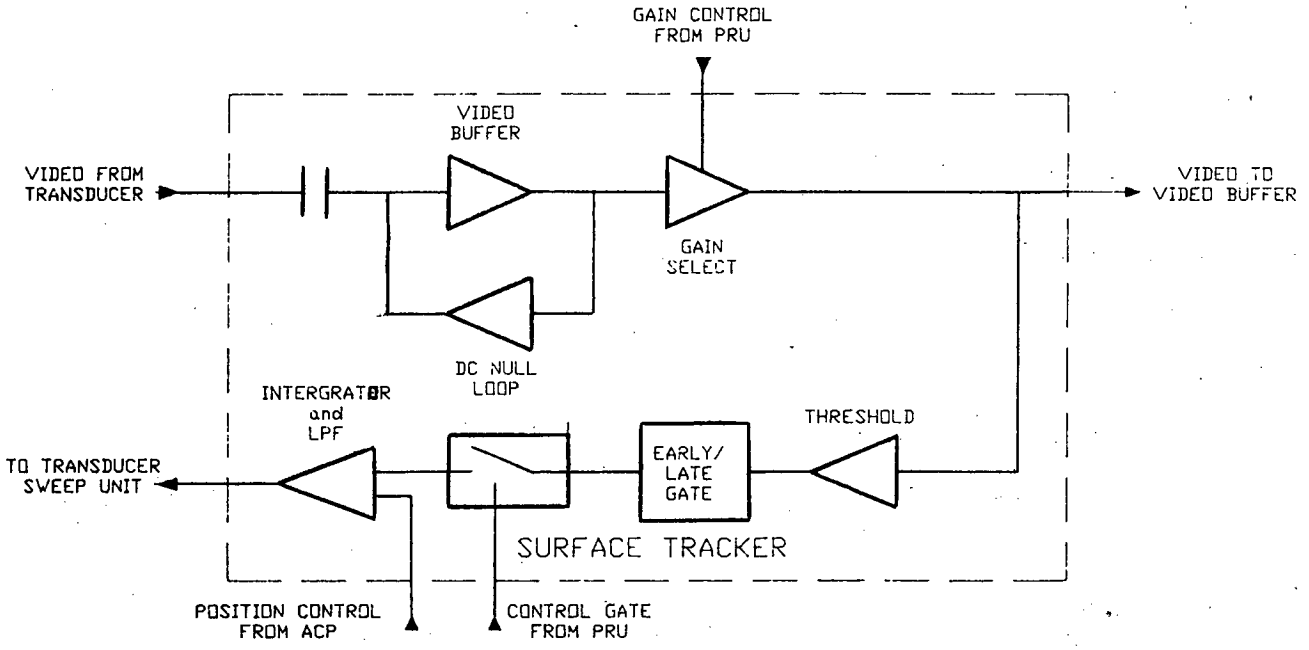

Figure B-6. Surface tracker block diagram.

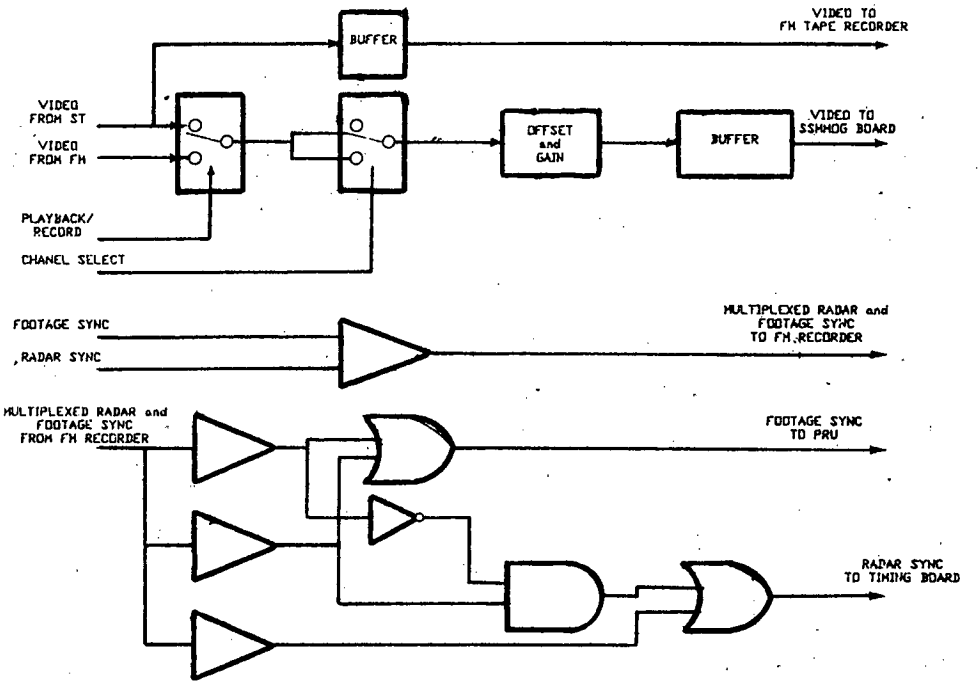

Figure B-7. Video buffer board block diagram.

main purpose of the board is to provide offset and gain to the real-time and the playback video that is passed on to the video processing board. This gain and offset are only applied to the channel of video that is selected to be output to the line scan recorder. In this enhanced radar subsystem, only one radar video channel at a time can be displayed on the line scan recorder. The remainder of the line scan recorder function displays the processed video results. All five channels of radar video data are recorded on the FM recorder and are passed through this board, but these channels are only buffered by this board to ensure isolation between FM channels. The board applies no further processing to the data. This guarantees that the data are recorded in an uncontaminated form and can be played back later to obtain the same results seen during data acquisition.

Another function of the video buffer board is to display the video on the oscilloscope. Because the oscilloscope has only two

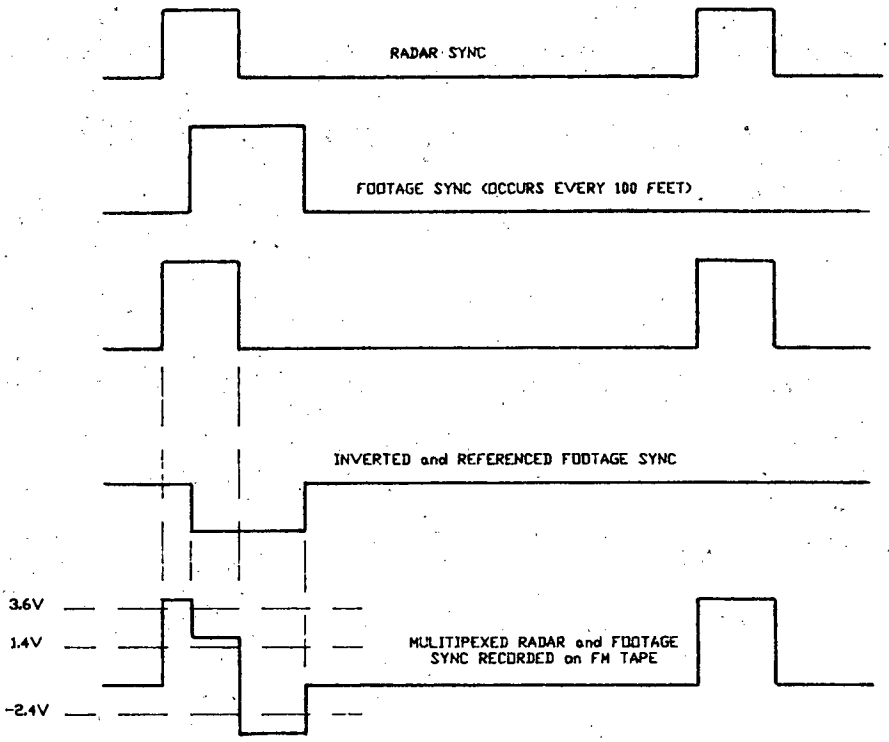

Figure B-8. Multiplexed waveforms for FM recording.

channels and there are five radar channels, a means to view all the radar video is needed for monitoring proper operation of the system. The channel of video that is passed to the processing board is also output to the oscilloscope. In order to verify the proper function of the five radar data channels, the video buffer board has a timing circuit that switches through the five channels of video and outputs this video to the oscilloscope in 1-sec per channel durations. In order to tell the operator which channel is displayed, the timing circuit holds the display of the first channel for 3 sec. This feature is only used as a reference to easily verify that all channels are functioning correctly, without manually switching between channels, and is not used for interpretation of the data.

The next function of the video buffer board is to multiplex the footage sync and the radar sync on one channel of the FM recorder. The footage sync is inverted and referenced to a minus voltage and then summed together with the radar sync. This one signal is then recorded on channel 7 of the FM recorder. Figure B-8 shows the input waveforms and the summed waveform.

The video buffer also demultiplexes the radar sync and footage sync. The multiplexed waveform is applied to three separate comparators that look at the voltage level and determine what sync pulse is present. These comparators reconstruct the appropriate sync pulses and then output the pulses to the timing board and the position reference board.

Conventional Video Processing Board

The conventional video processing board performs selected processing of the radar signals before they are plotted on the strip-chart recorder. The signal flow is shown in block diagram form in Figure B-9. The processing, which can be selected by the operator, consists of four basic functions. First, there is subsurface interface detection (SID), which extracts pavements layer interfaces and plots only these layer interfaces on the line scan recorder. Using this circuit, the operator is allowed to display a clean representation of layering without seeing any other features. Second, there is sensitivity time control (STC), which applies a time-varying gain to enhance small (or weak) returns. Third, there is positive/negative/bipolar video processing, which processes the signals and displays the appropriate polarity signal; and finally, there is the position marker, which is used to superimpose a time marker on the video signal so a measurement of depth (in time) can be made.

Although this board has a large number of processing features, it was necessary to develop a new processing board that could handle five channels of radar data. A new Enhanced Video Processing Board was designed. With the enhanced video processing board the original functions discussed above are retained for operator use if required.

Enhanced Radar Video Processing Board

For this project, a new processing scheme was developed that would help extract the data needed for determining void sizes. This new board, called the Enhanced Radar Video Processor, contains five circuits, one for each radar channel. The signals from these five circuits are output to the strip-chart recorder to produce a plan view of the void or anomaly. The enhanced radar video processing board is shown in block diagram form in Figure B-10

In this system, the radar scan rate is 20 msec. Because a major concern of this project is void sizing, all 20 msec of data are not needed. Void data are normally located at layer inter-

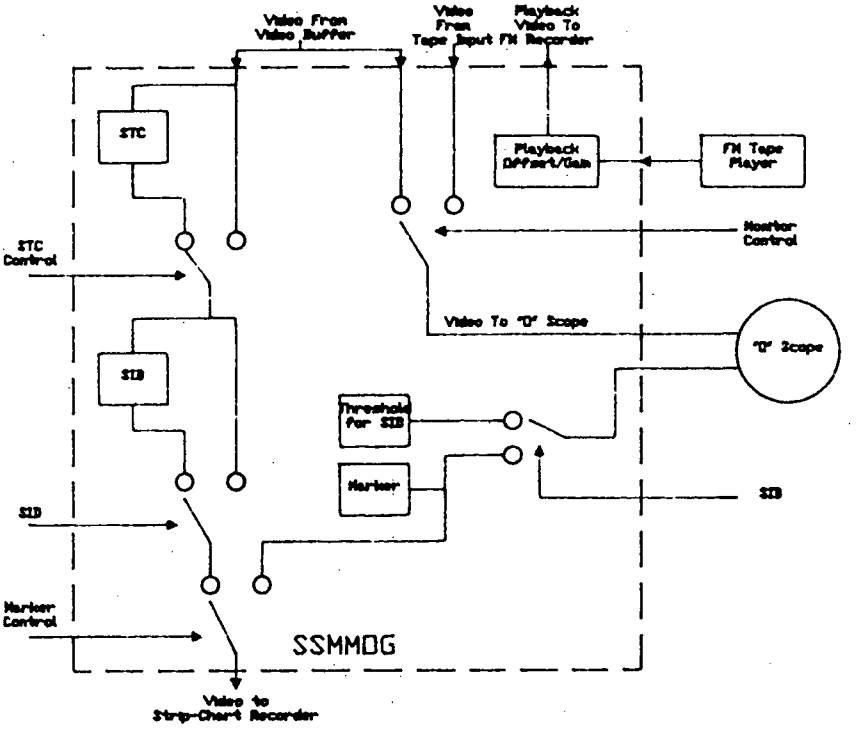

Figure B-9. Conventional radar video processing board signal flow diagram.

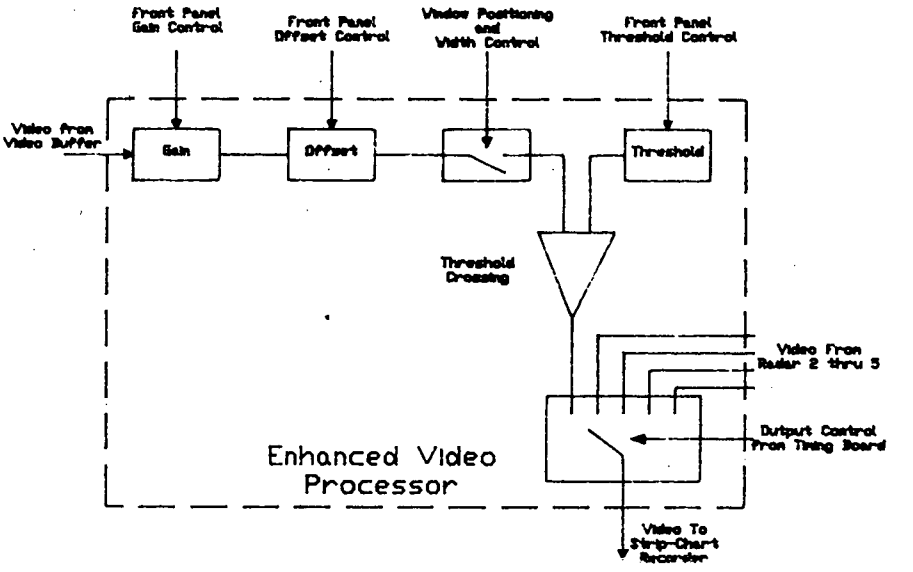

Figure B-10. Enhanced radar video processing board block diagram.

faces, so a method for eliminating all unnecessary data was designed. This circuit allows an adjustable window to be positioned in time at the pavement layer interface return. To further enhance the processing of the windowed data, an adjustment was made to narrow the window to further eliminate unwanted data. The operator must locate the interface in question and then position the window at this point. The next step is for the operator to narrow the window to allow only a small portion of the data to be passed on to the gain and offset stage. This unique feature allows the operator to adjust the gain and offset and have it affect only the windowed video. This is a major advantage because previous GAR systems had no capability to enhance the data in one area of interest. In GAR's conventional system, the offset and gain adjustment affects the entire 20 msec of data, and when a particular area of data needs to be enhanced, the entire 20-msec window is affected. This can make the data difficult to analyze. Figure B-11 shows how the new window adjustment scheme allows for a particular area of data to be enhanced. Only this small window of data is enhanced, processed, and printed on the strip chart recorder.

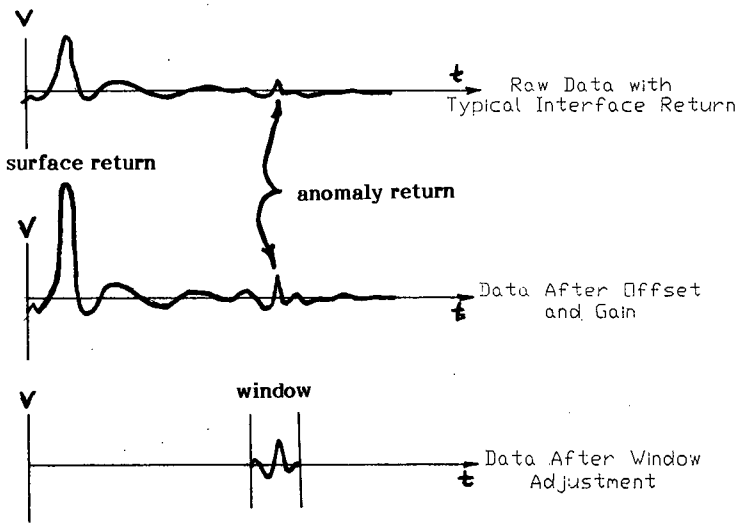

Figure B-11. Window adjustment for data enhancement.

The next two stages of the enhanced radar video processing board apply gain and offset to the video. The amount of adjustment to set up each channel of data is done on a trial and error basis and verified by coring. Because no two job sites will look the same, the amount of adjustment needed is job-dependent. The procedure for verifying the gain and offset adjustments by coring is discussed in the field test phase of this report. In order for the operator to reproduce the data in the office as it was seen on the job, a method of resetting these gain and offset adjustments was necessary.

The gain and offset adjustments are done by means of digital circuitry. The operator uses a set of three rocker switches for the gain and offset adjustments that allows him to increment or decrement the adjustments accordingly. In order to indicate the precise gain and offset settings, a set of liquid crystal displays is used to display the digital reference. The operator can then log this setting and reproduce this same setting at a later time.

The next stage of the board sums a digitally programmable threshold with the video. This setting indicates where the actual void extraction takes place. Through extensive data collection and laboratory testing, it was found that more void sizing information could be extracted from the negative video than from the positive portion of the video. For this reason, a negative threshold circuit was designed that would help extract void data. Because the possibility does exist that the positive video can yield some data, a switch was designed on the enhanced video processor control panel so the operator can select between a negative and positive threshold. The operator sets the threshold with a set of three rocker switches that control a digitally programmable D/A that outputs the threshold voltage and displays it on the LCD. Again, the operator must log the value represented on the LCD's so at a later date the same results can be reproduced if required. Figure B-12 shows pictorially how the threshold circuit extracts the void data. Figure B-12 (a) compares the video with no void to the selected threshold voltage. Figure B-12(c) compares the video with a void present to the threshold voltage. As shown in Figure B-12(c), the amplitude of the waveform at the interface increases when a void signature is present. Figure B-12(a) shows that the data do not cross the threshold voltage, so no output is produced from the threshold

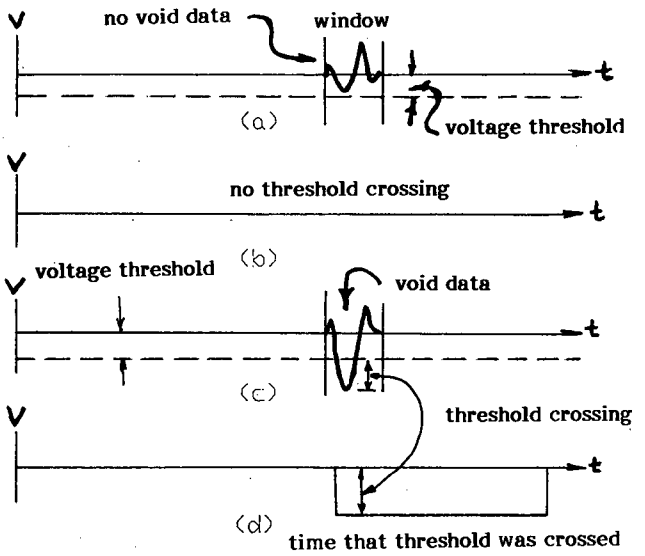

Figure B-12. Threshold circuit function.

detection circuit, Figure B-12(b). Figure B-12(c) shows the video crossing the threshold voltage which produces an output voltage from the threshold detection circuit, shown in Figure B-12(d). This threshold crossing produces an output voltage from the threshold detection circuit that has a direct relationship to the vertical dimension of the void.

The last stage of this board is a sample-and-hold circuit that takes the output from the threshold circuit and holds it until it is needed at the strip-chart recorder. A signal called "video 1/video 2" is produced on the PRU board that allows the first 20 msec of a line scan recorder sweep to print the selected channel of video and the last 20 msec to print the planned view of the five enhanced video outputs. A timing circuit, on the timing board, produces a counter waveform that controls an output switch for each of the five sample-and-hold circuits. After

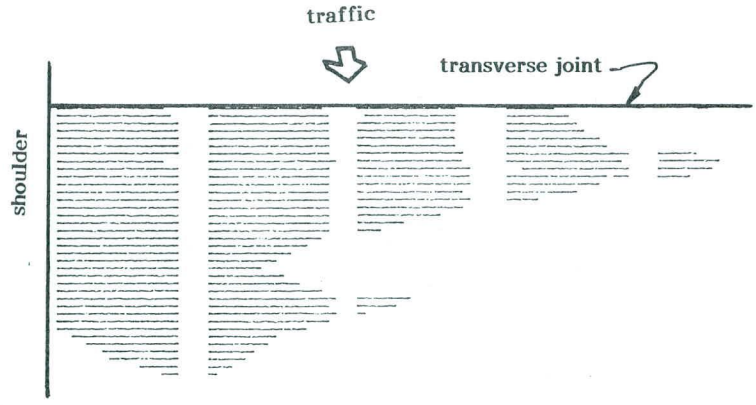

Figure B-13. Proposed output from gray-level recorder for representing horizontal extent of anomaly.

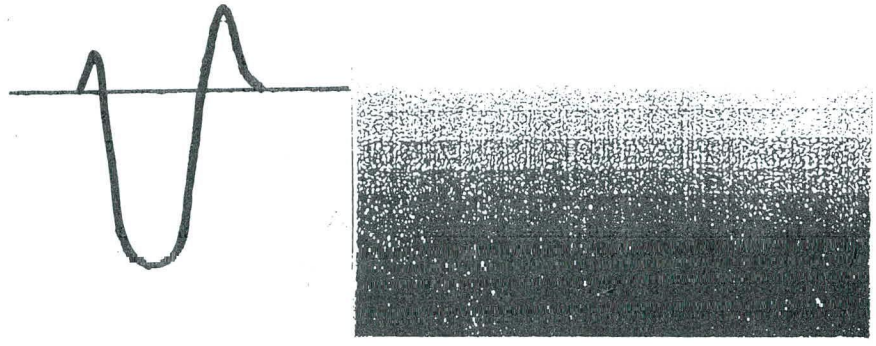

Figure B-14. Gray level recorder method of depicting signal amplitude.

the scan period of the radar (20 msec), the sample-and-hold circuits are all reset to zero volts, so on the next radar scan the threshold circuit will detect any new threshold crossings. The resetting time is of such a short duration that when the next 20-msec interval comes along, all five circuits will be ready to accept new data. The threshold crossing amplitude outputs are in the format of a voltage level that is reproduced in the line scan recorder as a gray level. This gray level is a direct representation of the thickness of the void. A sample of the output during the 20 msec of planned view time is shown in Figure B-13.

This figure shows how the void is represented in both the x and y dimensions. Because the antenna spacing is fixed, the y dimension is always known; and because the footage is represented on the line-scan recorder by footage marks, the x dimension is easily obtainable. By knowing these two dimensions, the void area is readily obtainable. Through experience, the operator can relate the gray-level variations on the strip-chart recorder to the vertical dimension of voids. Figure B-14 compares a void signature to a gray-level chart.

C—MASTER CONTROL PANEL

The master control panel contains all switches for signal recording, timing, and control (Figure B-15). This panel also has a set of thumbwheel switches that allow the operator to record run numbers on both FM tape and video tape.

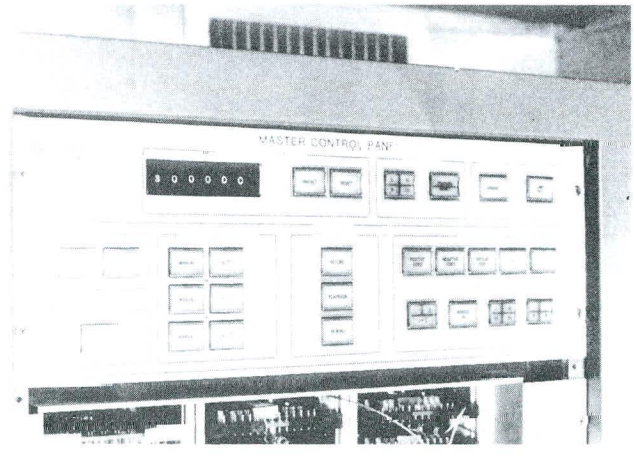

Figure B-15. Master control panel.

D—ENHANCED RADAR VIDEO PROCESSING CONTROL PANEL

The enhanced radar video processing control panel (Figure B-16) contains all the gain and offset controls and liquid crystal displays that interface with the enhanced video processing board. This panel also contains the window positioning control and

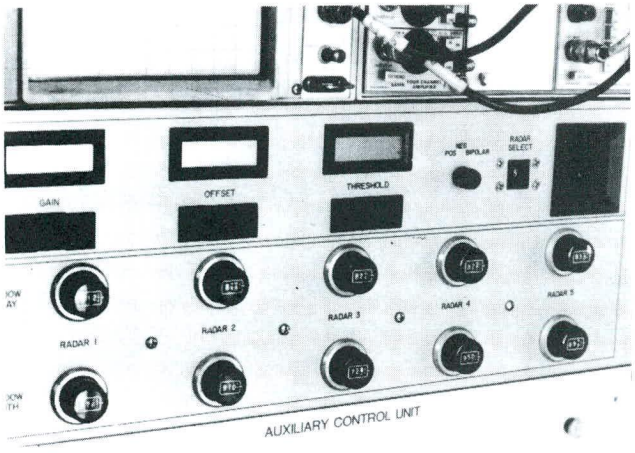

Figure B-16. Enhanced radar video processing control panel.

the window width adjustments. These potentiometers also have digital readouts, so that the operator can log the settings during acquisition and later reproduce these same settings during playback. Another feature of this panel is the ability to select any of the three available video forms (positive, negative, or bipolar). This selection controls only the video through the planned view time and not the video during the selected video time. This allows the operator to switch to a different format if more information can be extracted from that format.

E—ODOMETER/SPEEDOMETER

The odometer/speedometer includes one 3-digit display and one 6-digit display. The 3-digit display is used for indicating vehicle speed in miles per hour. The 6-digit display is used for indicating the distance traveled in feet. The odometer readings are referenced to a preset position on the fifth wheel, and the speedometer readings are determined from the rate of revolution of the fifth wheel. Both the operator and the driver have an odometer/speedometer display. The display operates during the playback mode for a visual indication of position on the roadway.

F—FIFTH WHEEL ASSEMBLY

The fifth wheel used is an off-the-shelf item. It has a transducer that produces 25 pulses per linear foot of distance. These pulses are used for determining speed and distance traveled.

G—FM TAPE RECORDER

The FM tape recorder is a Hewlett-Packard 8968A 8-channel recorder. An FM recorder is needed because the bandwidth of the processed video extends from DC to 10 kHz. This recorder also has several different speeds that allow data to be collected or played back at different rates. These different rates allow the operator to expand the data during the playback mode, so the information can be easily extracted.

H—LINE SCAN RECORDER

The line scan recorder is a Raytheon model number LSR-910M. This recorder is used mainly because it will accommodate an external sync that drives the recorder. The recorder paper speed can be set at a predetermined rate or can be driven by the speed of the vehicle. The sweep control is set to 40 msec so enough time is allocated for the selected channel to be printed (first 20 msec) and is allocated for the planned view (second 20 msec) to be printed.

APPENDIX C

VOID-SIZING ALGORITHM TEST DATA

This appendix contains the results of experiments made to determine the accuracy of the void-sizing algorithm. The controlled experiments performed on-site at the Gulf Applied Research facility produced the best tests for the prediction accuracy of the void thickness curves generated via the void signal model. In the controlled environment of the laboratory the void sizes could be varied by small, accurate increments, and the actual return data could be compared to predicted values from the curves obtained from the void signal modeling program.

WET SILTY CLAY BASE MATERIAL

The first laboratory test configuration included a 48 in. by 48 in. by 5.75 in. slab of portland cement concrete (PCC) and a mixture of wet, silty clay. The wet clay was used as the base material, and the concrete slab was placed over it with a carefully measured air gap in between to simulate the air void. The wet clay base material was made thick enough so that the return from the bottom of the clay did not interfere with the returns

from the top and bottom of the void. A thin sheet of plastic, which is transparent to the radar pulse, was placed over the wet clay to keep the clay from sticking to the bottom of the concrete as the concrete slab was lifted off the clay to produce the void. The radar antenna was placed close enough to the concrete slab so that the dimensions of the slab were large enough to eliminate any fringing effects at the edges of the concrete. The concrete slab was raised from resting on the silty clay surface in small increments to a maximum height of 1.5 in. off the surface of the silty clay. The radar returns were recorded on ¼-in. magnetic tape and then transformed into a digital data file for the IBM PC AT using the current Gulf Applied Research RDAS (Radar Data Acquisition System) unit. Samples of the output waveforms from the laboratory tests are provided in Appendix H of this report.

To simulate the laboratory test conditions, the signal modeling program, SIGMOD, was provided with the following test configuration parameters:

Pavement attenuation =	34 dB/m
Void attenuation =	0 dB/m
Pavement thickness =	5.75 in.
Pavement dielectric constant =	14
Void dielectric constant =	1
Clay dielectric constant =	37

Several examples of the output waveforms from the void modeling program are shown in Appendix H of this report. The changes in amplitudes of the negative and positive return peaks were recorded for void sizes ranging from 0.1 in. to 2.4 in. in 0.1-in. increments (24 total runs). The amplitude versus void size curves are shown in Figures C-1 and C-2.

The magnitude of the negative peak monotonically increased for the first 12 runs of the void signal modeling program. The best least squares cubic fit for the data points of the curve is given as follows:

$$y = 0.461504\,x^3 - 1.622874\,x^2 + 1.991878\,x - 0.03281505 \quad \text{(C-1)}$$

where y = radar return voltage amplitude (in volts), and x = void size in inches, 0.1 in. $\leq x \leq$ 1.2 in.

The magnitude of the positive peak monotonically increased for the first 9 runs of the signal modeling program. The best least squares cubic fit for the data points is given as follows:

$$y = 0.2766683\,x^3 - 1.65789\,x^2 + 2.101872\,x + 0.03738564 \quad \text{(C-2)}$$

where y = radar return voltage amplitude (in volts), and x = void size in inches, 0.1 in. $\leq x \leq$ 0.9 in.

To compare the output of the amplitude curves with the radar data it was necessary to remove the DC offset from the digitized radar return. The RDAS contains a 12-bit A/D converter which quantizes the analog signal to 4096 levels. The converter will accept a 10-volt peak-to-peak analog input where −5 volts is mapped to level 0 and +5 volts is mapped to level 4096. Therefore, a pseudo ground level occurs at value 2048, which appears to be a DC offset in the signal when the raw waveform is plotted. In order to compare the amplitudes of peaks in the actual radar return with predicted values from the amplitude and void size curves it is necessary to remove this offset. Also, the RDAS

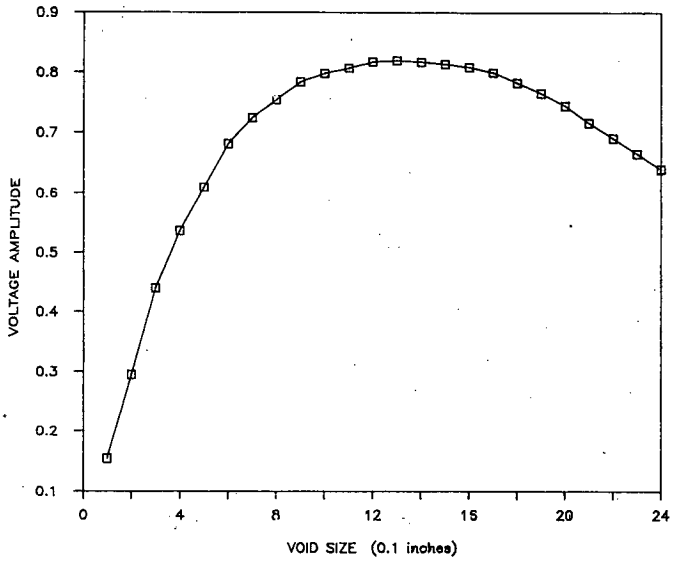

Figure C-1. Negative peak versus void size curve for wet silty clay base material.

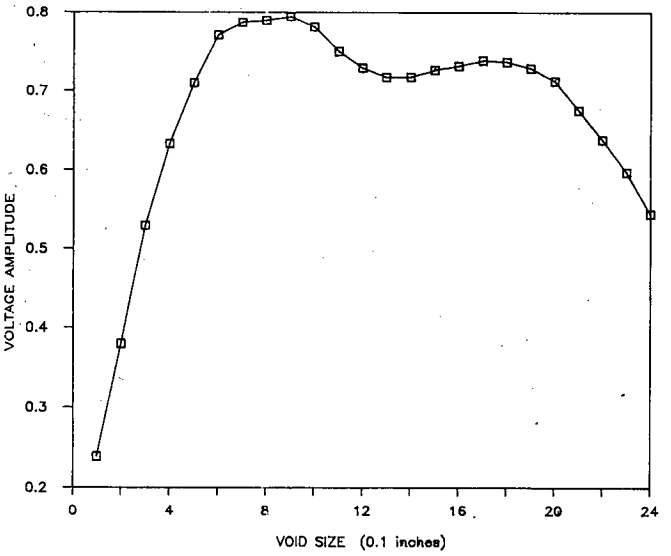

Figure C-2. Positive peak versus void size curve for wet silty clay base material.

contains a gain control that allows the operator to adjust the color pattern shown on his monitor. This gain must be compensated for in order to compare the two waveforms.

The solution to calibrating the radar signal for comparison with the computed values was to make the actual data match the predicted values for one of the void sizes. A window was first placed around the calibration void return in the radar signal, and the DC offset was removed from the waveform in the window as shown in Figures C-3 and C-4. The amplitude of the peaks in the window was measured and the multiplicative calibration constant required to make the projected value from

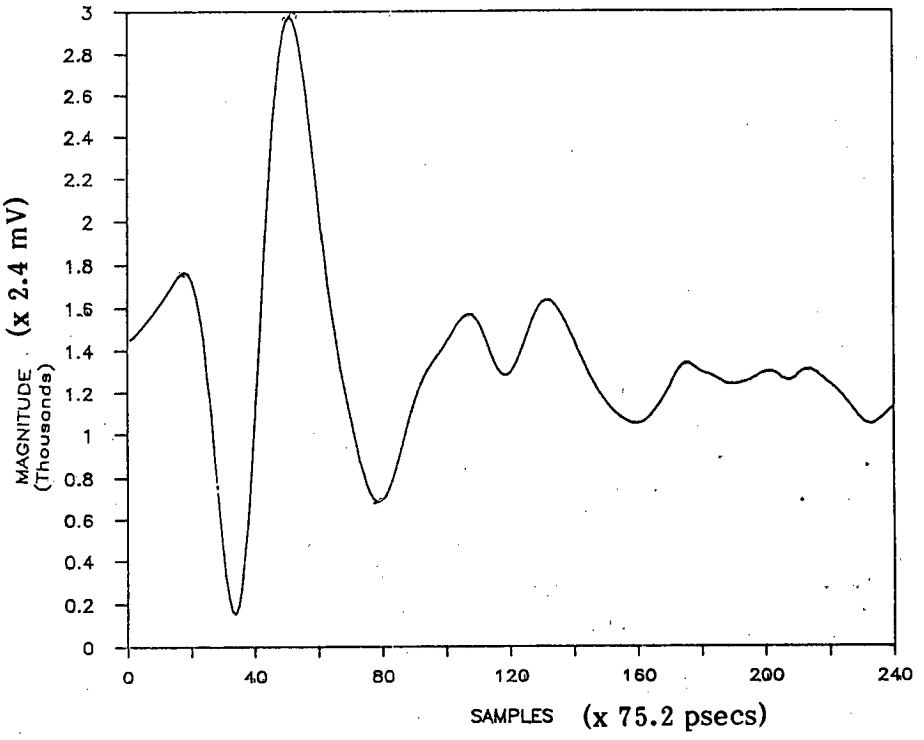

Figure C-3. Radar return waveform.

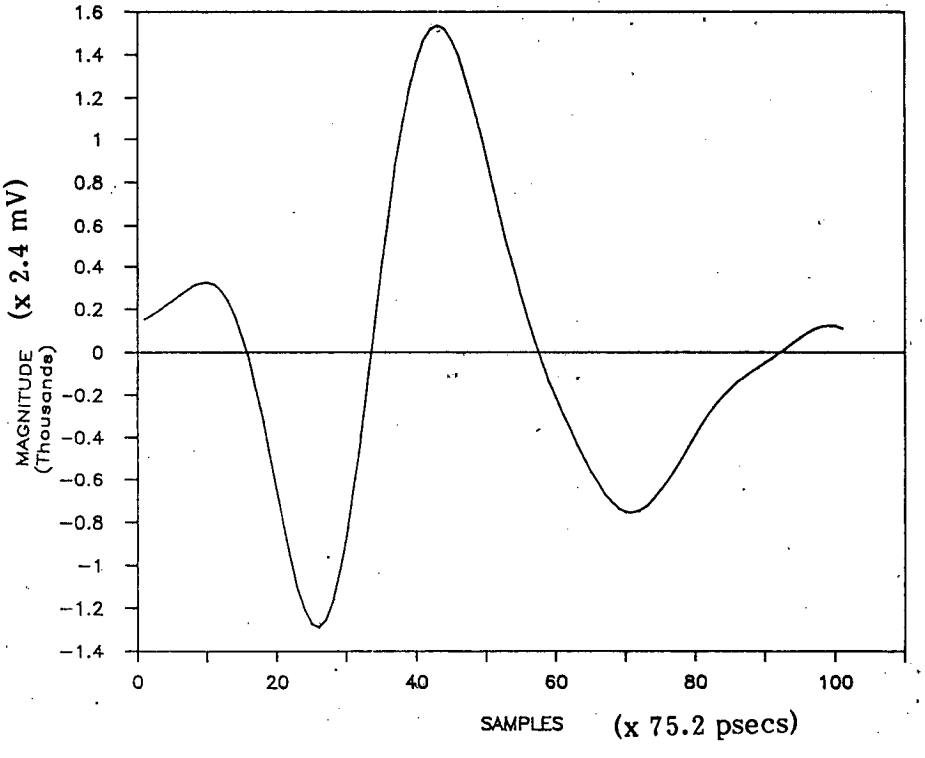

Figure C-4. Windowed void return with DC offset removed.

the amplitude and void size curves equal the actual value was computed:

Actual Radar Peak = Calibration Constant × Predicted Value

A separate calibration constant was computed for both the negative and positive peaks based on the ⅛-in. void return. These calibration constant multipliers were then used to compensate for payment attenuation and RDAS gain control for the rest of the void return peaks.

However, during the data analysis process it was found that in many cases it was difficult to determine precisely where the zero voltage level was in the radar window because of the undulations of the radar return. Therefore, to ensure that a small DC offset in the radar window did not affect the accuracy of the amplitude/void size curve predictions, the difference in amplitude between the positive and negative peaks was computed and compared to the actual data. Again, a calibration constant for the ⅛-in. void was computed to make the projected difference between positive and negative peaks fit the actual data for one void.

Once the actual peak values have been made to fit the predicted amplitude curves for the first void, the evaluation process of the amplitude curves involves simply seeing how well the actual values match the predicted curve. The results of this analysis for the laboratory wet silty clay data are provided in Table C-1. A graphical comparison of the predicted and actual peak values is given in Figures C-5 and C-6.

For void sizes greater than 2.2 in., the separation between the negative and positive peak returns, rather than the amplitudes of these returns, is required to predict void size. The linear portion of the time between the peaks versus void size curve corresponded to runs with greater than 2.2-in. separation. A graphical representation of the time separation between the positive and negative peaks is shown in Figure C-7. The least squares best line fit to the data points is given as follows:

$$y = 262.0993\text{E-}12\ x - 286.207\text{E-}12 \qquad \text{(C-3)}$$

where, y = separation time between peaks in picoseconds, and x = void size in inches, $x > 2.2$ in.

However, the reader should note that NCHRP Project 10-14 provided a thorough documentation of the algorithm's ability to predict large void sizes. The emphasis of this project has been focused on smaller void sizes; therefore, no data were compared with this predicted curve. The curve was computed for completeness of the algorithm and to determine the switch point where the curve could be used to predict void size.

DRY SAND BASE MATERIAL

The second laboratory configuration consisted of the same 48 in. by 48 in. by 5.75 in. slab of portland cement concrete (PCC) and a dry sand that was used as the base material. Again, the concrete slab was placed over the sand with a carefully measured air gap in between to simulate an air void. The sand base material was made thick enough so that the return from the bottom of the sand did not interfere with the returns from the top and bottom of the void. The radar antenna was placed close enough to the concrete slab so that the dimensions of the slab were large enough to eliminate any fringing effects at the edges of the concrete. This configuration was used to model the ¾-in. and 1½-in. void sizes that were encountered in the Florida test lane.

Table C-1. Results of void sizing algorithm for wet silty clay base material.

VOID SIZE		ACTUAL VALUE	PREDICTED VALUE	CALIBRATION CONSTANT	% ERROR
1/8"	POSITIVE PEAK	943.75	943.75	3434.86	-
	NEGATIVE PEAK	-328.25	-328.25	1712.2	-
	PEAK TO PEAK	1272.0	1272.0	2726.87	-
1/4"	POSITIVE PEAK	984.23	1592.3	-	61.8
	NEGATIVE PEAK	-422.77	-635.12	-	50.2
	PEAK TO PEAK	1407.0	2275.56	-	61.7
3/8"	POSITIVE PEAK	1114.8	2085.1	-	87.03
	NEGATIVE PEAK	-535.2	-857.86	-	60.3
	PEAK TO PEAK	1650.0	2361.3	-	43.1
1/2"	POSITIVE PEAK	1157.9	2433.4	-	110.16
	NEGATIVE PEAK	-625.1	1053.2	-	68.48
	PEAK TO PEAK	1783.0	3609.1	-	102.4
3/4"	POSITIVE PEAK	1291.9	2740.8	-	112.1
	NEGATIVE PEAK	-818.1	1272.04	-	55.49
	PEAK TO PEAK	2110.0	4201.75	-	99.14

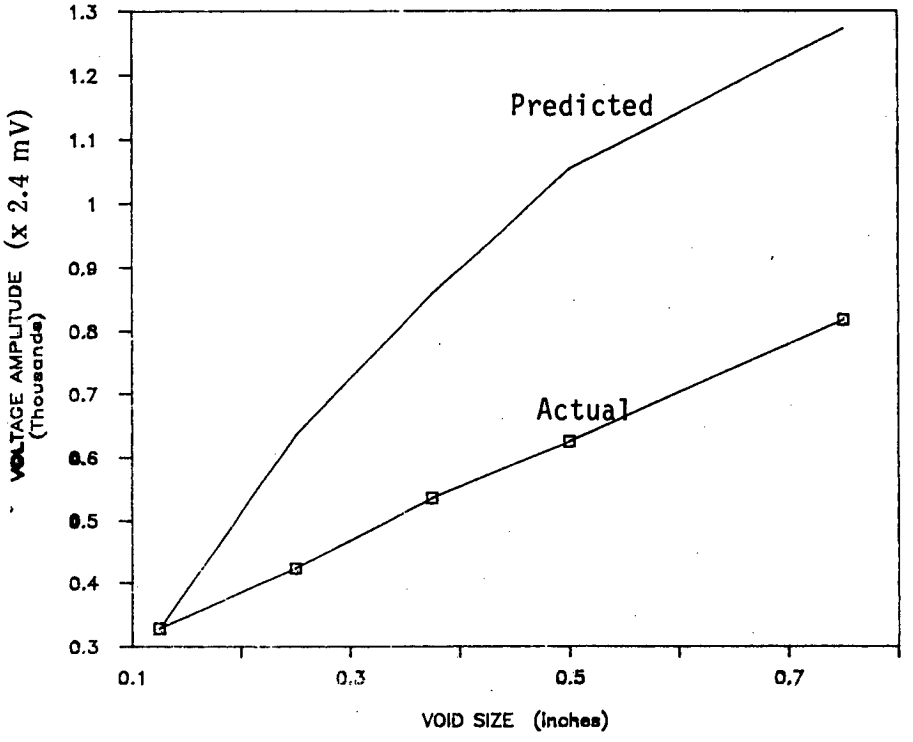

Figure C-5. Actual vs. predicted negative peak for wet silty clay base material.

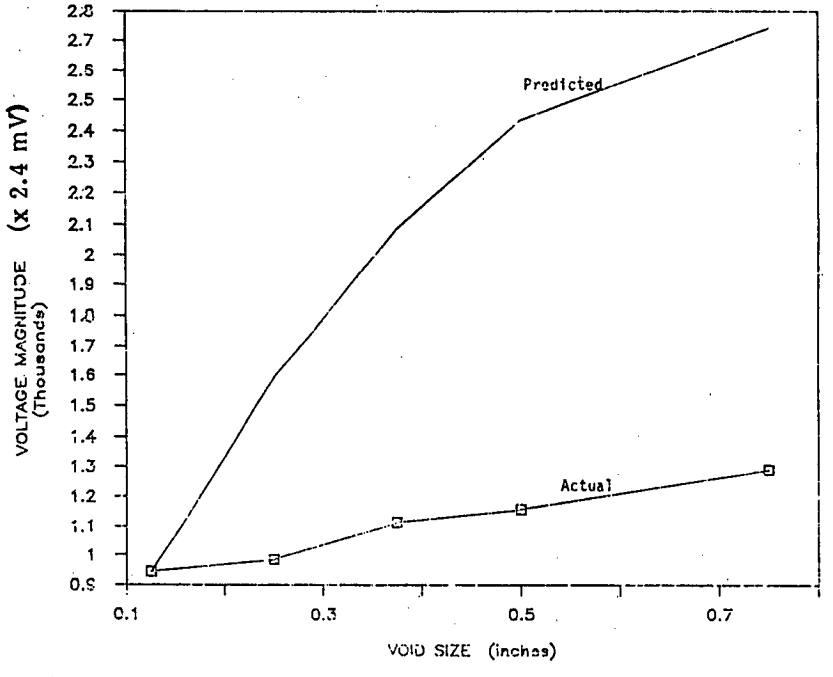

Figure C-6. Actual vs. predicted positive peak for wet silty clay base material.

To simulate these test conditions the signal modeling program, SIGMOD, was provided with the following test configuration parameters:

Pavement attenuation = 34 dB/m
Void attenuation = 0 dB/m
Pavement thickness = 5.75 in.
Pavement dielectric constant = 14
Void dielectric constant = 1
Sand dielectric constant = 4

Once again the output waveforms from the void modeling program were used to produce a set of amplitude and peak separation versus void size curves. The amplitude curves are shown graphically in Figures C-8 and C-9.

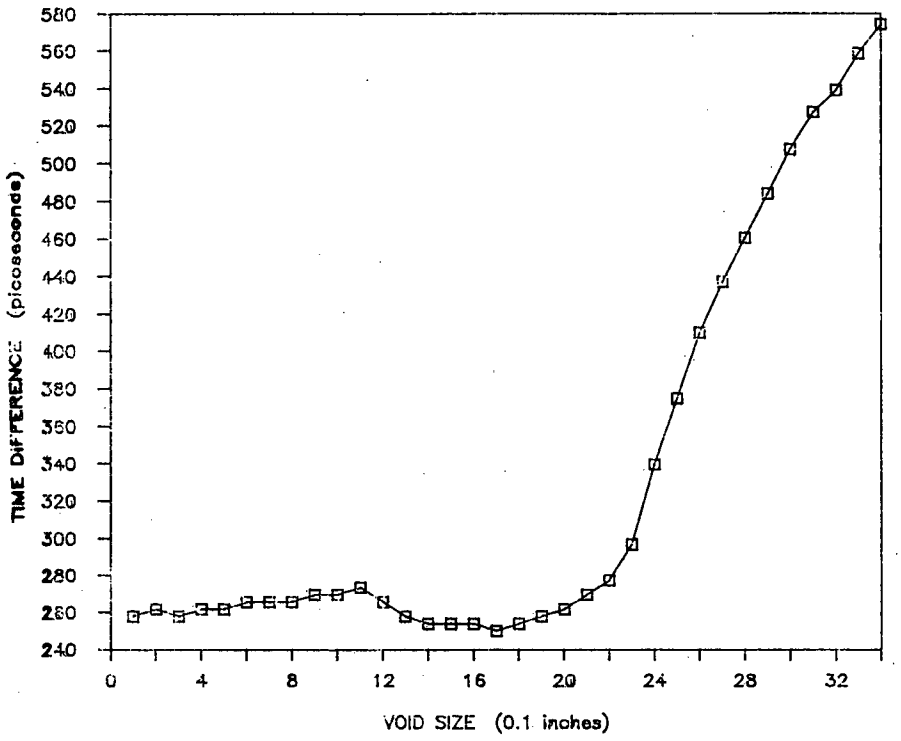

Figure C-7. Time separation between peaks for wet silty clay base material.

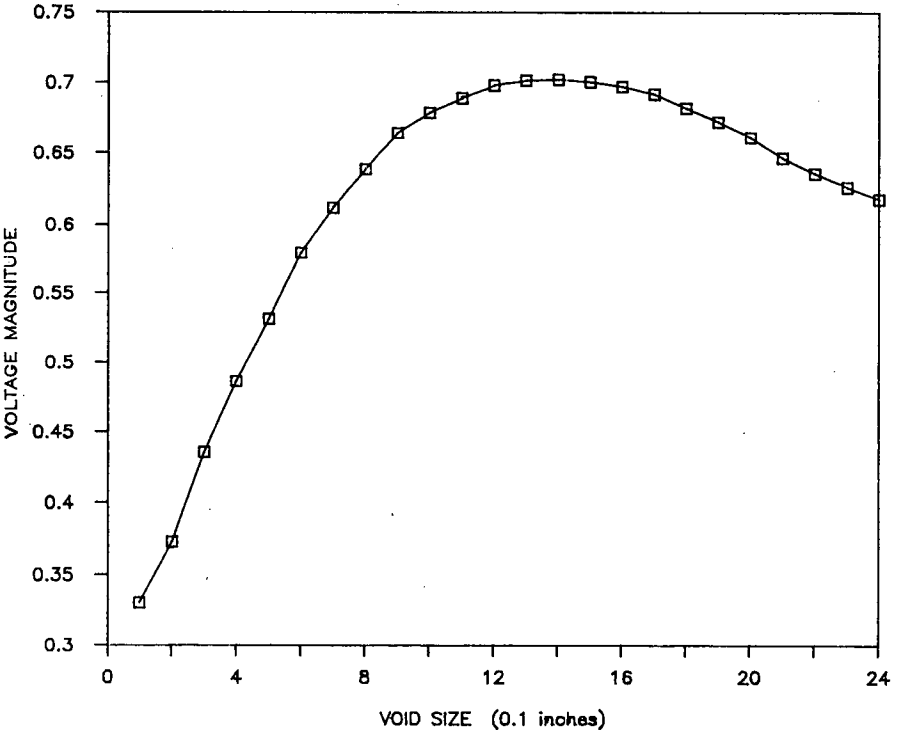

Figure C-8. Negative peak versus void size curve for dry sand base material.

The magnitude of the negative peak monotonically increased for the first 14 runs of the signal modeling program. The best least squares cubic fit for the data points of the curve is given as follows:

$$y = -0.01392801\,x^3 - 0.2364427\,x^2 + 0.6734927\,x + 0.2573286 \quad \text{(C-4)}$$

where y = radar return voltage amplitude in volts, and x = void size in inches, 0.1 in. $\leq x \leq$ 1.4 in.

The magnitude of the positive peak monotonically increased for the first 16 runs of the signal modeling program. The best least squares cubic fit for the data points is given as follows:

$$y = 0.09239492\,x^3 - 0.4906964\,x^2 + 0.8210303\,x + 0.08906468 \quad \text{(C-5)}$$

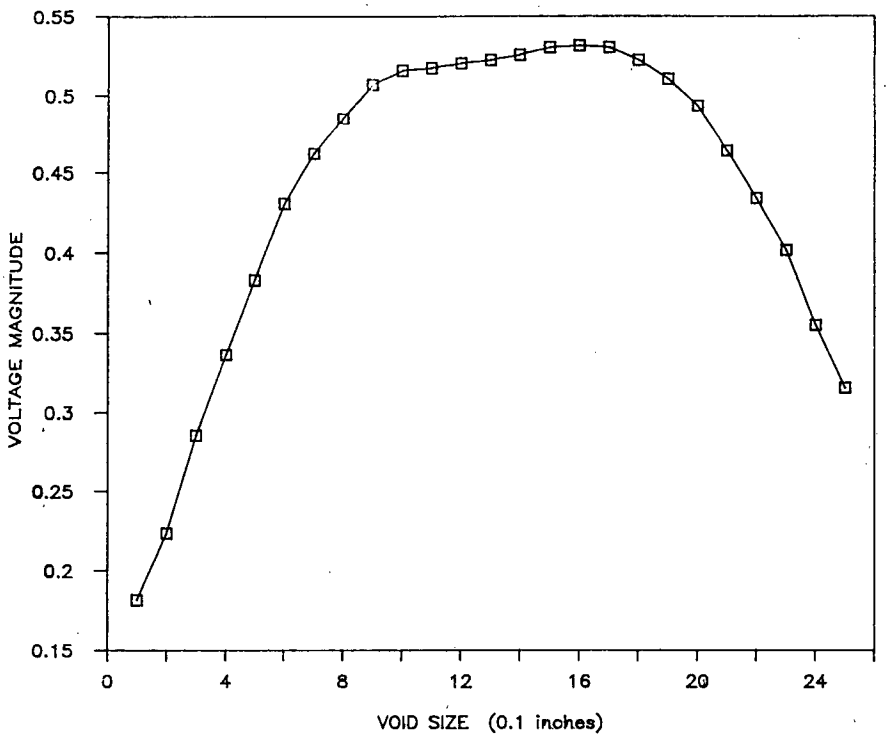

Figure C-9. Positive peak versus void size curve for dry sand base material.

where y = radar return voltage amplitude in volts, and x = void size in inches, 0.1 in. $\leq x \leq$ 1.6 in.

The comparison of the predicted values from the peak amplitude and void size curves with the actual measured data was accomplished by first removing the DC offset caused by the RDAS A/D converter from the digitized radar return. Next, the measured radar signal amplitude was calibrated with the projected values to make the actual data equal the predicted values for the no-void case. A calibration constant was computed which caused the negative peak of the no-void return from the signal modeling program to match the negative peak for the no-void return case from the radar signal. The results of the analysis with the laboratory sand data are provided in Table C-2. Notice that the positive peak amplitude curve was the only void sizing curve that could be used to examine the 1½-in. void.

The separation between peaks was determined to be a valid measure of void size for voids larger than 1.9 in. The corresponding curve is shown graphically in Figure C-10. The best least squares line fit to the linear portion of the curve is given below:

$$y = 78.12501\text{E-}12\ x + 112.7233\text{E-}12 \qquad \text{(C-6)}$$

where y = separation between peaks in picoseconds, and x = void size in inches, $x > 1.9$ in.

FLORIDA TEST LANE DATA

The void sizing program was also analyzed with data obtained from the void test lane at the Florida DOT's Materials and Research Laboratory in Gainsville, Florida. This test lane is comprised of a 9-in. thick PCC pavement surface with a sand subgrade. During the measurements taken by the RODAR system it was determined from the polarity of the no-void return that the sand subgrade contained water. The lane contains accurately measured ¾-in. and 1½-in. voids, which were formed from styrofoam blocks imbedded in the concrete.

The void signal modeling curves were generated from the following input parameters to the SIGMOD program:

Pavement attenuation	= 34 dB/m
Void attenuation	= 0 dB/m
Pavement thickness	= 9 in.
Pavement dielectric constant	= 14
Void dielectric constant	= 1
Wet sand dielectric constant	= 26

(The value for the dielectric constant of wet sand was obtained from previous measurements made by Dr. Glenn Smith of the School of Electrical Engineering at the Georgia Institute of Technology, a technical consultant for Gulf Applied Research.) The changes in amplitude of the negative and positive return peaks were recorded for void sizes ranging from 0.1 in. to 2.4 in. in 0.1-in. increments. The amplitude versus void size curves are shown in Figures C-11 and C-12.

The magnitude of the negative peak monotonically increased for the first 12 runs of the void signal modeling program. The best least squares cubic fit for the data points of the curve is given as follows:

$$y = 0.455044\ x^3 - 1.592589\ x^2 + 1.958275\ x - 0.03893512 \qquad \text{(C-7)}$$

where y = radar return voltage amplitude in volts, and x = void size in inches, 0.1 in. $\leq x \leq$ 1.2 in.

Table C-2. Results of void sizing algorithm for dry sand base material.

NO VOID CASE:

	ACTUAL VALUE	PREDICTED VALUE FROM MODEL	CALIBRATION CONSTANT
POSITIVE PEAK	33.33	.16731	199.21
NEGATIVE PEAK	-253.33	-.315498	802.964
PEAK TO PEAK	286.66	.48281	593.73

3/4" VOID CASE:

	ACTUAL VALUE	PREDICTED VALUE FROM MODEL	% ERROR
POSITIVE PEAK	46.33	93.1904	101.1
NEGATIVE PEAK	-336.67	-500.7068	48.7
PEAK TO PEAK	382.99	647.98	69.2

1-1/2" VOID CASE:

	ACTUAL VALUE	PREDICTED VALUE FROM MODEL	% ERROR
POSITIVE PEAK	104.8	105.26	0.44

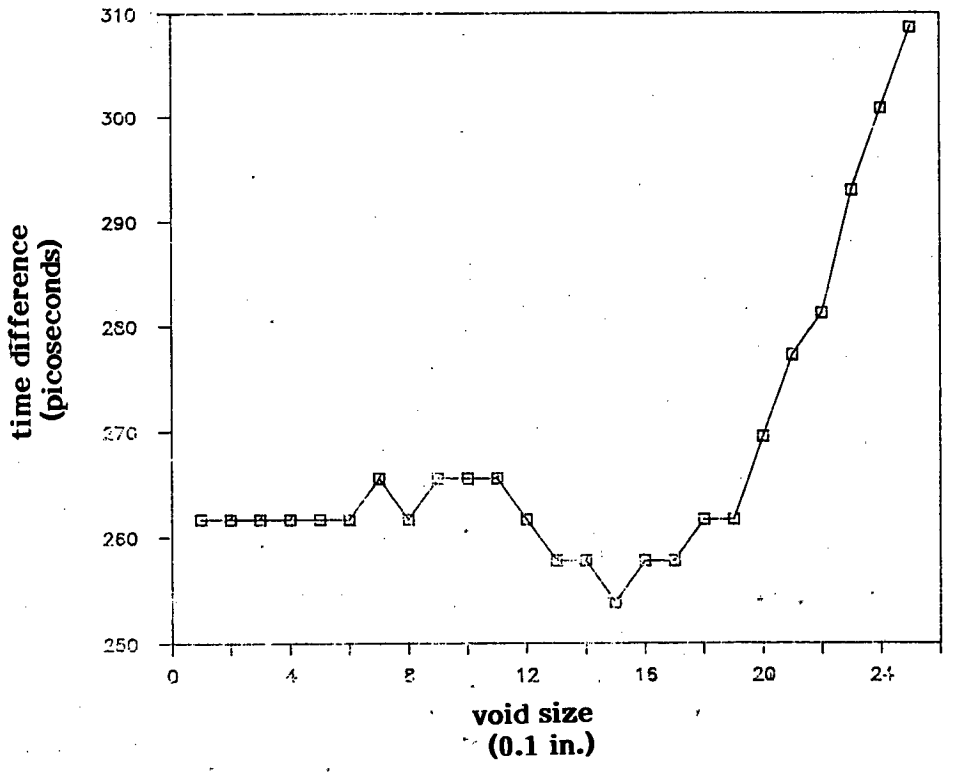

Figure C-10. Time separation between peaks for dry sand base material.

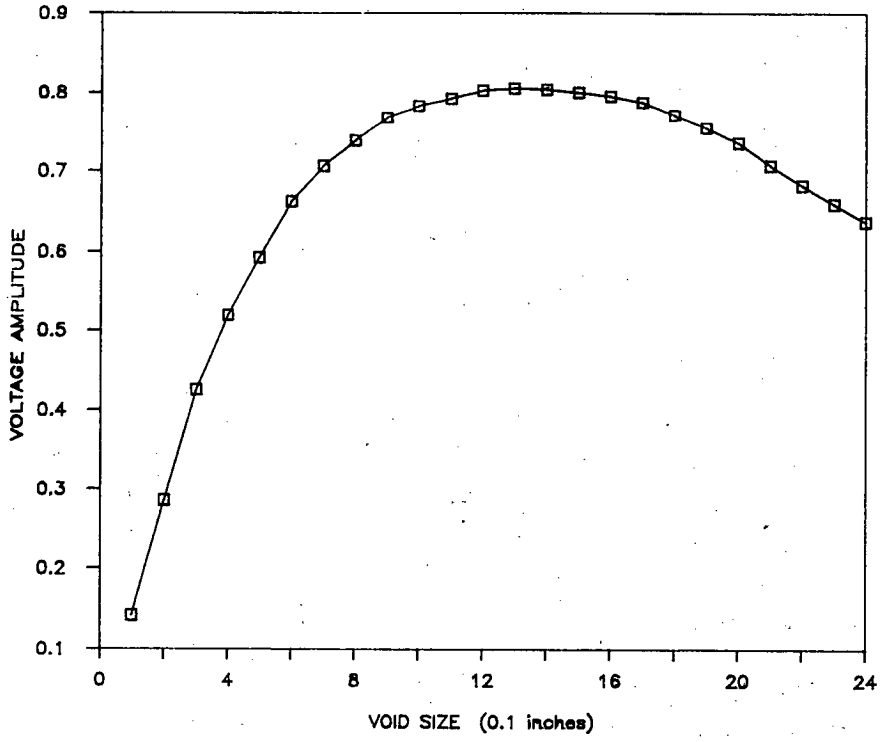

Figure C-11. Negative peak versus void size for wet sand base material.

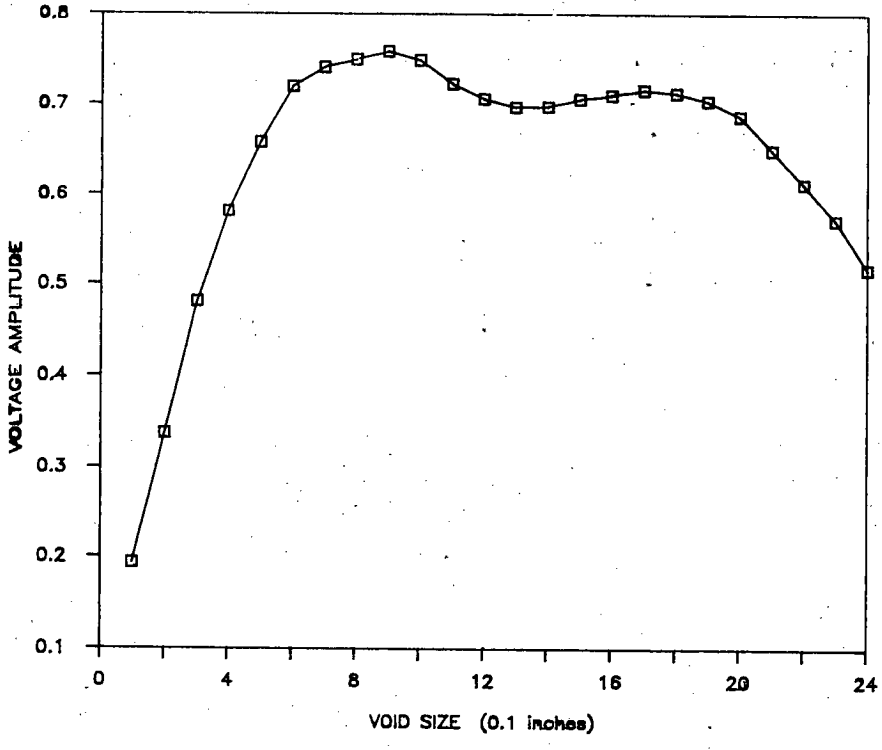

Figure C-12. Positive peak versus void size for wet sand base material.

The magnitude of the positive peak monotically increased for the first nine runs of the signal modeling program. The best least squares cubic fit for the data points of the curve is given as follows:

$$y = 0.449154\,x^3 - 1.825932\,x^2 + 2.130846\,x - 0.008395502 \quad \text{(C-8)}$$

where y = radar return voltage amplitude in volts, and x = void size in inches, 0.1 in. $\leq x \leq$ 0.9 in.

The predicted curves were calibrated to the actual return data by determining the calibration multiplier which forced the output from the signal modeling curves to equal the actual return data for the no-void case. The results of the comparison of the predicted values with the actual values for the ¾-in. void are

given in Table C-3. Notice that the 1½-in. void can not be determined by any of the void sizing curves. The 1½-in. void falls in a void size gap that exists between the reliable range of amplitude versus void size curve and the reliable range of separation between peaks versus void size curves.

The separation between peaks was determined to be a useful measure of void size for voids larger than 2.1 in. The corresponding curve is shown graphically in Figure C-13. The best least squares line fit to the linear portion of the curve is given below:

$$y = 214.8682\text{E-}12\ x - 187.5533\text{E-}12 \qquad \text{(C-9)}$$

where y = separation between peaks in picoseconds, and x = void size in inches, $x > 2.1$ in.

Table C-3. Results of void sizing for algorithm test lane, Florida wet sand base material.

NO VOID:

	ACTUAL VALUE	PREDICTED VALUE FROM MODEL	CALIBRATION CONSTANT
POSITIVE PEAK	806.74	.1597	5051.896
NEGATIVE PEAK	-1123.25	-.0847	13261.5
PEAK TO PEAK	1929.99	.2444	7896.85

3/4" VOID:

	ACTUAL VALUE	PREDICTED VALUE FROM MODEL	% ERROR
POSITIVE PEAK	501.2285	3799.73	658.1
NEGATIVE PEAK	-1348.77	-9626.69	613.7
PEAK TO PEAK	1849.999	11671.94	530.9

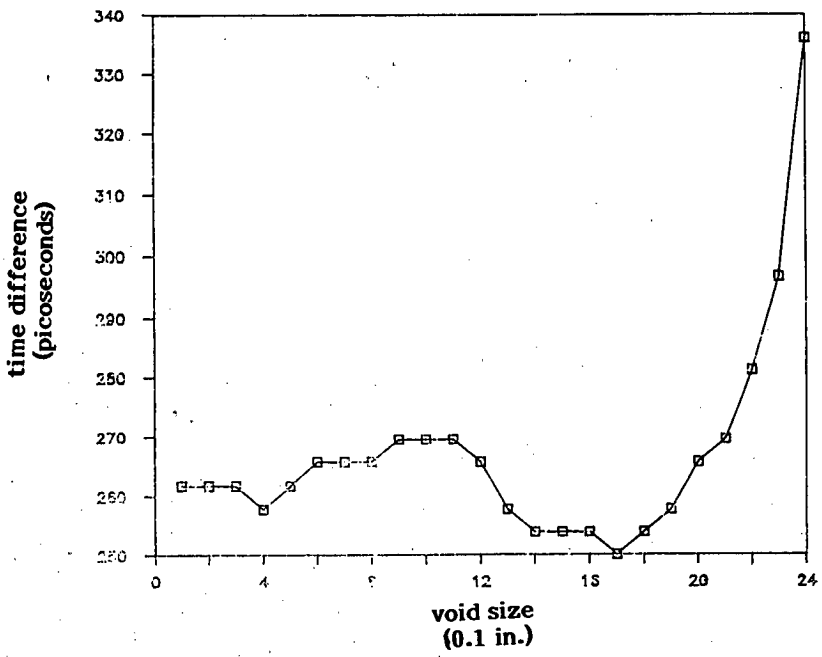

Figure C-13. Time separation between peaks for wet sand base material.

APPENDIX D

DEVELOPMENT OF THE SURFACE ANOMALY DETECTION ALGORITHM

DEVELOPMENT TOOLS

To conduct this portion of the research effort, Gulf Applied Research purchased a board-level video digitizer and display module that is plug-compatible with the IBM Personal Computer. This hardware card captures a standard RS-170 or RS-330 video signal at a rate of 30 frames per second, stores the image in an on-board 512 by 512 by 4- or 8- bit frame memory, and simultaneously displays the stored image on an external monitor. In addition, an advanced, menu-driven software package containing a variety of image acquisition and processing functions developed for use with an IBM PC was purchased to operate the hardware card. Also, the image processing software was required to provide some of the common image processing functions used to enhance raw video data.

DESIGN

The identification of surface distress features in the video data requires the successful solution of two separate and distinct image processing problems: image feature enhancement and feature extraction.

The first process, image/feature enhancement, attempts to increase the separation in intensity between the desired feature and the surrounding background. Ideally, this process will assign distinct, readily identifiable boundaries to the desired feature, which correlate with the original boundaries of the feature in the raw video. Once the extent of the desired feature has been determined by image enhancement, the feature extraction process is required to identify and classify the surface distress. However, the image/feature enhancement process proved to be the more difficult of the two tasks because of the small size of the desired surface features and the lack of contrast between the surface distresses and the surrounding background in the raw input image.

The CRAKFIND program attempts to separate the cracks from the pavement by reducing the raw video data to a binary (black/white) image consisting of black cracks and white background. Each image is composed of a grid of small, discrete blocks of light called pixels, the intensities of which range from black (0) to white (255). A histogram of the pixel intensities in a frame can be performed by the image processing software package. Typically, the pixel intensity histogram exhibits a Gaussian shape with the peak of the distribution roughly corresponding to the background intensity. However, when surface distresses such as cracks, spalls, and popouts containing pixels darker than the surrounding background appear in the image, they tend to form a tail on the black end of the histogram as shown in Figure D-1. Therefore, a cutoff pixel intensity value can be found that separates the darker feature pixels from the lighter background. By setting pixels whose intensities are lower

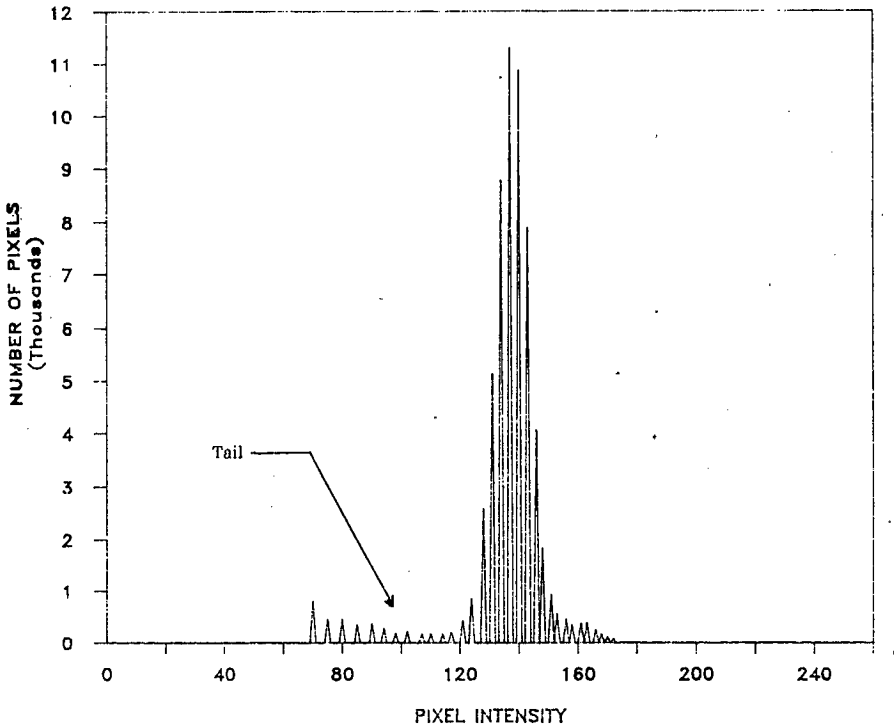

Figure D-1. Crack image histogram with black tail.

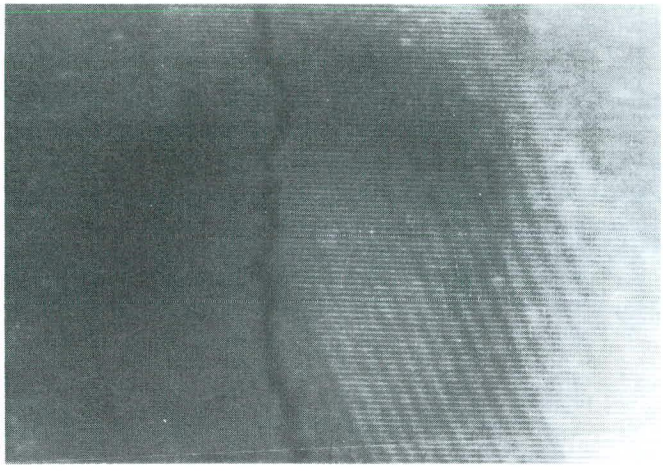

Figure D-2. Sample loading bay image.

Figure D-3. Sample loading bay image with a threshold of 3 standard deviations below the mean.

than the threshold to black (0), and the pixels whose intensities are higher than the threshold to white (255), a binary image is formed with black cracks on white background. This threshold detection approach has also been implemented in video pavement analysis systems proposed by the Arizona DOT and the Earth Technology Corp (see Refs. 4 and 5 of the main report).

Nonetheless, the value used as the pixel intensity threshold must be adaptable to variations in lighting and pavement color. Therefore, a statistical method for assigning the cutoff intensity was developed. The first step in calculating the threshold value is to compute the mean and standard deviation of the pixel intensities in the frame based on the histogram. The mean pixel intensity serves as a measure of the average background intensity. The cutoff value is then assigned by the operator in terms of the mean and standard deviation of the pixel intensities which make up the frame. During execution, the CRAKFIND program prompts the operator to enter the number of standard deviations below the mean intensity where the cutoff pixel intensity will be set. Once this cutoff is set, the program uses this value to produce the binary image. During program testing, a cutoff value of three standard deviations below the mean was found to produce the best results for the analyzed test data. However, the positioning of the threshold will require a calibration procedure prior to data analysis. Whether the data are analyzed in real time or off-line, an operator will be required to assign the cutoff value before the computer is allowed to take over the data analysis process.

This thresholding technique was performed on surface distress data obtained from a relatively clean loading bay apron located near the Gulf Applied Research (GAR) facility. A sample data frame from the loading bay is shown in Figure D-2. A threshold value of three standard deviations below the mean produced a well-defined silhouette of the desired features with very little background noise as shown in Figure D-3. The sensitivity of the output image to the choice of threshold value was examined by simply changing the number of standard deviations below the mean where the cutoff was set. As the number of standard deviations is decreased, the detected crack begins to widen and the amount of background speckle increases as more pixels in the raw data frame are mapped to black, as shown in Figure D-4. As the number of standard deviations is increased, the background becomes more noise-free and the crack begins to "wash-out" as shown in Figure D-5.

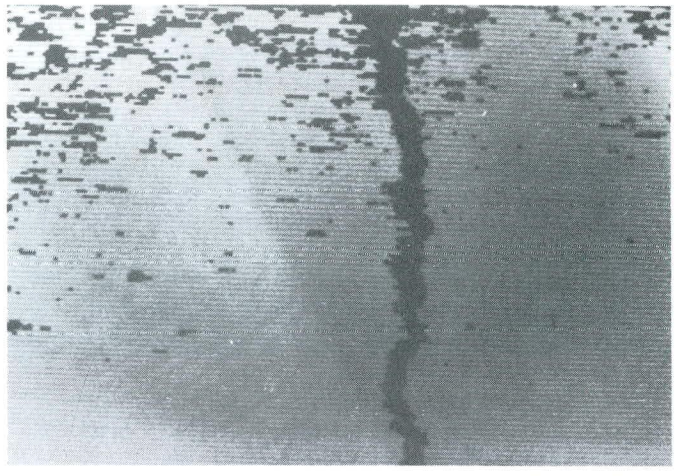

Figure D-4. Sample loading bay image with a threshold of 1 standard deviation below the mean.

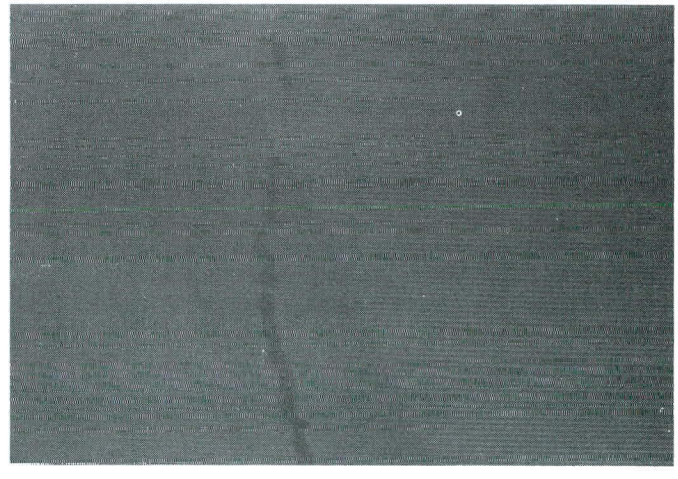

Figure D-5. Sample loading bay image with a threshold of 5 standard deviations below the mean.

However, in many cases, applying the thresholding to the raw video data did not produce the desired binary image. Particularly in test data taken from I-95 near Brunswick, Georgia, pavement coloring and lighting conditions did not provide the necessary separation between background and crack intensity for the reliable positioning of the threshold. The wheel paths of the highway road surface had been badly discolored by tire marks and the center of the lane contained black oil stains from the traffic. In addition, the road surface was illuminated by sunlight which varied greatly with the passing cloud cover, and the road surface itself was composed of concrete which contained a dark aggregate. All of these factors contributed in the reduction of the separation in pixel intensity between the darkened background and the desired surface features.

Therefore, the researchers concluded that feature enhancement of the raw video data is required to achieve the necessary contrast between the background and the desired surface features before application of the threshold. This increase in contrast reduces the sensitivity of the image to the exact choice of the threshold value. A number of enhancement techniques and their effectiveness in increasing the contrast in the test data were examined. Implementation of the techniques was simplified by using the menus of the image processing software package. The raw video frame could be processed by one of the software package programs and then saved to a disk file. The enhanced image in the hard disk file was then processed by the CRAKFIND program which applied the statistical threshold and then used the feature extraction techniques discussed later in this section to extract the desired surface distresses.

The enhancement testing phase required a method of evaluating the effectiveness of the enhancement techniques in increasing the intensity contrast between the background and the desired feature. A reasonable method of determining the effectiveness of an enhancement approach is to measure the change in the feature-to-background ratio, FBR, of the image before and after the application of the technique. The feature-to-background ratio is defined as follows:

$$\text{FBR} = 10 \log \left[\sqrt{E(x^2)} / \sqrt{E(n^2)} \right] \quad \text{(dB)} \quad \text{(D-1)}$$

where x = feature pixel intensity, n = background (noise) pixel intensity, and $E(\,)$ = expected value operator.

$E(n^2)$ can be rewritten using the following well-known identity:

$$E(n^2) = (E(n))^2 + \sigma_n^2 \quad \text{(D-2)}$$

where σ_n = standard deviation of the background pixel intensities.

Also, by approximating the expected value operator with the sample mean, Eq. D-2 can be written as:

$$E(n^2) = \mu_n^2 + \sigma_n^2 \quad \text{(D-3)}$$

where μ_n = average background pixel intensity.

Now, by substituting Eq. D-3 into Eq. D-1, the feature-to-background ratio, FBR, can be rewritten as:

$$\text{FBR} = 10 \log \left[\sqrt{E(x^2)} / \left(\sqrt{\mu_n^2 + \sigma_n^2} \right) \right] \quad \text{(dB)} \quad \text{(D-4)}$$

In order for a pixel to be labeled a feature pixel by the CRAKFIND program, the pixel must possess an intensity of:

$$x \leq \mu_p - T\sigma_p \quad \text{(D-5)}$$

where μ_p = average pixel intensity in the image, σ_p = standard deviation of the intensities in the image, and T = number of standard deviations below the mean where the threshold is set.

Because the intensity of the desired feature is lower in magnitude than the surrounding background, the most effective enhancement approach will minimize the feature-to-background ratio. In addition to a small FBR, the image enhancement technique should provide a maximum value for T. A large value for T serves to reduce the amount of background noise which is mapped to black by the chosen threshold. If the background noise is considered to be Gaussian, the amount of background which enters the image for a given threshold can be determined using a table of values for the standard normal distribution curve. For example, if a threshold is chosen at one standard deviation below the mean, approximately 84.1 percent of the background will be removed from the threshold image. Therefore, the higher the value for T, the more area of the normal distribution curve is excluded form being mapped to black. A clean, low-noise image is desired to reduce the possibility of confusing the feature extractor and falsely identifying background noise as a surface feature. In addition, a less cluttered image reduces the amount of processing time required to identify the desired surface features.

A program was written to compute the FBR in a rectangular region (10 pixels by 17 pixels) of the image which contains both crack and background. The operator is required to choose the region of the image and specify explicitly which pixels in the region belong to the crack and which pixels belong to the background. The FBR program calculates the feature-to-background ratio directly from the definition (Eq. D-1), using the sample mean in place of the expected value operator. The pixels that belong to the crack in the specified region were identified using the PIXEL FINDER and AREA PLOT functions in the image processing software menu.

In addition to the FBR calculations, the mean and standard deviation of the background were gathered using the built-in image processing software routines. To accomplish this, an Area Of Interest (AOI) containing only background was specified by the operator. Next, the HISTOGRAM function in the menu was called to produce the statistics of the specified region of the background. The HISTOGRAM function was also used to calculate the mean, μ_p, and standard deviation, σ_p, of the entire image.

The ability to calculate the FBR for a portion of the image and record the maximum value of T which provided detection of the crack by the CRAKFIND program provided criteria for evaluating and determining the most effective crack enhancement technique. In this application, the most effective technique was defined to be the one which produced a minimum feature-to-background ratio and a maximum number of standard deviations below the mean for positioning the threshold which still produced detection of the surface distress. A number of feature enhancement approaches were implemented with algorithms from the image processing software package and their performances were compared against the given criteria.

The evaluation process for the feature enhancement approaches involved using three "test images" which would be

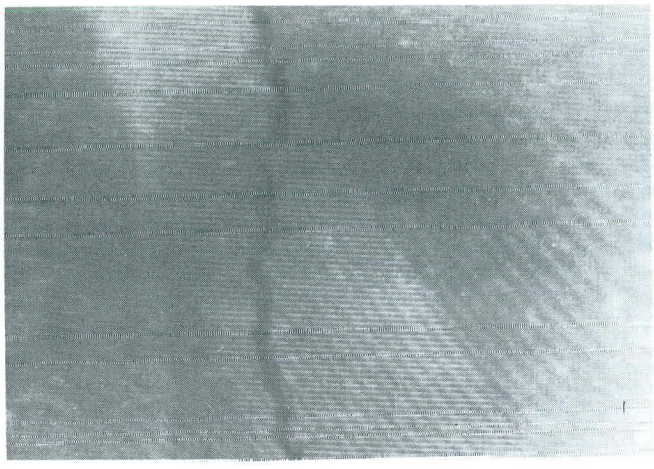

Figure D-6. Test image 1.

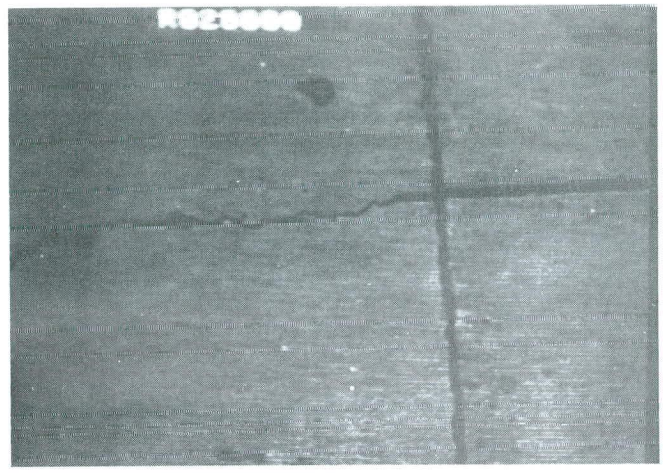

Figure D-7. Test image 2.

processed by each of the enhancement systems. The FBR of the unprocessed, raw test image was computed using the FBR program described above for a 10 by 17 pixel box centered around a portion of the crack in the image. Each enhancement system was applied to the image in turn, and the resultant FBR of the output image was computed for the same box of 10 by 17 pixels each time. The FBR's of the output images were compared with each other and with that of the raw image to determine which enhancement system produced the best results.

The first test image is shown in Figure D-6. This single longitudinal crack was obtained from the relatively clean concrete pavement of the loading bay apron behind the GAR facility. The box of pixels chosen for calculation of the FBR of the image extended from pixel 110 to pixel 127 in the transverse (horizontal) dimension and pixel 56 to pixel 66 in the longitudinal (vertical) dimension. The pixel in the top, left-hand corner of the image is transverse pixel 1 and longitudinal pixel 1. The pixel in the bottom, right-hand corner of the image is transverse pixel 255 and longitudinal pixel 240.

The second test image is shown in Figure D-7. This picture of a longitudinal and transverse crack was also obtained from the loading bay apron behind the GAR facility. The FBR pixel box for this image ranged from pixel 165 to pixel 182 in the horizontal dimension and from pixel 122 to pixel 132 in the vertical dimension.

The third test image is shown in Figure D-8. This image was obtained from road surface data taken on highway I-95 outside of Brunswick, Georgia. This picture was a calibration image of various size cracks taken before the RODAR™ vehicle began moving over the road surface. The FBR pixel box for this image extended from pixel 70 to pixel 87 in the horizontal dimension and from pixel 111 to pixel 121 in the vertical dimension.

The statistics of the raw, unprocessed test images are presented in Table D-1. The effectiveness of the enhancement techniques in enhancing the test images will be determined by observing the improvement in the statistics of the images. Again, the ideal enhancement technique will minimize the feature-to-background ratio and maximize the value of T which still provides detection of the desired surface features by the CRAKFIND feature extractor.

A block diagram of the first enhancement system evaluated is shown in Figure D-9. The system is composed of two channels,

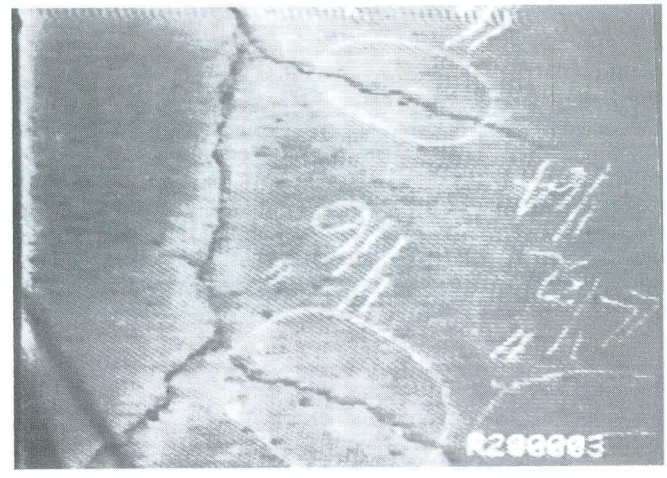

Figure D-8. Test image 3.

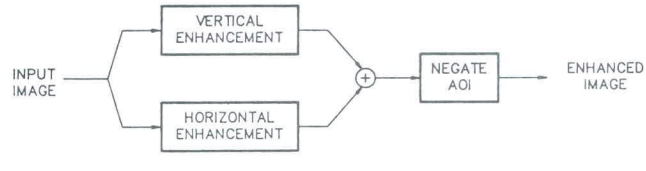

Figure D-9. Enhancement configuration 1.

one of which enhances features oriented vertically in the frame and the other of which enhances horizontal features. The system is provided with two copies of the raw, unprocessed video which are passed to both channels of the system. The VERTICAL ENHANCEMENT component of the enhancement system is a software package subroutine which performs a 5 × 3 convolution to enhance vertical lines in the image. The convolution kernel used is shown below:

Table D-1. Unprocessed test image statistics.

	FBR(dB)	μ_p	σ_p	μ_n	σ_n	MAXIMUM T
TEST IMAGE 1	-.3908016	228.62	6.31	230.43	3.91	6
TEST IMAGE 2	-2.601917	126.13	16.82	125.49	5.89	7
TEST IMAGE 3	-1.2334	136.30	17.83	144.18	8.73	1

$$\begin{matrix} 1 & 0 & -1 \\ 1 & 0 & -1 \\ 1 & 0 & -1 \\ 1 & 0 & -1 \\ 1 & 0 & -1 \end{matrix}$$

The HORIZONTAL ENHANCEMENT component is a software package subroutine which performs a convolution to enhance horizontal lines using the kernel shown below:

$$\begin{matrix} 1 & 1 & 1 & 1 & 1 \\ 0 & 0 & 0 & 0 & 0 \\ -1 & -1 & -1 & -1 & -1 \end{matrix}$$

Once the vertically and horizontally enhanced images have been generated, they are summed together to produce one image. The output of the edge enhancers is a portrayal of white enhanced cracks on a dark background. To prepare the enhanced image for input into the CRAKFIND algorithm, it is necessary to provide the NEGATE AOI intermediate step which inverts the intensities to produce dark enhanced features on a light background.

This enhancement configuration was applied to the three "test images". The resultant processed versions of the test images are shown in Figures D-10 through D-12. The statistics of the output images are tabulated and given in Table D-2. In comparing Tables D-2 and D-1, one should note that the feature-to-background ratio has decreased in all of the processed images, indicating a desirable increase in the separation between background pixel intensities and crack pixel intensities. However, the standard deviation of the background pixel intensities, σ_n, has also increased, which is an undesirable feature of the enhancement technique. It is important to keep in mind that all edge detectors will to some degree enhance spurious, speckle noise in the image. The maximum allowable value for T for the unprocessed test image 1 was 6. The maximum value for T, which still provided detection of the surface distress, for the processed test image 1 was 3. Obviously, this is a step in the wrong direction for enhancing the crack as far as the feature extractor is concerned. Again, this is because of the undesirably large increase in background standard deviation in comparison with the acquired decrease in feature-to-background ratio. In addition, the convolution kernels used in the VERTICAL and HORIZONTAL ENHANCEMENT subroutines are 5 pixels long. This means that to achieve maximum enhancement in the convoluted output image, the sections of the cracks in the input

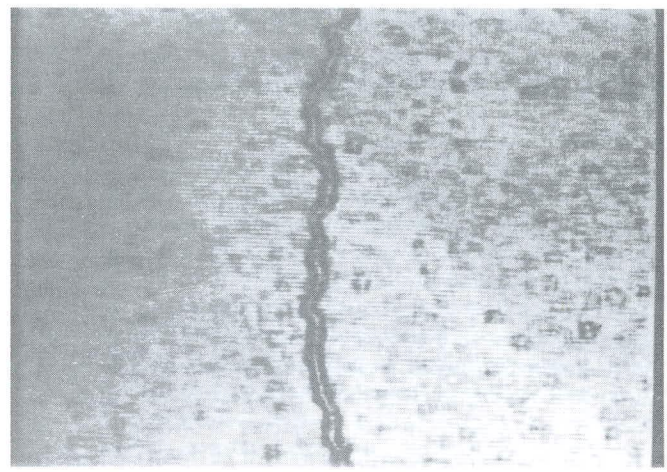

Figure D-10. Test image 1 enhanced with enhancement configuration 1.

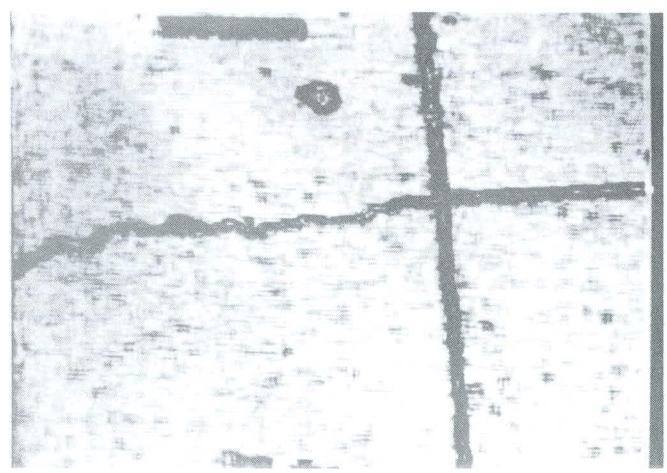

Figure D-11. Test image 2 enhanced with enhancement configuration 1.

Table D-2. Results of enhancement configuration 1 on test images.

	FBR(dB)	μ_p	σ_p	μ_n	σ_n	MAXIMUM T
TEST IMAGE 1	-1.174316	230.63	37.92	239.88	13.10	3
TEST IMAGE 2	-8.561419	206.96	57.57	221.99	21.10	3
TEST IMAGE 3	-2.3948	213.67	45.51	230.71	16.43	2

image must be perfectly vertical or perfectly horizontal for at least 5 pixels. This feature may result in the system failing to enhance the smaller, more undulating cracks because they do not fill the 3×5 and 5×3 kernels.

The second enhancement configuration is shown in Figure D-13. The SOBELOP component of the system is a software package subroutine which performs the Sobel Operator function on the input image. This operation extracts finer, more continuous edges in the image by using the following pair of 3×3 kernels:

$$\begin{matrix} -1 & 0 & 1 \\ -2 & 0 & 2 \\ -1 & 0 & 1 \end{matrix} \qquad \begin{matrix} 1 & 2 & 1 \\ 0 & 0 & 0 \\ -1 & -2 & -1 \end{matrix}$$

The convolution kernel on the left enhances vertical edges in the frame, while the one on the right enhances horizontal edges in the image. Also, the kernels operate in series on the same input image; therefore, only one input channel is needed to enhance both vertical and horizontal features. The Sobel Operator kernels assign high pixel intensities (white) to the edges in the image, so it is necessary to invert the look-up tables of the frame to produce darkened features on a white background in order to prepare the image for input to the CRAKFIND feature extractor. The Gaussian LOPASS filter component of the system is used to make the enhanced edges more continuous and to reduce the amount of "speckle" noise in the background obtained from edge enhancement.

This enhancement configuration was applied to the three raw "test" images. The three processed output images are shown in Figures D-14 through D-16. The statistics of the processed images are provided in Table D-3. Again, a decrease in the feature-to-background ratio was obtained with the processing system. However, an undesirably large increase in the standard deviation of the background pixel intensities was documented as a side effect of the edge enhancement algorithms. This stretching of the background pixel histogram produced an undesirable decrease in the maximum allowable value of T for detection in the first two test images. However, in comparing Table D-3 and Table D-1, the third test image obtained from the Brunswick data showed an increase in the maximum value of T. Also, the smaller cracks (encircled in Figure D-8), which branch off from the main longitudinal crack, were greatly enhanced by this processing configuration. This improvement in test image 3 supported the hypothesis that the Sobel Operator might provide a solution for the detection of very fine cracks in the road surface. In the case of the Brunswick test image, cracks that were too fine to be detected in the raw video were enhanced and extracted by the CRAKFIND feature extractor. In addition, the Sobel Operator contained convolution kernels that were spatially small (3 by 3) so that they could provide better enhancement for small undulating cracks in the image.

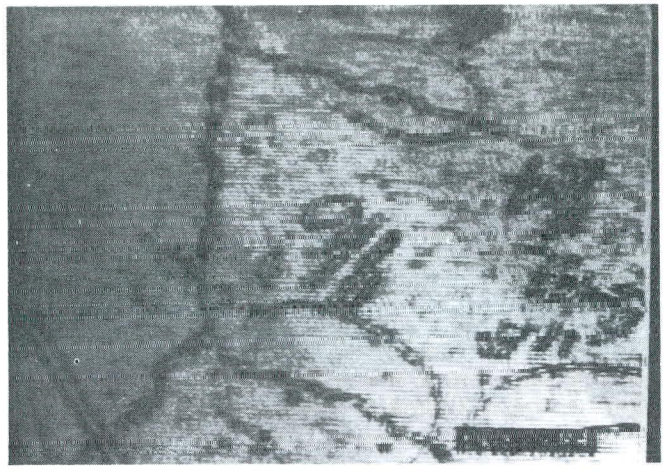

Figure D-12. Test image 3 enhanced with enhancement configuration 1.

Figure D-13. Enhancement configuration 2.

Another enhancement approach that was applied to the test images is shown in Figure D-17. This approach used the same configuration as approach 2 with the addition of a MEDIAN filter placed in front of the LOPASS filter. The MEDIAN filter is designed to filter out spurious "spot" noise in the background of the image produced by the edge enhancer. The 3 by 3 filter replaces the value of the center pixel in the kernel with the median value of the selected pixels around it. The filter kernel used in the system is as follows:

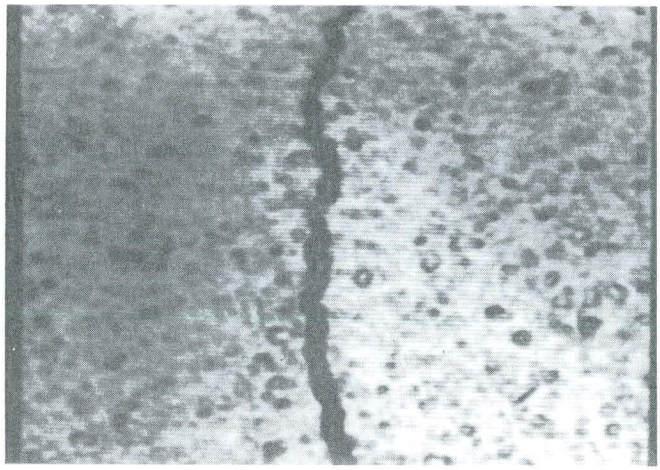

Figure D-14. Test image 1 enhanced with enhancement configuration 2.

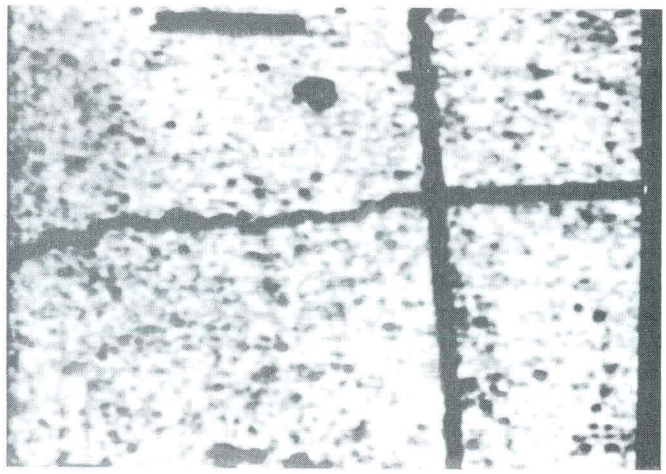

Figure D-15. Test image 2 enhanced with enhancement configuration 2.

$$\begin{matrix} 0 & 1 & 0 \\ 1 & 1 & 1 \\ 0 & 1 & 0 \end{matrix}$$

Thus, this filter kernel replaces the input pixel with the median value of the pixels directly above, below, and on either side of the input pixel. This kernel structure is designed to reject features in the image which do not have extent in either horizontal or vertical directions. Therefore, horizontal and vertical cracks in the image should retain approximately the same signal strength while "spot" noise is reduced.

Again, this enhancement system was applied to three "test" images, and the resulting output videos are shown in Figures D-18 through D-20. The statistics of the output images are provided in Table D-4. This approach also produced a significant decrease in the feature-to-background ratio while also increasing the background pixel standard deviation. However, the MEDIAN filter proved very effective in removing "spot" noise from the background which did not exhibit the features of a vertical or horizontal crack.

Series of attempts were made to modify the third enhancement system to improve the results obtained. Efforts to further reduce the spot noise resulted in a simultaneous reduction in the strength of the desired feature. Therefore, several configurations were tried to increase the strength of the feature intensities rather than to reduce the background intensities around it. A block diagram of one of these configurations is shown in Figure D-21. This system uses the SHARPEN IMAGE subroutine of the software menu to increase the contrast of the image before trying to separate the crack from the background. The kernel used by the SHARPEN IMAGE subroutine is shown below:

$$\begin{matrix} -1 & -1 & -1 \\ -1 & 12 & -1 \\ -1 & -1 & -1 \end{matrix}$$

This configuration was applied to the test images, and the corresponding output images are shown in Figures D-22 through D-24. The statistics of the output images are given in Table D-5.

Figure D-16. Test image 3 enhanced with enhancement configuration 2.

The analysis of the enhancement configurations showed the dependence of the maximum allowable value for T on the FBR and the standard deviation of the background intensities. Also, the algorithms providing the most improvement in the feature-to-background ratio were the edge enhancing operators. This is because edge enhancement algorithms take advantage of the fact that cracks in the video appear as edges in the image. However, as the size of the convolution kernel of the edge enhancer is reduced so that the enhancer is more sensitive to the smaller, more undulating cracks, the smaller, localized discolorations in the pavement background are also enhanced. This "spot" noise contributes to the darkness of the background which produces a stretching of the background pixel intensity histogram. This increase in the standard deviation of the background pixel intensities results in a processed image that is more sensitive to the chosen threshold. Therefore, a balance must be found between the decreased feature-to-background ratio and the residual increase in the background standard deviation. The enhance-

Table D-3. Results of enhancement configuration 2 applied to test images.

	FBR(dB)	μ_p	σ_p	μ_n	σ_n	MAXIMUM T
TEST IMAGE 1	-2.407177	209.22	35.66	217.30	18.68	4
TEST IMAGE 2	-6.712979	173.73	49.01	184.71	24.10	3
TEST IMAGE 3	-3.9252	179.62	50.83	205.20	20.62	2

ment configuration tested during the research effort, which produced the largest maximum allowable values of T for detection of the surface distresses the lowest FBRs, was the third system outlined earlier. However, additional work should be done in this area before an operational system is implemented, which is capable of reliably finding fine cracks in large images of the road surface.

The feature extraction techniques in the CRAKFIND Video Frame Analyzer software were tested with video data taken from the concrete loading bay apron near the GAR facility. The concrete slabs that were examined by the feature extractor were relatively clean and could be properly enhanced to a binary image which contained black cracks and white background. The CRAKFIND feature extractor was designed to locate popouts, spalls, and longitudinal, skewed and transverse cracks. This portion of the software successfully located and identified the surface distress features found in the test slabs.

The feature extractor uses the shape of the black silhouettes of the surface distresses in the frame to identify the desired surface features. The feature extractor was provided with a set of "frame analysis parameters" from the operator which describe the shape of the desired features. In general, the frame

Figure D-17. Enhancement configuration 3.

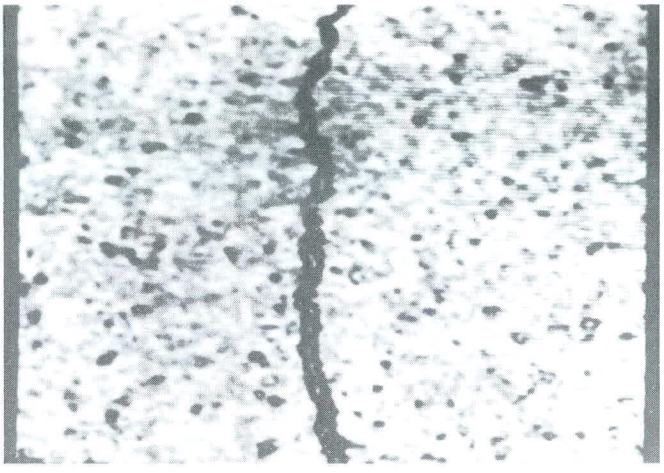

Figure D-18. Test image 1 enhanced with enhancement configuration 3.

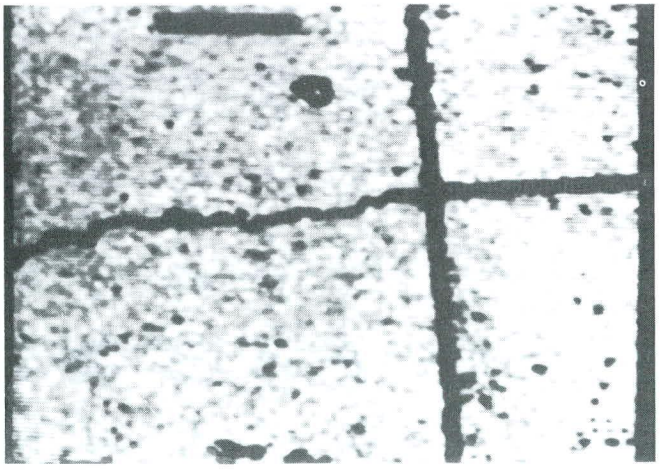

Figure D-19. Test image 2 enhanced with enhancement configuration 3.

Figure D-20. Test image 3 enhanced with enhancement configuration 3.

Table D-4. Results of enhancement configuration 3 applied to test images.

	FBR(dB)	μ_p	σ_p	μ_n	σ_n	MAXIMUM T
TEST IMAGE 1	-2.576287	205.25	35.55	214.62	16.66	4
TEST IMAGE 2	-7.925	170.95	48.32	183.07	19.47	3
TEST IMAGE 3	-4.7668	177.09	50.48	201.76	17.86	2

Figure D-21. Enhancement configuration 4.

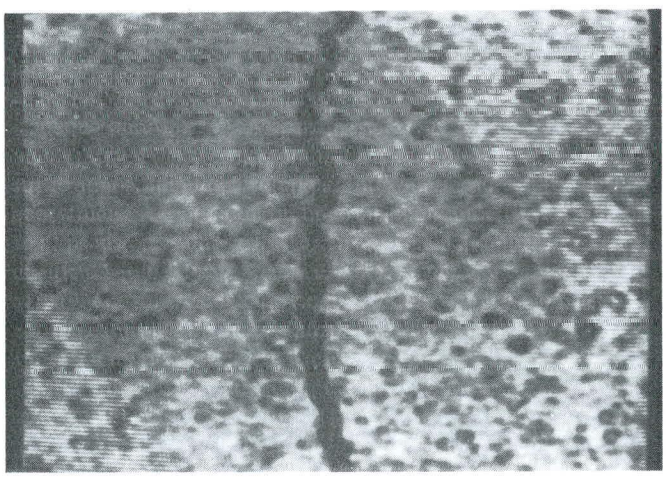

Figure D-22. Test image 1 enhanced with enhancement configuration 4.

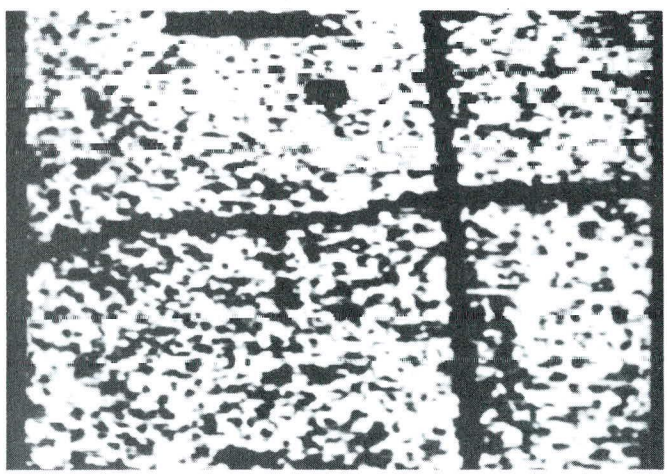

Figure D-23. Test image 2 enhanced with enhancement configuration 4.

analysis parameters define a longitudinal crack as a long slender silhouette that is oriented predominantly vertical in the frame. Similarly, a long, slender silhouette running horizontally in the frame is considered to be a transverse crack. The parameters define a spall as a wide section of a silhouette that otherwise appears to be a crack. A popout is defined as a relatively large clustering of black pixels in the frame whose dimensions are greater than the width of a crack. By programming the computer with this set of rules which describe the geometry of common surface distresses, an algorithm is obtained which is capable of discerning the features from the noise "speckle" in the background of the enhanced image. A similar approach to feature extraction and identification using the shape of the dark silhouettes in the enhanced binary image has also been implemented in the system designed by EarthTech (see Ref. 5 in the main report).

Once the video has been reduced to a binary image, the algorithm searches the picture for bodies of black pixels, which are then examined with the frame analysis parameters to determine if they are surface distresses. The algorithm moves line by line from top to bottom on the image, scanning horizontally across the screen for black pixels. The black pixels found on each horizontal line are grouped together into small horizontal strings. The computer then connects the horizontal strings that are aligned vertically into long vertical chains of black pixels. These long chains are then compared to the feature geometries described by the frame analysis parameters in order to determine if they are the silhouettes of cracks in the picture.

Table D-5. Results of enhancement configuration 4 on test images.

	FBR(dB)	μ_p	σ_p	μ_n	σ_n	MAXIMUM T
TEST IMAGE 1	-4.466787	179.85	39.72	188.37	25.93	3
TEST IMAGE 2	-8.11986	124.58	55.38	128.68	46.35	2
TEST IMAGE 3	-5.4828	142.83	59.89	173.26	29.84	2

The CRAKFIND program begins by reading a 256 by 240 pixel image from the hard disk of the computer into quadrant 0 of the video screen. The quadrants defined for the video screen are as shown below:

Quadrant 0	Quadrant 1
Quadrant 2	Quadrant 3

Also, CRAKFIND whites out quadrant 1 of the screen so that cracks that are found by the system in the original image (quadrant 0) can be written into this quadrant for display to the operator.

The feature extraction program begins by prompting the operator to enter the set of frame analysis parameters that will be used to locate and classify the silhouette shapes in the video. The program does not run any enhancement convolution for image enhancement because this process was previously done manually to the raw image using the image processing software during project development. The program then uses the software menu subroutine HISTOGRAM to obtain a histogram of the pixel intensities contained in the image. From the pixel histogram the algorithm calculates the mean and standard deviation of the pixel intensities in the image. The program uses the frame analysis parameter TIMES to set the intensity threshold for creating the binary (black/white) image. The frame analysis parameter TIMES is equal to the number of standard deviations below the mean where the pixel intensity threshold is set by the algorithm. The program then creates the binary image by mapping pixels whose intensities are below the threshold to black and pixels whose intensities are above the cutoff to white. The CRAKFIND program copies this binary image into quadrant 2 of the screen so that it can be compared with the cracks that will be displayed in the output image in quadrant 1.

Once the binary image is created, the program uses the subroutine RHLINE to read a horizontal line of pixels from the top of the image into the array LINE. The subroutine PIXFIND is called to locate groups of black pixels in the horizontal line which might be cross sections of longitudinal cracks in the frame.

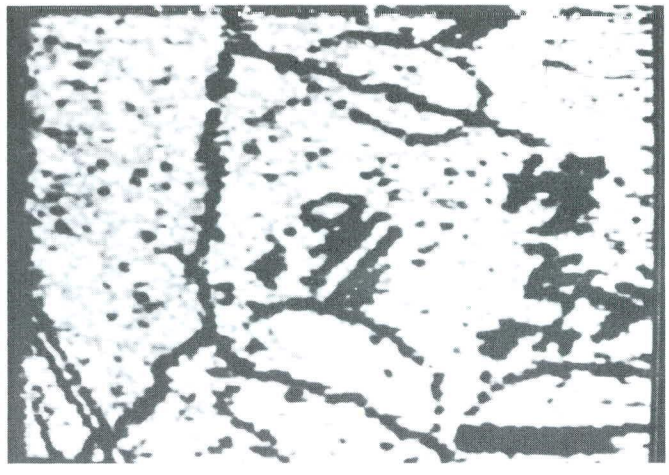

Figure D-24. Test image 3 enhanced with enhancement configuration 4.

The subroute begins by scanning the array LINE for a black pixel intensity. If a black pixel is found, the computer records the position in the array START which contains the position of the left side of each black pixel group found in the current horizontal line. The routine searches the next JUMP number of pixels for another black pixel. The variable JUMP is a frame analysis parameter entered by the operator, which determines the maximum separation between two black pixels that may be grouped together as one group or body.

If no other black pixels are found in the JUMP window, the single black pixel location is written into the array STOP, which contains the position of the right side of each black pixel group found in the current horizontal line. If a black pixel is found, the process of scanning another pixel window of length JUMP is repeated until a window containing only white pixels is found. The last black pixel found in a JUMP pixel window is recorded in the array STOP. The subroutine continues scanning the array for another black pixel which will become the left side of the next group of black pixels. In this way, a horizontal line is segmented into groups of black pixels that are separated by at least JUMP white pixels.

The arrays containing the left and right sides of the black pixel segments are returned to the main routine to be grouped

with pixel segments found on previous horizontal scan lines. The horizontal black pixel segments that can be aligned vertically in the image form potential cracks, called traces, down the length of the image. The program maintains a set of bookkeeping arrays that keep track of the location of the left and right sides of each trace based on the position of the most recent black pixel segment associated with the trace. The array LEFSIDE contains the position of the left side of the ongoing traces, while the array RIGSIDE contains the position of the right side of all the ongoing traces. The program tries to associate each string of black pixels on the current scan line in the arrays START and STOP with an ongoing trace whose last horizontal position was no more than JUMP pixels to either side of the black pixel segment.

If no ongoing trace is found within JUMP pixels of the black pixel group, the pixel segment becomes the beginning of a new trace. If the string is within JUMP pixels of an ongoing trace and the length of the black pixel segment is less than the frame analysis parameter MAXWID, the current string is associated with the trace and the current position of the left and right side of the trace is updated by the location of the left and right side of the new black pixel segment. The frame analysis parameter MAXWID is equal to the maximum width of a crack which can be identified by the program. If a black pixel group can be associated with an ongoing trace and contains more pixels than MAXWID, the black pixel segment is considered to be a potential spall of the vertical trace and its position is entered into a set of bookkeeping arrays that keep track of the sections of a trace that are wider than the width of a crack. If a trace is found to fulfill the geometric criteria of a crack, these wide sections are examined to see if they fulfill the criteria of a spall.

If two black pixel segments are found to be inside of the JUMP pixel window of the same trace, a decision must be made between the two pixel segments as to which is the new addition to the trace. This is accomplished by linearly projecting where the next trace cross section should occur based on recent pixel segment updates of the trace. The frame analysis parameter WINDOW is used to determine the number of previous trace updates that will be used to calculate the projected location of the next trace update. The smaller this number, the more "short-time" the update position estimate becomes, which allows the trace to react quickly to sudden changes in direction. If the window is long, the update prediction becomes more insensitive to sudden changes in direction.

The prediction is made by calculating the average slope between the positions of the left side of the trace found in the window. Given this slope and the position of the most recent left side of the trace, one can predict where the left side of the trace should be on the current horizontal line. The black pixel segment whose left end is closest to the projected left side of the trace is chosen as the update to the trace.

If a segment of black pixels is not associated with an ongoing trace and the length of the pixel segment is small enough to be a potential crack width (its length is less than MAXWID), the segment is used as the first entry for a new trace. If the length of the pixel segment is greater than MAXWID, the segment is considered to be too large to be a crack width and the pixel segment is discarded. This situation could occur if the pixel segment is a cross section of a large popout or a lengthwise section of a transverse crack running horizontally across the frame. In either case, the program will search for these surface distresses later in the processing.

Once the black pixel segments have been used to create new traces and update ongoing traces, the existing traces are examined for inactivity. The frame analysis parameter JUMP determines how many horizontal scan lines may be processed without updating a trace with new black pixels before the trace is closed because of inactivity. If a trace is found to be inactive, it is examined with the frame analysis parameters to determine if it satisfies the geometric criteria of a crack. The number of horizontal scan lines containing the trace is computed and compared with the frame analysis parameter MINLEN. The MINLEN variable contains the minimum length of a detectable crack. If the length of the trace is greater than MINLEN, the trace is labeled a crack by the program.

If the trace fulfills the criteria for a crack, the algorithm uses the bookkeeping arrays which keep track of the wide sections of the trace to determine if they satisfy the criteria for spalling. The frame analysis parameter SPALLEN contains the minimum length of a detectable spall recognizable by the system. For each wide section in the trace, the number of horizontal scan lines contained in the wide section is calculated and compared with the variable SPALLEN. If the length of a wide section is greater than the value of SPALLEN, the section is labeled a spall on the crack.

However, if an inactive trace does not satisfy the crack criteria, the trace is scheduled by the program for erasing from the bookkeeping arrays. The subroutine REORDER is called, which writes the array index that corresponds to the trace in the bookkeeping arrays into the array SORT. This array is used later to overwrite the inactive trace.

The program then examines the traces to determine if two traces have converged on the same black pixel segment. This situation occurs when the horizontal scan line reaches the bifurcation of two cracks. The algorithm examines the newer trace of the two and determines if it fulfills the criteria for a crack. If the trace is long enough to be labeled a crack, the wide sections of the trace are examined to determine if spalling has occurred on the crack. Again, if the trace does not fulfill the crack requirements, the subroutine REORDER is called and the corresponding trace index is written into the array SORT.

Once all the inactive traces have been tagged by the subroutine REORDER, they are erased from the bookkeeping arrays. The program pulls the index of the first trace to be erased from the top of the SORT array. The SORT array is created so that the lowest index trace is in the first index of the array and the highest index trace is in the highest index in the array. The program overwrites the inactive trace data by simply moving the other traces in the trace bookkeeping arrays (LEFSIDE, RIGSIDE, BOTTOM, TOP, STARLEF, STARRIG, LAST LEF, LASTBOT, DELCNT, CRKFLAG, and CHECKED) up by one index. Once the overwriting procedure has rippled through the bookkeeping arrays, the program pulls the next trace entry from the SORT array and repeats the procedure. As the program erases the trace from the trace/crack bookkeeping arrays, it also overwrites any wide sections that were associated with the inactive trace in the bookkeeping arrays used to tag spalling (SPALFLG, SPALTOP, SPALBOT, and SPALDIR).

Once the traces on the current horizontal scan line have been examined, the program reads another horizontal scan line into the array LINE and repeats the procedure of recording the traces, cracks, and spalls until the entire image has been examined. Once the end of the image has been reached, there may

be traces that are still active and have not been examined to determine if they are cracks. Thus, the program compares the traces that are still active in the bookkeeping arrays with the frame analysis parameter MINLEN to determine if the traces are cracks. Again if a trace is labeled a crack, the wide sections of the crack recorded in the spalling section of the bookkeeping arrays are compared with the frame analysis parameter SPALLEN to determine if the sections represent spalling on the crack. The search for cracks and spalls in the image has been completed once the traces that were still active when the program reached the bottom of the frame have been examined with the frame analysis parameters.

It was noted during preliminary testing of the feature extractor that many hairline cracks became two or more cracks in the binary (black/white) image because of poor intensity contrast between the thin crack and the background. Also, it is possible to have a crack that is physically separated by small sections of unbroken pavement, producing the appearance of several cracks. In both of these cases, it is desirable for the feature extractor to recognize and record only one crack. This goal is accomplished by supplying the program with the frame analysis parameter GROUP. The GROUP parameter represents the minimum number of pixels which must separate the end points of a crack from other crack end points before the crack can be labeled as a single distinct crack. The program assigns a box of pixels around the end points of the crack. The length of the box is twice the length of GROUP, as shown in Figure D-25. If the beginning of another crack is found inside the box, the two cracks are considered to be part of one large crack. The end point of the first crack is updated with the end point of the second crack, and the procedure is repeated until all the recorded cracks are labeled as separate cracks. In this way, the program knits together cracks that are made up of sections of broken pavement that lie along the same line of stress.

Also during the first pass through the image, the program determines whether the cracks found in the frame are longitudinal or skewed. This is accomplished by calculating the slope of a straight line drawn from the top to the bottom of a crack. If the slope of the line is less than 60 deg, the crack is labeled a skewed crack. If the slope of the line is greater than 60 deg, the crack is called longitudinal by the feature extractor. The program then displays the number of spalls and longitudinal and skewed cracks found in the frame to the operator.

Once the program has identified the longitudinal and skewed cracks in the frame, it erases them from the image to eliminate the possibility that the program will find the cracks again while scanning for transverse cracks. This is done by starting at the top of the image and reading in horizontal lines of pixels and searching the pixel lines for segments of the cracks stored in the bookkeeping arrays. If a crack segment is found on a horizontal scan line, the subroutine ERASE is called to remove the crack segment from the scanned image in quadrant 0 of the screen and to write the crack segment into quadrant 1 of the screen for comparison with the original binary image stored in quadrant 2 of the screen.

Once the cracks found during the longitudinal pass through the frame have been erased from the scanned image, the program rotates the image counterclockwise 90 deg and repeats the entire process again for transverse cracks. This rotation of the image serves to orient transverse cracks vertically on the screen so that the exact same technique of scanning horizontal lines of pixels for cross-sectional segments of the cracks can be used to locate

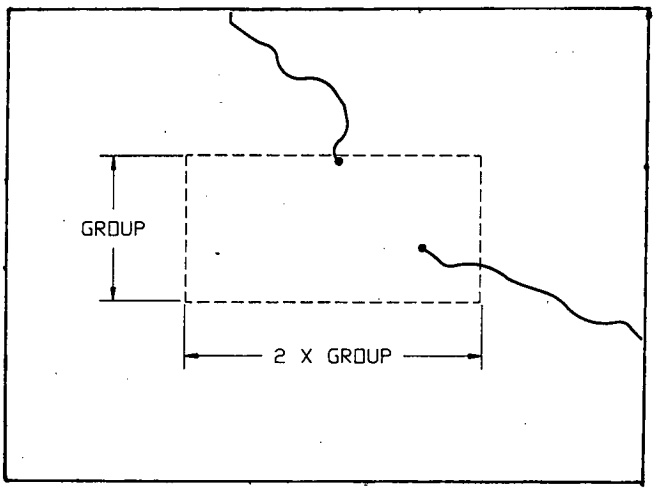

Figure D-25. Grouping crack segments.

the transverse cracks and spalls in the image. The image in quadrant 1 is also rotated for writing the transverse cracks found by the system into the output image. Once the quadrant has been rotated, the screen is rescanned as before, and the transverse cracks and spalls are erased from quadrant 0 and written into the output image in quadrant 1. The program also prints the number of transverse cracks and spalls to the operator's terminal.

Next, the program searches the image for popouts in the road surface. Again, the program starts at the top of the frame and begins reading horizontal lines of pixels into the array LINE. Once again the horizontal image lines are scanned for black pixel segments. The black pixel segments are compared to the frame analysis parameter POPLEN which represents the minimum number of pixels in a popout cross section that can be detected by the system. If a black pixel segment is found that is more than POPLEN pixels in width, it is stored in the bookkeeping arrays. If, during the next JUMP horizontal scan lines, another black pixel segment that is larger than POPLEN is found within JUMP pixels of the currently tracked potential popout, the position of the potential popout is updated in the bookkeeping arrays.

However, if a potential popout has not been updated in the last JUMP horizontal scan lines, the program counts the number of horizontal scan lines contained in the trace. If the number of horizontal lines is less than the POPLEN parameter, the trace is not labeled a popout and it is removed from the bookkeeping arrays, as before, with the subroutine ERASE. However, the trace is labeled a popout by the system if more than POPLEN horizontal scan lines are contained inside the trace.

During a scan of a horizontal pixel line, the traces are examined to determine if any of the traces have converged on the same black pixel segment. If two traces have converged on the same segment, the length of the newer trace is calculated and compared with the parameter POPLEN. If the trace is longer than POPLEN, it is labeled a popout by the system; however, if the trace is shorter than the POPLEN parameter, it is erased from the bookkeeping arrays. This procedure is continued line-by-line until the end of the frame is reached.

One should note that the expected position of the left side of

the popout is not computed from the slope of a line drawn through previous left-side positions of the popout as was done with cracks. This procedure was deemed unnecessary because the edges of the popouts should not be concealed by intersecting cracks. Once the end of the frame is reached, the traces that are still active are compared with the POPLEN parameter to determine if they are popouts. The popouts that are found by the system are erased from quadrant 0 and written into quadrant 1, using the same procedure described earlier for cracks.

Once the output image (quadrant 1) has been completed, it is rotated 270 deg counterclockwise for comparison with the original (pre-analyzed) binary image located in quadrant 2. The program finishes by printing out to the operator's terminal the number of popouts, spalls, as well as longitudinal, skewed, and transverse cracks found by the system. Also, a list of the frame analysis parameters used by the algorithm to detect the road surface distresses is printed to the operator's screen. The end of program execution is reached once the output data are provided to the operator.

APPENDIX E

VIDEO ANALYSIS SUBSYSTEM DESIGN

The video subsystem for analyzing pavement surface conditions may be implemented in one of several forms. Two approaches are outlined in this appendix. The off-line analysis subsystem is a relatively inexpensive implementation which utilizes off-the-shell equipment and proven analysis techniques, while the real-time analysis subsystem is expensive but allows for immediate pavement assessment. This appendix describes in detail the proposed two subsystem designs.

OFF-LINE ANALYSIS SUBSYSTEM DESIGN

A block diagram of the off-line version of the automated video analysis subsystem in shown in Figure E-1. The system is designed to simply record the image data on video tape during a survey run so that the tape can be returned to a central facility to be processed by computer. The system consists of a high-resolution video camera, a studio quality VCR, a personal computer, and the paint mark controller system that has already been developed for the RODAR™ system.

The paint mark controller system was developed by Gulf Applied Research 2 years ago to correlate the RODAR™ system on-board road surface measurement system with roadway station numbers. The RODAR™ system contains a fifth wheel that rolls alongside the truck during a survey run. This wheel is connected to a pulse generator, which fires a set number of evenly spaced pulses during one complete rotation of the wheel. Therefore, as the truck travels down the road, the wheel generates a pulse train waveform. The circumference of the fifth wheel is precisely known; therefore, the length of road surface covered during one period of the output pulse train can be accurately determined. This output pulse train from the fifth wheel is known as the footage signal. The paint mark controller is an electronic circuit, which counts the pulses of the footage signal. The operator is allowed to enter a road surface length into the paint mark system through a thumb wheel switch in the truck. When the controller measures the desired length in footage pulses, it generates its own pulse which fires a paint gun

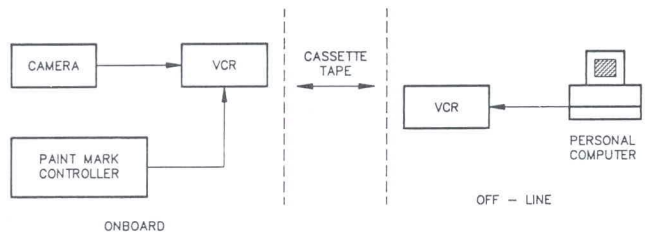

Figure E-1. Block diagram of off-line automated video analysis subsystem.

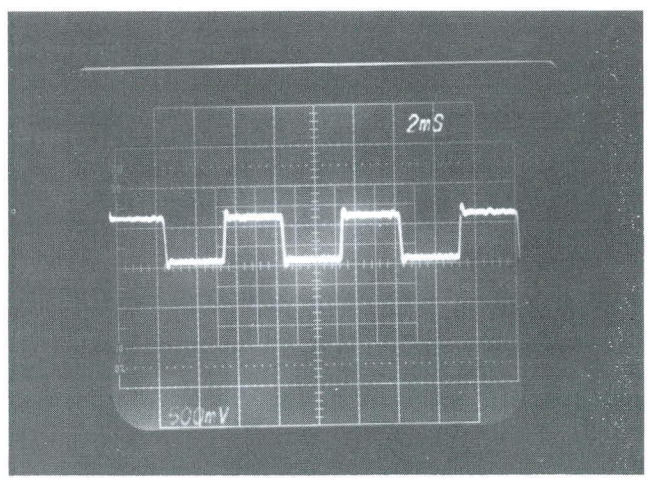

Figure E-2. Pulse train generated by paint mark controller.

that paints a small spot on the road surface. These paint marks provide a physical means of comparing the footage signal from the fifth wheel with station numbers on the surface of the road. The pulse train generated by the paint mark system, shown in Figure E-2, is recorded on the audio channel of the VCR for identification of video "frames".

The image subsystem acquires video data of the road surface through a high-resolution video camera mounted on the RODAR™ vehicle. The speed of data acquisition will require the use of a high-speed camera with an optical shutter, such as the camera purchased by GAR during this project. Although this camera is capable of taking clear high-speed images with good resolution, it was observed during the current project that the images from the camera lacked the level of contrast obtained by the camera system currently used in the RODAR™ system. The degree of contrast in the image is directly related to the camera components. Therefore, a camera with very high contrast capability will be required for an operational system.

The composite RS-170 standard video output from the camera will be stored on a high quality VCR for off-line automated data analysis. It is important to choose a VCR that is capable of maintaining the resolution provided by the camera. If the VCR has poor bandwidth and SNR for storage of the image data, it defeats the purpose of using a quality camera which provides good resolution and contrast. The VCR used to store image data during this project was a Panasonic AG-6200 industrial quality ¾-in. video recorder which provided 380 lines of resolution with a 42-dB signal-to-noise ratio. This VCR was already available for video surface logging with the RODAR system; however, other higher quality video recorders have been identified during the current project.

There are several broadcast quality recorders that use 1-in. video tape, but they are not rugged enough to use in the RODAR™ vehicle A more acceptable system would use video cassettes in order to be durable enough to survive the truck environment. One of these systems is the Panasonic M2 format broadcast quality recorder, which uses ½-in. tape and provides 420 to 450 lines of resolution with a 48-dB signal-to-noise ratio. Another system which provides the same durability, resolution, and contrast is a Sony Beta broadcast-quality format recorder. Either of these recording systems would be suitable for image storage on-board the proposed system.

In addition to the raw image data, the off-line computer must be instructed when to grab and process an image frame. This is accomplished by recording the output pulse train from the paint mark controller on the audio channel of the VCR. Again, each pulse from the paint mark controller represents a length of roadway that is preset by the operator. The computer will use these pulses to trigger the "grabbing" of a frame for processing. Therefore, the road surface separation between two adjacent images processed by the system would be set by dialing the desired separation into the paint mark controller on-board the truck. However, the output pulse train of the paint mark controller contains a 50 percent duty cycle regardless of the pulse period. Thus, the pulse width of the waveform changes with the speed of rotation of the fifth wheel. As the pulse width of the waveform expands, the bandwidth of the signal contracts; as the pulse width contracts, the bandwidth expands.

However, the bandwidth of the audio channel of the VCR is fixed to that of signals that are audible to the human ear (approximately 20 Hz to 20 kHz). In fact, depending on the quality of the recorder, this operating bandwidth may be smaller. Therefore, distortion of the paint mark pulse train is encountered when its bandwidth ranges outside the bandwidth of the VCR. Figure E-3 shows an example of the distortion for low fifth wheel speeds. When the pulse train is read from the VCR by the off-line computer, the signal will probably require some conditioning to regain its original shape. For example, the squared edges of the pulse train could be recovered by passing the pulse train through electronic hardware such as a Schmitt trigger.

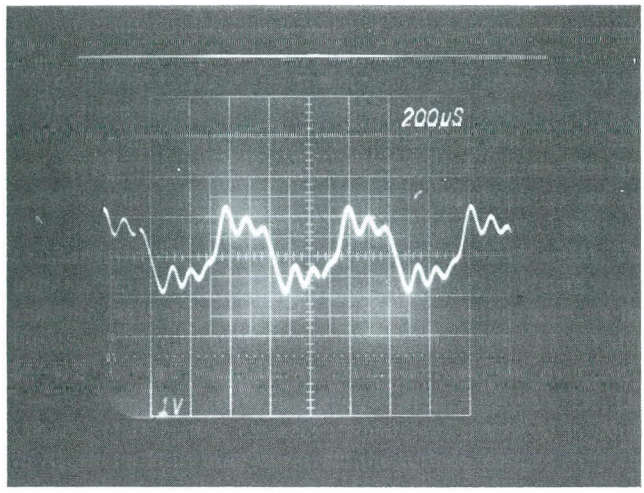

Figure E-3. Paint mark pulse train distorted by bandwidth limitation of the VCR audio channel.

Once the survey has been completed, the VCR tape containing the road surface video and the paint mark controller waveform can be removed from the truck and returned to the GAR facility for analysis. The tape is loaded into a studio quality VCR that is controlled by a personal computer. The remote connector on the back of the VCR is connected to a parallel port of the computer which controls the play, rewind, and stop functions of the recorder. The audio channel of the VCR is connected to another parallel port of the computer which reads the pulse train output and determines when to grab a frame and stop the VCR.

The software residing in the personal computer for analysis of the video data consists of an administrative program, a frame enhancer, the CRAKFIND feature extractor, and an assembly code program that reads the paint mark pulse train from the parallel port of the computer. The other programs are written in a high level language such as FORTRAN or C, with an optimizing compiler used to increase the run time speed. The administrative program is the main program of the system which calls the other programs and maintains a running count of the number of surface anomalies found by the CRAKFIND analyzer. The frame enhancer is a feature-to-background enhancement scheme like the ones described in Appendix D. The CRAKFIND feature extractor, which was described in detail in Appendix D, is used to extract the surface features from the enhanced video.

The off-line analysis system begins with the administrative program using the remote control connection with the VCR to start the playback of the road surface data. The assembly language program is then called which will read the paint mark pulse from the parallel port of the computer. The assembly language code is simply a loop that waits for one line of the port to go from a low voltage to a high voltage, indicating the rising edge of a new pulse. The assembly language program then returns control to the administrative program which will call the software package subroutine GRAB to hold a frame in

memory. Once the image has been captured, the administrative program sends a message to the remote port of the VCR to stop the tape. The administrative program then calls the feature enhancer to improve the contrast between the desired features and the background. Next, the administrator calls the CRAK-FIND feature extractor which locates the desired features and reports them to the administrative main program. Once the frame has been analyzed, the administrator starts the video tape and calls the assembly language program to begin searching for the next rising edge of the paint mark pulse train.

The paint mark pulse train was chosen over the raw footage pulses of the fifth wheel for encoding onto the audio channel of the VCR for several reasons. First, the pulse repetition rate is much lower for the paint mark pulse (1 pulse per 4 ft versus 25 pulses per 1 ft), which allows it to fit more easily into the bandwidth of the VCR's audio channel at high vehicle speeds. Second, the paint mark waveform eases the burden on the software required to determine when to grab an image. If the raw footage pulse train was encoded on the VCR, the program would be required to count the footage pulses to determine when to grab an image. However, if the paint mark pulse train is used, the program is only required to wait for the rising edge of a new pulse to grab an image. The amount of roadway separating two paint mark pulses would be set by the operator in the survey vehicle prior to the survey run. Also, the VCR has a transient period during the stopping and starting of the tape which could cause the assembly program to miss some of the footage pulses. However, if the images to be grabbed are far enough apart for a given vehicle speed, the transients of the VCR will not interfere with the next pulse of the paint mark controller.

Although the off-line system is unable to report the number of surface distresses immediately following the end of the survey run, it still possesses several advantages. First, the system remains fully automated, allowing the road surface analysis to proceed independently without constant operator interface. The system could be allowed to analyze the data continuously overnight, thus providing the operator with the surface distress analysis upon his return the next day. Second, the off-line system would be relatively low cost in comparison with a real-time system. The off-line system would not require the expensive, dedicated components of a real-time system. Also, the off-line system would be easier to implement because the software for the system is not required to be run-time critical. The programs would be written to be run-time efficient to provide the fastest analysis time possible; however, they would not be required to meet critical, high-speed timing requirements imposed by analyzing the road as the truck moves at highway speeds.

To determine the limitations of the system, several key factors must be considered to achieve the desired system performance. First, the size of the smallest crack to be detected by the system must be considered by the operator. This requirement will determine the height of the video cameras above the road surface needed to achieve the desired resolution. The considerations of camera height versus resolution have been addressed in Chapter Two of the main report. If the camera height is chosen to be close to the road surface to detect small cracks in the pavement, several cameras working in parallel may be required to cover the entire lane. The use of multiple cameras would require a slightly more complex software administrative scheme as well as more processing time for data enhancement and feature extraction. Each camera would require a separate VCR for the recording of the camera image data and the paint mark pulse.

In addition, the maximum speed of the survey and the length of road surface between processed images must be considered. These factors will determine the bandwidth of the paint mark pulse train which is encoded on the audio channel of the recorder. Therefore, the vehicle speed and the needed paint mark pulse repetition rate will determine the amount of distortion that is encountered when the signal is written onto the audio channel of the recorder. The transients of the VCR will also determine the minimum separation between processed images for a given truck speed. If the vehicle is traveling at a high rate of speed, the paint mark pulse repetition rate must be chosen so that the transients of stopping and starting the VCR have died away before the next pulse is encountered on playback by the computer. Finally, the vehicle speed must not exceed the ability of the optically shuttered camera to freeze the motion of the road surface in the image.

REAL-TIME ANALYSIS SUBSYSTEM DESIGN

The real-time video analysis subsystem needed to analyze the road surface at highway speeds will require more sophisticated hardware and more time for implementation. This system will require a faster video sensor for gathering the data at the higher vehicle speeds. Also, the on-board computer system must contain high-speed pipelined processors to handle the increased data rates. The software used by the on-board computer analyzer must be fast enough to process the data as the information is passed to it by the pipelined hardware. These real-time requirements pose significant problems in designing a system that would provide the desired high vehicle speed, data rate and image resolution. In addition, the system should be constructed by integrating pieces of existing technology, because development of new technologies for this application would be very expensive and would impose severe technical risks.

The real-time system must use a high-resolution video sensor that is fast enough to freeze the motion of the road surface at highway speeds. The research work performed during this project indicated that most optically shuttered high-speed video cameras would be unable to prevent the blurring of the video frame. This finding is supported by researchers at EarthTech (see Ref. 5 in the main report) who are working on the problem of high-speed road surface analysis. However, there are video linear sensors that have scan rates that are capable of preventing the blurring of the image. These line scan sensors are charge coupled devices (CCD's) which use a monolithic component containing a single row of image sensing elements called photosites. The line scan camera generates a single row of image pixels from the surface area placed directly below the sensor. The vertical dimension of the image is produced as the truck travels down the roadway bringing the road surface under the line scan sensor.

The line scan camera prohibits blurring of the image because of the short exposure time needed to acquire a line of pixels. There are commercially available line scan sensors that can acquire a 1 by 512 array of pixels in 52 μsec. In this case the minimum time required to fill an entire 512 by 512 frame of data would be 13.3 msec. Therefore, if each frame corresponded to a 4-ft square of road surface, the truck would be allowed to travel as fast as 204.9 mph (theoretically) without distorting the image data. This high-speed acquisition rate is ideal for highway speed road surface video acquisition.

However, the system must also contain high-speed image processing hardware and software to enhance and extract the features at the rate provided by the linear sensor. Fortunately, there are manufacturers of pipelined image processing hardware that can take advantage of this high data throughput. Generally, these companies produce a line of digital hardware boards that perform common image processing functions. The real-time processing speed is achieved by designing each board to be dedicated to one specific processing function. The boards can be purchased individually, allowing a designer to choose only the boards needed to configure the specific processing system. The processing boards are controlled through a central bus system (usually Multibus or VMEbus) by the designer's single board computer (SBC), which also contains the designer's software for the specific application. Therefore, in the video analysis system application, the processing boards could perform the image enhancement functions in hardware at real-time speeds, while the CRAKFIND feature extraction algorithm analyzes the enhanced image from a high-speed CPU on the master SBC.

The first processing board required would be a video data acquisition module. The output from the linear sensor is an analog pulse train whose magnitudes are linearly related to the amount of light captured by the photosites of the CCD detector in the camera. The video processing companies recognize the existence of these sensors and manufacture boards that are designed to handle video inputs that are not in a standard RS-170 or CCIR format. In fact, there are commercially available boards that will A/D convert nonstandard video input at data rates as high as 20 MHz. The video A/D converter stores the incoming data in another board provided by the image processing hardware company. There are commercially available video frame storage boards that can contain up to 2 megabytes of the video data. Therefore, if a frame consists of 512 by 512 array of 8-bit pixels, the frame storage board contains enough memory to store seven frames at one time. The ability to store more than one frame at a time is a useful asset, because the feature extraction software can be processing one frame while another frame is being gathered by the hardware.

The system will also require a board which will perform two-dimensional convolutions on the image for feature enhancement. There are boards that are commercially available that can perform up to 640 million multiple-accumulates per second. This processing rate will allow a 512 by 512 image to be convolved with a feature enhancement filter in $\frac{1}{30}$ of a second. Again, if the image is a 4-ft square of the road surface, this frame throughput rate of 30 frames per second would correspond to a truck speed of 81.8 mph.

The image hardware companies also produce boards which will perform histograms of the video image at real-time frame rates. These commercially available boards will also perform a histogram of a 512 by 512 image at a rate of 30 frames a second. During the current research effort, it was discovered that calculation of the image histogram was one of the most time-consuming processes performed by the CRAKFIND program. However, adding this hardware feature would only require the CRAKFIND algorithm to read the gray level histogram and compute its mean and standard deviation before setting the crack cutoff intensity.

The system would require a master single board computer (SBC) which would control the dedicated image processing boards and perform the feature extraction function. There are commercially available SBC's which will perform at real-time processing speeds. One manufacturer produces a real-time VMEbus single board computer which uses the Motorola 32-bit MC68020 microprocessor at a clock rate of 25 MHz. This board level computer is also equipped with the Motorola MC68881 FPU coprocessor which will serve to increase the speed of the central processing unit. This high-speed Motorola microprocessor was used extensively in the system developed by EarthTech researchers.

Thus, the real-time video analysis system would contain a high-speed line scan sensor, dedicated image processing boards, and a high-speed central master computer board. A simplified block diagram of this system is shown in Figure E-4. The image data would be acquired continuously through the line scan sensor as the truck travels down the highway. The truck speed would be tied to the exposure time of the linear sensor in order to capture a 4-ft square of road surface in each image frame. This would provide a coverage of less than a $\frac{1}{10}$ in. per pixel for a 512 by 512 pixel image. This coverage would require a three-sensor system to span a 12-ft wide highway lane. The incoming video data would be digitized and stored in the real-time processing boards.

Once the video sensor has completed its scan of an entire frame, then preprocessing for image enhancement can begin on the input image. As the current frame of video data is enhanced and the features are extracted, the video sensor and high-speed A/D and storage boards will continue building up the next frame of data. The high-speed convolution board will be used to implement the convolutions of the Sobel Operator, MEDIAN, and LOPASS filter kernels with the input image. Once the image has been preprocessed for feature enhancement, then the real-time histogram board will be used to compute the gray scale histogram. The master single board computer (SBC) will read the pixel histogram and compute the threshold level for crack detection. The SBC will then proceed to analyze the image with the frame analyzer. The number of surface distresses in the image will be logged with the administrative program, and the next preprocessed image from the real-time enhancement boards will be obtained from the system hardware.

The feature extractor of this system is similar to the CRAKFIND algorithm developed during this research project with some minor modifications. First, the computer will not be required to rewrite the pixels in the frame to form a black and white image. This was done during the development process to allow the researchers to see which pixels were being labeled as cracks by the program. During the operation of the real-time system, this time-consuming read/write process will not be required because each image pixel can be compared directly with the computed cutoff value. Also, the frame storage board will allow access to both the columns and rows of the pixels in the image. This feature will allow the master computer to extract both longitudinal and transverse surface distresses in the image without rotating the frame by 90 deg.

The proposed real-time system possesses several desirable features. First, the system will be constructed from commercially available hardware. This feature ensures that system development engineers will have the support of the processing hardware companies during system integration. The hardware is widely used; therefore, the boards have been previously debugged and integrated into operational real-time image processing systems. In addition, the real-time nature of the system will allow the analysis of a large volume of road surface data on-site, during the pavement survey. Also, the dedicated system hardware will

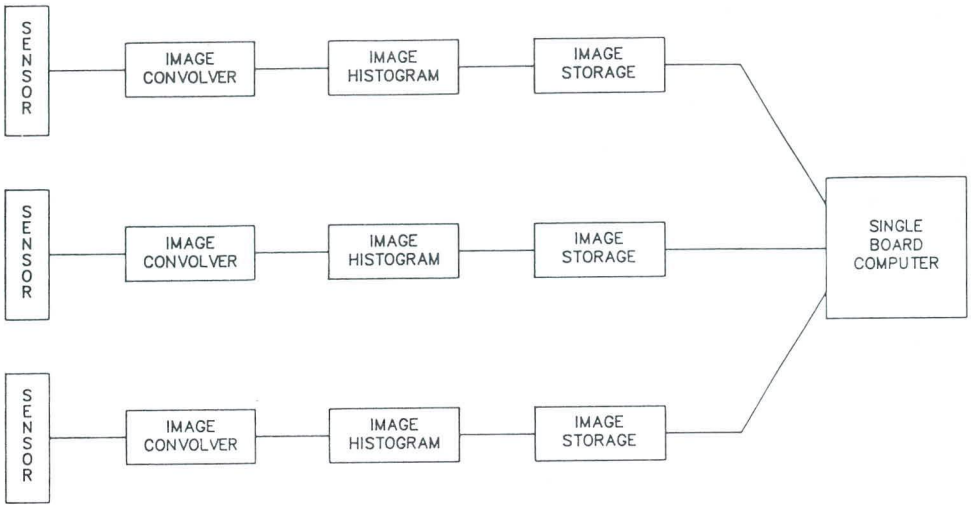

Figure E-4. Simplified block diagram.

allow the road surface survey to be taken at appreciable highway speeds. The processing rate of 30 frames per second for the hardware will allow the truck to take road surface data at speeds approaching 81 mph, subject to applicable traffic laws, of course. However, a limiting factor in vehicle speed will be the run time of the feature extraction and administrative code residing in the master computer.

As opposed to the off-line system, this system will require more development time to integrate the hardware and software into an operational system. Also, the cost of the proposed real-time system will be higher than that of the off-line system. In addition, more development time will be required to streamline the feature extraction and administrative software so that it can be implemented in real-time to take advantage of the high-speed hardware.

APPENDIX F

LABORATORY TESTING

Early in the system testing phase of this project, it became apparent that the "short-flare" antenna, developed specifically for the enhanced radar system, did not perform quite as well as the standard "long-flare" antenna of the RODAR™ system. Figure F-1 is a photograph of both of these antennas. It was felt that a laboratory comparison of several configurations of horn antennas would be a valuable addition to this project.

Some sample data from the laboratory testing phase of this project can be found at the end of this appendix. The data are presented in the form of plots of actual waveforms that resulted from the various test arrangements. These data plots were obtained by using a dynamic recording oscilloscope and a plotter at the time of the actual tests. In some cases data from similar test arrangements are plotted on the same graph for ease of interpretation.

Three different styles of horn antennas were used: a long flare, a short flare, and a medium flare. The long and short flare were used in the bistatic mode as well and the monostatic mode. In the monostatic mode, one antenna serves as both the transmitter and receiver. In the bistatic mode, two antennas are used, one

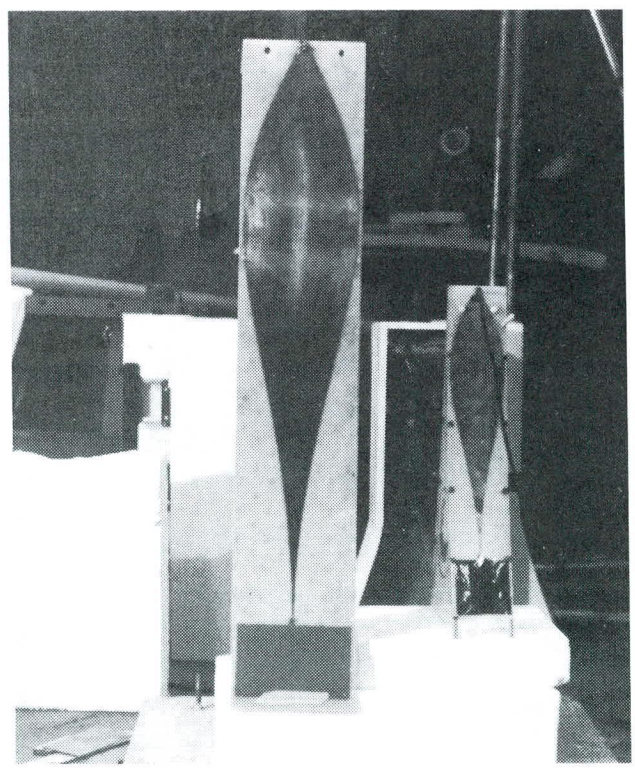

Figure F-1. Long and short flare antennas used in both laboratory and field tests.

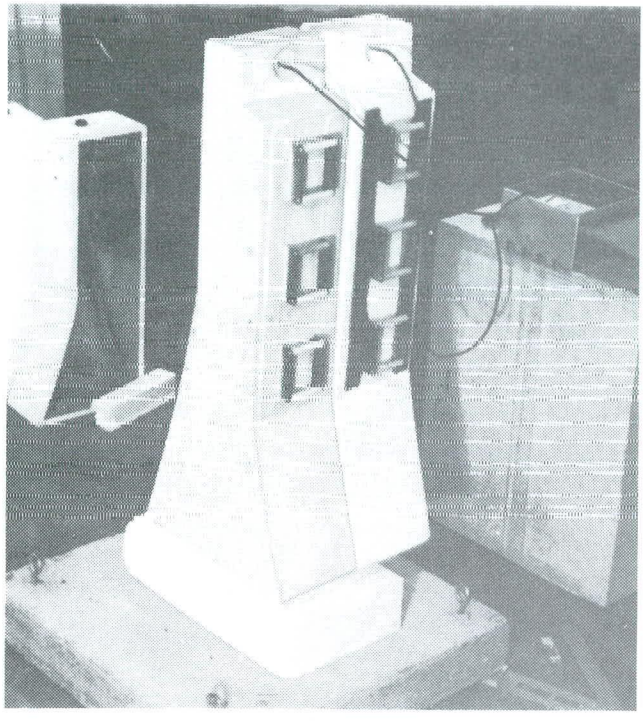

Figure F-2. Long flare antenna in bistatic mode during laboratory tests.

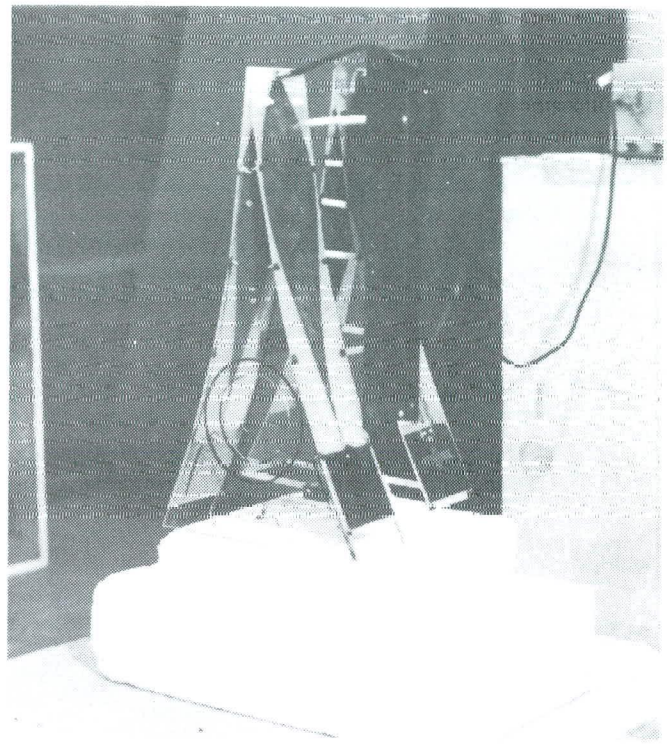

Figure F-3. Short flare antenna in bistatic mode during laboratory tests.

serves to transmit the pulse and the other receives the reflections. Figures F-2 and F-3 are photographs of the long- and short-flare antennas being used in the bistatic mode. Early research in the area of ground-penetrating radar indicated that bistatic antenna configurations reduced the amount of clutter in the return signal. During these tests, all factors were held constant except the antenna configuration.

A performance comparison of the monostatic and bistatic configurations of horn antennas can be seen in Data Plots 1 and 2 at the end of this appendix. These data were taken on a concrete slab of sufficient thickness so that the only significant return in the received data was due to the surface reflection. The data on these two plots contain the surface (marked) and only system clutter and noise beyond the surface. The antenna configurations used were long flares in monostatic and bistatic modes. On the basis of these test results two points can be made: first, the surface return had a somewhat higher amplitude in the bistatic mode, indicating higher transmission reception efficiency; and, second, the area of data downrange in time from the surface return is flatter in the bistatic mode, indicating less system clutter.

To compare the performances of the various antenna configurations a test slab was chosen that would provide sufficient reflections. This slab was 6 in. thick, had ½-in. reinforcing steel embedded at mid-depth, and was placed on a high dielectric material to ensure a large reflection at the slab bottom. Data Plots 3, 4, 5, and 6 are the results of these antenna comparison tests. Four antenna configuration results are shown in these plots: long-flare monostatic, medium-flare monostatic, short-flare bistatic, and long-flare bistatic. Two features of these data plots are of interest for this comparison: the amplitude of the surface return and the amplitude of the signal return from the slab bottom. The amplitude of the return from the slab bottom is of particular interest because this pulse has traveled through the surface, the steel layer, reflected from the slab bottom, passed through the steel layer again and back through the surface. By comparing these four plots, one can see that the long-flare bistatic antenna is superior, and the short-flare bistatic antenna is slightly better than the long-flare monostatic antenna. The medium-flare monostatic antenna fared worst, with the amplitude of the signal return from the slab bottom approximately one-half that of the long-flare bistatic antenna. A data plot from the short-flare monostatic antenna was generated but is not included here. The performance of the short-flare monostatic antenna was somewhat worse that of the medium-flare monostatic antenna.

On the basis of these tests, it was concluded that the bistatic mode is superior for several reasons. The long-flare antenna performs best, but the short-flare antenna is a reasonable substitute if size is a critical factor.

ANTENNA ORIENTATION

The application of electromagnetic theory to horn-type antennas indicates that the field generated by the antenna has a definite orientation. This field orientation is important because reinforcing steel in a concrete pavement can produce more or less pulse reflection, depending on relative antenna orientation. If antenna orientation can reduce the reflection from reinforcing steel, more energy is available for deeper penetration. Because in most reinforced PCC pavements the steel is predominantly longitudinal, the optimum antenna orientation could enhance the ability to detect subsurface anomalies.

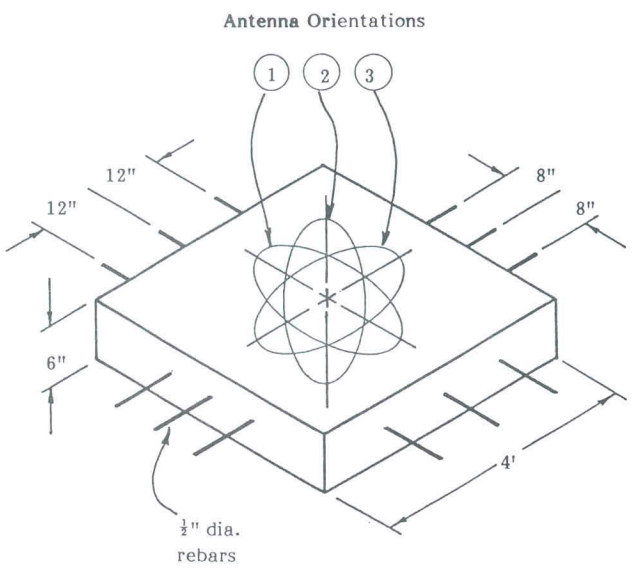

Figure F-4. Test slab for investigating antenna orientation relationship with reinforcing steel.

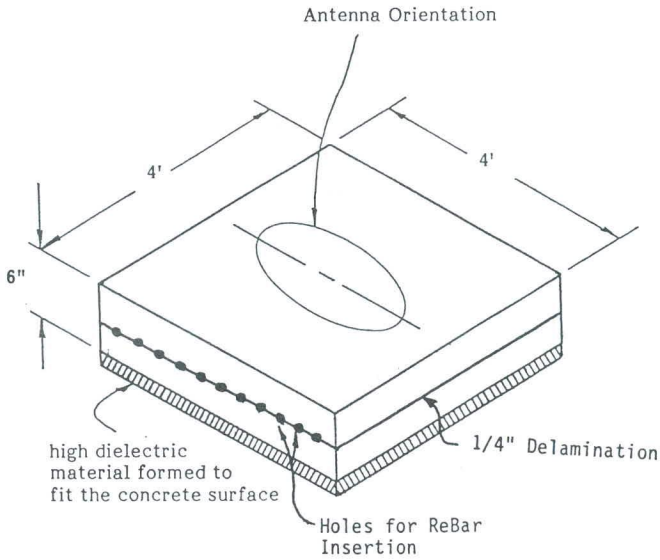

Figure F-5. Test slab for investigating antenna orientation relationships with reinforcing steel.

To experiment in the area of antenna orientation, two different slabs were used. The first slab was 6 in. thick and had ½-in. reinforcing steel embedded at mid-depth. This slab had steel oriented in two directions, one direction had an 8-in. spacing between bars, the other direction had a 12-in. spacing between bars. Data were plotted with the antenna oriented both parallel and perpendicular to the steel bars and at a 45-deg orientation with respect to the bars (Figure F-4). The data from all three of the antenna orientations are plotted in Data Plot 7. It is obvious from this plot that antenna orientation has an effect on radar returns from reinforcing steel.

The second slab used to investigate further the effects of antenna orientation on signal return from the reinforcing bars was constructed in two parts. The two parts of this slab separate horizontally at the plane of the reinforcing bars (Figure F-5). This separation allows the spacing of the reinforcing steel to be varied by adding or removing bars (Figure F-6). The construction of this test slab resulted in a ¼-in. "delamination" at the plane of the steel bars. The reinforcing bars run in one direction only in this test slab. Data were plotted for reinforcing steel spacings of 3 in., 6 in., 9 in., and 12 in.; "no steel-with delamination" condition; and "no steel-no delamination" condition. The "no steel-no delamination" condition consisted of a slab, poured at the same time as the previously mentioned two-part slab, but as a solid unit without steel or delamination. The "no steel-with delamination" condition was accomplished by simply removing the steel from the two-part slab.

Each of these conditions was repeated for both antenna orientations. Data Plot 8 contains the data from the slabs with various steel spacings, with the antenna oriented perpendicular to the axis of the steel. Data Plot 9 contains the same data, but with the antenna oriented parallel to the steel axis. As can be readily seen by comparing these two plots, the orientation of the antenna has a radical effect on signal reflection from the reinforcing bars. It would appear from Data Plot 9 that with the correct antenna orientation, the effect of reinforcing steel on pulse penetration can be minimized. It can also be seen in Data Plot 8 that, with the wrong antenna orientation, reinforcing steel spacing has a pronounced effect on radar penetration and clutter.

Figure F-6. Bottom of test slab with variable reinforcing steel spacing capability.

VOID MODELING

To model voids, two test slabs were used: one was a 6-in. thick plain concrete slab, the other was a 6-in. thick concrete slab with reinforcement (Figures F-7 and F-8). These slabs were placed on a high dielectric constant material and shims were used to raise the slabs for void simulations (Figure F-9). As before, the actual signal return curves were plotted for various size voids. These curves were placed on the same plot for ease of evaluation. Data Plot 10 contains the results of various void

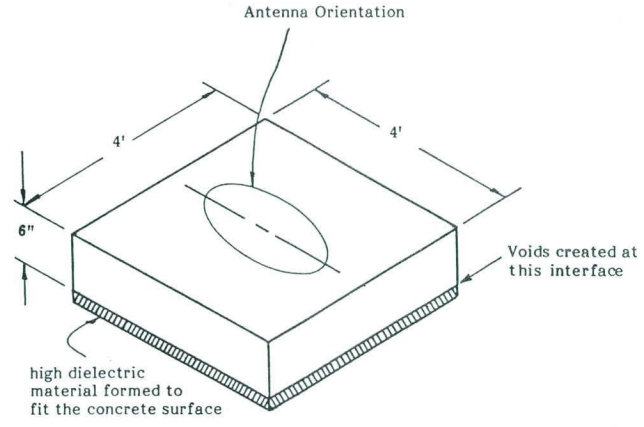

Figure F-7. Plain test slab used for void modeling.

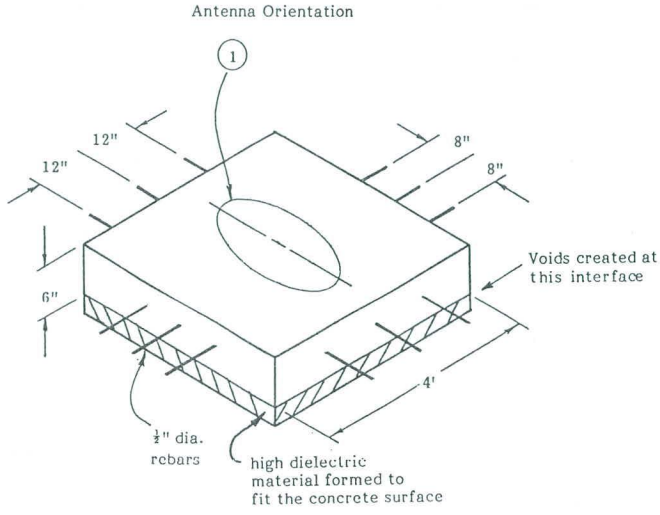

Figure F-8. Reinforced test slab used for void modeling.

sizes under the plain concrete slab. Although several of the antenna configurations were used to make these measurements, the long-flare antenna, used in the monostatic mode, was chosen for presentation here. The results from the other antenna configurations were similar. Data Plot 11 contains the same void size variation curves generated using the reinforced slab. The medium-flare antenna in the monostatic mode was used in the plot.

As can be readily seen in these two data plots, the effect of void size under these slabs is very obvious. These data took the general form of the predicted theoretical model developed in Appendix C. These data were used for verification in the development of the void-sizing algorithm.

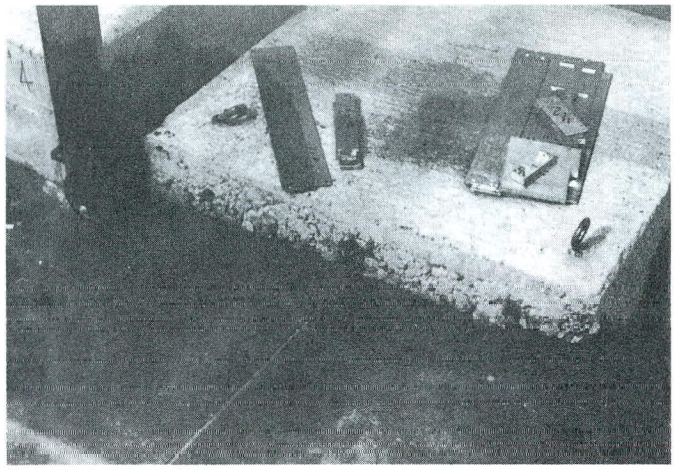

Figure F-9. Test slab and shims used in laboratory test phase.

WATER-FILLED VOIDS

To model the effect of water in a void, a special test had to be devised. A 6-in thick plain PCC slab was placed on the concrete floor of the laboratory. Shims were used to establish a ¼-in. and a ½-in. thick void between the slab and the concrete floor. Signal return data curves from these two air voids were plotted. A structure was placed around the slab and flooded with water. The signal return data from the corresponding ¼- and ½-in. thick water-filled void were plotted along with the data from the air voids for direct comparison. Data Plot 12 contains these four signal return data curves. The long-flare antenna in the monostatic mode was used to make these measurements.

The effect of water filling an air void can be predicted by electromagnetic theory. The signal return from an air void and from a water-filled void should have nearly opposite phases. (In this case, the phases are not exactly opposite because of the composite effect of the two returns associated with a void.) In addition, the amplitude of the signal return from the water-filled void should be considerably higher than that from the air void because of the high reflection coefficient of water. Both of these factors (phase and amplitude) are seen in Data Plot 12. Water-filled voids result in a much different signal return than do air voids.

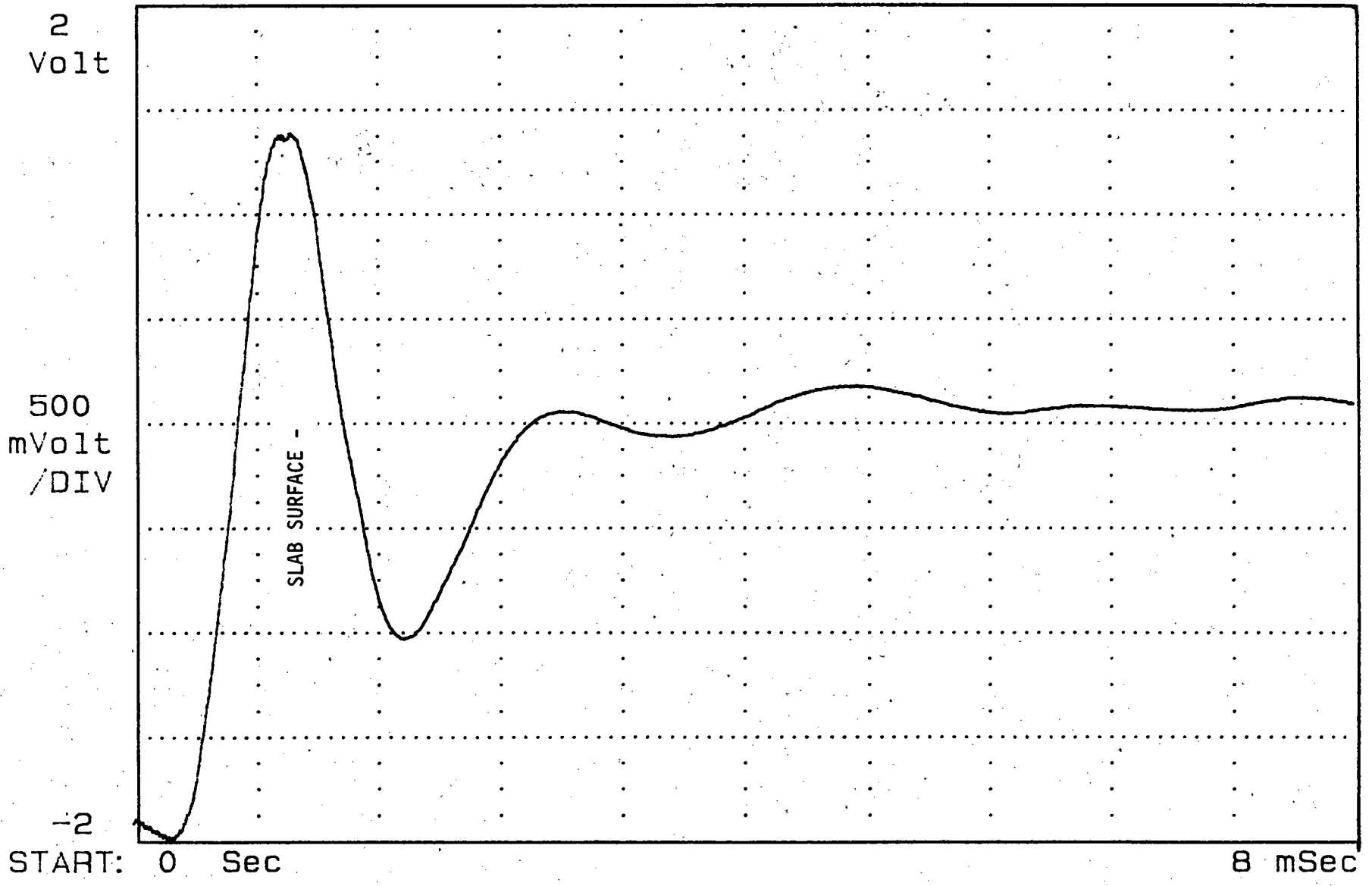

Data Plot #1: Long Flare Antenna - Monostatic Mode (Very Thick Concrete Slab, No Returned Signal)

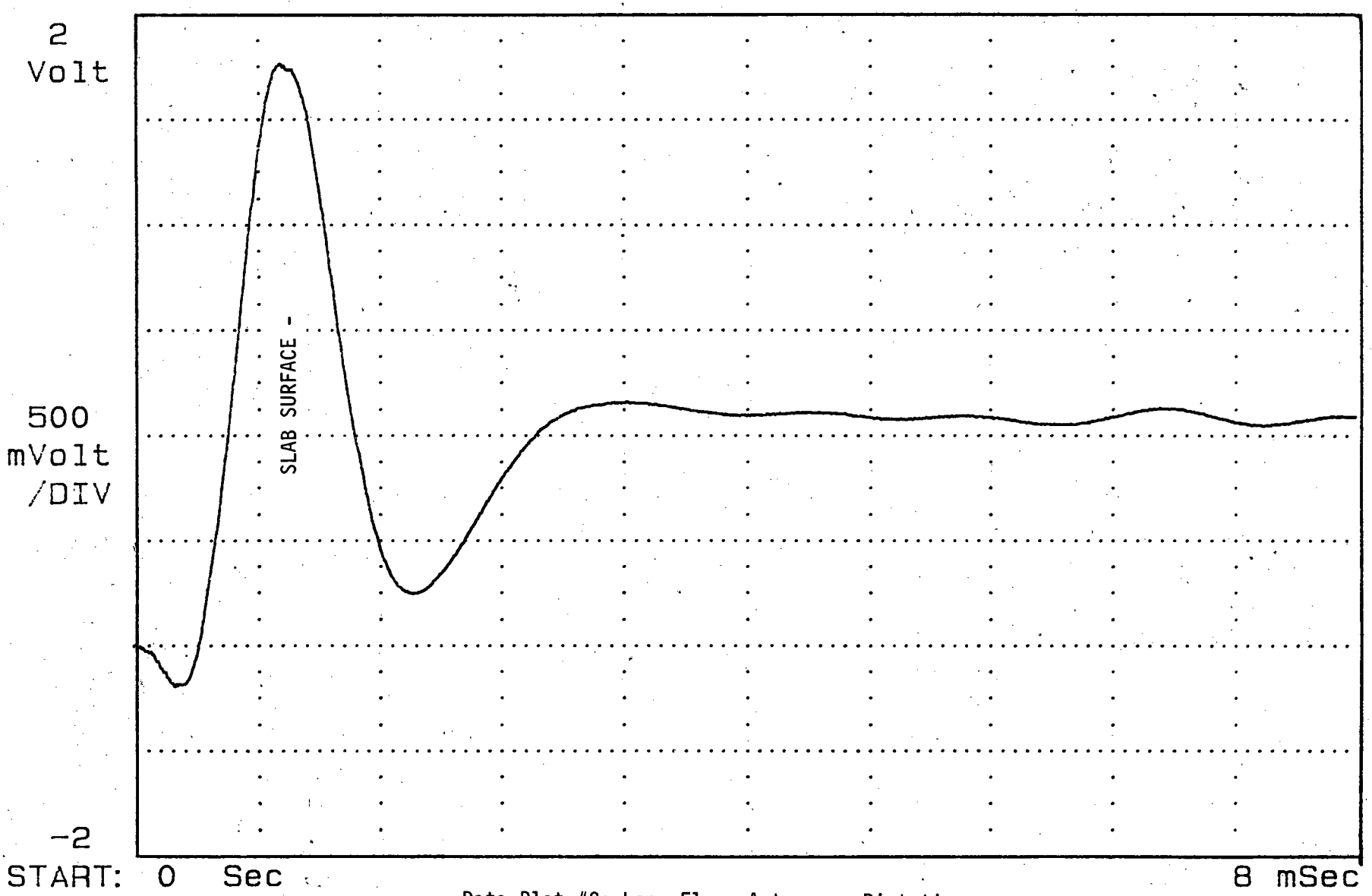

Data Plot #2: Long Flare Antenna - Bistatic Mode (Very Thick Concrete Slab, No Returned Signal)

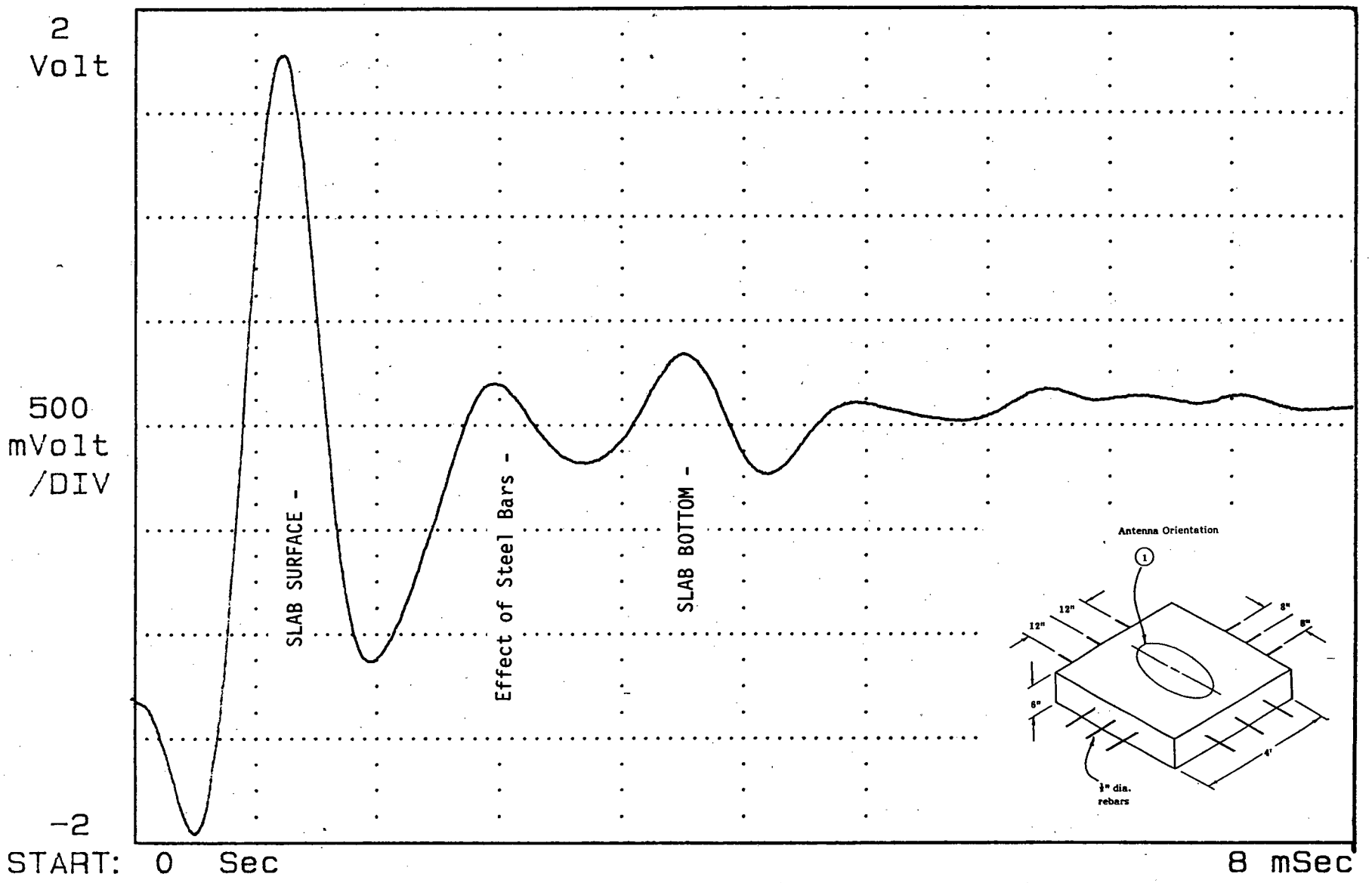

Data Plot #3: Long Flare Antenna - Mono-static Mode

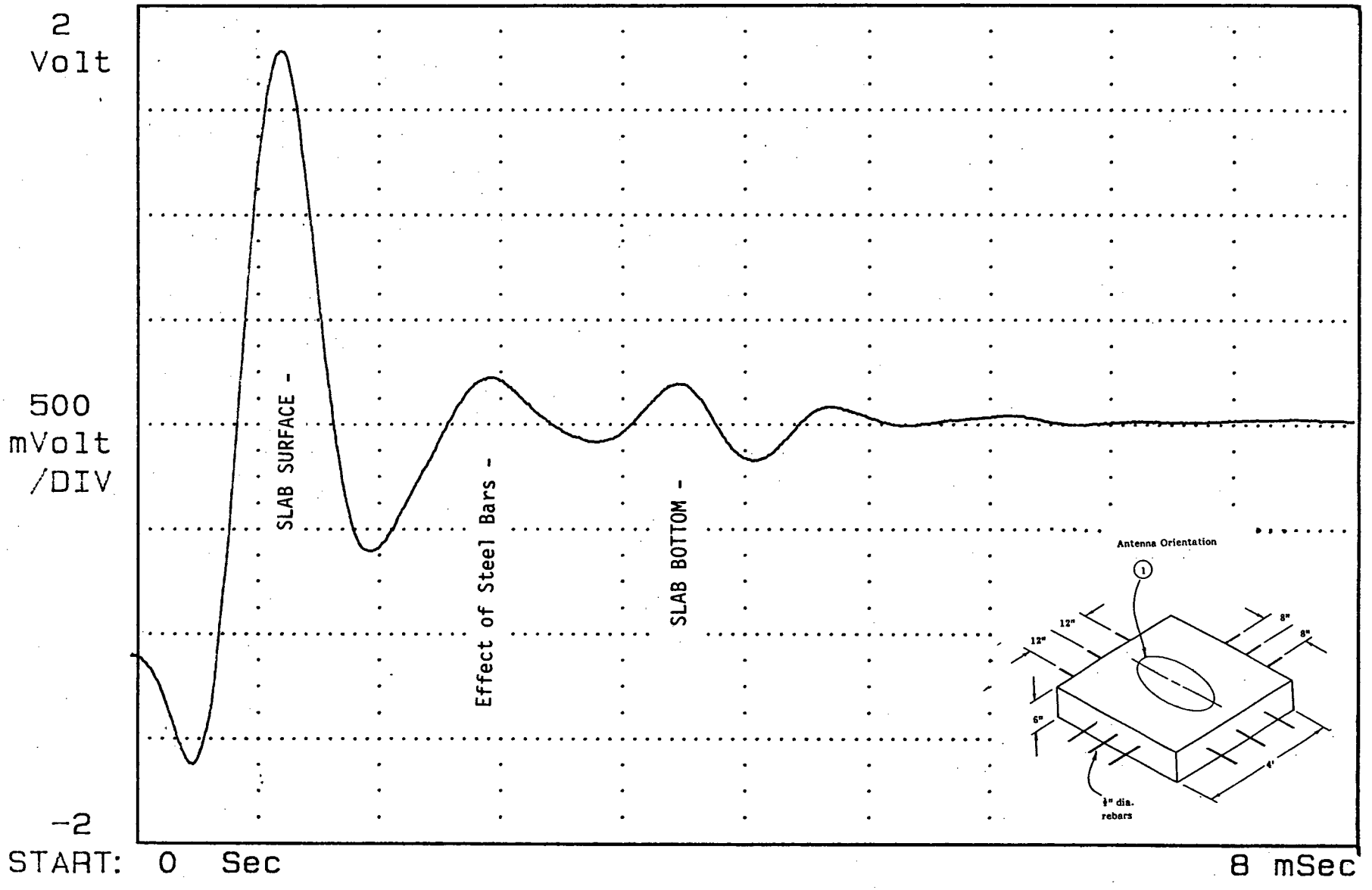

Data Plot #4: Medium Flare Antenna - Mono-static Mode

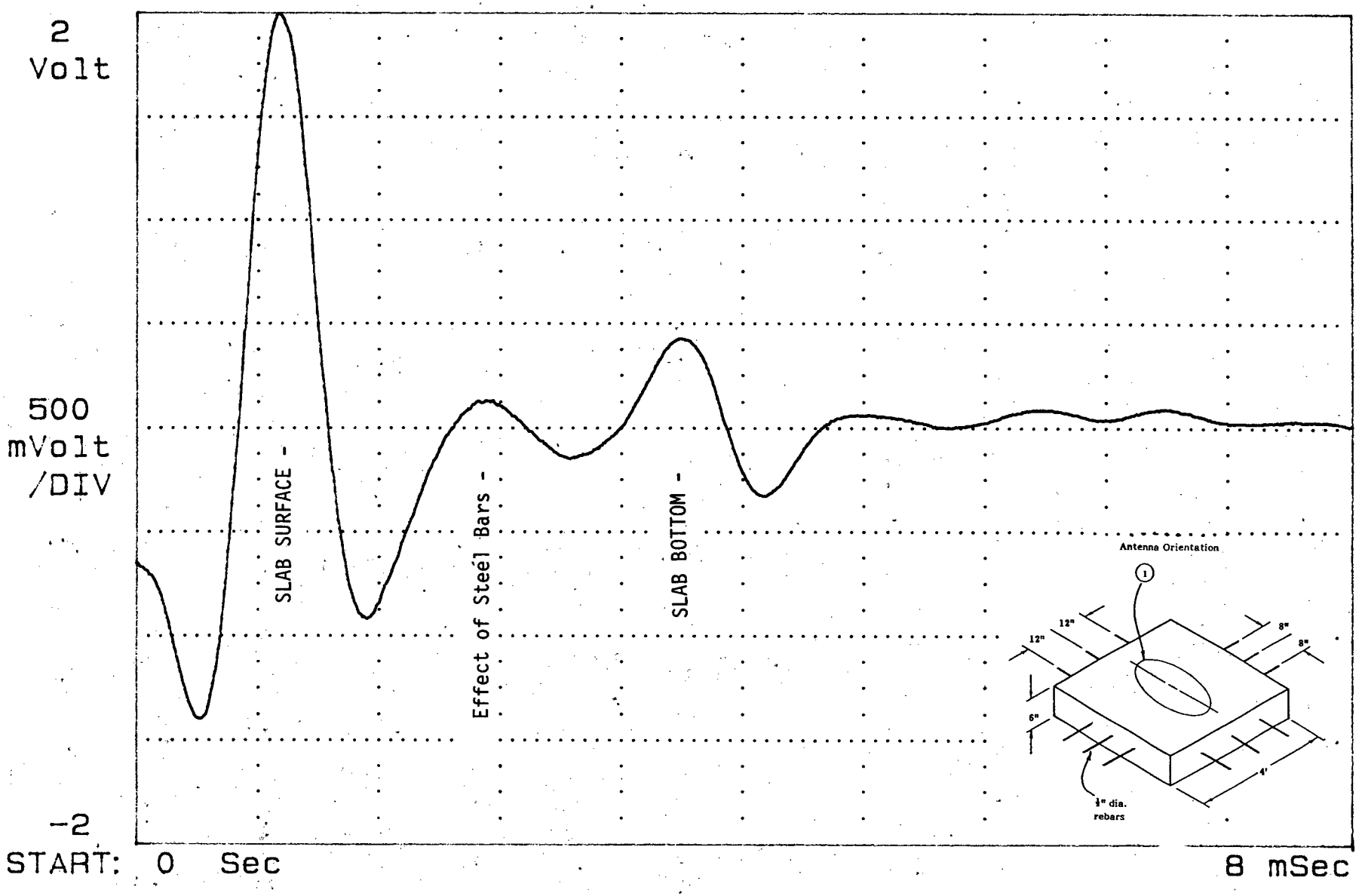

Data Plot #5: Long Flare Antenna - Bistatic Mode

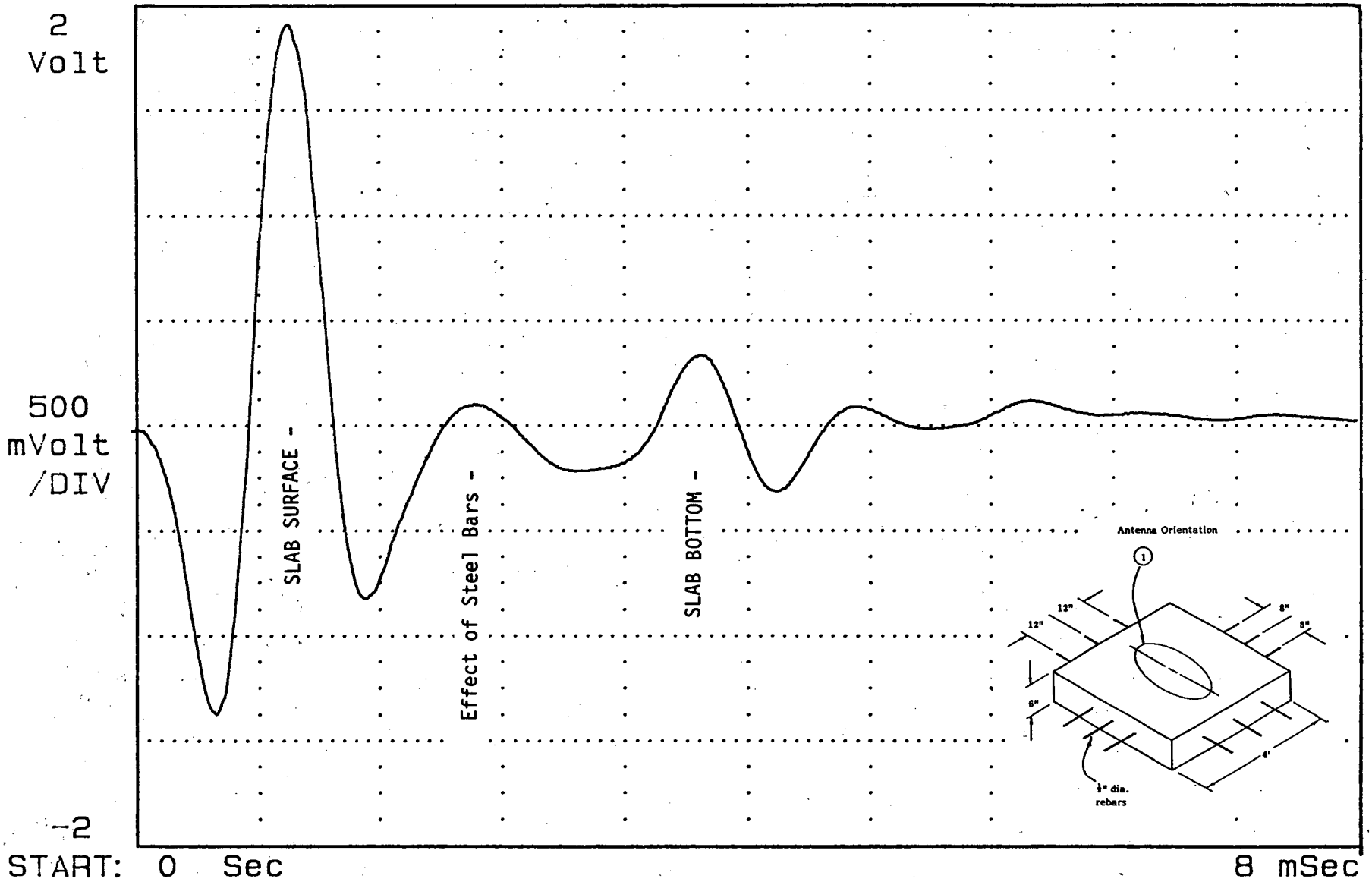

Data Plot #6: Short Flare Antenna - Bistatic Mode

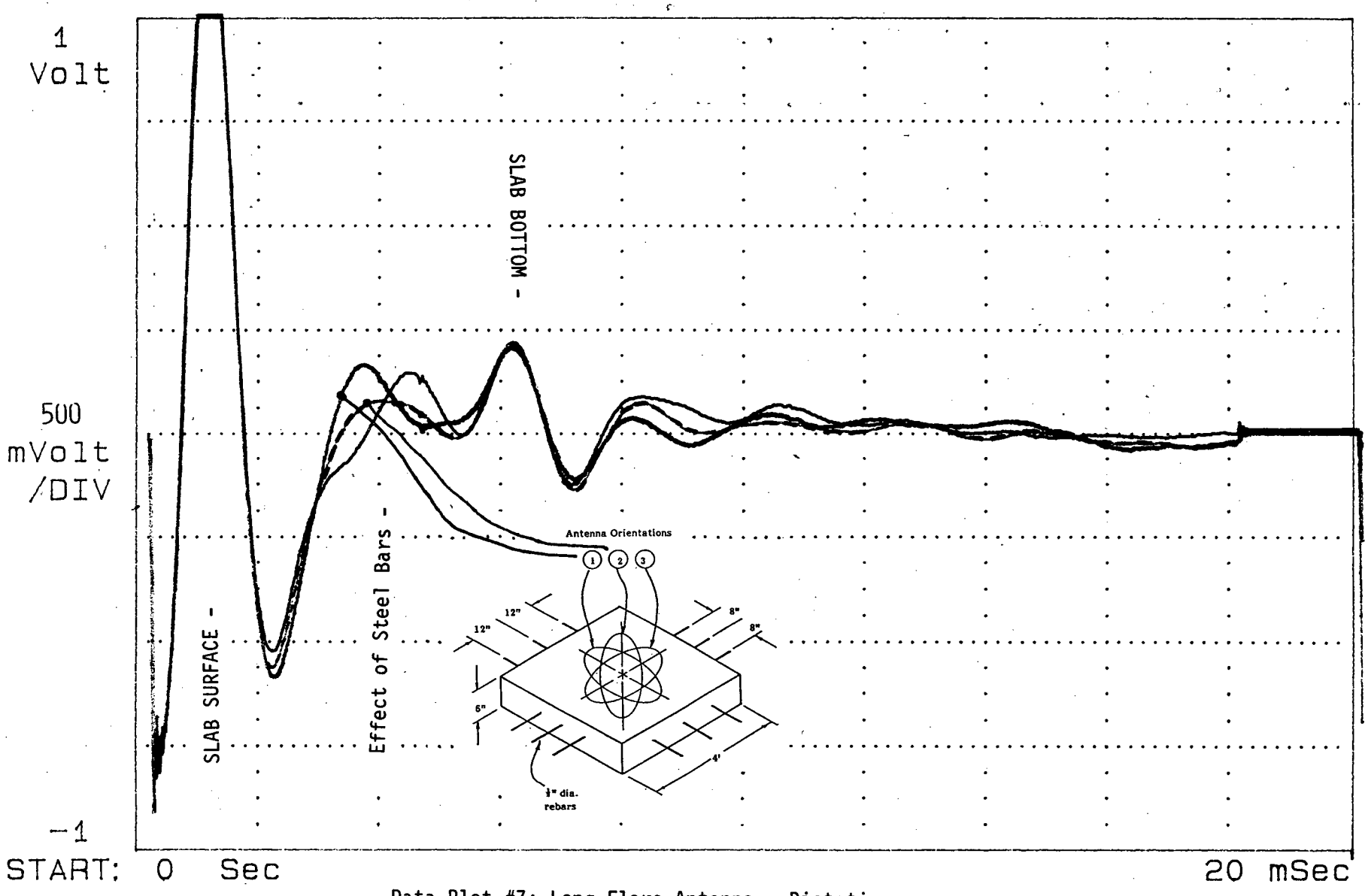

Data Plot #7: Long Flare Antenna - Bistatic Mode (Antenna Orientation Effects)

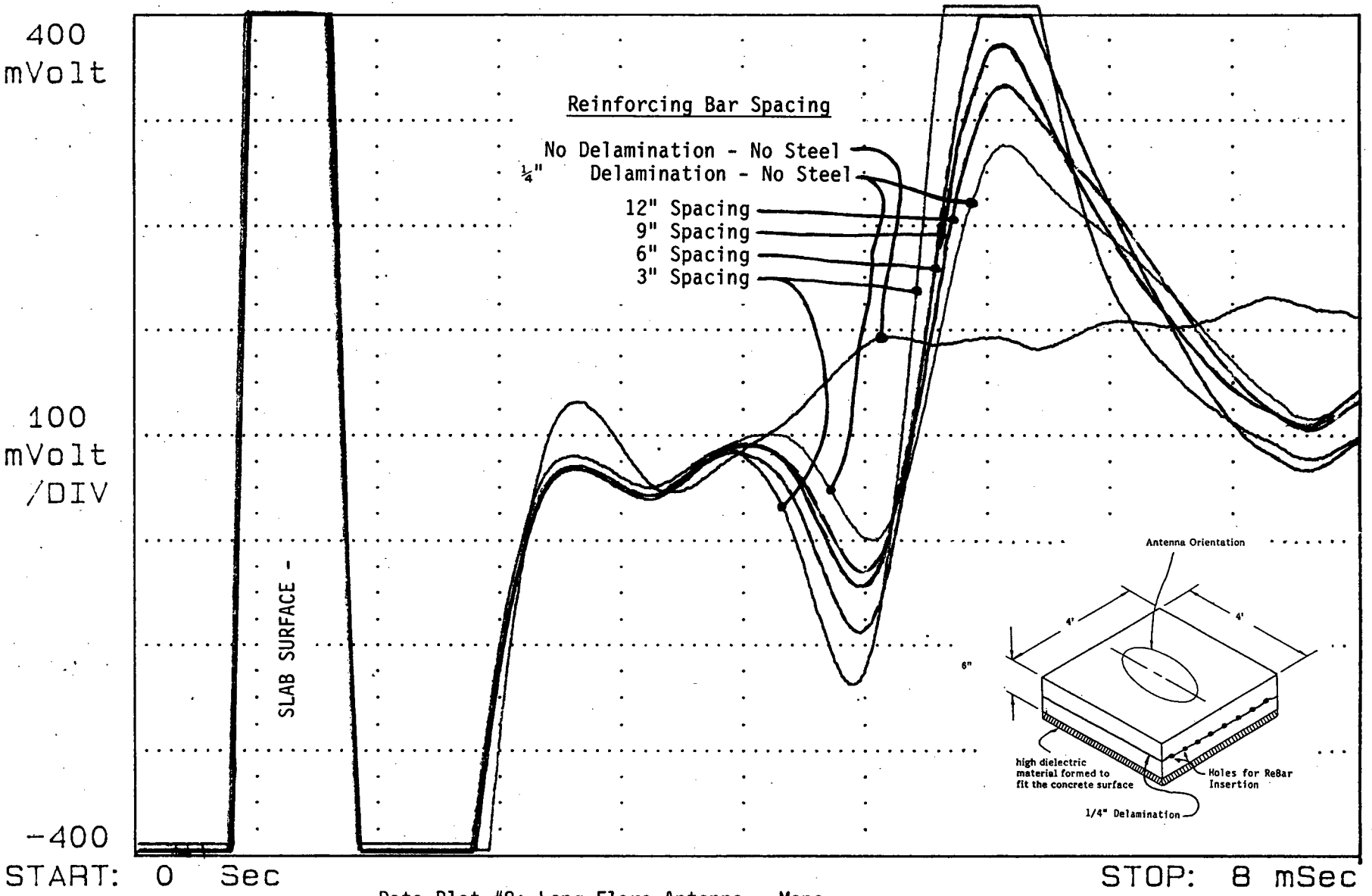

Data Plot #8: Long Flare Antenna - Mono-static Mode (Antenna Orientation Effects - A)

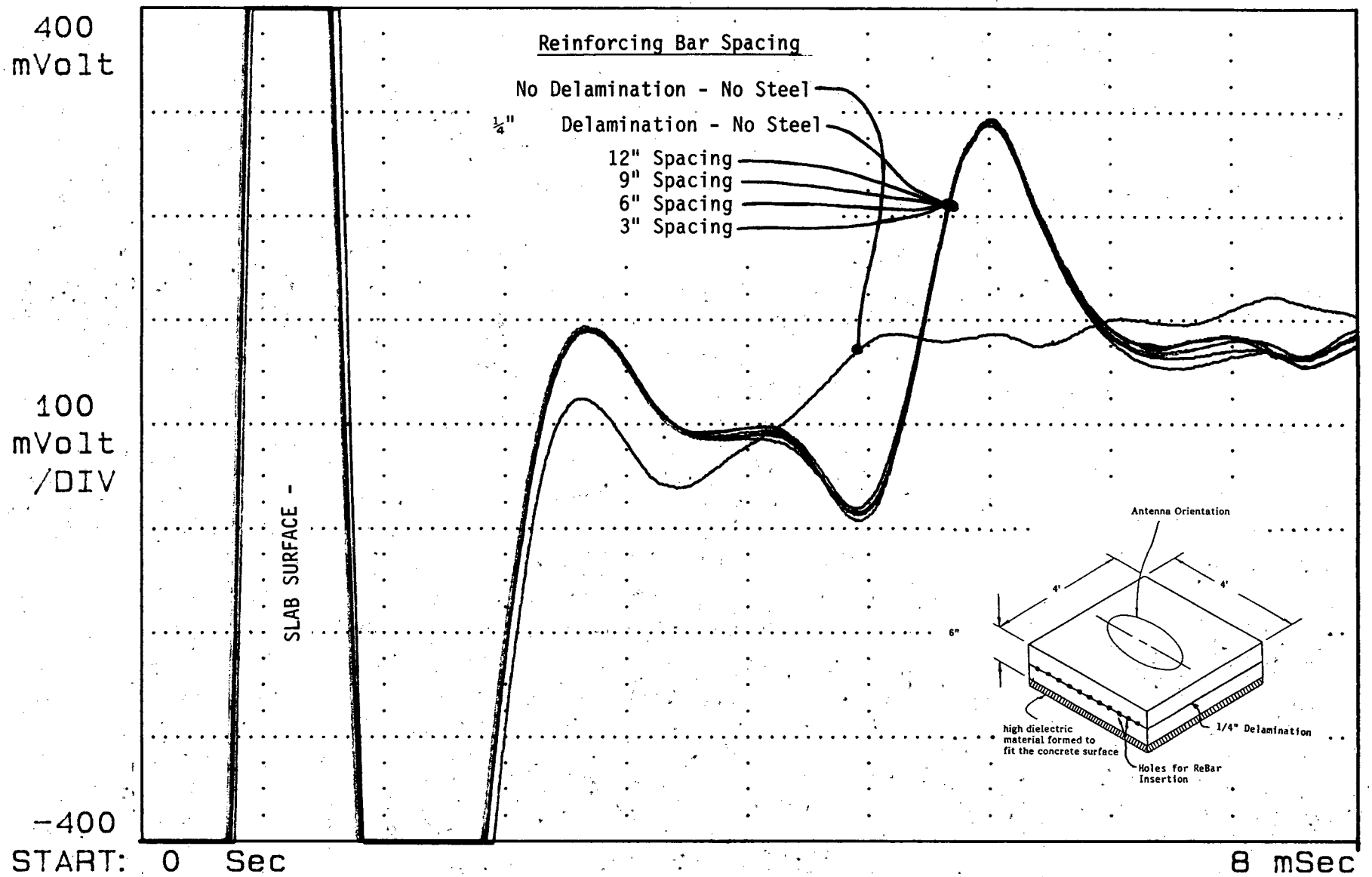

Data Plot #9: Long Flare Antenna - Monostatic Mode (Antenna Orientation Effects - B)

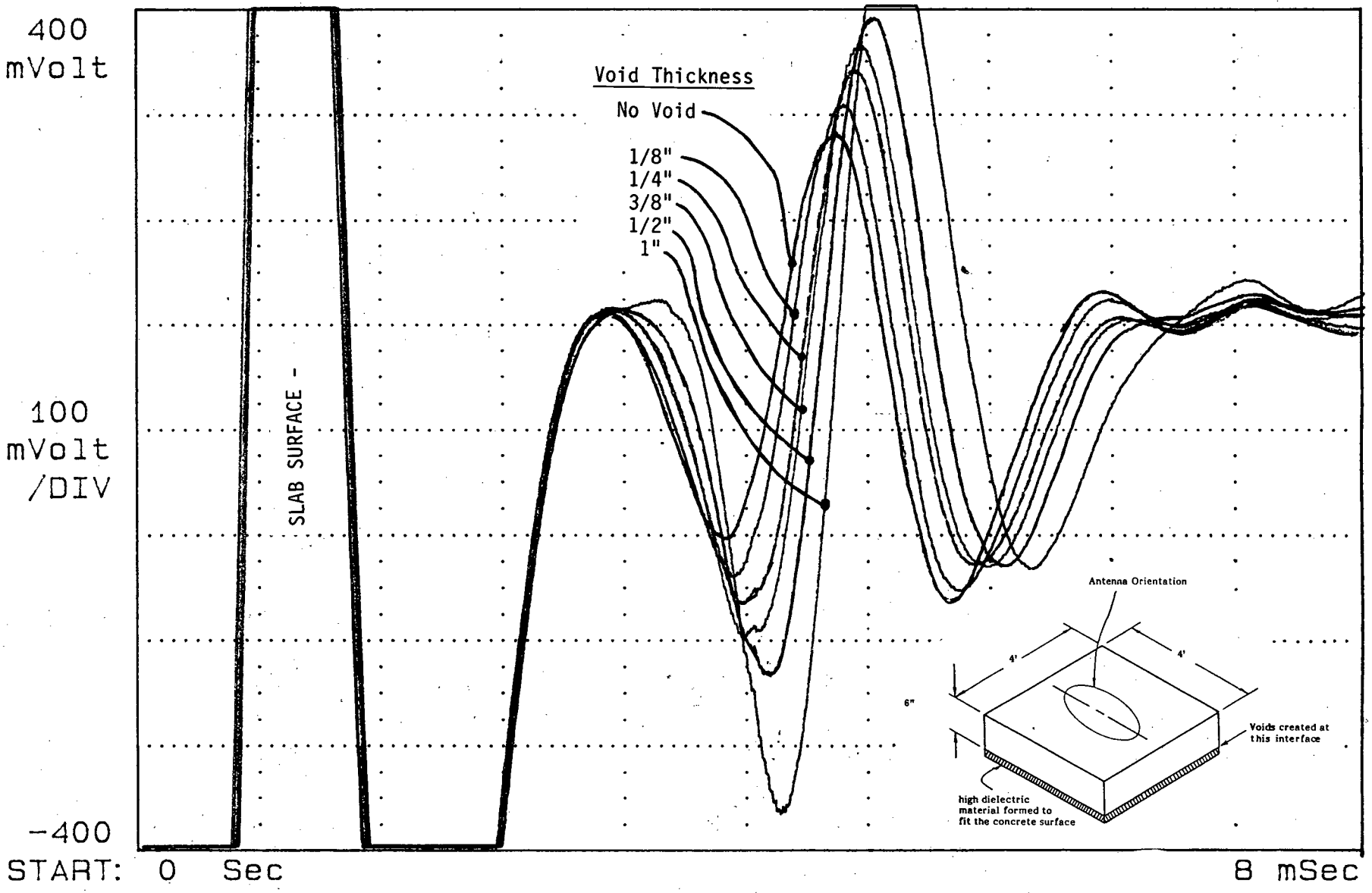

Data Plot #10: Long Flare Antenna - Monostatic Mode (Void Modeling - Plain Concrete)

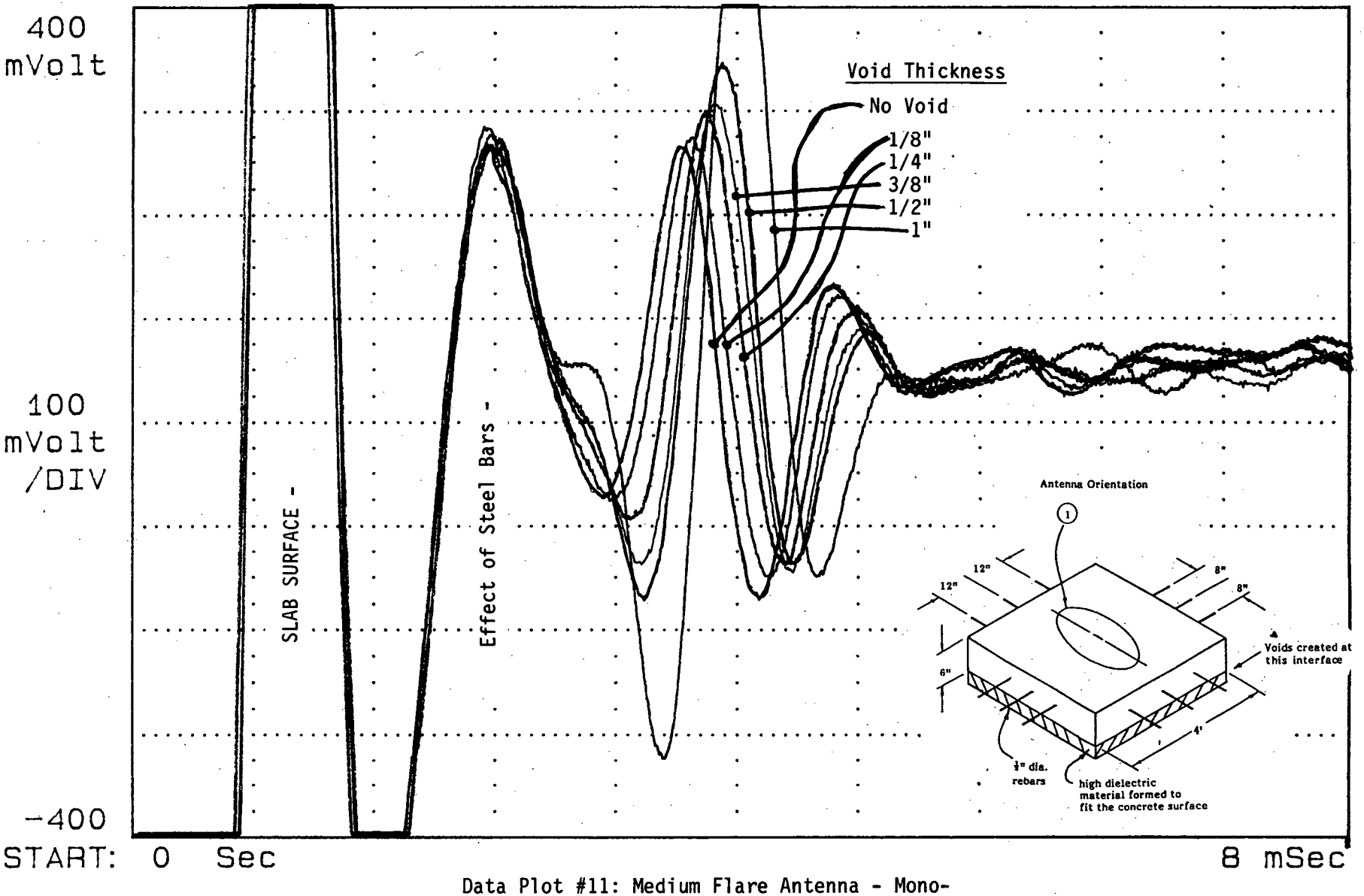

Data Plot #11: Medium Flare Antenna - Monostatic Mode (Void Modeling - Reinforced Concrete)

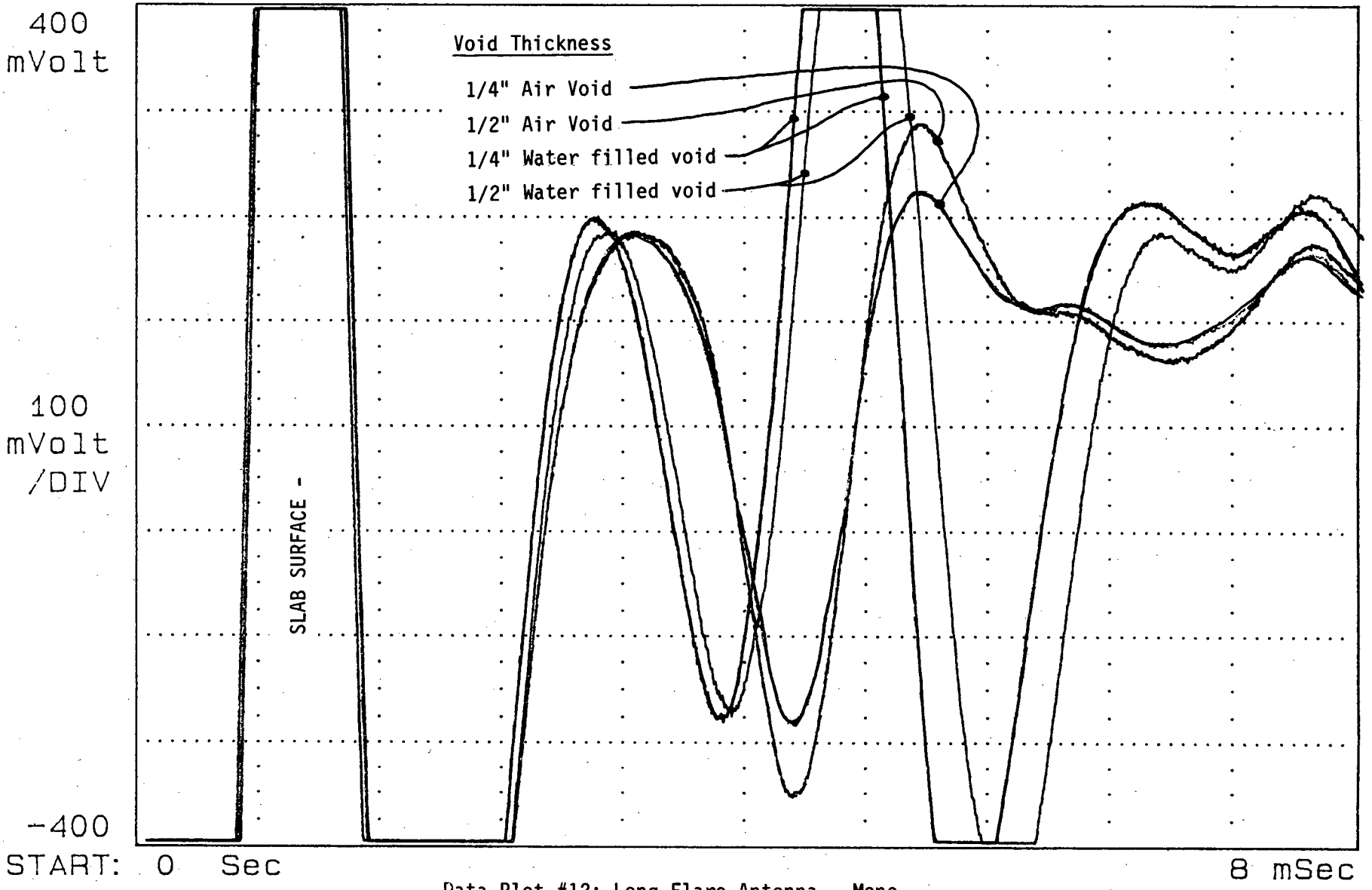

Data Plot #12: Long Flare Antenna - Mono-static Mode (Effect of Water Filled Void)

APPENDIX G

FIELD TESTING PROGRAM

Several sites were chosen to conduct field tests of the radar and video systems. The five-antenna system was employed on most test sites to verify operational performance. A standard RODAR™ vehicle was used on every test site for comparison with the five-channel system and in the determination of the limits of ground-penetrating radar in determining various subsurface distresses. The surface video system was employed on several of these test sites. Verification of the subsurface distress was carried out with a variety of methods: deflection tests (Falling Weight Deflectometer, Dynaflect, Benkleman Beam), grouting, slab removal, and a special "water infiltration" test discussed in the main report. This water infiltration test was widely used during the field testing program. The following sites were chosen for the field testing portion of this project:

I-475 Bibb County, Georgia
I-40 Iredell County, North Carolina
US 90 Hancock County, Mississippi (Jointed)
US 90 Hancock County, Mississippi (CRC)
I-95 Glynn County, Georgia
I-85 Gwinnett County, Georgia
I-10 Waller County, Texas
I-74 Champaign County, Illinois

I-475 BIBB COUNTY, GEORGIA

This pavement consisted of 9 in. of PCC. The pavement was not reinforced and the joints were not dowelled. The joints were not skewed and had a 30-ft spacing. I-475 serves as a bypass around Macon, Georgia, and carries the majority of the I-75 traffic. I-75 serves as the major north-south route from the midwestern states through the southeastern states to Florida, and carries a large traffic volume with a substantial truck percentage.

The pavement exhibited little joint-related distress and had few broken slabs. The two major distresses in evidence were faulting at the joints and slab pumping. At the time of this field test, Georgia DOT personnel were conducting deflection tests in an attempt to determine the existence and extent of voids.

Ground-penetrating radar was used on a 1-mile section of I-475 from sta. 275+00 to sta. 225+00 in the southbound lane. The survey was conducted and five locations were chosen for verification. The verification was carried out using the water-infiltration test described earlier. The water infiltration test identified three general subsurface conditions: air voids (very rapid infiltration), sound pavement/base contact (little short-term infiltration), and deteriorated base material (slow/moderate infiltration rate). The "deteriorated base material" was generally wet and had coarse gradations indicating loss of fines. The original base material was a well-graded, bituminous stabilized, crushed aggregate. The "deteriorated base material" areas had widely varying infiltration rates indicating very small voids or coarse material at the pavement/base interface causing these variations in infiltration rates. The radar signatures associated with these three general areas were very different (Figures G-1, G-2, G-3).

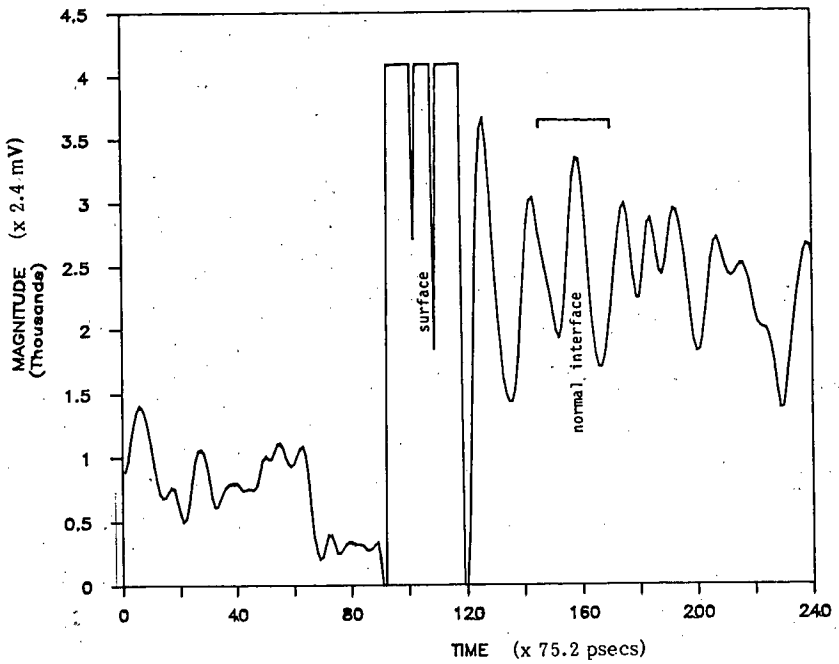

Figure G-1. Radar signal return data plot from I-475 test section—good area.

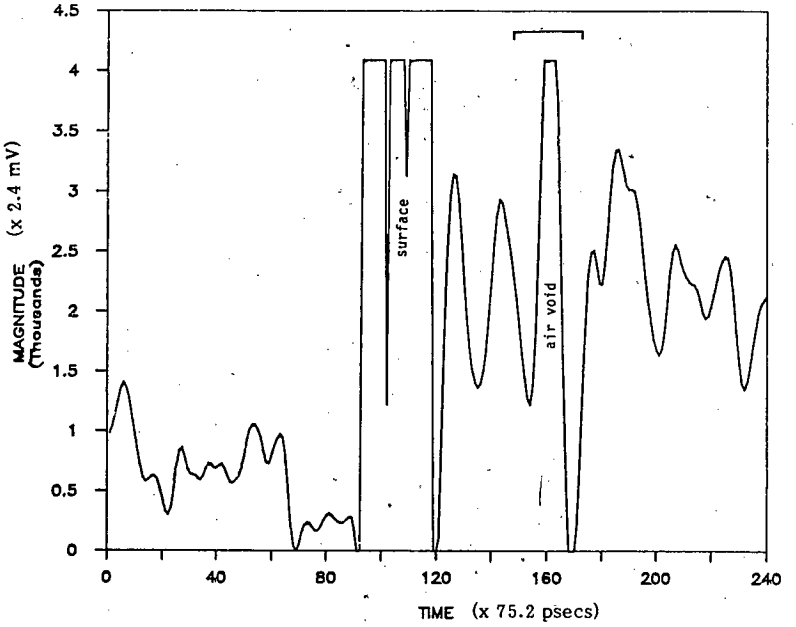

Figure G-2. Radar signal return data plot from I-475 test section—air void.

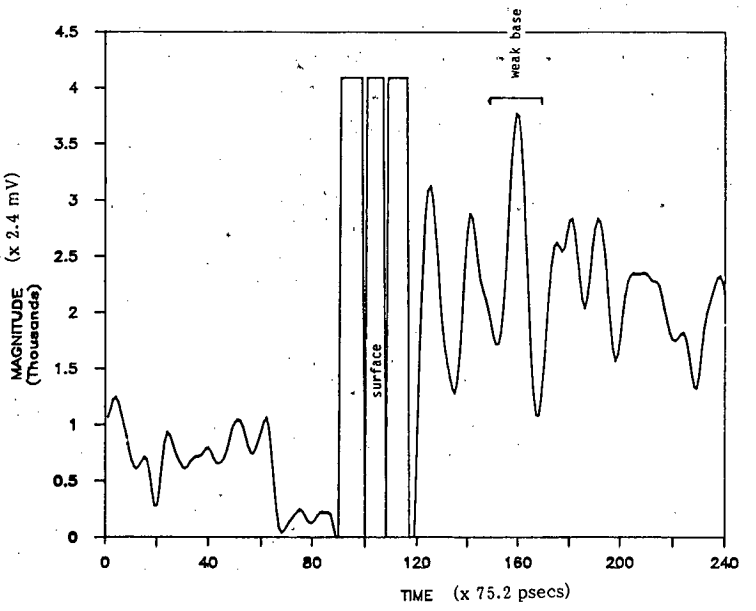

Figure G-3. Radar signal return data plot from I-475 test section—deteriorated base material.

Based on the obvious return signal, the air void in Figure G-2 can readily be detected. Using the same logic, the difference in radar signature between areas of sound pavement-base interface and areas of "deteriorated base material" make the detection of the deteriorated areas visually obvious and certainly feasible using automatic processing techniques.

Surface video data on this project was of little value because there was no surface manifestation of the subsurface distresses. Shoulder distresses, although occasionally an important factor, were not included in the scope of this research. No broken slabs or joint-related distresses of the concrete pavement existed on this project.

I-40 IREDELL COUNTY, NORTH CAROLINA

This field test was performed on a 1,000-ft section of the westbound, outside lane of I-40 near Statesville, North Carolina. I-40 is a major east-west route and carries heavy traffic levels. This portion of I-40 consists of 9 in. of PCC pavement and 6 in. of graded aggregate base. The pavement is not reinforced; the joints are not dowelled; and the joints have a 30-ft spacing and are not skewed. The only surface indication of distress was slab faulting. No signs of pumping and no broken slabs existed.

The goal of this test was to determine the existence of voids, the horizontal extent of the voids, and the effectiveness of pres-

sure grouting in filling the voids. For verification, several methods of void detection were used during this test for comparison with radar results. Other methods of void detection included: Falling Weight Deflectometer, Dynaflect, and Benkleman Beam. The sequence of testing was as follows:

Day 1 a.m.—radar and deflection testing
p.m.—grout each slab with standard hole pattern
Day 2 a.m.—radar and deflection testing
p.m.—remove selected slabs

The testing was performed early in the morning because of widespread acceptance that deflection testing is most effective at this time because of lower temperatures. The tests were performed both before and after grouting to compare void detection capability and grouting effectiveness. The Benkleman Beam was used, and the data were evaluated in a manner specified by the North Carolina DOT. The Falling Weight Deflectometer was operated, and the data were evaluated by a method developed as part of NCHRP Project 1-21. The Dynaflect was operated, and the data were evaluated in an accepted manner.

The radar data were verified at three joints using the "water infiltration" procedure. This gave positive correlation between radar signatures and actual voids. Both the 5-antenna radar system and the standard RODAR™ vehicle were used during this test. Based on the physical evidence provided by the "water infiltration" test, the radar data were analyzed to determine the length of void (longitudinal) in each antenna path across the roadway (lateral). The data could then be combined to determine the shape of the void. The results of the radar data analysis are shown in Figures G-4 through G-7. In these figures, the lengths of the voids in each of four antenna paths are shown for each of the 34 joints in this test section. An example estimate of the horizontal void shape is included in these figures.

After the grouting was completed and the post-grout testing was performed, the radar data were evaluated based on the obvious radar signal changes that the existence of grout causes. Figures G-8 through G-11 show the existence of grout overlayed on the pre-grout voids. These figures are very interesting because the relationship between grout flow and voids can be seen.

The results from all the various testing methods, both pre-grout and post-grout, are tabulated in Figure G-12. A general, and subjective, indication of whether the slab "accepted" grout or not is also included in this figure. Based on a comparison of the various deflection measurements with radar, there was an 80 to 90 percent agreement concerning the existence of voids.

One should keep in mind that deflection testing can only determine "loss of support" beneath concrete pavements. This "loss of support" may be void-related or occasionally can be related to weak base materials or slab curl. Because the radar data interpretation was based on physical evidence of voids, and the agreement between deflection tests and the radar testing was high, the "loss of support" measured by the deflection tests was assumed to be void-related in this case.

The correlation between deflection test results and radar data after the grouting was mixed. This was a result of the differences in the measurement techniques. Deflection tests indicated reductions in deflections caused by the presence of grout under the slab, with no indication that the grout fully filled the voids under the slab. The radar signal return from a grout layer under the slab is very obvious, and the extent of grout flow under the slab can be readily detected. Differences in the post-grout results between deflection tests and radar can probably be attributed to the fact that grout pumped beneath a slab will increase the stability of that slab regardless of how well all voids are filled, and radar can detect how far the grout actually flowed and whether voids are filled. This obvious difference, in what is actually measured, between deflection tests and radar accounts

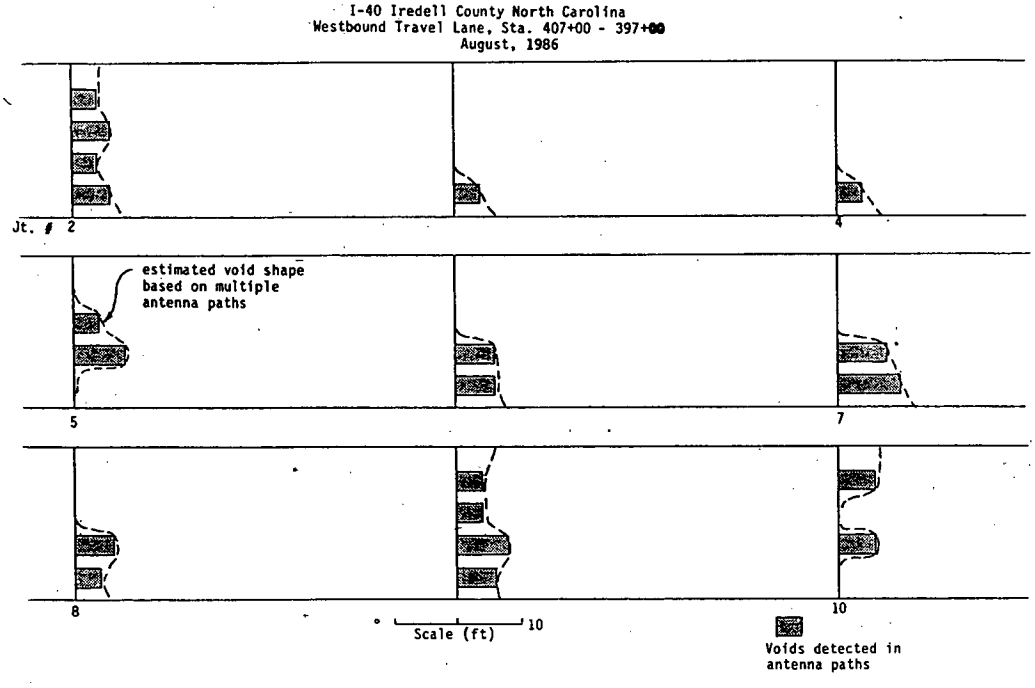

Figure G-4. Results of radar analysis for void horizontal shape on I-40 test section (JTS. 2-10).

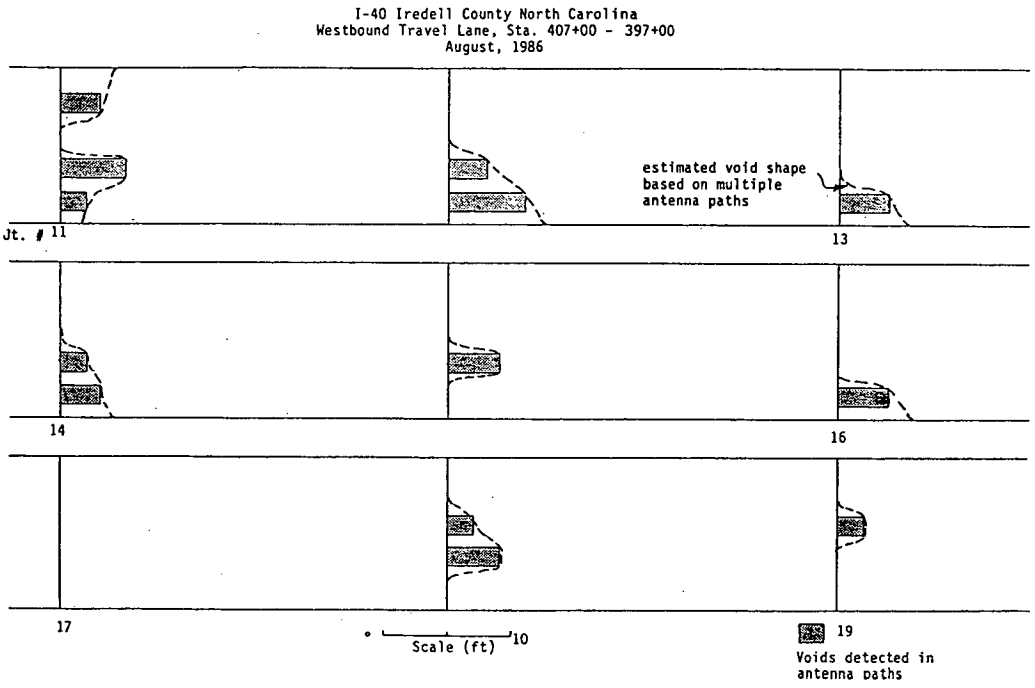

Figure G-5. Results of radar analysis for void horizontal shape on I-40 test section (JTS. 11-19).

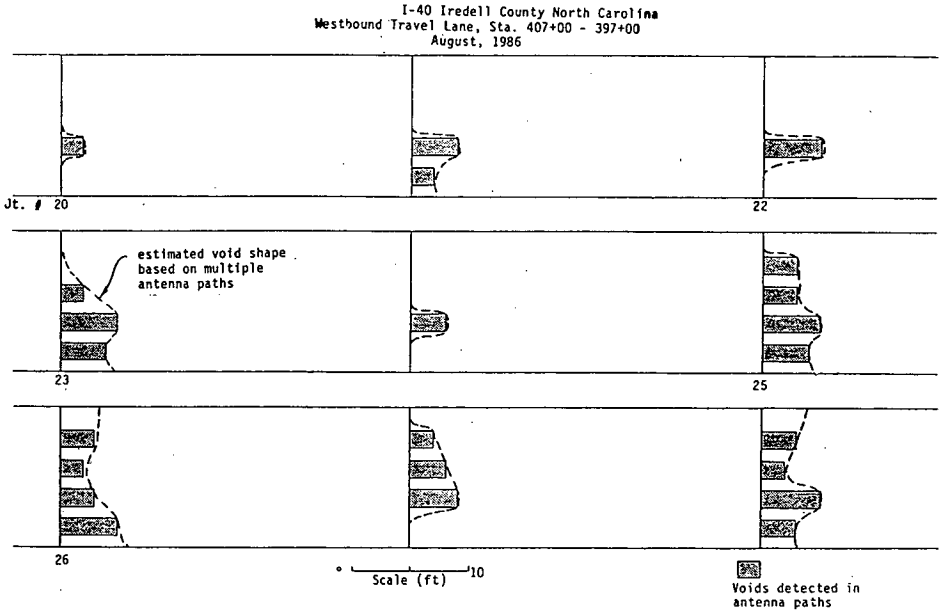

Figure G-6. Results of radar analysis for void horizontal shape on I-40 test section (JTS. 20-28).

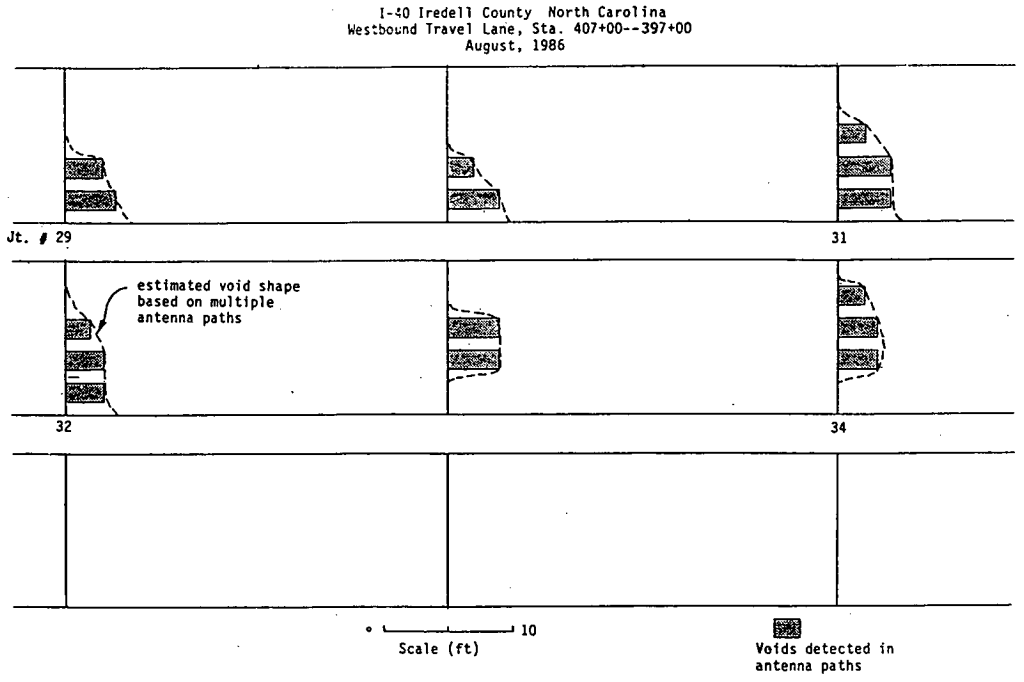

Figure G-7. Results of radar analysis for void horizontal shape on I-40 test section (JTS. 29-34).

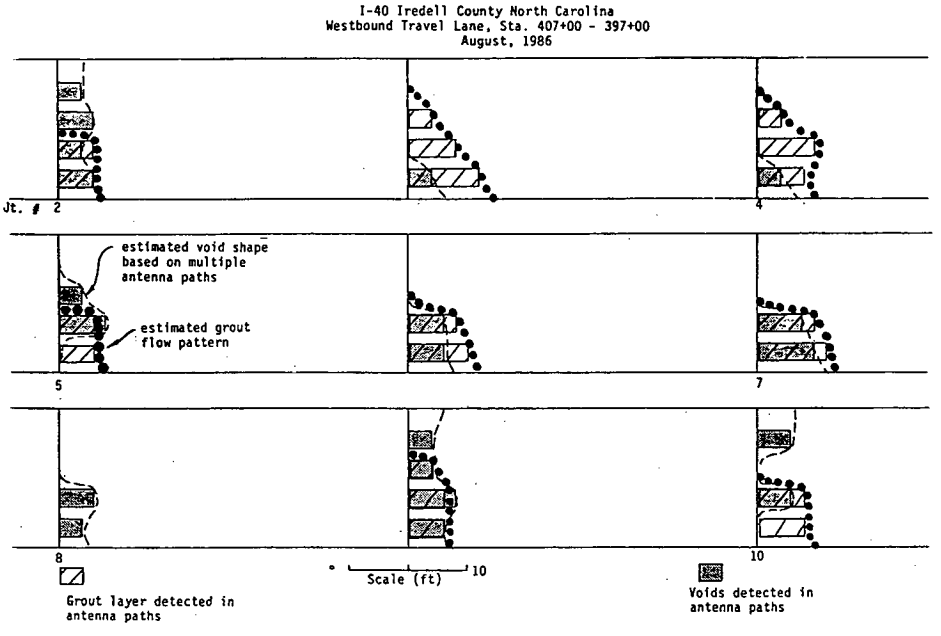

Figure G-8. Results of radar analysis for grout flow on I-40 test section (JTS. 2-10).

for any discrepancies in the correlation of post-grout test results. In several cases, radar detected grout under a slab, but all the voided area under the slab was not filled with grout (Figures G-8 through G-11), and the existence of ungrouted voids under certain slabs was indicated by the radar. On the other hand, some slabs had grout pumped into areas with no previous voids.

After the post-grout measurements were completed, four slabs were chosen to be removed in order to determine how the grout had flowed during pumping. There was very good correlation between the radar-indicated grout layer extent and the actual layer of grout under the slab.

Although this field test was concerned with void detection, void extent and grouting effectiveness, additional analysis of these data revealed some interesting features. Figure G-13 is a photograph of a portion of the field data, as displayed on the color enhanced Radar Data Analysis System, a feature of the RODAR™ system. This figure represents the radar data from

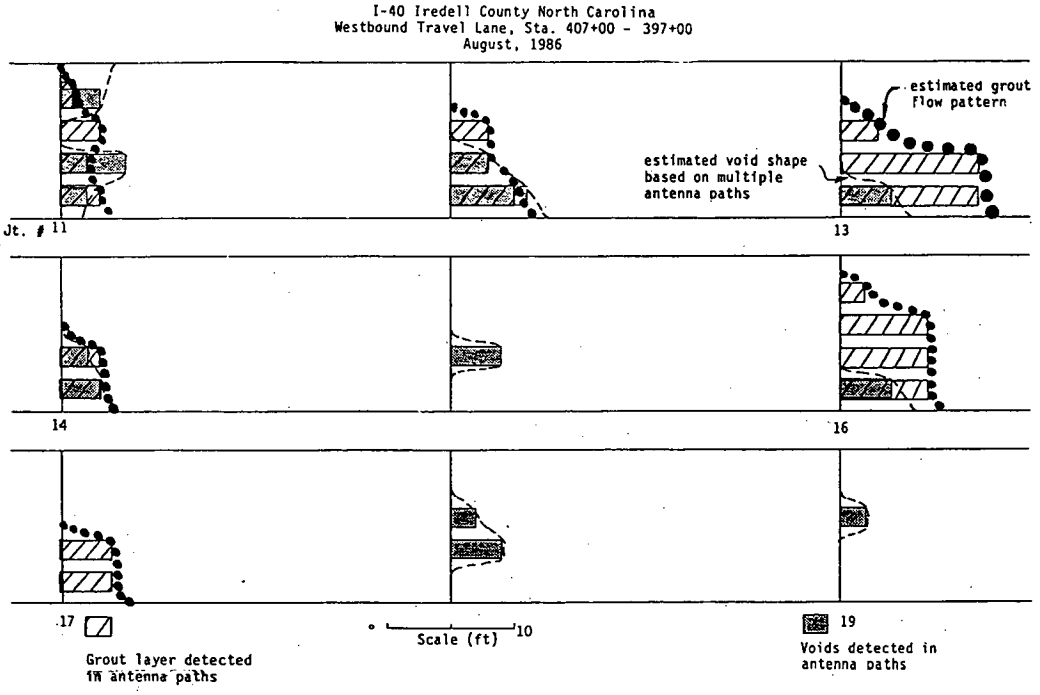

Figure G-9. Results of radar analysis for grout flow on I-40 test section (JTS. 11-19).

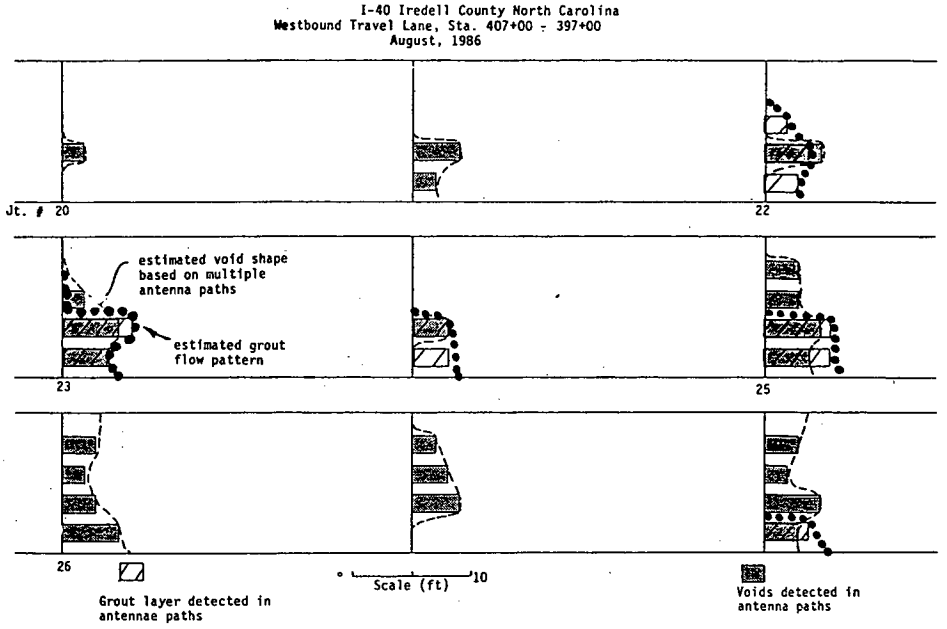

Figure G-10. Results of radar analysis for grout flow on I-40 test section (JTS. 20-28).

one antenna path in the area that includes the last three joints in this test section.

From Figure G-13, the pavement surface is obvious as a green band at the top of this figure. Approximately in the center of the figure is a straight dotted line which marks the radar signal return from the bottom of the concrete pavement. The three circled areas are joint areas. The joint on the left was verified as a void. At the other two joints, no voids were found. The red color at the joint on the left, which represents a higher amplitude negative return, indicates the presence of a void. The uneven dotted line toward the bottom of the slide marks the bottom of a 6-in. graded aggregate base coarse material. It is interesting how this line fluctuates under each joint. What this indicates is that the base material under the joints has a higher dielectric constant than the base material between the joints. This increase in dielectric slows down the radar pulse and makes the thickness of the base layer under the joints appear to be greater. This higher dielectric could only be caused by water coming through the joints and saturating the base material in the area around the joint. This increase in apparent thickness

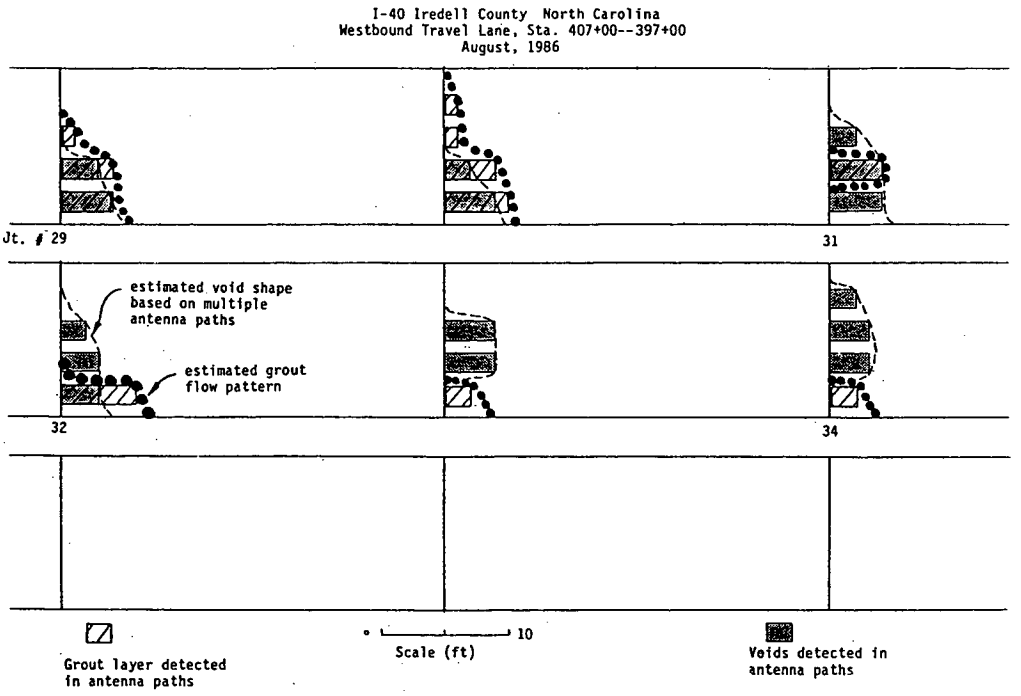

Figure G-11. Results of radar analysis for grout flow on I-40 test section (JTS. 29-34).

always occurs directly under a joint, so the only logical reason for this apparent increase in thickness is an increase in dielectric constant. Because base materials are generally uniform, dielectric constant variations must be caused by moisture entering at the joints. It is interesting that the joint areas on the left and right-hand side of this figure have more effect from dielectric variation (apparent thickness) than the joint in the center which would indicate more water is getting through the joints and wetting the base material on the left and right joints in this figure, and less water is penetrating and saturating the base under the joint in the center of the figure. On the basis of these variations in radar pulse velocities caused by moisture variations, if the relationship between moisture content and dielectric constant for a particular base material is determined, it appears feasible to be able to determine the moisture content (and variations in the moisture content) of that base material using radar measurements.

Another interesting feature of Figure G-13 is the fact that the interface at the bottom of the base material (green band just above footage marks) on the left and right-hand side of the figure has a bright red color associated with it. This bright red is an indication of a stronger interface return. The cause of this stronger interface return is greater differences in dielectric constant between the base material and the subgrade material. The most plausible causes would be either a saturation of the subgrade or water standing at the interface between the base and subgrade. Summarizing the preceding discussion, it appears that surface water is entering the joints and saturating the base material in the vicinity of the joints. Further, this water has entered in sufficient quantity to either saturate the subgrade just below the base or to collect at the base-subgrade interface in the vicinity of the joints.

Another interesting point is that these apparent effects of infiltrating water vary from joint to joint. In Figure G-13 the joints on the left and right sides of this figure, and not the joint in the center, have very obvious effects from water infiltrating the base. This would tend to indicate that some of the joints on this project were more effectively sealed than others.

Although the moisture content of the base and subgrade material was not verified during this field test, a combination of radar theory and knowledge of pavement structure point out the feasibility of using radar data to determine unusual subsurface moisture conditions in a pavement system. This 1,000-ft test section had no surface defects. Surface video data were thus of little value.

U.S. 90 HANCOCK COUNTY, MISSISSIPPI (JOINTED)

As part of the field testing program, a portion of U.S. 90 in Hancock County, Mississippi, was surveyed. The five-antenna system was used to survey a 1,000-ft area. The standard two-antenna RODAR™ system was also used on this area for comparison and on other areas of this project for investigative purposes. This test area was on U.S. 90 near the State Route 607 intersection, approximately 5 miles west of Waveland, Mississippi.

This section of U.S. 90 has been in service for nearly 40 years. Until the opening of I-10, U.S. 90 carried the heavy traffic east-west along the Gulf coast. Currently, this portion of U.S. 90

experiences moderate traffic levels. A rehabilitation of this portion of U.S. 90 is planned and there is concern over the subsurface condition of this old area of roadway.

This pavement consists of PCC concrete surface with a variable depth cross section (7 in.–9 in.) The pavement is reinforced with wire mesh and has dowelled joints. The joint spacing is 20 ft and the joints are not skewed. Sand was used to stabilize the top 3 in. of subgrade material to serve as a base material. The shoulders are not paved. The only visible signs of distress on this project were some faulting at the joints and a few cracked

JT. NO.	BB B A	FWD B A	R B A	D	GROUT	JT. NO.	BB B A	FWD B A	R B A	D	GROUT
1	N N	Y Y	Y +	8%	N	18	Y Y	+Y Y	Y Y	+7%	N
2	Y Y	+Y Y	Y N		L	19	Y Y	Y Y	N N	+20%	N
3	Y N	+Y N	Y N	+48%	L	20	Y Y	+Y Y	Y Y	7%	N
4	Y N	+Y Y	Y N	+43%	N	21	N N	Y N	Y Y	Ø	L
5	Y N	+Y N	Y.N	+20%	G	22	N N	+Y N	+Y Y	+37%	G
6	Y N	+Y N	Y N	+40%	G	23	Y N	+Y N	+Y N	-22%	G
7	Y N	+Y N	Y N	+45%	G	24	Y N	Y N	N N	+13%	G
8	Y Y	+Y Y+	Y N	+40%	N	25	Y N	+Y N	+Y N	+7%	G
9	Y N	Y N	Y N		G	26	Y Y	+Y Y+	+Y Y	+6%	N
10	Y N	+Y N	Y N	-25%	G	27	Y Y	+Y Y+	Y Y	Ø	N
11	Y N	Y Y	Y N	-20%	G	28	Y Y	+Y Y+	Y Y	Ø	G
12	Y N	+Y Y	+Y N	-27%	G	29	Y Y	+Y Y+	+Y Y	+60%	G
13	Y N	Y N	+Y N		G	30	Y N	+Y N	+Y N		G
14	Y Y	+Y Y	Y N	-15%	G	31	Y N	Y Y+	Y N	+25%	L
15	Y Y	+Y N	Y Y	-17%	N	32	Y Y	Y Y+	Y N	+25%	G
16	Y N	+Y N	N N	-25%	G	33	Y N	N N	Y Y	-32%	G
17	Y N	N N	N N	-13%	G	34	Y Y	Y N	Y Y	Ø	G

BB = Benkleman Beam
FWD = Falling Weight Deflectometer
R = Ground Penetrating Radar
D = Dynaflect: % increase (+) or decrease (-) in deflection after grouting
Grout = Subjective opinion on grout "take" during pumping: G = good take, N = none, L = little "take"
B = Before grouting
A = After grouting
N = No void indicated by test
Y = Void indicated by test
-Y = Small void indicated
Y+ = Large void indicated

Figure G-12. Results of various test methods used for void detection on I-40 test section.

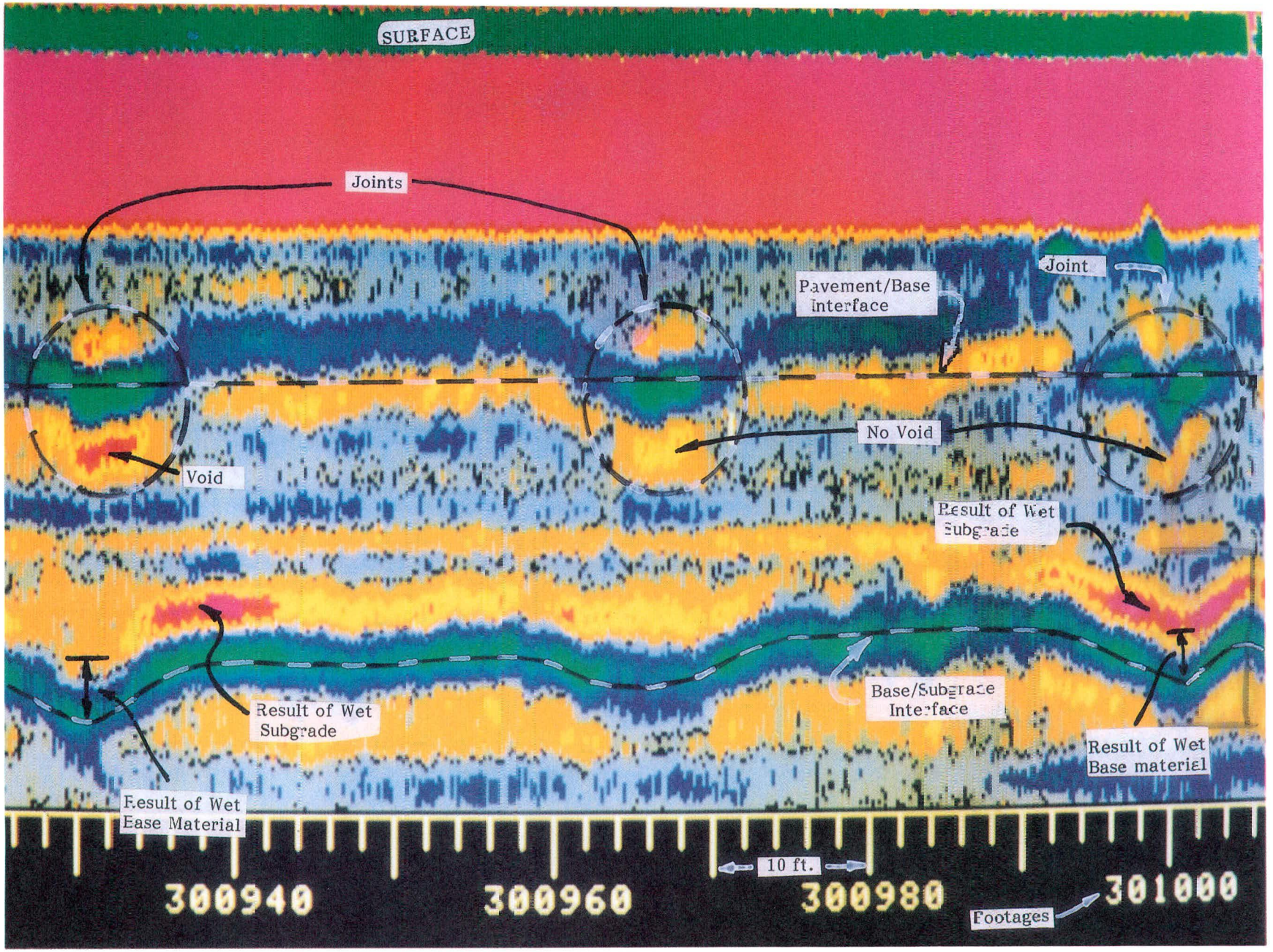

Figure G-13. Data from color enhanced radar analysis system on I-40 test section.

slabs. There was no sign of slab pumping at the shoulder joint. The data were collected, and verification was performed using the water infiltration test. The results of the data verification tests indicated that substantial moisture existed under the concrete slabs in some areas of this project. In the vicinity of joints, a few small water-filled voids were detected, based on the verification tests. Also based on the verification tests, the remaining "water affected" areas could be broken into two categories: (1) areas with excess moisture at the pavement-base interface, but where no voids exist (contact between pavement and base is tight); and (2) areas with materials in the base, just below the pavement, that exhibit a significant degree of cohesiveness (clay). These materials can hold a substantial amount of moisture and give the appearance of free moisture to the radar. It is speculated that this cohesive material has entered the base material from below because of excess moisture and traffic action.

This speculation is based on the fact that these areas occur only near transverse joints or near the longitudinal centerline joint (sources of water infiltration) and occurred only in certain areas. This type of "water-affected" area had no voids in evidence and a firm pavement-base interface.

The reduction in radar pulse transmission power attributed to use of the short-flare antenna (Appendix F) was apparent in this field test. The losses associated with the steel mesh reinforcement in this pavement made the detection of anomalies at the pavement-base interface difficult. The five-antenna system functioned well and recorded all necessary data, but when the data were evaluated and compared to the same data taken with the standard long-flare antennas, the signal return strength superiority of the longer antenna was obvious.

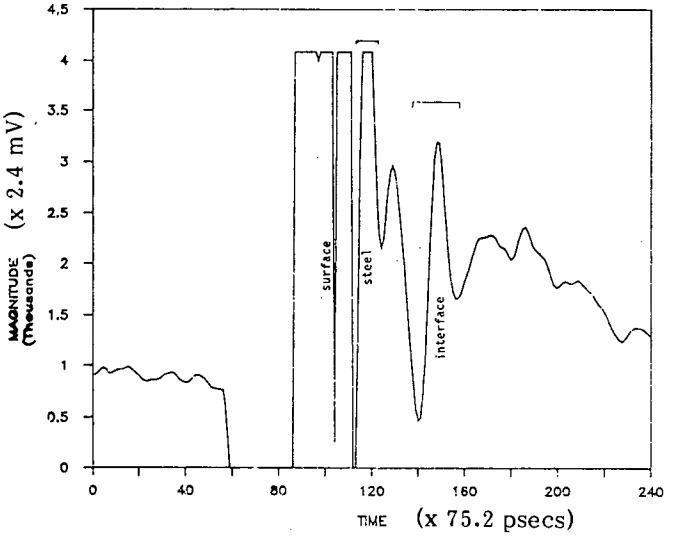

Figure G-14. Data plot from U.S. 90, "normal" antenna orientation.

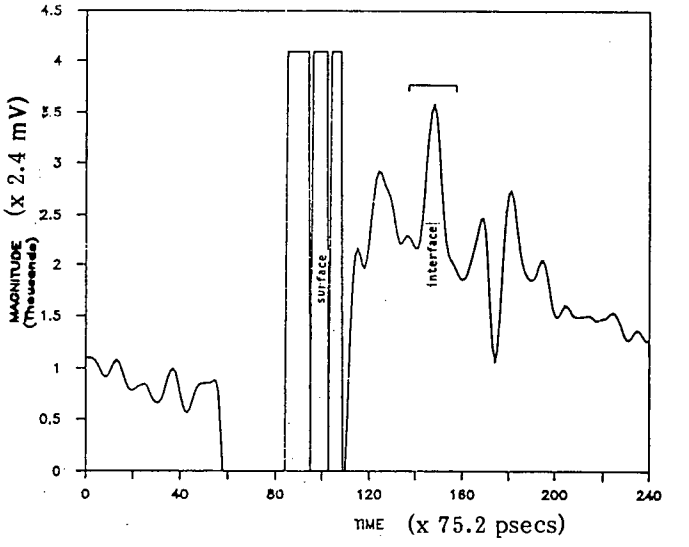

Figure G-15. Data plot from U.S. 90, 90 degree shift from normal antenna orientation.

U.S. 90 HANCOCK COUNTY, MISSISSIPPI (CRC)

This section of U.S. 90 is near the test area described in the previous section. The pavement is a continuously reinforced concrete with reinforcing bars used rather than wire mesh. The steel percentage in this pavement was 0.6 percent. The object of this test was the field verification of the effects of antenna orientation on the penetration of reinforced pavements by radar pulses. Laboratory tests discussed in Appendix F indicated a substantial effect of antenna orientation on radar pulse penetration of reinforced pavements.

A short section of this area of U.S. 90 was chosen for testing. Because these data were to be used as a field verification of laboratory results, only one antenna was used. Radar data were collected on this area twice: once with the antenna in the "normal" orientation and once with a 90-deg change in antenna orientation. Figures G-14 and G-15 are plots of actual data from the same point on the pavement surface, but with different antenna orientations. Comparing the strengths of the returns from the steel and from the pavement-base interface from these two figures, it is obvious that the effect of antenna orientation on radar data from reinforced pavements is substantial. A weaker return from the reinforcing steel means that less energy is being reflected by the steel, so that more energy is available to produce returns from deeper interfaces. This would tend to make the detection and identification of subsurface anomalies in reinforced pavements a much easier matter.

This portion of U.S. 90 had some areas with tightly spaced cracks. Some cracks were spalled and some spalls were patched with asphaltic concrete. The video system was used to collect data for evaluations. Five different runs were made over the same area of roadway. These runs had varying camera heights and f-stops to aid in the study of pavement surface defect video image resolution. With the video camera at a height of 4 ft, cracks with a width of $\frac{1}{16}$ in. could be detected. Spalling as small as $\frac{1}{4}$-in. wide could also be resolved.

I-95 GLYNN COUNTY, GEORGIA

A portion of I-95 in Glynn County, Georgia, was surveyed as part of the field testing program. The surveyed area was in the northbound travel lane near the intersection with SR-99. I-

95 is the major route along the eastern seaboard and carries substantial traffic levels. This pavement has been in service for approximately 15 years. The pavement consisted of 9 in. of continuously reinforced concrete (CRC) pavement over a bituminous stabilized base. The general cracking pattern consisted of reasonably uniformly spaced (15–20 ft) transverse cracks considered normal for CRC pavements of this age. Considerable longitudinal cracking was present, and at a few of the cracks some minor spalling was present. A few areas existed with a series of tightly spaced transverse cracks (3 to 5 cracks, 1 to 2 ft apart). The cracks on this project were generally ⅛-in. wide or less.

This project was considered a good test for the video survey subsystem, because the cracks were tight and the pavement surface was relatively dark in color, a good combination to test the limits of the video subsystem capabilities. A 500-ft section of this roadway was selected for video data collection. The lighting consisted of natural sunlight (clear sky, no haze). The sun was at an orientation and angle that created shadows inside the cracks and spalls which resulted in adequate definition of these features. The video data were collected for a camera height of both 4 ft and 6 ft above the surface. Several runs were made on this test section, with varying camera adjustments and vehicle speed.

The initial analysis of the I-95 video data resulted in less than desirable results. Additional efforts aimed at preprocessing the raw video data to enhance features of interest were employed. The introduction of the preprocessing of the video data as part of the enhancement portion of the video analysis software resulted in much improved analysis results from marginal data. These image enhancement modifications are included in Appendix D. It is felt that the enhancement methodology developed for the data, significantly improved the overall capabilities of the computer-based video data analysis subsystem.

The analysis of the video data indicated that a $\frac{1}{16}$-in. wide crack could be reliably detected using the previously discussed camera system (Chapter Two) at a height of 4 ft. The camera had a 380 × 380 pixel resolution format. The camera and lens system, at a height of 4 ft, resulted in the recording of an area that included 4 × 4 ft of roadway surface. Therefore, each pixel represented $\frac{1}{8} \times \frac{1}{8}$ in. of road surface. The use of the computer-based video analysis subsystem developed for this project allows for the reliable detection of cracks that are less than one pixel wide.

I-85 GWINNETT COUNTY, GEORGIA

An area of the southbound lane of I-85 in Gwinnett County, Georgia, was surveyed as part of the field testing program. I-85 is a major route from the northeastern portion of the United States to the southeast U.S. and carries a considerable traffic loading with a large percentage of trucks. This particular area of I-85 is a special test area for the Georgia DOT and consists of several types of reinforced and nonreinforced PCC overlays of existing PCC pavement. The crack patterns of the CRC overlays have been manually recorded over the past several years as part of the Georgia DOT research program. It was believed that this known crack information would be of value in testing the video recording and analysis subsystem.

When the surface video data were recorded, it was apparent that several factors existed that made this pavement surface a problem for video data analysis. First, the surface had an unusual deeply "tined" texture. A "tined" texture is transverse grooves spaced less than 1-in. apart, placed for improved skid resistance. This texture on I-85 was placed during construction, while the concrete was still plastic. These transverse grooves were deep enough that material had accumulated in the bottom of the grooves, resulting in a considerably darker color. The areas between the grooves were much lighter in color because of traffic wear. The second problem was the width of the cracks on this project. Most of the cracks were transverse (parallel to the grooved texture) and considerably less than ⅛-in. wide. The combination of the transversely grooved surface texture and the very thin transverse cracks made this surface video data impossible to adequately analyze, because the thin transverse cracks were similar in video contrast to the dark areas of the transversely grooved texture.

I-10 WALLER COUNTY, TEXAS

An area of the eastbound lane of I-10 near the Brazos River in Waller County, Texas, was surveyed. The pavement consisted of 10 in. of PCC pavement reinforced with welded wire mesh. The base material was a select borrow material. The pavement had been in service for more than 20 years and had carried extensive truck traffic. The Texas DOT suspected that some joint-related distress (delamination or D-cracking) might be present. Although no surface evidence of these types of distress existed, a portion of the roadway was surveyed. No obvious radar signal returns related to joint deterioration in the concrete were found; nonetheless, several joints were chosen for coring. No physical evidence (cores, visual, radar) verified the existence of joint-related distress (delamination or D-cracking) in the concrete pavement. It is believed that no such deterioration existed.

Several areas of excess moisture and small voids in the vicinity of joints at the pavement-base interface were detected and verified. The corresponding radar data took a form similar to the data from Bibb County, Georgia.

I-74 CHAMPAIGN COUNTY, ILLINOIS

A portion of the eastbound lane of I-74 in Champaign County, Illinois, near the Vermillion County line, was surveyed as part of this project. I-74 is a major east-west route across the midwest United States and carries substantial traffic levels. The PCC pavement was 9 in. thick, had dowelled joints, and was reinforced. The aggregate used in the paving concrete was a limestone that is prone to suffer D-cracking. This project suffered from extensive D-cracking. As examples of the extent of D-cracking on this project, Figures G-16 and G-17 are photographs of two typical joints in the surveyed area.

The amount of steel at the joints (dowels and reinforcement) interferes with the radar signal returns from the D-cracking. Reinforcing steel creates a very large radar signal return, and because the steel is usually in the same area of the concrete as the D-cracking, the radar returns from the two features (steel and D-cracked area) interfere to some extent. The effects of the D-cracking were not readily recognizable in a single signal return waveform, but when all the signal return waveforms, taken across a D-cracked area, are displayed in sequence (as on the

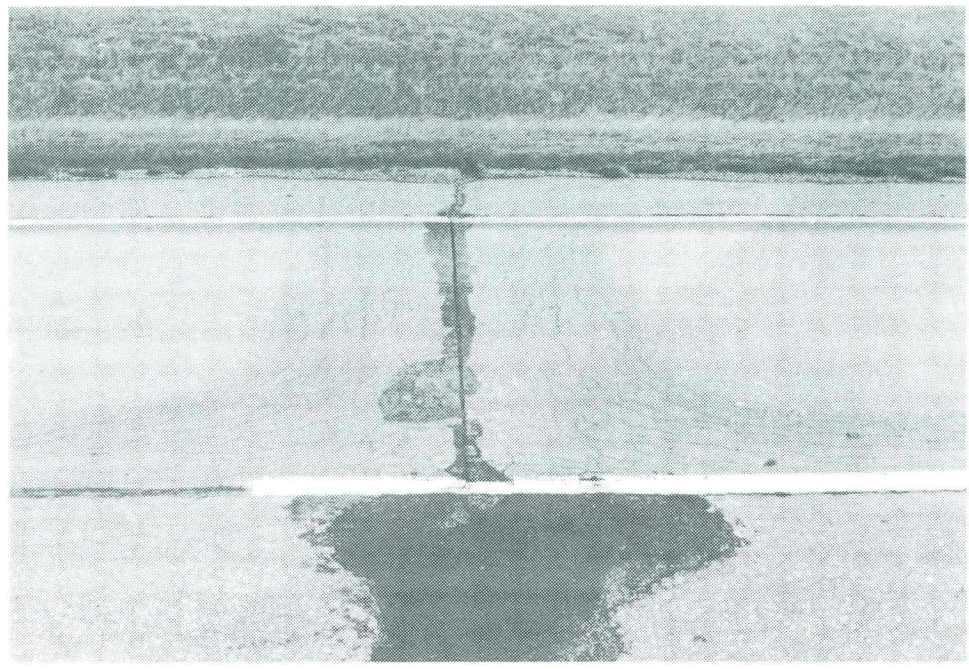

Figure G-16. Typical D-cracking pattern on I-74.

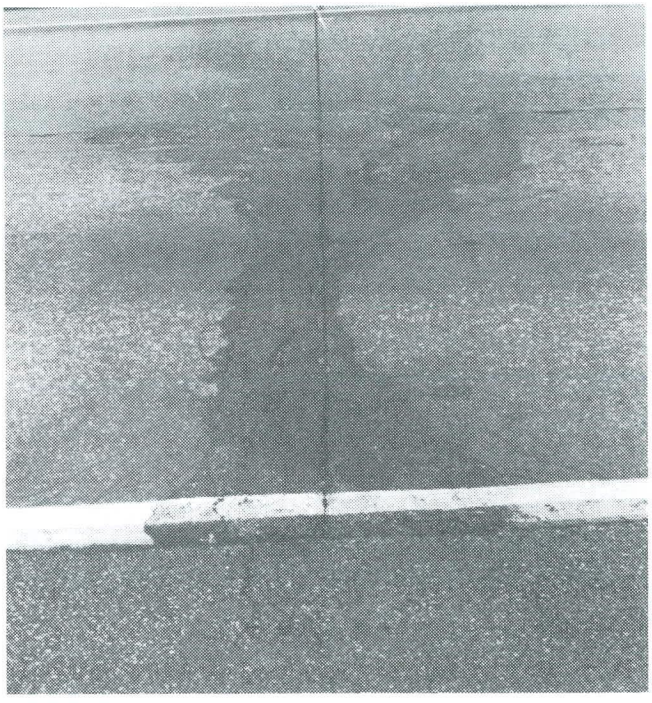

Figure G-17. Typical D-cracking pattern on I-74.

RDAS color-enhanced system), a pattern was evident as a result of D-cracking of the concrete pavement.

The radar waveform pattern resulting from D-cracked concrete shows an increase in the time required for the radar pulse to travel through the concrete in the vicinity of the joint. The D-cracked concrete has a higher dielectric constant than sound concrete, mainly because of moisture content. This higher dielectric constant slows the radar pulse, resulting in a pattern on the RDAS that makes the concrete pavement appear to get thicker in the vicinity of D-cracking. The fifth wheel-based measuring system associated with the radar system allows the determination of the lateral extent of the D-cracking, because it can be assumed that the distance along the roadway that the radar signal return is affected is related to the actual lateral extent of the D-cracking. Figure G-18 is a photograph of actual data from the RDAS monitor showing an example of the effects of D-cracking on the return waveform.

This same effect was reported in an interview with Donohue and Associates personnel, an engineering firm specializing in the application of radar technology to pavement assessment. On a PCC pavement with no dowels or reinforcement, Donohue technicians obtained an excellent correlation between areas where the radar pulse was slowed by the concrete layer (apparent thicker concrete layer on the line scan recorder) and D-cracking as verified through coring.

Although the dowels and reinforcing steel affected the radar return data, the effect of subsurface D-cracking deterioration in this I-74 pavement could be seen in the radar return waveform patterns. This field test was conducted before the laboratory tests proved how radar antenna orientation can significantly reduce the effect of reinforcing steel in pavements. A different antenna orientation would have made these data easier to analyze, by reducing the effect of the reinforcing steel.

As can be seen in Figures G-16 and G-17, surface manifestations of D-cracking consisted mainly of concrete discoloration and very thin cracks. Both of these manifestations are extremely difficult to resolve with a surface video analysis system. Surface discoloration caused by D-cracking is difficult to distinguish from other areas of discoloration (such as the area between the wheelpaths discolored by oil). The difficulty in detecting very thin cracks is discussed in Chapter Two of this report. The wider cracks in the D-cracking pattern ($> 1/16$ to $1/8$ in.) could

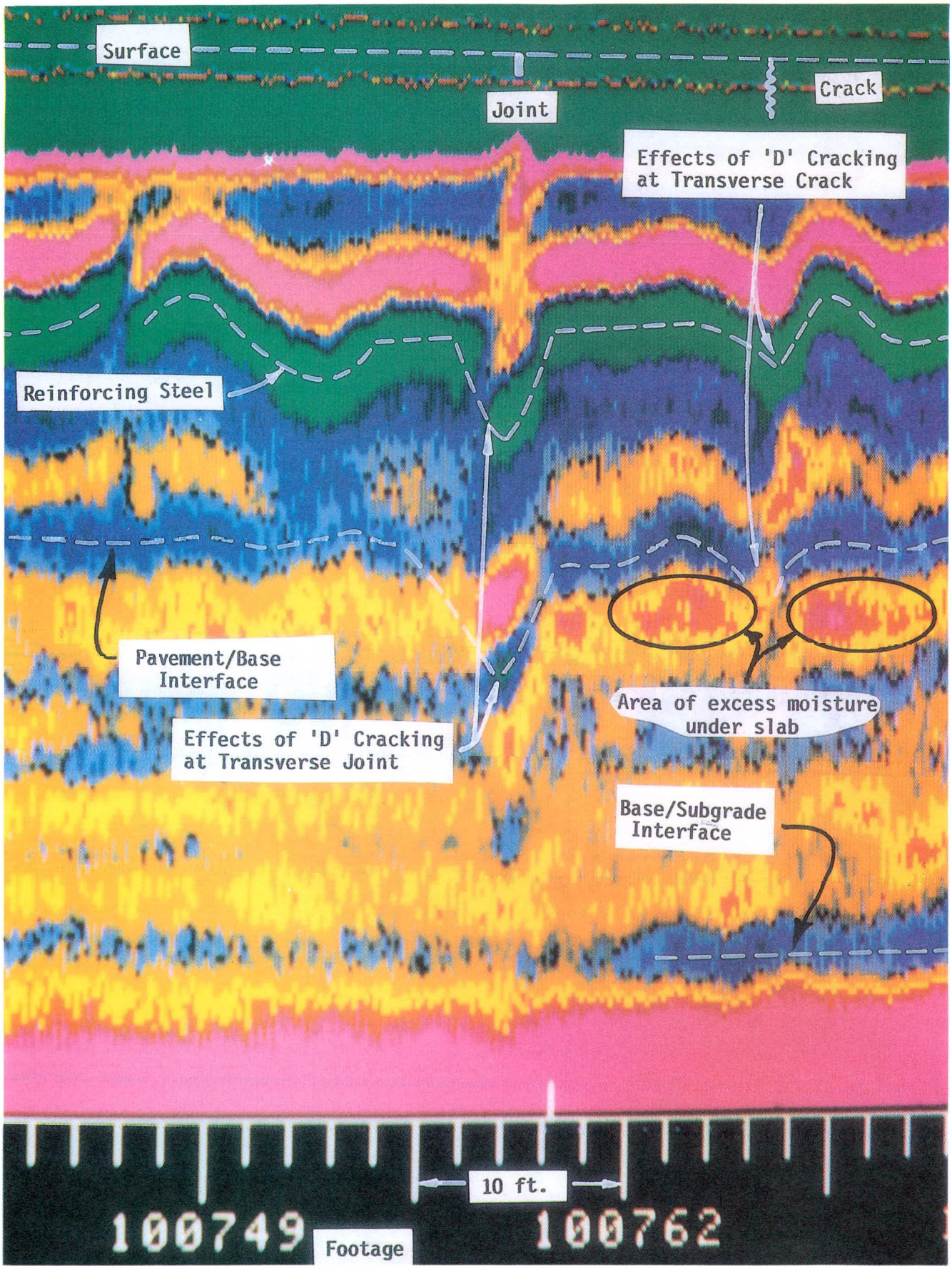

Figure G-18. Color enhanced radar signal return from a D-cracked area of I-74.

be detected, but the entire extent of the D-crack pattern was not resolvable. If the D-cracking has advanced to the stage of wide surface cracks, the video system can detect the existence of D-cracks on the surface, but it cannot accurately detect the extent of the distress because the very thin cracks are not resolvable.

The ability of the radar portion of the survey system to detect D-cracking is important, because the subsurface effects of the distress are detected. The subsurface effects of D-cracking, as detected by radar, along with some limited coring for calibration, potentially can be used to determine the extent of the resulting structural damage along extensive areas of roadway.

APPENDIX H

DEVELOPMENT OF THE VOID RADAR RETURN EQUATION

A physical model approximating a void between the concrete pavement surface and the underlying base material is shown in Figure H-1. It is reasonable to assume that the soil layer is deep enough so that reflections from the bottom of the soil layer are insignificant. Given this geometry, the following terms can be written which describe the primary radar returns from the top and bottom of the void as shown in Figure H-2.

Top of Void:

$$(1-\rho_1)\,\rho_2(1-(-\rho_1))\,A_P\,X_{(t-\tau_A-\tau_P)}$$

Bottom of Void:

$$(1-\rho_1)\,(1-\rho_2)\rho_3(1-(-\rho_2))\,(1-(-\rho_1))\,A_P A_V\,X_{(t-\tau_A-\tau_P-\tau_V)}$$

where:

- X_t = transmitted pulse (waveform);
- ρ_1 = reflection coefficient at the top of the pavement;
- ρ_2 = reflection coefficient at the top of the void;
- ρ_3 = reflection coefficient at the bottom of the void;
- A_P = attenuation due to the round-trip transit through the pavement;
- A_V = attenuation due to the round-trip transit through the void;
- τ_A = round-trip time from the antenna to the top of the pavement;
- τ_P = round-trip time through the pavement; and
- τ_V = round-trip time through the void.

Note that the reflection coefficients in the foregoing terms are defined for a wave traveling downward through the subsurface layers. In addition to the primary reflections, a series of secondary double bounce paths occur that must be taken into account in considering the return waveform. The NCHRP 10-14 project does not include all of the double bounce returns included in this model. The following terms can be written describing secondary bounces at the top and bottom of the void shown in Figure H-3:

Top of Void:

$$(1-\rho_1)\rho_2(-\rho_1)\rho_2(1-(-\rho_1))\,A_P^2\,X_{(t-\tau_A-2\tau_P)}$$

Bottom of Void:

$$2(1-\rho_1)\,(1-\rho_2)\,\rho_3[(1-(-\rho_2))\,(-\rho_1)\,\rho_2(1-(-\rho_1))\,A_P^2\,A_V$$

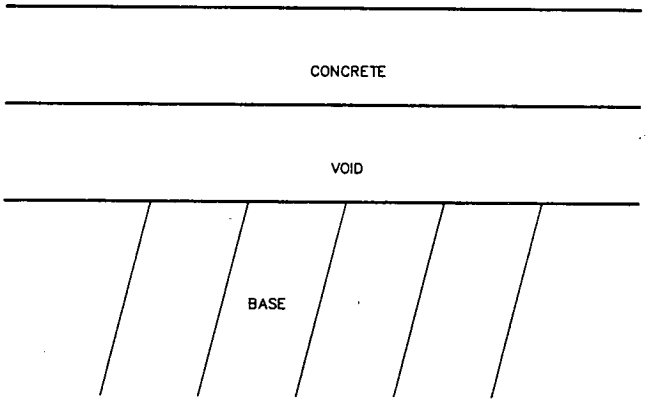

Figure H-1. Model of void under pavement.

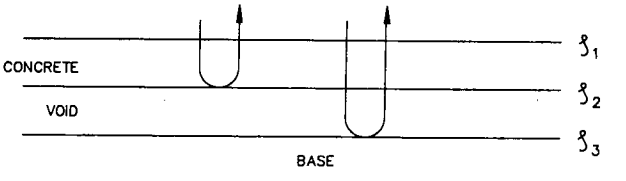

Figure H-2. Primary void returns.

$$X_{(t-\tau_A-2\tau_P-\tau_V)}] + (1-\rho_1)\,(1-\rho_2)\,\rho_3[(-\rho_2)\,(\rho_3)(1-(-\rho_2))\,(1-(-\rho_1))\,A_P\,A_V^2\,X_{(t-\tau_A-\tau_P-2\tau_V)}]$$

Finally, the current computer model accounts for the tertiary bounces at the top and bottom of the void shown in Figure H-4 as described in the following (the NCHRP 10-14 project does not include any of the tertiary returns in its mathematical model):

Top of Void:

$$(1-\rho_1)(\rho_2)(-\rho_1)(\rho_2)(-\rho_1)(\rho_2)(1-(-\rho_1))A_P^3\,X_{(t-\tau_A-3\tau_P)}$$

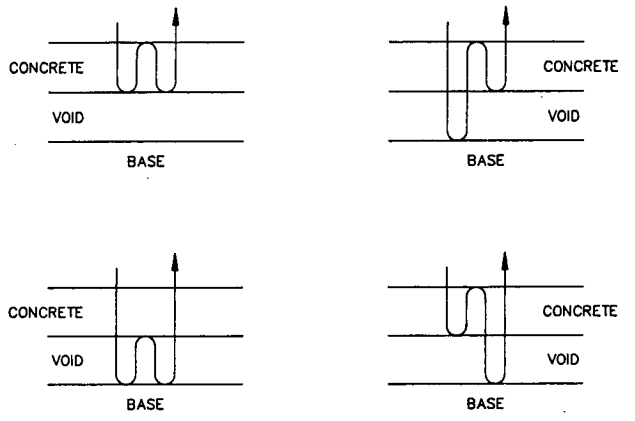

Figure H-3. Secondary void returns.

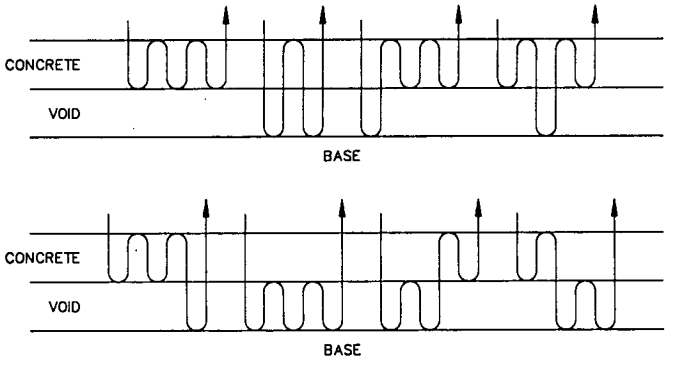

Figure H-4. Tertiary void returns.

radar return waveform can be written based on the preceding expressions for the primary, secondary, and tertiary returns:

$$
\begin{aligned}
S(t) = {} & \rho_2 X(t) \\
& + (1-\rho_2^2)\,\rho_3 A_V X_{(t-\tau_V)} \\
& - \rho_1\rho_2^2 A_P X_{(t-\tau_P)} \\
& - 2\rho_1\rho_2(1-\rho_2^2)\,\rho_3 A_P A_V X_{(t-\tau_P-\tau_V)} \\
& - \rho_2(1-\rho_2^2)\,\rho_3^2 A_V^2 X_{(t-2\tau_V)} \\
& + \rho_1^2\rho_2^3 A_P^2 X_{(t-2\tau_P)} \\
& + 3\rho_1^2\rho_2^2(1-\rho_2^2)\rho_3 A_P^2 A_V X_{(t-2\tau_P-\tau_V)} \\
& + \rho_2^2(1-\rho_2^2)\,\rho_3^3 A_V^3 X(t-3\tau_V) \\
& + [2(1-\rho_2^2)\,\rho_2^2 - (1-\rho_1)^2(1+\rho_2)^2]\rho_1\rho_3^2 A_P A_V^2 \\
& X_{(t-\tau_P-2\tau_V)}
\end{aligned}
$$

This equation was coded in Microsoft FORTRAN on an IBM PC AT. A copy of the program, called SIGMOD, can be found in Appendix I of this report. The program was designed to create a series of data files which contained the output waveform $S(t)$ for varying void sizes for a given geometry. The operator-furnished inputs to the program are the thickness of the pavement, the minimum and maximum thickness of the void, the void thickness increment (for stepping from one void size to another), the attenuation through the void, the attenuation through the pavement, as well as the dielectric constant of the pavement, void, and base material.

This appendix concludes with sample plots that compare the output waveforms of the void modeling program, SIGMOD, with the actual void return waveforms reported by the radar (see Figures H-5 through H-10). Three pairs of waveforms are plotted, corresponding to void thicknesses of ⅛ in., ½ in., and 1 in. For reference, a source listing of the FORTRAN program SIGMOD is included in Appendix I.

Bottom of Void:

Case 1:

$$(1-\rho_1)(1-\rho_2)\rho_3(1-(-\rho_2))(-\rho_1)(1-\rho_2)\rho_3(1-(-\rho_2))(1-(-\rho_1))\,A_P^2 A_V^2 X_{(t-\tau_A-2\tau_P-2\tau_V)}$$

Case 2:

$$3(1-\rho_1)(1-\rho_2)\rho_3(1-(-\rho_2))(-\rho_1)\rho_2(-\rho_1)\rho_2(1-(-\rho_1))\,A_p^3 A_V X_{(t-\tau_A-3\tau_P-\tau_V)}$$

Case 3:

$$(1-\rho_1)(1-\rho_2)\rho_3(-\rho_2)\rho_3(-\rho_2)\rho_3(1-(-\rho_2))(1-(-\rho_1))\,A_P A_V^3 X_{(t-\tau_A-\tau_P-3\tau_V)}$$

Case 4:

$$2(1-\rho_1)(1-\rho_2)\rho_3(-\rho_2)\rho_3(1-(-\rho_2))(-\rho_1)\rho_2(1-(-\rho_1))\,A_P^2 A_V^2 X_{(t-\tau_A-2\tau_P-2\tau_V)}$$

The programmed model assumes that all higher order bounces are insignificant because they occur too far out in time to interfere with the primary returns. In addition, the higher order bounces will typically be attenuated into the noise floor of the receiver and these are of little concern. Therefore, by neglecting the common terms $((1-\rho_1)\,(1-(-\rho_1))A_P)$ and the common delay $(\tau_A + \tau_P)$, the following expression for the composite

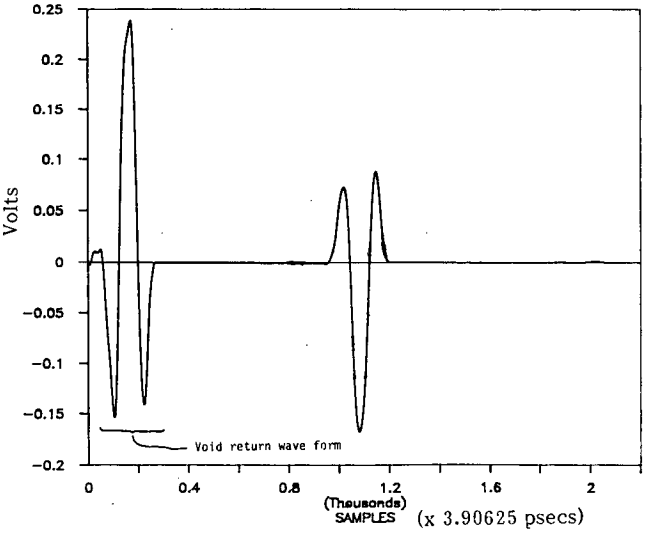

Figure H-5. SIGMOD *output for ⅛-inch void.*

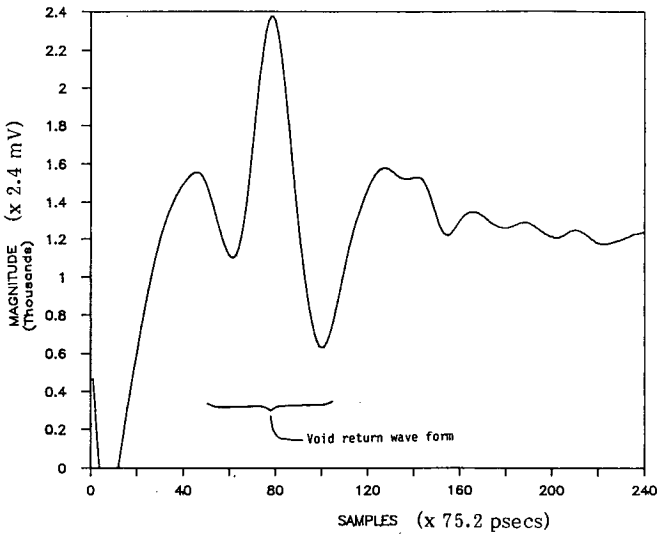

Figure H-6. Actual radar return for ⅛-inch void.

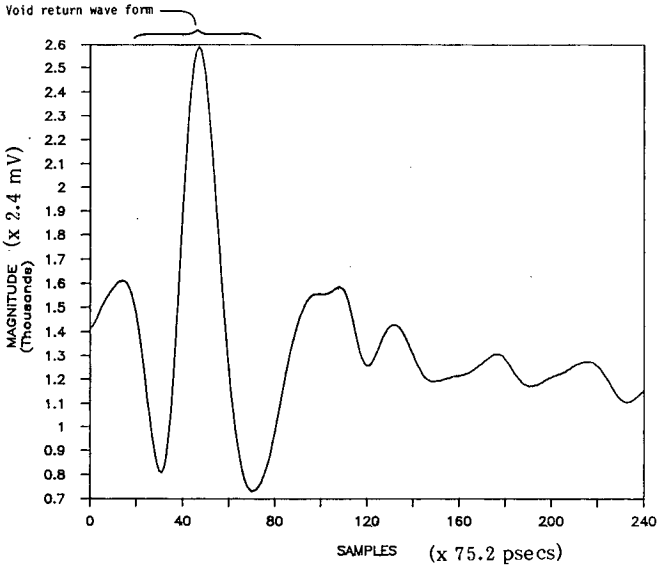

Figure H-8. Actual radar return for ½-inch void.

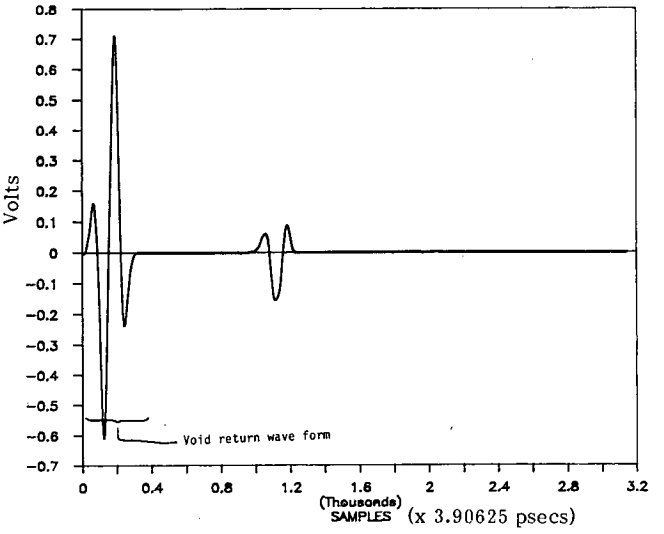

Figure H-7. SIGMOD *output for ½-inch void.*

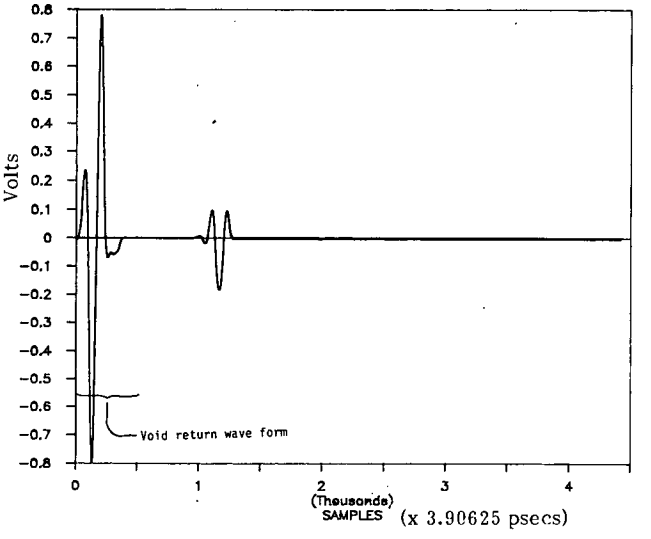

Figure H-9. SIGMOD *output for 1-inch void.*

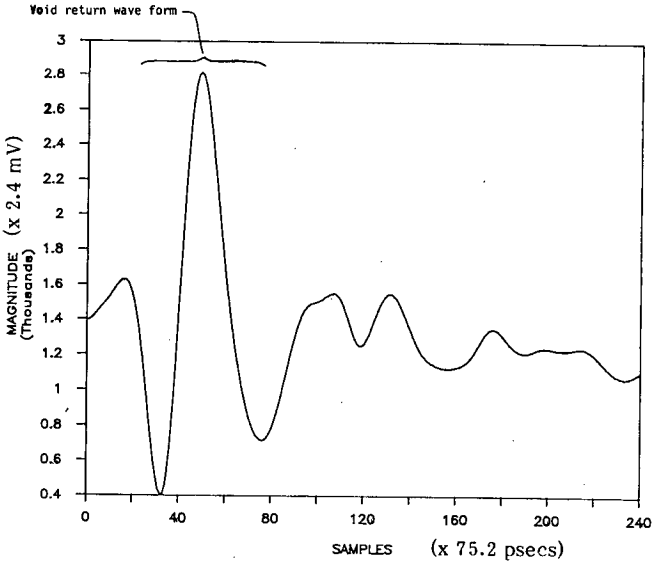

Figure H-10. Actual radar return for 1-inch void.

APPENDIX I

SIGMOD SOURCE LISTING

This appendix contains a listing of the Microsoft FORTRAN program SIGMOD, which was used to produce the theoretical radar return waveform from an air void. The equation for the void return waveform, $S(t)$, is given in Appendix H. The waveforms generated by the following program were used to create the peak amplitude versus void size curves that were used in developing the void-sizing algorithm (see Chapter Two).

```
$NOTRUNCATE

      PROGRAM  SIGMOD

C
C  Author:        Jeffrey L. Smart,   Gulf Applied Research
C
C  Filename:      SIGMOD.FOR
C
C
C  Function:      This program models the radar return waveform obtained
C                 from an air void.  This is accomplished by calculating
C                 the reflection coefficients and time delays resulting
C                 from multiple bounces of the radar signal between the
C                 top and bottom of the void.  The void return waveform
C                 is then constructed by weighting and delaying the
C                 transmitted waveform.  The program is capable of
C                 calculating return waveforms for a range of void sizes.
C                 The values of the void return waveform are stored in
C                 sequentially numbered files on the computer's hard disk.
C
C  Project:       NCHRP
C
C
C
C  Declare program parameters.
C

      INTEGER    TEMP_COUNT,     UP_SAMPLE_FACTOR,
START_PADDING,
     +           I,              J,                    X_COUNT,
     +           TIME,           MAX_SHIFT

      REAL       TEMP_X(32),     X(258),               S(8192),
     +           LIGHT_SPEED,    NORMALIZE,            MAX_VOID_DEPTH,
     +           MIN_VOID_DEPTH

      CHARACTER  FILENAME*7

      FILENAME(1:1) = 'S'
      FILENAME(4:7) = '.DAT'

C  Set the value of the speed of light.
C

      LIGHT_SPEED   =   3.0E+8

C
C  Set the maximum shift in the number of samples.
C

      MAX_SHIFT     =   7936

C
C  Initialize the output array record length.
C

      OUTPUT_RECORD_LENGTH  =   0

C
C  Hardwire 32 values of X(t), the transmitted waveform.
C

      TEMP_COUNT  =  32
      TEMP_X(1)   =  1536.0
      TEMP_X(2)   =  1536.0
      TEMP_X(3)   =  1509.0
      TEMP_X(4)   =  1467.0
      TEMP_X(5)   =  1405.0
      TEMP_X(6)   =  1294.0
      TEMP_X(7)   =  1135.0
      TEMP_X(8)   =  927.0
      TEMP_X(9)   =  752.0
      TEMP_X(10)  =  634.0
```

```
      TEMP_X(11)   =    624.0
      TEMP_X(12)   =    747.0
      TEMP_X(13)   =    1049.0
      TEMP_X(14)   =    1635.0
      TEMP_X(15)   =    2295.0
      TEMP_X(16)   =    2971.0
      TEMP_X(17)   =    3384.0
      TEMP_X(18)   =    3552.0
      TEMP_X(19)   =    3518.0
      TEMP_X(20)   =    3351.0
      TEMP_X(21)   =    3072.0
      TEMP_X(22)   =    2576.0
      TEMP_X(23)   =    1955.0
      TEMP_X(24)   =    1252.0
      TEMP_X(25)   =    743.0
      TEMP_X(26)   =    460.0
      TEMP_X(27)   =    447.0
      TEMP_X(28)   =    625.0
      TEMP_X(29)   =    891.0
      TEMP_X(30)   =    1188.0
      TEMP_X(31)   =    1432.0
      TEMP_X(32)   =    1432.0

C
C  Invert the hardwired values.
C

      DO  32  I  =  1, 32

         TEMP_X(I)    =     - TEMP_X(I)

32    CONTINUE

C
C  Up-sample the TEMP_COUNT hardwired values of X(t) to the desired
C  X_COUNT 256 values.
C
C  Begin by setting the value of the up-sample factor.
C

      UP_SAMPLE_FACTOR     =    8

C
C  Spread the TEMP_COUNT hardwired samples out across the extent of the
C  array.
C

      START_PADDING    =    2
      J                =    1
      DO  10  I  =  1, TEMP_COUNT

         X(J)          =    TEMP_X(I)
         STOP_PADDING  =    START_PADDING + UP_SAMPLE_FACTOR - 2
         DO  20  J  =  START_PADDING, STOP_PADDING

            X(J)  =  0.0

20       CONTINUE
         START_PADDING  =  START_PADDING + UP_SAMPLE_FACTOR

10    CONTINUE

C
C  Pass the upsampled array to the Fourier Transform routine FFA.
C

      X_COUNT    =     TEMP_COUNT * UP_SAMPLE_FACTOR

C
C  Pass the array X(t) to the Fourier Transform subroutine FFA.
C

      CALL  FFA( X, X_COUNT )

C
C  Lopass filter the array X(t) by zeroing array components beginning
C  with the index CUTOFF_FREQUENCY.
C

      CUTOFF_FREQUENCY   =   ( 0.5 * TEMP_COUNT ) + 3
      DO  30  I  =   CUTOFF_FREQUENCY, (X_COUNT + 2)

         X(I)  =  0.0

30    CONTINUE
```

```
C
C  Remove the DC offset from the transmitted waveform.
C
      X(1)  =   0.0

C
C  Obtain the expanded transmitted waveform by passing the X(t) array
C  to the inverse Fourier Transform routine FFS.
C
      CALL  FFS( X, X_COUNT )

C
C  Normalize the transmitted waveform.
C
      NORMALIZE    =     245.9932

      DO  4000  I = 1, X_COUNT

         X(I)   =   X(I) / NORMALIZE

4000  CONTINUE

      DO  39  I  =   1, X_COUNT

         X(I)  =   X(I) - 0.047

39    CONTINUE

C
C  Write the transmitted waveform out to a data file for examination.
C
      OPEN (10,FILE='X.DAT',STATUS='UNKNOWN')
      WRITE (10,*)  X_COUNT
      DO  140  I  =  1, X_COUNT

         WRITE (10,*)  X(I)

140   CONTINUE
```



```
C
C  Prompt the operator to input parameters describing the void.
C
      WRITE (*,*) 'Enter the thickness of the pavement (inches)'
      READ (*,*) PAVEMENT_DEPTH
      PAVEMENT_DEPTH   =     PAVEMENT_DEPTH * 0.0254

430   CONTINUE

      WRITE (*,*) 'Enter the minimum thickness of the void (inches)'
      READ (*,*) MIN_VOID_DEPTH
      MIN_VOID_DEPTH       =     MIN_VOID_DEPTH * 0.0254

      IF  ( MIN_VOID_DEPTH  .EQ.  0 )  THEN
         WRITE (*,*) ' '
         WRITE (*,*) '****** NOT A VALID INPUT ********'
         WRITE (*,*) ' '
         GOTO 430
      ENDIF

      WRITE (*,*) 'Enter the maximum thickness of the void (inches)'
      READ (*,*) MAX_VOID_DEPTH
      MAX_VOID_DEPTH       =     MAX_VOID_DEPTH * 0.0254

      WRITE (*,*) 'Enter the void thickness increment (inches)'
      READ (*,*) DELTA_VOID_DEPTH
      DELTA_VOID_DEPTH     =     DELTA_VOID_DEPTH * 0.0254

      WRITE (*,*) 'Enter the pavement attenuation (dB/meter)'
      READ (*,*) PAVEMENT_ATTEN

      WRITE (*,*) 'Enter the void attenuation (dB/meter)'
      READ (*,*) VOID_ATTEN

      WRITE (*,*) 'Enter the Dielectric Constant of the Pavement'
      READ (*,*) PAVEMENT_ER

      WRITE (*,*) 'Enter the Dielectric Constant of the Void'
      READ (*,*) VOID_ER

      WRITE (*,*) 'Enter the Dielectric Constant of the Soil'
```

```
      READ (*,*) SOIL_ER

C
C  Calculate the total round trip attenuation through the pavement (AP)
C  and the void (AV).
C

      VOID_COUNT     =    INT ( ( MAX_VOID_DEPTH - MIN_VOID_DEPTH ) /
     +                        DELTA_VOID_DEPTH ) + 1

      DO  1000  II  =   1, VOID_COUNT

        IF  ( II  .EQ.  1 )  THEN
          VOID_DEPTH     =      MIN_VOID_DEPTH
        ELSE
          VOID_DEPTH     =      VOID_DEPTH + DELTA_VOID_DEPTH
        ENDIF

        AP    =     PAVEMENT_ATTEN * PAVEMENT_DEPTH * 2.0
        AV    =     VOID_ATTEN * VOID_DEPTH * 2.0

C
C  Convert the entered round trip attenuation (in dB) into a power ratio.
C

        AP    =    10.0 ** ( - AP / 10.0 )
        AV    =    10.0 ** ( - AV / 10.0 )

C
C  Calculate the round propagation time through the pavement (TP) and
C  the void (TV).  These values are equal to twice the thickness of the
C  medium divided by the phase velocity of the signal through the medium.
C

        ER_P_ROOT    =    SQRT( PAVEMENT_ER )
        ER_V_ROOT    =    SQRT( VOID_ER )
        ER_S_ROOT    =    SQRT( SOIL_ER )
        TP           =    2.0 * ER_P_ROOT * PAVEMENT_DEPTH /
LIGHT_SPEED
        TV           =    2.0 * ER_V_ROOT * VOID_DEPTH / LIGHT_SPEED

C
C  Calculate the reflection coefficient at the air-pavement interface (P1),
C  the pavement-void interface (P2) and the void-soil interface (P3).
C

        P1    =    ( 1.0 - ER_P_ROOT ) / ( 1.0 + ER_P_ROOT )
        P2    =    ( ER_P_ROOT - ER_V_ROOT ) / ( ER_P_ROOT +
ER_V_ROOT )
        P3    =    ( ER_V_ROOT - ER_S_ROOT ) / ( ER_V_ROOT +
ER_S_ROOT )

C
C  Set the amount of time between samples in the transmitted waveform.
C

        SAMPLE_SPACING     =     3.90625E-12

C
C  Initialize the output waveform, S(t).
C

        DO  50   I  =  1, 8192

          S(I)   =   0.0

50      CONTINUE

C
C  Enter the DO loop which will weight and delay the transmitted waveform
C  to form the waveform received at the radar (S).
C

        DO  100  I  =  1, 9

C
C  Calculate the magnitude weight and time delay for the first term.
C

          IF  ( I .EQ. 1 )  THEN
            WEIGHT    =    P2
            TIME      =    0
          ENDIF

C
C  Calculate the magnitude weight and time delay for the second term.
```

```
C
      IF  ( I .EQ. 2 )  THEN
         WEIGHT   =    (1 - P2 ** 2.0 ) * P3 * AV
         TIME     =    INT( TV / SAMPLE_SPACING )
      ENDIF

C
C  Calculate the magnitude weight and time delay for the third term.
C

      IF  ( I .EQ. 3 )  THEN
         WEIGHT   =    - P1 * (P2 ** 2.0) * AP
         TIME     =    INT( TP / SAMPLE_SPACING )
      ENDIF

C
C  Calculate the magnitude weight and time delay for the fourth term.
C

      IF  ( I .EQ. 4 )  THEN
         WEIGHT   =    - 2.0 * P1 * P2 * (1 - P2 ** 2.0)
     +                   * P3 * AP * AV
         TIME     =    INT( (TP + TV) / SAMPLE_SPACING )
      ENDIF

C
C  Calculate the magnitude weight and time delay for the fifth term.
C

      IF  ( I .EQ. 5 )  THEN
         WEIGHT   =    - P2 * (1 - P2 ** 2.0) * (P3 ** 2.0)
     +                   * (AV ** 2.0)
         TIME     =    INT( (2.0 * TV) / SAMPLE_SPACING )
      ENDIF

C
C  Calculate the magnitude weight and time delay for the sixth term.
C

      IF  ( I .EQ. 6 )  THEN
         WEIGHT   =    (P1 ** 2.0) * (P2 ** 3.0) * (AP ** 2.0)
         TIME     =    INT( (2.0 * TP) / SAMPLE_SPACING )
      ENDIF

C
C  Calculate the magnitude weight and time delay for the seventh term.
C

      IF  ( I .EQ. 7 )  THEN
         WEIGHT   =    3.0 * (P1 ** 2.0) * (P2 ** 2.0)
     +                   * (1 - P2 ** 2.0) * P3 * (AP ** 2.0) * AV
         TIME     =    INT( ( (2.0 * TP) + TV ) / SAMPLE_SPACING )
      ENDIF

C
C  Calculate the magnitude weight and time delay for the eighth term.
C

      IF  ( I .EQ. 8 )  THEN
         WEIGHT   =    (P2 ** 2.0) * (1 - P2 ** 2.0)
     +                   * (P3 ** 3.0) * (AV ** 3.0)
         TIME     =    INT( (3.0 * TV) / SAMPLE_SPACING )
      ENDIF

C
C  Calculate the magnitude weight and time delay for the ninth term.
C

      IF  ( I .EQ. 9 )  THEN
         WEIGHT   =    P1 * P3**2.0 * AP * AV**2.0 *
     +                 ( ( 2.0 * (1.0 - P2**2.0) * P2**2.0 ) -
     +                 ( (1.0 - P1)**2.0 * (1.0 + P2)**2.0 ) )
         TIME     =    INT( (TP + 2.0*TV) / SAMPLE_SPACING )
      ENDIF

C
C  Check the number of shifted samples.  If the number of shifted
C  samples (TIME) is greater than the MAX_SHIFT then exit the loop
C  and report the error to the operator.
C

      IF  ( TIME  .GT.  MAX_SHIFT )  THEN
         WRITE (*,*) '***** ERROR *******'
         WRITE (*,*) 'TIME DELAY TOO LARGE FOR OUTPUT
WAVEFORM'
```

```
            GOTO  70
          ENDIF

C
C  Update the output array record length.
C

          IF  ( TIME  .GT.  OUTPUT_RECORD_LENGTH )  THEN
            OUTPUT_RECORD_LENGTH   =   TIME
          ENDIF

C
C  Write the weighted and delayed transmitted waveform to the output
C  waveform S(t).
C

          DO  200  J  =  1, X_COUNT

            OUTPUT         =   X(J) * WEIGHT
            S(J + TIME)    =   S(J + TIME) + OUTPUT

200       CONTINUE

100     CONTINUE

C
C  Write the received waveform out to a data file.
C

        IF  ( II .LT. 10 )  THEN
          FILENAME(2:2)  =   48
          FILENAME(3:3)  =   CHAR(II + 48)
        ELSE
          I_NAME   =    II / 10
          FILENAME(2:2)  =   CHAR(I_NAME + 48)
          I_NAME   =    II  -  (I_NAME * 10)
          FILENAME(3:3)  =   CHAR(I_NAME + 48)
        ENDIF

        OUTPUT_RECORD_LENGTH    =    OUTPUT_RECORD_LENGTH + 256

        OPEN (11,FILE=FILENAME,STATUS='UNKNOWN')
        WRITE (11,*)  INT( OUTPUT_RECORD_LENGTH )

          DO  40  I  =  1, OUTPUT_RECORD_LENGTH

            WRITE (11,*)  S(I)

40        CONTINUE

          CLOSE(11)

1000    CONTINUE

C
C  End of the program.
C

70      CONTINUE

        END
```

APPENDIX J

CRAKFIND SOURCE LISTING

This appendix contains a listing of the Microsoft FORTRAN program CRAKFIND, the experimental frame analyzer program for the computer-based video data analysis subsystem described in Appendix D. The following program was designed to locate cracks, spalls, and popouts in video data taken of the road surface.

```
      PROGRAM  CRAKFIND

$INCLUDE:'ITEXPC.INC'

C
C  Author:          Jeffrey L. Smart,   Gulf Applied Research
C
C  Program Title:   CRAKFIND
C
C  Filename:        CRAKFIND.FOR
C
C  Function:        This FORTRAN program identifies,locates and counts
C                   cracks,spalls and popouts in asphalt and CRC (Continously
C                   Reinforced Concrete) roadway surfaces.  The algorithm
C                   is provided with a video image of the road surface through
C                   calls to subroutines provided by the IMAGEACTION image
C                   analysis software package.  The picture is analyzed
C                   using a set of frame analysis parameters which are
C                   dependent on the amount of surface area in the frame
C                   and the F - stop of the camera.
C
C  Project:         NCHRP
C
C  Date:            7/15/86
C
C  Update:
C

      IMPLICIT INTEGER*2 (A-Z)

      INTEGER*4 MEM4BASE,REG4BASE
      CHARACTER*127 COMLIN
      CHARACTER*10  INFILE
      CHARACTER*11  OUTFILE
      CHARACTER*1   ANSWER
      INTEGER*4     PEAK
      INTEGER*4     HISTAR(512)
      REAL*4  VAR,TPIXS,PROB,TERM,STADEV,SUM,MEAN
      INTEGER*2  LINE(256),START(500),BOTTOM(100)
      INTEGER*2  STOP(100),LEFSIDE(100),RIGSIDE(100)
      INTEGER*2  SORT(100),LASTBOT(100),LASTLEF(100)
      INTEGER*2  STARLEF(100),STARRIG(100),TOP(100)
      INTEGER*2  CHECKED(100),VIEW(256),SPALDIR(100)
      INTEGER*2  SPALBOT(100),SPALTOP(100),SPALFLG(100)
      INTEGER*2  DELCNT(100),CRKFLAG(100),DELTAS(30,100)
      REAL*4  SLOPE,XCHANGE,YCHANGE

C
C  Define the pixel intensity for BLACK and WHITE.
C

      BLACK = 0
      WHITE = 255

C
C  This procedure defines the hardware addresses for PCVISION Frame Grabber,
C  and tells ITEX/PC that we do have pseudocolor (bwflag = 1).  The base
C  address of the registers is set to hex FF00 (65280-dec) and the base
C  address of frame memory is set to D0000.  Because only 16 bits of value
C  can be passed, this address is specified without the last 4 bits,
C  D000 (or dec 53248).
C

      WRITE (*,*) 'Initializing system '
      REG4BASE = 65280
      MEM4BASE = 53248
      REGBASE = INT (REG4BASE)
      MEMBASE = INT (MEM4BASE)
      BWFLAG  = 1
      CALL SETHDW(REGBASE,MEMBASE,BWFLAG)
      CALL INITIA

C
C  Readft reads a 256 X 256 image from the disk file 'IMAGIN.IMG' and puts it
```

```
C  in Quadrant 0. Any comment line stored with the is returned in comline.
C  If the image was stored in compressed mode, it is automatically
C  decompressed when it is read in.
C
      ERRVAL = READFT(0,0,256,256,'IMAGIN.IMG',COMLIN)

C
C  White out Quadrant 1 which will be used to display the cracks,spalls
C  and popouts found by the system.
C
      DO 109 YS = 0,239
         DO 123 I = 1,256
            VIEW(I) = WHITE
123      CONTINUE
         CALL  WHLINE(256,YS,256,VIEW)
109   CONTINUE

C
C  Prompt the user for sharpening a blurry image with the IMAGEACTION
C  subroutine SHARPE.  This routine is useful for eliminating fuzzy
C  areas in the picture.
C
      WRITE (*,*) 'Do you want to sharpen the image (Y/N)'
      READ  (*,367)  ANSWER
367   FORMAT(A1)

      IF (ANSWER .EQ. 'Y') THEN
         CALL  SHARPE(0,0,256,240,2)
      ENDIF

C
C  Prompt the user for rolling the lookup tables of the video frame.
C  The variable ROLL should be an integer ranging from -255 to 255.
C  The higher the number the darker the picture will become.
C
      WRITE (*,*) 'Do you want to roll the look up table (Y/N)'
      READ (*,68) ANSWER
68    FORMAT (A1)

      IF (ANSWER .EQ. 'Y') THEN
         BANK = 3
         COLOR = 3
         CALL  SETLUT(COLOR,BANK)

         WRITE (*,*) 'Enter the amount of roll to LUT'
         READ (*,*) ROLL

         CALL  ROLLUT(ROLL)
         CALL  MAPLUT(0,0,256,240)
      ENDIF

C
C  Set the default frame analysis parameters.
C
      TIMES = 3
      JUMP = 5
      MAXWID = 7
      GROUP = 25
      MINLEN = 40
      POPLEN = 7
      SPALLEN = 15
      WINDOW = 10

C
C  Print the default frame analysis parameters to the screen.
C  Definition of frame analysis parameters:
C     TIMES - Number of standard deviations below the mean where
C             the cutoff for crack intensity is set.
C     JUMP - Maximum acceptable separation between black pixels
C            which can be grouped together as one set.
C     MAXWID - Maximum width of black pixels which is still
C              identified as a crack width.
C     GROUP - Enter the number of pixels that a potential crack
C             must be separated from another potential crack
C             without the two cracks being combined by the
C             processor as one crack.
C     MINLEN - Minimum detectable crack length.
C     POPLEN - Minimum size of a detectable popout.
C     SPALLEN - Minimum length of a detectable spall.
C     WINDOW - Length of updates.
C
```

```
      WRITE (*,*) 'The Default Frame Analysis Parameters are:'
      WRITE (*,*) ' '
      WRITE (*,*) ' '
      WRITE (*,*) 'Crack Intensity Threshold = ',TIMES,' SD'
      WRITE (*,*) 'Maximum gap between black pixels = ',JUMP
      WRITE (*,*) 'Maximum crack width  = ',MAXWID
      WRITE (*,*) 'Maximum gap between cracks  = ',GROUP
      WRITE (*,*) 'Minimum detectable crack length = ',MINLEN
      WRITE (*,*) 'Minimum size of a detectable popout = ',POPLEN
      WRITE (*,*) 'Minimum detectable spall length = ',SPALLEN
      WRITE (*,*) 'Window Length for slope calculation = ',WINDOW
      WRITE (*,*) ' '
      WRITE (*,*) ' '

C
C  Prompt the user to change the default frame analysis parameters.
C

      WRITE (*,*) 'Do you want to change the frame analysis parameters?'
      READ (*,423) ANSWER
423    FORMAT(A1)
      IF (ANSWER .EQ. 'Y') THEN
         WRITE (*,*) 'Enter TIMES'
         READ (*,*) TIMES
         WRITE (*,*) 'Enter JUMP'
         READ (*,*)  JUMP
         WRITE (*,*) 'Enter MAXWID'
         READ (*,*) MAXWID
         WRITE (*,*) 'Enter GROUP'
         READ (*,*) GROUP
         WRITE (*,*) 'Enter MINLEN'
         READ (*,*) MINLEN
         WRITE (*,*) 'Enter POPLEN'
         READ (*,*) POPLEN
         WRITE (*,*) 'Enter SPALLEN'
         READ (*,*) SPALLEN
         WRITE (*,*) 'Enter WINDOW'
         READ (*,*) WINDOW
      ENDIF

C
C  Use the IMAGEACTION subroutine to obtain a HISTOGRAM of the
C  pixel intensities in the video image.
C

      CALL  HISTOGRAM (0,0,256,240,1,1,HISTAR)

C
C  Compute the mean pixel intensity.
C

      TPIXS = 0.0
      DO 23 I = 1,256
         TPIXS = TPIXS + HISTAR(I)
23    CONTINUE
      MEAN = 0.0
      DO 57 I = 1,256
         PROB = HISTAR(I)/TPIXS
         TERM = (I - 1.0) * PROB
         MEAN = MEAN + TERM
57    CONTINUE

C
C  Compute the standard deviation of the pixel intensities.
C

      VAR = 0.0
      DO 34 I = 1,256
         PROB = HISTAR(I)/TPIXS
         TERM = ((I - 1.0 - MEAN)**2.0) * PROB
         VAR = VAR + TERM
34    CONTINUE
      STADEV = VAR ** 0.5

C
C  Set the pixel intensity CUTOFF value separating black crack from
C  white background.  The variable TIMES determines the number of
C  standard deviations below the mean pixel intensity where the
C  CUTOFF value is set.
C

      IMEAN = INT(MEAN)
      SD = INT(STADEV)
      CUTOFF = IMEAN - (TIMES * SD)
```

```
C
C  Map pixels with magnitudes greater than CUTOFF to white background
C  and pixels less than the CUTOFF equal to black crack.
C
      DO 502 YS = 0,239
         CALL  RHLINE(0,YS,256,LINE)
         DO 504 I = 1,256
            IF ( LINE(I)  .GT.  CUTOFF  )  THEN
               LINE(I) = WHITE
            ELSE
               LINE(I) = BLACK
            ENDIF
504      CONTINUE
         CALL  WHLINE (0,YS,256,LINE)
502   CONTINUE

C
C  Copy the binary (black/white) image to Quadrant 2.
C
      CALL  CAREA(0,0,256,256,0,256,256,256)

C
C  Write the binary image to the hard disk file 'IMAGOUT.IMG'.
C
      COMLIN = 'asph1 in binary format !'
      ERRVAL = SAVEFT (0,0,256,240,COMFLG,'IMAGOUT.IMG',COMLIN)

C
C  Analyze the binary image for longitudinal,transverse and skewed
C  cracks.  During the first pass through the loop when ANALYZE
C  is equal to 1 then scan for longitudinal and skewed cracks.
C  During the second pass through the loop when ANALYZE is equal to
C  2 then rotate the image being processed (Quadrant 0) and Quadrant 1
C  where the cracks found by the system are displayed and scan for
C  transverse cracks.
C
      DO 1 ANALYZE = 1,2

         IF (ANALYZE .EQ. 1) THEN
            TRACE = 0
            CRACK = 0
            LONTUDE = 0
            SKEWED = 0
            SPALLS = 0
            SPALPIX = 0
            SPALCNT = 0
            LINECNT = 256
            ROWCNT = 239
         ELSE
            CALL  ROT90(0,0,256,256)
            CALL  ROT90(256,0,256,256)
            TRACE = 0
            CRACK = 0
            TRANS = 0
            SPALCNT = 0
            LINECNT = 240
            ROWCNT = 255
         ENDIF

C
C  Use the IMAGEACTION subroutine RHLINE to read in a LINE  of
C  pixels from row YS.  The call PIXFIND to obtain the STARTing
C  and STOPping points of sets of black pixels on the current scan
C  line.  The variable CURRENT is the number of groups of black pixels
C  found on the scan line.  The variable JUMP is the maximum number
C  of white pixels separating blacks pixels which belong to the same
C  set or group.
C
         DO 100 YS = 0,ROWCNT
            CALL  RHLINE(0,YS,LINECNT,LINE)
            CALL  PIXFIND(LINECNT,LINE,STOP,START,CURRENT,JUMP)

C
C  Determine whether the groups of black pixels found on the current scan
C  line are part of the traces (potential cracks) which are still
C  active (CRKFLAG = 0).  If a group of pixels on the current scan line
C  lies within JUMP of an ongoing crack then it is used in the crack and
C  the location of the LEFSIDE and RIGSIDE of the crack is updated.  The
C  array DELTAS contains a history of the change in X - coordinate per
C  change in Y - coordinate of the LEFSIDE of the crack.  DELCNT is equal
C  to the number of DELTAS stored in the array which may not exceed WINDOW.
```

```
C  The average change in X per change Y is computed in DELTAX and used
C  to calculate EXPECT where the LEFSIDE of the crack should occur.  If
C  a decision must be made between two potential crack widths then the one
C  which is closest to EXPECT is chosen.
C
      DO 61 TRCCNT = 1,TRACE
         IF (CRKFLAG(TRCCNT) .EQ. 0) THEN
            CANDATE = 0
            IF (DELCNT(TRCCNT) .GT. 0) THEN
               ISUM = 0
               DO 67 I = 1,DELCNT(TRCCNT)
                  ISUM = ISUM + DELTAS(I,TRCCNT)
67             CONTINUE
               DELTAX = ISUM/DELCNT(TRCCNT)
               EXPECT = LASTLEF(TRCCNT) + (YS -
BOTTOM(TRCCNT))*DELTAX
            ENDIF
            LEFT = LEFSIDE(TRCCNT) - JUMP
            RIGHT = RIGSIDE(TRCCNT) + JUMP
            DO 27 CURCNT = 1,CURRENT
               IF (START(CURCNT) .GT. 0) THEN
                  IF (STOP(CURCNT) .GE. LEFT .AND. START(CURCNT)
     -            .LE. RIGHT) THEN
                     IF (CANDATE .EQ. 0) THEN
                        CANDATE = CURCNT
                     ELSE
                        IF (DELCNT(TRCCNT) .GT. 0) THEN
                           CANLEN = ABS(EXPECT - START(CANDATE))
                           CURLEN = ABS(EXPECT - START(CURCNT))
                           IF (CURLEN .LT. CANLEN) CANDATE = CURCNT
                        ENDIF
                     ENDIF
                  ENDIF
               ENDIF
27          CONTINUE

C
C  If a group of black pixels is associated with an ongoing crack then
C  the width of the black pixels is calculated.  If the width exceeds the
C  value of MAXWID then the width is treated as a potential spall.  If
C  the width is less than MAXWID then the width filed as a part of the
C  ongoing crack and the array DELTAS is updated with the current change
C  in X per change in Y.
C
            IF (CANDATE .GT. 0) THEN
               TWIDTH = STOP(CANDATE) - START(CANDATE) + 1
               IF (TWIDTH .LE. MAXWID) THEN
                  DELCNT(TRCCNT) = DELCNT(TRCCNT) + 1
                  NEWDEL = (START(CANDATE) - LASTLEF(TRCCNT))
     -            /(YS - LASTBOT(TRCCNT))
                  IF (DELCNT(TRCCNT) .GT. WINDOW) THEN
                     DELCNT(TRCCNT) = WINDOW
                     DO 82 MOVE = 2,WINDOW
                        DELTAS(MOVE - 1,TRCCNT) =
DELTAS(MOVE,TRCCNT)
82                   CONTINUE
                  ENDIF
                  DELTAS(DELCNT(TRCCNT),TRCCNT) = NEWDEL
                  LASTLEF(TRCCNT) = START(CANDATE)
                  LASTBOT(TRCCNT) = YS
               ELSE
                  FOUND = 0
                  DO 71 SCAN = 1,SPALCNT
                     IF (SPALDIR(SCAN) .EQ. TRCCNT) THEN
                        RANGE = YS - SPALBOT(SCAN)
                        IF (RANGE .LT. JUMP) THEN
                           SPALBOT(SCAN) = YS
                           FOUND = 1
                        ENDIF
                     ENDIF
71                CONTINUE
                  IF (FOUND .EQ. 0) THEN
                     SPALCNT = SPALCNT + 1
                     SPALFLG(SPALCNT) = 0
                     SPALDIR(SPALCNT) = TRCCNT
                     SPALTOP(SPALCNT) = YS
                     SPALBOT(SPALCNT) = YS
                  ENDIF
               ENDIF
               LEFSIDE(TRCCNT) = START(CANDATE)
               RIGSIDE(TRCCNT) = STOP(CANDATE)
               BOTTOM(TRCCNT) = YS
               START(CANDATE) = 0
            ENDIF
```

```
            ENDIF
61        CONTINUE

C
C  If a group of black pixels was not associated with an ongoing trace
C  and the width is less or equal to MAXWID, then a new trace is started
C  with the current as width as its first entry.
C

          DO 90 CURCNT = 1,CURRENT
             TWIDTH = STOP(CURCNT) - START(CURCNT) + 1
             IF (START(CURCNT) .GT. 0  .AND.  TWIDTH .LE. MAXWID) THEN
                TRACE = TRACE + 1
                STARLEF(TRACE) = START(CURCNT)
                STARRIG(TRACE) = STOP(CURCNT)
                LEFSIDE(TRACE) = START(CURCNT)
                RIGSIDE(TRACE) = STOP(CURCNT)
                LASTLEF(TRACE) = START(CURCNT)
                LASTBOT(TRACE) = YS
                TOP(TRACE) = YS
                DELCNT(TRACE) = 0
                BOTTOM(TRACE) = YS
                CRKFLAG(TRACE) = 0
                CHECKED(TRACE) = 0
             ENDIF
90        CONTINUE

C
C  If an ongoing trace has not been updated in the last JUMP scans of
C  the image then exam the trace to determine if it is a crack.  If the
C  trace satisfies the criteria for a crack then set the CRKFLAG equal to
C  1 and keep the crack location (top left corner,top right corner,bottom
C  left corner,bottom right corner) in memory.  If the trace does not
C  satisfy the crack criteria then erase the trace from memory.  Also,
C  examine the potential spalls associated with the trace.  If the trace is
C  to be erased then call the subroutine REORDER which writes the index of
C  closed trace to the array SORT.
C

          ORDER = 0
          DO 542 SCAN = 1,TRACE
             IF (CRKFLAG(SCAN) .EQ. 0) THEN
                RANGE = YS - BOTTOM(SCAN)
                LENGTH = BOTTOM(SCAN) - TOP(SCAN)
                IF (RANGE .GT. JUMP) THEN
                   IF (LENGTH .GT. MINLEN) THEN
                      CRACK = CRACK + 1
                      CRKFLAG(SCAN) = 1
                      DO 35 I = 1,SPALCNT
                         IF (SPALDIR(I) .EQ. SCAN) THEN
                            SPSIZE = SPALBOT(I) - SPALTOP(I)
                            IF (SPSIZE .GE. SPALLEN) THEN
                               SPALLS = SPALLS + 1
                               SPALFLG(I) = 1
                            ENDIF
                         ENDIF
35                    CONTINUE
                   ELSE
                      CALL  REORDER(SORT,ORDER,SCAN)
                   ENDIF
                ENDIF
             ENDIF
542       CONTINUE

C
C  If two traces intersect then determine if the most recent trace is
C  a crack.  If the trace is a crack then close the trace by setting
C  CRKFLAG equal to 1 and save it in memory.  Continue scanning the
C  older trace.  Again, if the trace is to be erased call the subroutine
C  REORDER which writes the index of the closed trace to the array SORT.
C

          DO 83 LOOK = 1,TRACE
             IF (CRKFLAG(LOOK) .EQ. 0) THEN
                DO 84 SCAN = (LOOK + 1),TRACE
                   IF (CRKFLAG(SCAN) .EQ. 0) THEN
                      IF (LEFSIDE(SCAN) .EQ. LEFSIDE(LOOK)) THEN
                         LENGTH = BOTTOM(SCAN) - TOP(SCAN)
                         IF (LENGTH .GT. MINLEN) THEN
                            CRACK = CRACK + 1
                            CRKFLAG(SCAN) = 1
                            DO 635 I = 1,SPALCNT
                               IF (SPALDIR(I) .EQ. SCAN) THEN
                                  SPSIZE = SPALBOT(I) - SPALTOP(I)
                                  IF (SPSIZE .GE. SPALLEN) THEN
```

```
                        SPALLS = SPALLS + 1
                        SPALFLG(I) = 1
                      ENDIF
                    ENDIF
635                 CONTINUE
                  ELSE
                    CALL  REORDER(SORT,ORDER,SCAN)
                  ENDIF
                ENDIF
              ENDIF
84          CONTINUE
          ENDIF
83      CONTINUE

C
C  Update the trace and spall bookkeeping arrays by overwriting the
C  trace entries which are listed in the array SORT.
C

        IF (ORDER .GT. 0) THEN
          IF (TRACE .EQ. 1) THEN
            TRACE = 0
            SPALCNT = 0
          ELSE
            DO 16 SCAN = 1,ORDER
              DO 13 MOVE = ( SORT(SCAN) + 1 ),TRACE
                DO 14 SWITCH = 1,DELCNT(MOVE)
                  DELTAS(SWITCH,MOVE - 1) = DELTAS(SWITCH,MOVE)
14              CONTINUE
                LEFSIDE(MOVE - 1) = LEFSIDE(MOVE)
                RIGSIDE(MOVE - 1) = RIGSIDE(MOVE)
                BOTTOM(MOVE - 1) = BOTTOM(MOVE)
                TOP(MOVE - 1) = TOP(MOVE)
                STARLEF(MOVE - 1) = STARLEF(MOVE)
                STARRIG(MOVE - 1) = STARRIG(MOVE)
                LASTLEF(MOVE - 1) = LASTLEF(MOVE)
                LASTBOT(MOVE - 1) = LASTBOT(MOVE)
                DELCNT(MOVE - 1) = DELCNT(MOVE)
                CRKFLAG(MOVE - 1) = CRKFLAG(MOVE)
                CHECKED(MOVE - 1) = CHECKED(MOVE)
13            CONTINUE
              SHIFT = 0
              DO 137 I = 1,SPALCNT
                IF ((SPALDIR(I) .EQ. SORT(SCAN)) .AND.
                SPALFLG(I) .EQ. 0) THEN
                  SHIFT = SHIFT + 1
                ELSE
                  SPALTOP(I - SHIFT) = SPALTOP(I)
                  SPALBOT(I - SHIFT) = SPALBOT(I)
                  SPALFLG(I - SHIFT) = SPALFLG(I)
                  IF (SPALDIR(I) .GT. SORT(SCAN)) THEN
                    SPALDIR(I - SHIFT) = SPALDIR(I) - 1
                  ELSE
                    SPALDIR(I - SHIFT) = SPALDIR(I)
                  ENDIF
                ENDIF
137           CONTINUE
              SPALCNT = SPALCNT - SHIFT
              DO 714 MOVE = ( SCAN + 1 ),ORDER
                SORT(MOVE) = SORT(MOVE) - 1
714           CONTINUE
              TRACE = TRACE - 1
16          CONTINUE
          ENDIF
        ENDIF
100   CONTINUE

C
C  Once all the rows of the picture have been scanned examine the traces
C  which are still active in the bookkeeping arrays.  If the traces satisfy
C  the criteria for a crack then set the CRKFLAG equal to 1.
C

      DO 571 SCAN = 1,TRACE
        IF (CRKFLAG(SCAN) .EQ. 0) THEN
          LENGTH = BOTTOM(SCAN) - TOP(SCAN)
          IF (LENGTH .GT. MINLEN) THEN
            CRACK = CRACK + 1
            CRKFLAG(SCAN) = 1
            DO 935 I = 1,SPALCNT
              IF (SPALDIR(I) .EQ. SCAN) THEN
                SPSIZE = SPALBOT(I) - SPALTOP(I)
                IF (SPSIZE .GE. SPALLEN) THEN
                  SPALLS = SPALLS + 1
                  SPALFLG(I) = 1
                ENDIF
```

```
            ENDIF
935         CONTINUE
          ENDIF
        ENDIF
571   CONTINUE

C
C  Cracks which begin and end within GROUP pixels of each other are grouped
C  together as the same crack.  This helps eliminate the possibility that a
C  crack is lost as it travels through an intersection with another crack
C  as is picked up again on the other side as a new crack.  Also, it groups
C  together cracks which lie along the same line of stress, but are not
C  connected in the video by either poor enhancement of the image or the
C  pavement is not yet broken.  During the first pass (ANALYZE = 1), if the
C  crack is positioned at less than a 60 degree angle in the frame it is
C  called a SKEWED crack.  If the angle of orientation is greater than 60
C  degrees then it is termed a longitudinal crack.  During the second pass
C  (ANALYZE = 2) the crack is labeled a transverse crack.
C

      DO 60 SCAN = 1,TRACE
        IF (CRKFLAG(SCAN) .EQ. 1  .AND.  CHECKED(SCAN) .EQ. 0) THEN
          CHECKED(SCAN) = 1
          TEMPBOT = BOTTOM(SCAN)
          TEMPLEF = LEFSIDE(SCAN)
          TEMPRIG = RIGSIDE(SCAN)
          DO 91 LOOK = (SCAN + 1),TRACE
            NEAR = ABS(TEMPBOT - TOP(LOOK))
            IF (NEAR .LT. GROUP) THEN
              NEARLEF = TEMPLEF - GROUP
              NEARRIG = TEMPRIG + GROUP
              IF (STARRIG(LOOK) .GE. NEARLEF  .AND.
     -        STARLEF(LOOK) .LE. NEARRIG)  THEN
                CHECKED(LOOK) = 1
                TEMPBOT = BOTTOM(LOOK)
                TEMPLEF = LEFSIDE(LOOK)
                TEMPRIG = RIGSIDE(LOOK)
              ENDIF
            ENDIF
91        CONTINUE
          IF (ANALYZE .EQ. 1) THEN
            XCHANGE = REAL(TEMPLEF) - REAL(STARLEF(SCAN))
            YCHANGE = REAL(TEMPBOT) - REAL(TOP(SCAN))
            IF (XCHANGE .EQ. 0) THEN
              LONTUDE = LONTUDE + 1
            ELSE
              SLOPE = ABS(YCHANGE/XCHANGE)
              IF (SLOPE .GT. 1.73) THEN
                LONTUDE = LONTUDE + 1
              ELSE
                SKEWED = SKEWED + 1
              ENDIF
            ENDIF
          ELSE
            TRANS = TRANS + 1
          ENDIF
        ENDIF
60    CONTINUE

C
C  Write the number of cracks and spalls found by the system on the current
C  pass to the screen.
C

      WRITE (*,*) ' '
      WRITE (*,*) ' '
      IF (ANALYZE .EQ. 1) THEN
        WRITE (*,*) 'Number of Longitudinal Cracks = ',LONTUDE
        WRITE (*,*) 'Number of Skewed Cracks = ',SKEWED
        WRITE (*,*) 'Number of Spalls = ',SPALLS
        VSPALLS = SPALLS
      ELSE
        HSPALLS = 0
        HSPALLS = SPALLS - VSPALLS
        WRITE (*,*) 'Number of Transverse Cracks = ',TRANS
        WRITE (*,*) 'Number of Spalls = ',HSPALLS
      ENDIF
      WRITE (*,*) ' '
      WRITE (*,*) ' '

C
C  If a crack was detected during the current pass through the video
C  image then erase the cracks and spalls found so they will not be
C  detected again during processing of video.  The identified crack is
C  also written into QUADRANT 1 for comparison with the original image
C  in QUADRANT 2.  The video image is re - scanned as before with a
```

```
C  call to the subroutine ERASE for removing the identified crack from
C  the processed image.  The IMAGEACTION subroutine WHLINE is used to
C  write the processed scan line of pixels to the image.
C
      IF (CRACK .GT. 0) THEN
         DO 134 YS = 0,ROWCNT
            CALL  RHLINE(0,YS,LINECNT,LINE)
            CALL  RHLINE(256,YS,LINECNT,VIEW)
            DO 992 TRCCNT = 1,TRACE
               IF (CRKFLAG(TRCCNT) .EQ. 1) THEN
                  IF (YS .GE. TOP(TRCCNT)  .AND.
                  YS .LE. BOTTOM(TRCCNT)) THEN
                     CALL  PIXFIND(LINECNT,LINE,STOP,START,CURRENT,JUMP)
                     CANDATE = 0
                     IF (YS .EQ. TOP(TRCCNT)) THEN
                        DELCNT(TRCCNT) = 0
                        LASTLEF(TRCCNT) = STARLEF(TRCCNT)
                        LASTBOT(TRCCNT) = YS
                        LEFSIDE(TRCCNT) = STARLEF(TRCCNT)
                        RIGSIDE(TRCCNT) = STARRIG(TRCCNT)
                        CALL  ERASE(LEFSIDE,RIGSIDE,LINE,VIEW,TRCCNT)
                     ELSE
                        IF (DELCNT(TRCCNT) .GT. 0) THEN
                           ISUM = 0
                           DO 467 I = 1,DELCNT(TRCCNT)
                              ISUM = ISUM + DELTAS(I,TRCCNT)
467                        CONTINUE
                           DELTAX = ISUM/DELCNT(TRCCNT)
                           EXPECT = LASTLEF(TRCCNT) + (YS -
                           LASTBOT(TRCCNT))*DELTAX
                        ENDIF
                        LEFT = LEFSIDE(TRCCNT) - JUMP
                        RIGHT = RIGSIDE(TRCCNT) + JUMP
                        DO 75 CURCNT = 1,CURRENT
                           IF (STOP(CURCNT) .GE. LEFT .AND.
                           START(CURCNT) .LE. RIGHT) THEN
                              IF (CANDATE .EQ. 0) THEN
                                 CANDATE = CURCNT
                              ELSE
                                 IF (DELCNT(TRCCNT) .GT. 0) THEN
                                    CANLEN = ABS(EXPECT - START(CANDATE))
                                    CURLEN = ABS(EXPECT - START(CURCNT))
                                    IF (CURLEN .LT. CANLEN)
                                    CANDATE = CURCNT
                                 ENDIF
                              ENDIF
                           ENDIF
75                         CONTINUE
                        ENDIF
                        IF (CANDATE .GT. 0) THEN
                           TWIDTH = STOP(CANDATE) - START(CANDATE) + 1
                           IF (TWIDTH .LE. MAXWID) THEN
                              DELCNT(TRCCNT) = DELCNT(TRCCNT) + 1
                              NEWDEL = (START(CANDATE) - LASTLEF(TRCCNT))
                              /(YS - LASTBOT(TRCCNT))
                              IF (DELCNT(TRCCNT) .GT. WINDOW) THEN
                                 DELCNT(TRCCNT) = WINDOW
                                 DO 723 MOVE = 2,WINDOW
                                    DELTAS(MOVE - 1,TRCCNT) =
                                    DELTAS(MOVE,TRCCNT)
723                              CONTINUE
                                 DELTAS(WINDOW,TRCCNT) = NEWDEL
                              ELSE
                                 DELTAS(DELCNT(TRCCNT),TRCCNT) = NEWDEL
                              ENDIF
                              LEFSIDE(TRCCNT) = START(CANDATE)
                              RIGSIDE(TRCCNT) = STOP(CANDATE)
                              LASTLEF(TRCCNT) = START(CANDATE)
                              LASTBOT(TRCCNT) = YS
                              CALL  ERASE(LEFSIDE,RIGSIDE,LINE,VIEW,TRCCNT)
                           ELSE
                              LEFSIDE(TRCCNT) = START(CANDATE)
                              RIGSIDE(TRCCNT) = STOP(CANDATE)
                              DO 316 SCAN = 1,SPALCNT
                                 IF (SPALDIR(SCAN) .EQ. TRCCNT) THEN
                                    IF (YS .GE. SPALTOP(SCAN) .AND.
                                    YS .LE. SPALBOT(SCAN)) THEN
                                    IF (SPALFLG(SCAN) .EQ. 1) THEN
                                       SPALPIX = SPALPIX + (RIGSIDE(TRCCNT)
                                       - LEFSIDE(TRCCNT) + 1)
                                       CALL  ERASE(LEFSIDE,RIGSIDE,LINE,
                                       VIEW,TRCCNT)
                                    ENDIF
                                 ENDIF
                                 ENDIF
```

```
316                     CONTINUE
                      ENDIF
                    ENDIF
                  ENDIF
                ENDIF
992           CONTINUE
              CALL  WHLINE(0,YS,LINECNT,LINE)
              CALL  WHLINE(256,YS,LINECNT,VIEW)
134         CONTINUE
          ENDIF

1         CONTINUE

C
C  Initialize the counters for scanning for POPOUTS in the video image.
C

          TRACE = 0
          POPOUTS = 0
          LINECNT = 240

C
C  Again, read in a line of pixels and determine START and STOP which
C  represents the beginning and end of a string of black pixels on the
C  current scan line.
C

          DO 314 YS = 0,255
            CALL  RHLINE(0,YS,LINECNT,LINE)
            CALL  PIXFIND(LINECNT,LINE,STOP,START,CURRENT,JUMP)

C
C  Search through the existing potential POPOUTS to associate a current
C  START and STOP of black pixels with an ongoing POPOUT.  The expected
C  location of the LEFSIDE of the POPOUT is not computed, because the
C  POPOUT should not be concealed by intersecting cracks.
C

            DO 436 CURCNT = 1,CURRENT
              TWIDTH = STOP(CURCNT) - START(CURCNT) + 1
              DO 87 TRCCNT = 1,TRACE
                IF (CRKFLAG(TRCCNT) .EQ. 0) THEN
                  LEFT = LEFSIDE(TRCCNT) - JUMP
                  RIGHT = RIGSIDE(TRCCNT) + JUMP
                  IF (STOP(CURCNT) .GE. LEFT .AND. START(CURCNT)
                  .LE. RIGSIDE(TRCCNT)) THEN
                    IF (TWIDTH .GE. POPLEN) THEN
                      BOTTOM(TRCCNT) = YS
                      LEFSIDE(TRCCNT) = START(CURCNT)
                      RIGSIDE(TRCCNT) = STOP(CURCNT)
                      START(CURCNT) = 0
                    ENDIF
                  ENDIF
                ENDIF
87            CONTINUE

C
C  If the START and STOP pair could not be associated with an existing
C  trace (potential POPOUT) and the current width satisfies the potential
C  for a POPOUT width then begin a new trace.
C

              IF (START(CURCNT) .GT. 0  .AND.  TWIDTH .GE. POPLEN) THEN
                TRACE = TRACE + 1
                CRKFLAG(TRACE) = 0
                STARLEF(TRACE) = START(CURCNT)
                STARRIG(TRACE) = STOP(CURCNT)
                LEFSIDE(TRACE) = START(CURCNT)
                RIGSIDE(TRACE) = STOP(CURCNT)
                TOP(TRACE) = YS
                BOTTOM(TRACE) = YS
              ENDIF

436         CONTINUE

C
C  If a new piece has not been added to a POPOUT within the last JUMP scans
C  then examine the trace to see if it fits the criteria for a POPOUT. If
C  the trace fits the criteria for a POPOUT then keep the location of the
C  POPOUT in memory.  If the trace fails the test then call the subroutine
C  REORDER which writes the index of the trace to the array SORT for later
C  erasing of trace from the bookkeeping arrays.
C

            ORDER = 0
            DO 342 SCAN = 1,TRACE
```

```
            IF (CRKFLAG(SCAN) .EQ. 0) THEN
               RANGE = YS - BOTTOM(SCAN)
               LENGTH = BOTTOM(SCAN) - TOP(SCAN)
               IF (RANGE .GT. JUMP) THEN
                  IF (LENGTH .GT. POPLEN) THEN
                     POPOUTS = POPOUTS + 1
                     CRKFLAG(SCAN) = 1
                  ELSE
                     CALL  REORDER (SORT,SCAN,ORDER)
                  ENDIF
               ENDIF
            ENDIF
342      CONTINUE

C
C  Scan the tracings to see if two or more are overlapping. If two tracings
C  are overlapping then the most recent trace for a POPOUT.  If the trace is
C  a POPOUT then retain its location.  If the trace fails then call the
C  subroutine REORDER which writes the index of the trace to the array
C  SORT for later erasing of the trace from the bookkeeping arrays.
C

         DO 481 LOOK = 1,TRACE
            IF (CRKFLAG(LOOK) .EQ. 0) THEN
               DO 768 SCAN = ( LOOK + 1 ),TRACE
                  IF (CRKFLAG(SCAN) .EQ. 0) THEN
                     IF (LEFSIDE(SCAN) .EQ. LEFSIDE(LOOK)) THEN
                        LENGTH = BOTTOM(SCAN) - TOP(SCAN)
                        IF (LENGTH .GT. POPLEN) THEN
                           POPOUTS = POPOUTS + 1
                           CRKFLAG(SCAN) = 1
                        ELSE
                           CALL  REORDER (SORT,SCAN,ORDER)
                        ENDIF
                     ENDIF
                  ENDIF
768            CONTINUE
            ENDIF
481      CONTINUE

C
C  Use the SORT array provided by the subroutine REORDER to update the
C  bookkeeping arrays for traces which have been closed and failed the POPOUT
C  criteria.
C

         IF (ORDER .GT. 0) THEN
            IF (TRACE .EQ. 1) THEN
               TRACE = 0
            ELSE
               DO 2161 SCAN = 1,ORDER
                  DO 711 MOVE = ( SORT(SCAN) + 1 ),TRACE
                     LEFSIDE(MOVE - 1) = LEFSIDE(MOVE)
                     RIGSIDE(MOVE - 1) = RIGSIDE(MOVE)
                     BOTTOM(MOVE - 1) = BOTTOM(MOVE)
                     TOP(MOVE - 1) = TOP(MOVE)
                     STARLEF(MOVE - 1) = STARLEF(MOVE)
                     STARRIG(MOVE - 1) = STARRIG(MOVE)
711               CONTINUE
                  DO 114 MOVE = ( SCAN + 1 ),ORDER
                     SORT(MOVE) = SORT(MOVE) - 1
114               CONTINUE
                  TRACE = TRACE - 1
2161           CONTINUE
            ENDIF
         ENDIF

314      CONTINUE

C
C  Once the end of the picture has been reached scan the still currently
C  active tracings for POPOUTS.
C

         DO 157 SCAN = 1,TRACE
            IF (CRKFLAG(SCAN) .EQ. 0) THEN
               LENGTH = BOTTOM(SCAN) - TOP(SCAN)
               IF (LENGTH .GE. POPLEN) THEN
                  POPOUTS = POPOUTS + 1
                  CRKFLAG(SCAN) = 1
               ENDIF
            ENDIF
157      CONTINUE


C
```

```
C  If POPOUTS were detected during scanning of the image then erase
C  them from the processed image (Quadrant 0) and write them out to
C  Quadrant 1.  The subroutine ERASE is used to change the color of
C  the pixels.
C
      IF (POPOUTS .GT. 0) THEN
         DO 991 YS = 0,255
            CALL  RHLINE(0,YS,LINECNT,LINE)
            CALL  RHLINE(256,YS,LINECNT,VIEW)
            CALL  PIXFIND(LINECNT,LINE,STOP,START,CURRENT,JUMP)
            DO 734 CURCNT = 1,CURRENT
               DO 521 TRCCNT = 1,TRACE
                  IF (CRKFLAG(TRCCNT) .EQ. 1) THEN
                     IF (YS .GE. TOP(TRCCNT) .AND. YS .LE.
     -                    BOTTOM(TRCCNT)) THEN
                        IF (YS .EQ. TOP(TRCCNT)) THEN
                           LEFT = STARLEF(TRCCNT) - JUMP
                           RIGHT = STARRIG(TRCCNT) + JUMP
                        ELSE
                           LEFT = LEFSIDE(TRCCNT) - JUMP
                           RIGHT = RIGSIDE(TRCCNT) + JUMP
                        ENDIF
                        IF (STOP(CURCNT) .GE. LEFT .AND. START(CURCNT)
     -                       .LE. RIGHT) THEN
                           LEFSIDE(TRCCNT) = START(CURCNT)
                           RIGSIDE(TRCCNT) = STOP(CURCNT)
                           CALL  ERASE(LEFSIDE,RIGSIDE,
     -                          LINE,VIEW,TRCCNT)
                        ENDIF
                     ENDIF
                  ENDIF
521            CONTINUE
734         CONTINUE
            CALL WHLINE(0,YS,240,LINE)
            CALL  WHLINE(256,YS,240,VIEW)
991      CONTINUE
      ENDIF

C
C  Print the frame analysis results to the screen.
C
      DO 64 I = 1,20
         WRITE (*,*) ' '
64    CONTINUE
      WRITE (*,*) 'FRAME ANALYSIS PARAMETERS:'
      WRITE (*,*) ' '
      WRITE (*,*) 'Crack Intensity Threshold = ',TIMES,' SD'
      WRITE (*,*) 'Maximum gap between black pixels = ',JUMP
      WRITE (*,*) 'Maximum crack width  = ',MAXWID
      WRITE (*,*) 'Maximum gap between cracks  = ',GROUP
      WRITE (*,*) 'Minimum detectable crack length = ',MINLEN
      WRITE (*,*) 'Minimum size of a detectable popout = ',POPLEN
      WRITE (*,*) 'Minimum detectable spall length = ',SPALLEN
      WRITE (*,*) 'Window Length for slope calculation = ',WINDOW
      WRITE (*,*) ' '
      WRITE (*,*) ' '
      WRITE (*,*) ' '
      WRITE (*,*) ' '
      WRITE (*,*) 'FRAME ANALYSIS RESULTS:'
      WRITE (*,*) ' '
      WRITE (*,*) 'Number of Longitudinal Cracks = ',LONTUDE
      WRITE (*,*) 'Number of Skewed Cracks = ',SKEWED
      WRITE (*,*) 'Number of Transverse Cracks = ',TRANS
      WRITE (*,*) 'Number of Spalls = ',SPALLS
      WRITE (*,*) 'Number of Spalled Pixels = ',SPALPIX
      WRITE (*,*) 'Number of Popouts = ',POPOUTS

C
C  Rotate the 1st quadrant.
C
      DO 7  I = 1,3
         CALL ROT90(256,0,256,256)
7     CONTINUE

C
C  End of Program.
C
      END
```

```
C
C ******************************************************
C
C    SUBROUTINE:    PIXFIND
C
C ******************************************************
C
C
C  This subroutine locates the starting and stopping position
C  in the X coordinate for a group of black pixels on the
C  current scan line.  The array LINE contains the row of
C  pixels obtained from the image.  The variable LINECNT equals
C  the number of entries in the LINE array.  The variable
C  JUMP is the maximum number of white pixels which may
C  separate black pixels which are grouped together in one
C  set.  The variable CURRENT is the number of entries in the
C  arrays START and STOP.
C

      SUBROUTINE  PIXFIND(LINECNT,LINE,STOP,START,CURRENT,
     - JUMP)

      IMPLICIT INTEGER*2 (A-Z)

      INTEGER*2  LINE(256),START(100),STOP(100)

      BLACK = 0
      WHITE = 255
      CURRENT = 0
      OPENFLG = 0
      DO 25 SCAN = 1,LINECNT
         IF ( LINE(SCAN) .EQ. BLACK ) THEN
            CHECK = SCAN - JUMP
            IF ( CHECK .LT. 1 ) THEN
               SEARCH = 1
            ELSE
               SEARCH = CHECK
            ENDIF
            PIXFLAG = WHITE
            DO 42 I = SEARCH,(SCAN - 1)
               IF ( LINE(I) .EQ. BLACK ) PIXFLAG = BLACK
42          CONTINUE
            IF ( PIXFLAG .EQ. WHITE ) THEN
               IF ( OPENFLG .EQ. 1 ) THEN
                  STOP(CURRENT) = START(CURRENT)
                  CURRENT = CURRENT + 1
                  START(CURRENT) = SCAN
               ELSE
                  CURRENT = CURRENT + 1
                  START(CURRENT) = SCAN
                  OPENFLG = 1
               ENDIF
            ENDIF
            IF ( PIXFLAG .EQ. BLACK ) THEN
               STOP(CURRENT) = SCAN
               OPENFLG = 0
            ENDIF
         ENDIF
25    CONTINUE
      IF ( OPENFLG .EQ. 1 ) STOP(CURRENT) = START(CURRENT)
      RETURN
      END
C
C ******************************************************
C
C    SUBROUTINE:    REORDER
C
C ******************************************************
C
C
C  This subroutine produces the array SORT which contains the
C  indices in the bookkeeping arrays of the traces which were
C  closed from inactivity and did not meet the requirements
C  of cracks or popouts.  The variable SCAN is the index of the
C  trace to be erased.  The variable ORDER is the number of
C  entries in the array SORT.  The array SORT is arranged so that
C  the lowest index trace is in the first index of SORT and the
C  highest index trace is the highest index in SORT.
C

      SUBROUTINE  REORDER(SORT,ORDER,SCAN)

      IMPLICIT INTEGER*2 (A-Z)

      INTEGER*2  SORT(100)
```

```
      FOUND = 0
      DO 210 I = 1,ORDER
         IF (SORT(I) .EQ. SCAN) FOUND = 1
210   CONTINUE
      IF (FOUND .EQ. 0) THEN
         ORDER = ORDER + 1
         SORTED = 0
         DO 211 N = 1,(ORDER - 1)
            IF (SORTED .EQ. 0) THEN
               IF (SCAN .LT. SORT(N)) THEN
                  DO 212 I = ORDER,(N + 1),-1
                     SORT(I) = SORT(I - 1)
212               CONTINUE
                  SORT(N) = SCAN
                  SORTED = 1
               ENDIF
               IF (SCAN .GT. SORT(N) .AND. N .EQ. (ORDER - 1)) THEN
                  SORT(N + 1) = SCAN
               ENDIF
            ENDIF
211      CONTINUE
         IF (ORDER .EQ. 1) SORT(1) = SCAN
      ENDIF
      RETURN
      END

C
C ****************************************************************
C
C    SUBROUTINE:  ERASE
C
C ****************************************************************
C
C  This subroutine erases the crack from Quadrant 0 and write the
C  crack to Quadrant 1.  The array LINE contains pixels from Quadrant 0
C  and the array VIEW contains the pixels from Quadrant 1.  The
C  LEFSIDE and RIGSIDE of the crack is passed to the subroutine and
C  the pixels in Quadrant 0 are changed to white while the white pixels
C  in Quadrant 1 are changed to black.
C

      SUBROUTINE  ERASE(LEFSIDE,RIGSIDE,LINE,VIEW,TRCCNT)

      IMPLICIT INTEGER*2 (A-Z)

      INTEGER*2  LEFSIDE(100),RIGSIDE(100),LINE(256)
      INTEGER*2  VIEW(256)

      BLACK = 0
      WHITE = 255
      DO 35 CHANGE = LEFSIDE(TRCCNT),RIGSIDE(TRCCNT)
         IF (LINE(CHANGE) .EQ. BLACK) VIEW(CHANGE) = BLACK
35    CONTINUE
      DO 78 CHANGE = LEFSIDE(TRCCNT),RIGSIDE(TRCCNT)
         LINE(CHANGE) = WHITE
78    CONTINUE
      RETURN
      END
```

THE TRANSPORTATION RESEARCH BOARD is a unit of the National Research Council, which serves the National Academy of Sciences and the National Academy of Engineering. It evolved in 1974 from the Highway Research Board which was established in 1920. The TRB incorporates all former HRB activities and also performs additional functions under a broader scope involving all modes of transportation and the interactions of transportation with society. The Board's purpose is to stimulate research concerning the nature and performance of transportation systems, to disseminate information that the research produces, and to encourage the application of appropriate research findings. The Board's program is carried out by more than 270 committees, task forces, and panels composed of more than 3,300 administrators, engineers, social scientists, attorneys, educators, and others concerned with transportation; they serve without compensation. The program is supported by state transportation and highway departments, the modal administrations of the U.S. Department of Transportation, the Association of American Railroads, the National Highway Traffic Safety Administration, and other organizations and individuals interested in the development of transportation.

The National Academy of Sciences is a private, nonprofit, self-perpetuating society of distinguished scholars engaged in scientific and engineering research, dedicated to the furtherance of science and technology and to their use for the general welfare. Upon the authority of the charter granted to it by the Congress in 1863, the Academy has a mandate that requires it to advise the federal government on scientific and technical matters. Dr. Frank Press is president of the National Academy of Sciences.

The National Academy of Engineering was established in 1964, under the charter of the National Academy of Sciences, as a parallel organization of outstanding engineers. It is autonomous in its administration and in the selection of its members, sharing with the National Academy of Sciences the responsibility for advising the federal government. The National Academy of Engineering also sponsors engineering programs aimed at meeting national needs, encourages education and research, and recognizes the superior achievements of engineers. Dr. Robert M. White is president of the National Academy of Engineering.

The Institute of Medicine was established in 1970 by the National Academy of Sciences to secure the services of eminent members of appropriate professions in the examination of policy matters pertaining to the health of the public. The Institute acts under the responsibility given to the National Academy of Sciences by its congressional charter to be an adviser to the federal government and, upon its own initiative, to identify issues of medical care, research, and education. Dr. Samuel O. Thier is president of the Institute of Medicine.

The National Research Council was organized by the National Academy of Sciences in 1916 to associate the broad community of science and technology with the Academy's purpose of furthering knowledge and advising the federal government. Functioning in accordance with general policies determined by the Academy, the Council has become the principal operating agency of both the National Academy of Sciences and the National Academy of Engineering in providing services to the government, the public, and the scientific and engineering communities. The Council is administered jointly by both Academies and the Institute of Medicine. Dr. Frank Press and Dr. Robert M. White are chairman and vice chairman, respectively, of the National Research Council.

TRANSPORTATION RESEARCH BOARD
National Research Council
2101 Constitution Avenue, N.W.
Washington, D.C. 20418

ADDRESS CORRECTION REQUESTED

000015M003
MATERIALS ENGR

IDAHO TRANS DEPT DIV OF HWYS
P O BOX 7129
BOISE ID 83707